SANDIA REPORT
SAND98–1171/1 • TTC 1525
Unlimited Release
Printed May 1998

Data and Methods for the Assessment of the Risks Associated with the Maritime Transport of Radioactive Materials Results of the SeaRAM Program Studies

Volume 1: Main Report

Jeremy L. Sprung, Stephen J. Bespalko, Francis L. Kanipe, Sieglinde Neuhauser, James D. Smith, Richard Yoshimura, Philip C. Reardon, Clinton J. Shaffer, Rod Fisk, Holly Tomasik, Robert J. Heid

Prepared by
Sandia National Laboratories
Albuquerque, New Mexico 87185 and Livermore, California 94550

Sandia is a multiprogram laboratory operated by Sandia Corporation, a Lockheed Martin Company, for the United States Department of Energy under Contract DE-AC04-94AL85000.

Sandia National Laboratories

Issued by Sandia National Laboratories, operated for the United States Department of Energy by Sandia Corporation.

Available to DOE and DOE contractors from
Office of Scientific and Technical Information
P.O. Box 62
Oak Ridge, TN 37831

Prices available from (615) 576-8401, FTS 626-8401

Available to the public from
National Technical Information Service
U.S. Department of Commerce
5285 Port Royal Rd
Springfield, VA 22161

NTIS price codes
Printed copy: A21
Microfiche copy: A01

DISCLAIMER

SAND--98-1171/1

SAND98-1171/1
Unlimited Release
Printed May 1998

TTC-1525/1

Data and Methods for the Assessment of the Risks Associated with the Maritime Transport of Radioactive Materials Results of SeaRAM Program Studies Volume I–Main Report

Jeremy L. Sprung, Stephen J. Bespalko, Francis L. Kanipe, Sieglinde Neuhauser, James D. Smith, and Richard Yoshimura
Transportation Systems Analysis Department
Sandia National Laboratories
P.O. Box 5800
Albuquerque, NM 87185

Philip C. Reardon
PCRT Technologies
8416 Yeager Drive NE
Albuquerque, NM 87109

Clinton J. Shaffer
Science and Engineering Associates, Inc.
6100 Uptown Boulevard NE
Albuquerque, NM 87190

Rod Fisk and Holly Tomasik
Edlow International Co.
1666 Connecticut Avenue NW, Suite 201
Washington, DC 20009

Robert J. Heid
Engineering Computer Optecnomics, Inc.
1356 Cape St. Claire Road
Annapolis, MD 21401

Abstract

This report describes ship accident event trees, ship collision and ship fire frequencies, representative ships and shipping practices, a model of ship penetration depths during ship collisions, a ship fire spread model, cask-to-environment release fractions during ship collisions and fires, and illustrative consequence calculations.

Contents

Figures

Tables

ACRONYMS AND ABBREVIATIONS

ABS	American Bureau of Shipping
ACL	Atlantic Container Line
BNFL	British Nuclear Fuels Limited
CAPSTAN	Computer Aided Planning Stowage and Networking
DOE	U.S. Department of Energy
DOT	U.S. Department of Transportation
EA	environmental assessment
EIS	environmental impact statement
GESAMP	Group of Experts on the Scientific Aspects of Marine Pollution
HSV	high-sided vehicles
IAEA	International Atomic Energy Agency
IMDG	International Maritime Dangerous Goods
IMO	International Maritime Organization
INF	irradiated nuclear fuel
ISO	International Standards Organization
LNG	liquefied natural gas
LPG	liquefied propane gas
M	magnitude
MEPC	Marine Environmental Protection Committee
MSMS	Marine Safety Management System
NEPA	National Environmental Policy Act
NRC	U.S. Nuclear Regulatory Commission
NTSB	National Transportation Safety Board
OPRC	Oil Pollution Preparedness, Response and Co-operation
P	probability of occurrence
PNTL	Pacific Nuclear Transport Limited
PuO_2	plutonium dioxide
R	risk
RAM	radioactive materials
Ro-Ro	roll-on/roll-off
SAR	Safety Analysis Report
SCM	Special Consultative Meeting
SNL	Sandia National Laboratories
TDW	tons deadweight
TI	Transport Index
UFSAR	Updated Final Safety Analysis Report
UNCLOS	United Nations Convention on the Law of the Sea
UNEP	United Nations Environment Program
USCG	U.S. Coast Guard
VHLW	vitrified high level waste

1. INTRODUCTION

1.1 Background

Substantial quantities, about one billion curies per year from 1992 through 1996, of radioactive materials (RAM) (for example, spent reactor fuel, plutonium dioxide, and vitrified high-level wastes) are routinely transported in ships on the world's oceans. Citizens, Greenpeace, and members of congress have all expressed concerns about the safety of these shipments.

The United States will ship or receive large quantities of radioactive materials across the oceans during the next decade. For example, a 1996 Record of Decision issued by the U.S. Department of Energy (DOE) approves the acceptance from foreign research reactors of 700 to 800 shipments of spent fuel containing some 500 million curies of radioactivity. In addition, shipment of radioactive military waste materials and spent fuel from power reactors to Europe for reprocessing into vitrified high-level waste and mixed oxide fuel is one option being considered for the disposal of military wastes that contain plutonium. All of these shipments must be made in accordance with regulations established by the U.S. Nuclear Regulatory Commission (NRC) and the Department of Transportation (DOT). The safety of shipments while in United States ports is overseen by the U.S. Coast Guard (USCG).

The National Environmental Policy Act (NEPA) mandates evaluation of the impacts on the environment of government activities, such as the shipment of radioactive materials. DOE assesses the risks of specific shipping campaigns and documents the findings by preparing Environmental Assessments (EAs) or Environmental Impact Statements (EISs). Previous assessments [1-4] of the risks associated with the maritime transport of radioactive materials may have substantially overestimated these risks because these assessments

- Greatly overestimated the probability that an accident will lead to a release of radioactivity,
- Significantly underestimated retention by deposition onto cask surfaces of the radioactive vapors and aerosols released to the cask interior as a result of the accident, and
- Sometimes overestimated population exposures because real non-uniform population distributions were replaced by approximate uniform distributions, which caused the number of people situated near to the accident site and consequently population doses both to be overestimated.

Because of the number of ocean shipments likely to occur during the near future and because of the widespread concerns expressed about these shipments, during the summer of 1994, DOE initiated a general study of ship accident risks with the intent of substantially enhancing the technical data and methods available for the assessment of these risks and the goal of allaying concerns about the safety of these shipments. Sandia National Laboratories (SNL) was selected to perform the study, which was given the name SeaRAM.

1.2 SeaRAM Program

The SeaRAM Program has four objectives. First, to define and describe a robust methodology for the assessment of the risks associated with the shipment of radioactive materials by sea. Second, to illustrate the use of this methodology by the performance of illustrative calculations. Third, to develop credible technical estimates of the probabilities of ship collisions and ship fires and the likelihood that collisions and/or fires will damage a RAM transport cask so severely that radioactive materials are released from the cask. And fourth, to model the details of a few severe, real ship accidents in order to determine

whether these accidents would have damaged a RAM transport cask had one been on board the ship involved in the accident.

Because this is a generic study, DOE stated that the analyses should be substantial but not exhaustive, and that all calculations performed should be illustrative, that is they should not attempt to examine any specific RAM shipping campaign. The following approach was selected to fulfill this mandate. First, an appropriate risk assessment methodology was identified and described. Then, the methodology was illustratively applied to the transport of spent commercial reactor fuel in a typical transport cask on board a charter freighter and a break-bulk freighter. Data needed to support these calculations or to develop or validate the models used in these calculations was developed, where necessary, by the performance of experiments and detailed collision and/or fire calculations. Finally, illustrative consequence calculations that examine the risks posed by accidents that might occur while these ships were sailing at sea, in coastal waters, and in ports were performed. After these studies were completed, studies of other radioactive materials (plutonium dioxide and vitrified high-level wastes) and of two other transport ships (container and purpose-built ships) were to be performed if funding permitted and review suggested that these added analyses were advisable.

The SeaRAM Program was expected to produce the following results: (1) construction of generic events trees depicting important ship accident scenarios, (2) development of estimates of the probabilities of at least several of the more important scenarios, (3) calculation from historic ship accident data of the probabilities of ship collisions, ship fires, and ship collisions that lead to ship fires, (4) preparation of credible estimates of the probabilities that collisions or fires will actually cause a radioactive material transport cask to be damaged, (5) performance of experiments (e.g., fire tests) and calculations (finite element ship collision calculations, detailed fire and heat transport calculations, probabilistic ship collision, and fire spread calculations) required to develop these damage probabilities, (6) use of risk codes (e.g., RADTRAN, MACCS, MARINRAD) to model the amounts of radioactivity likely to actually be released from a damaged cask during a severe ship accident, and (7) estimation of the magnitude of the consequences that these radioactive releases might cause.

1.3 References

1. *Environmental Assessment on Shipment of Taiwanese Research Reactor Spent Fuel*, DOE/EA-0321. U.S. Department of Energy, Washington, DC, December 1986.

2. *Environmental Assessment on Shipment of Taiwanese Research Reactor Spent Fuel (Phase II)*, DOE/EA-0363. U.S. Department of Energy, Washington, DC, June 1988.

3. *Environmental Assessment of the Risks of the Taiwan Research Reactor Spent Fuel Project*, DOE/EA-0515. U.S. Department of Energy, Washington, DC, June 1991.

4. *Environmental Assessment of Urgent-Relief Acceptance of Foreign Research Reactor Spent Nuclear Fuel*, DOE/EA-0912. U.S. Department of Energy, Washington, DC, April 1994.

2. RISK ASSESSMENT

2.1 Risk Equations

Risk (R) is the product of the magnitude (M) of an unfavorable consequence and the probability of occurrence (P) of that consequence. Thus, $R = P \times M$.

For accidents that might happen during the transportation of RAM, the unfavorable consequences of the accident include (1) exposure of people to radiation emitted by the radioactive gases and particulates released from the failed transportation cask, (2) the occurrence of radiation induced health effects in the population exposed to the radiation, and (3) the costs associated with any emergency response and post-accident cleanup actions.

Consequence magnitudes are usually calculated using computer codes (e.g., MACCS [1, 2] for accidents that happen at known locations, RADTRAN [3, 4] for accidents that can happen somewhere along a transportation route, and MARINRAD [5] for accidents that lead to releases of radioactivity into the ocean). In Section 10.0 of this report, illustrative consequence calculations are described that model the consequences caused by the release of RAM following a ship collision that occurs in a port, while sailing in coastal waters, and while sailing at sea.

Although accident consequences are complicated functions of many input variables, past studies [6] have shown that consequence magnitudes depend principally on the size of the accident source term, the degree to which the source term is diluted during downwind transport (ocean transport for ocean releases) before it reaches population groups, and the size of the exposed population groups. Thus,

$$M = f(\text{source term, prevailing meteorology, exposed population})$$

For transportation accidents, the amount of radionuclide i released to the environment (M_{STi}) is the product of the inventory (I_i) of that radionuclide in the transport cask and the fraction of that inventory (F_i) that is released to the environment from the failed cask. Because release usually occurs in two stages, first from the radioactive material (m) to the cask interior (c) and then from the cask interior to the environment (e), the overall release fraction F_i can be represented as a product of two release fractions, F_{mci} and F_{cei}, where F_{mci} is the release fraction for radionuclide i from the radioactive material to the cask interior and F_{cei} is the release fraction for that radionuclide from the cask interior to the environment. Thus, the accident source term (M_{ST}) is given by

$$M_{ST} = \sum_i M_{STi} = \sum_i I_i F_i = \sum_i I_i F_{mci} F_{cei}$$

Release fractions from RAM casks involved in transportation accidents have been examined by several studies [7–10] and values for F_{mci} have been estimated from experimental data [11]. Because experimental data from which to estimate values for F_{cei} is sparse or non-existent, F_{cei} values have either been based on expert opinion [R] or have been conservatively assumed to be unity [12]. As assuming $F_{cei} = 1.0$ neglects aerosol and vapor deposition inside of the cask and is thus very conservative, a more realistic value for F_{cei} was developed by performing calculations using a compartment code, MELCOR [13], that implements a full-set of thermal-hydraulic and aerosol and vapor transport phenomena. The results of these calculations are summarized in Section 9.0 and are described fully in Appendix IV.

Consequence probabilities (P) are the product of the probability of the source term (P_{ST}), the probability that a particular type of weather (set of meteorological conditions) will prevail at the time the accident occurs (P_W), and the probability that a particular population group will be exposed by the release of radioactivity to the environment (P_{pop}) given the prevailing weather conditions. Thus,

$$P = P_{ST}P_WP_{Pop}$$

For transportation accidents, the probability that an accident will lead to a source term of size j (P_{STj}) is the product of the probability that any accident in single broad class of accidents (e.g., ship collisions) will occur (P_{Acc}) and the fraction of these accidents that are severe enough to cause the release of source term j. Thus, $P_{STj} = P_{Acc}F_{Sev.,j}$ where $F_{Sev.,j}$ is called a severity fraction.

2.2 Accident Scenarios and Probabilities

Risk analyses never specifically consider all of the individual accidents that might occur or even all that historically have occurred. Instead, all of the possible accidents are divided (binned) into classes (groups) and a representative accident is developed (defined) for each group. One powerful way to perform this binning process is by the construction of event trees. An event tree is a diagram that maps paths through accident space. The space is defined by a series of events that may or may not occur given the set of preceding events. Thus, the occurrence or non-occurrence of each event on the tree produces a branch on the tree, a specific set of outcomes for the events on the tree defines a unique path through accident space, and the set of events defined by a unique path constitutes a specific accident scenario. For example, for ship accidents, where the initiating event is a two-ship collision, the second event might be hitting the hold of the struck ship in which the RAM cask is stowed; the third event, deep penetration of that hold by the bow of the striking ship; the fourth event, the initiation of a fire on the struck ship; and the fifth event, the spreading of that fire to the RAM hold. If the RAM hold is both struck and deeply penetrated, then the cask may be damaged by the penetrating bow of the striking ship or, if cargo is present in the hold, by the crushing of cargo about the RAM cask. Alternatively, even if the RAM hold is not struck, the collision may cause a fire that spreads to that hold and there burns hot enough and long enough to eventually causes cask failure and the release of radioactivity from the cask.

Thus, an accident scenario is a specific sequence of events that is initiated by one accident in a broad class of accidents (e.g., a ship collision) and then progresses to a specific set of final conditions (specific mechanical and/or thermal loads on the RAM cask) that cause the release of a source term of a specific composition and size (i.e., source term j). The product of the probabilities of occurrence (P_{jk}) of all of the events on path j that follow the initiating event, then gives the severity fraction for the radioactive release (the release of source term j) that is the result of the j^{th} accident scenario. Thus,

$$F_{Sev,j} = \prod_{k=1}^{n} P_{jk} \quad \text{and therefore} \quad P_{STj} = P_{Acc}F_{Sev.j} = P_{Acc}\prod_{k=1}^{n} P_{jk}$$

Values for ship accident probabilities (P_{Acc}) are developed in Section 4.0 for fires, for collisions, and for collisions that lead to fires. Section 6.0 develops estimates of the chance that a RAM cask is damaged by mechanical forces during a ship collision, given that the striking ship has struck the hold in which the RAM cask is stowed. Appendix II and Appendix III present data developed by ECO, Inc., that were used in these analyses. The chance that a fire spreads to the RAM hold and there burns long enough and hot enough to cause the RAM cask to fail and radioactivity to be released is examined in Section 7.0. Shipping practices that might affect the probability or magnitude of radioactive releases

from RAM casks during ship accidents are summarized in Section 5.0 with supporting material presented in Appendix I. Finally, Section 3.0 develops illustrative ship accident event trees and Section 8.0 develops scenario probabilities for some of the scenarios on the trees.

2.3 References

1. D. I. Chanin et al., *MELCOR Accident Consequence Code System (MACCS), Volume I: User's Guide*, NUREG/CR-4691. Sandia National Laboratories, Albuquerque, NM, February 1990.

2. H. N. Jow et al., *MELCOR Accident Consequence Code System (MACCS), Volume II: Model Description*, NUREG/CR-4691. Sandia National Laboratories, Albuquerque, NM, February 1990.

3. K. S. Neuhauser and F. L. Kanipe, *RADTRAN 4, Volume II: Technical Manual*, SAND89-2370. Sandia National Laboratories, Albuquerque, NM, May 1994.

4. K. S. Neuhauser and F. L. Kanipe, *RADTRAN 4, Volume III: User Guide*, SAND89-2370. Sandia National Laboratories, Albuquerque, NM, January 1992.

5. D. A. Esminger et al., *User's Guide to MARINRAD IV: Model for Assessing the Consequences of Release of Radioactive Material into the Oceans*. The Analytical Sciences Corp., Reading, MA, September 1987.

6. D. C. Aldrich et al., *Technical Guidance for Siting Criteria Development*, SAND81-1549. Sandia National Laboratories, Albuquerque, NM, December 1982.

7. E. L. Wilmot, *Transportation Accident Scenarios for Commercial Spent Fuel*, SAND80-2124. Sandia National Laboratories, Albuquerque, NM, July 1984.

8. R. P. Sandoval et al., *Estimate of CRUD Contribution to Shipping Cask Containment Requirements*, SAND88-1358. Sandia National Laboratories, Albuquerque, NM, January 1991.

9. T. L. Sanders et al., *A Method for Determining the Spent-Fuel Contribution to Transport Cask Containment Requirements*, SAND90-2406. Sandia National Laboratories, Albuquerque, NM, November 1992.

10. J. L. Sprung et al., *Radiological Consequences of Ship Collisions that Might Occur in U.S. Ports during the Shipment of Foreign Research Reactor Spent Nuclear Fuel to the United States in Break-Bulk Freighters*, SAND96-0400. Sandia National Laboratories, Albuquerque, NM, August 1996.

11. R. A. Lorenz et al., *Fission Product Release from Highly Irradiated LWR Fuel*, NUREG/CR-0722. Oak Ridge National Laboratory, Oak Ridge, TN, February 1980.

12. L. E. Fischer et al., *Shipping Container Response to Severe Highway and Railway Accident Conditions*, NUREG/CR-4829, UCID-20733. Lawrence Livermore National Laboratory, Livermore, CA, 1987.

13. R. M. Summers et al., *MELCOR 1.8.0: A Computer Code for Nuclear Reactor Severe Accident Source Term and Risk Assessment Analyses*, NUREG/CR-5531, SAND90-0364. Sandia National Laboratories, Albuquerque, NM, January 1991.

3. EVENT TREES

Figures 3-1a, 3-1b, 3-1c, and 3-1d present a generic ship accident event tree. The tree is divided into four subtrees: the Ship Tree (Figure 3-1a), the RAM Ship Tree (Figure 3-1b), the Oil Tanker Tree (Figure 3-1c), and the Fire/Sink Tree (Figure 3-1d). The boxes at the top of each tree list the events (questions) on the tree. The box labeled OUTCOME indicates either connections between the subtrees or, for the Fire/Sink Tree that terminates each accident scenario (each path through ship accident space), the probabilities of the specific accident scenarios (P_1, ..., P_6). These trees were constructed using the SANET code [1]. That code allows event probabilities to be attached to each branch of the tree and, when given a complete set of branch probabilities, automatically calculates the resulting path (scenario) probabilities. Here, specific values for scenario probabilities are lacking because no branch probabilities were input to SANET when these trees were generated. Probabilities for several important paths on this generic tree are developed in Section 8.0 of this report.

The Ship Tree (Figure 3-1a) asks the following questions: Does an accident (a collision or a fire) occur during the ship voyage? Is the accident a collision or a fire? If the accident is a collision, is the RAM ship the struck ship? If the RAM ship is the striking ship, is the struck ship an oil tanker? Ramming of fixed structures (e.g., bridge piers) and grounding are not addressed by this tree because RAM casks should not be damaged by either of these accidents (ramming of a fixed structure can inflict considerable damage on the bow of the RAM transport ship but rarely would damage cargo significantly; groundings usually do not damage cargo and if a grounding leads to a sinking, recovery of the RAM cask should not be difficult from the shallow water where the grounding occurred). If the accident is not a collision, then the Ship Tree connects directly to the Fire/Sink as the accident must be a fire. The oil tanker question is included on the Ship Tree for two reasons: first, because the striking of an oil tanker by the RAM transport ship could lead to a serious, long duration fire on the RAM transport ship; and second, because even though this accident has never occurred, tracing its path through accident space illustrates how specific highly improbable sequences possibly of concern can be examined using an event tree.

The RAM Ship Tree (Figure 3-1b) describes a collision where the RAM transport ship is struck by some other ship. The second, third, and fourth questions on this tree determine whether the RAM hold is struck. That question is not asked by a single question because collision data indicate that ships are more likely to be struck fore or aft than amidship. Therefore, because RAM casks are more often stowed in center holds than in fore or aft holds, the probability that the striking ship collides with the RAM transport hold requires that both strike and cask location be examined. If the RAM hold is struck, penetration of the bow of the striking ship far enough into that hold to cause cask damage by cask overrun or by crushing of cargo about the cask is examined next. Because release of radioactivity may be enhanced during fire events if the cask has multiple failures, the occurrence of cask puncture or shear failures in addition to seal failures is examined. Finally, all of the paths on this subtree connect to the Fire/Sink Tree as all of these collisions might cause a fire on the RAM transport ship and/or the sinking of that ship.

The Oil Tanker Tree (Figure 3-1c) describes the following very unlikely accident that has never actually occurred: the striking of an oil hold of an oil tanker by a RAM transport ship, specifically, a small charter freighter that has only two cargo holds and is carrying the RAM cask in its forward hold. This hypothetical accident is examined because at least conceptually it could lead to a severe, hot, long duration fire, if oil in the struck hold is able to pour through the hole in the shell of the oil tanker into the forward hold of the charter freighter and there catches fire. Thus, the consideration of this extremely unlikely accident scenario illustrates how the probability of possibly extremely severe accidents that have never occurred historically can be examined.

Finally, the Fire/Sink Tree (Figure 3-1d) asks whether a fire occurs on the RAM transport ship, either as an isolated event or as the result of a collision, whether the fire starts in or spreads to the RAM hold and then damages the cask, and last, whether the RAM transport ship sinks. The Fire/Sink Tree has six possible outcomes. Because one of the four paths on the Ship Tree (Figure 3-1a), all of the ten paths on the RAM Ship Tree (Figure 3-1b), and all four paths on the Oil Tanker Tree (Figure 3-1c) each connect to the Fire/Sink Tree, these four generic ship accident event subtrees (Figures 3-1a, 3-1b, 3-1c, and 3-1d together) together constitute a single tree that actually has 90 separate outcomes (paths through accident space [90 = 6 (15) = 6 (1 + 10 + 4)]). Because even a simple tree can by branching lead to many outcomes, this study made no attempt to estimate all of the branch probabilities needed to fully quantify this illustrative generic tree, and did not even contemplate trying to construct a tree that exhaustively describes ship accident space. Nevertheless, in Section 8.0, path (scenario) probabilities are developed for several of the more important accident scenarios depicted on this generic ship accident event tree.

3.1 References

1. A.L. Camp and L. P. Abeyta, *SANET 1.0 User's Guide and Reference Manual*, SAND91-2864. Sandia National Laboratories, Albuquerque, NM, December 1991.

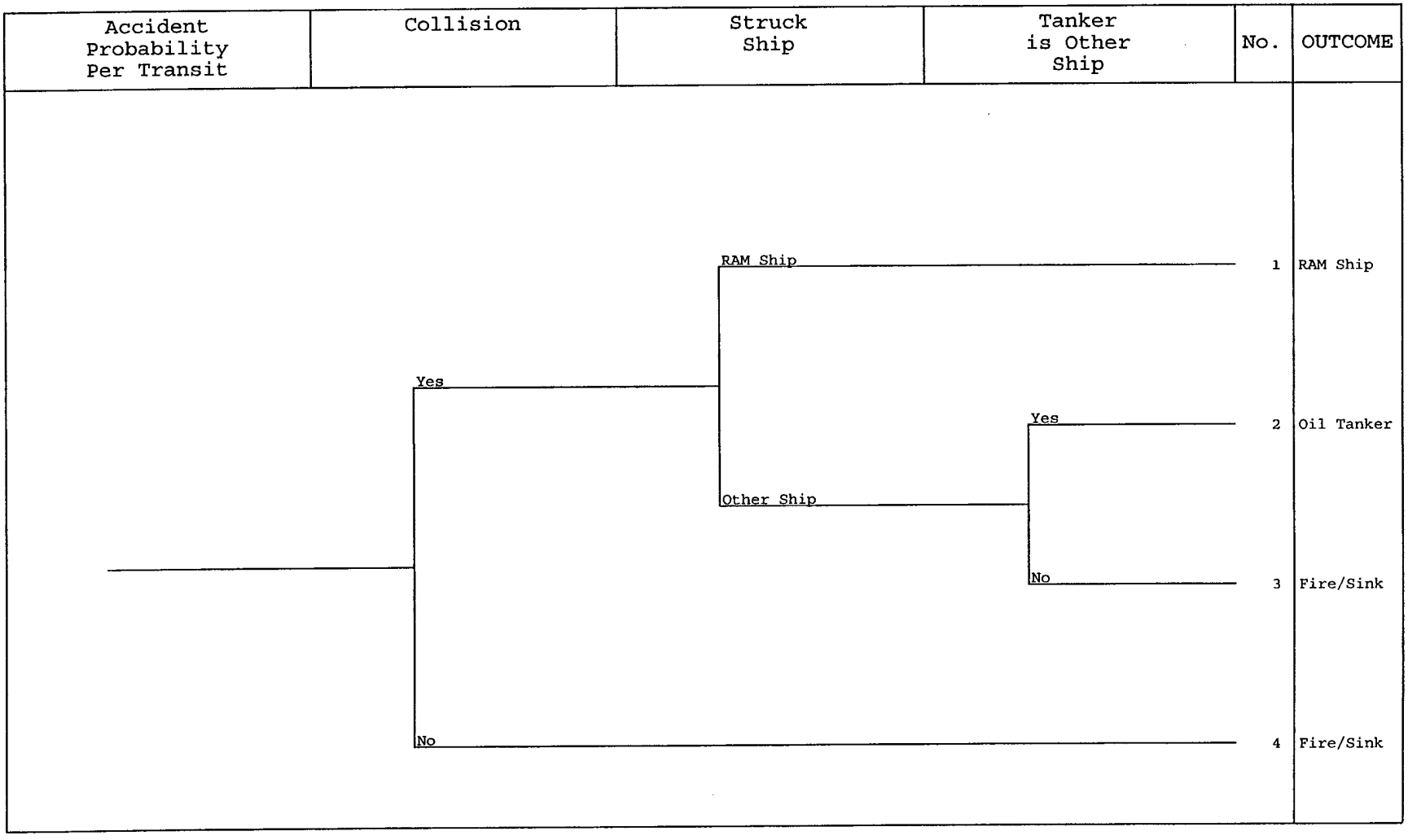

Figure 3-1a. Ship Tree.

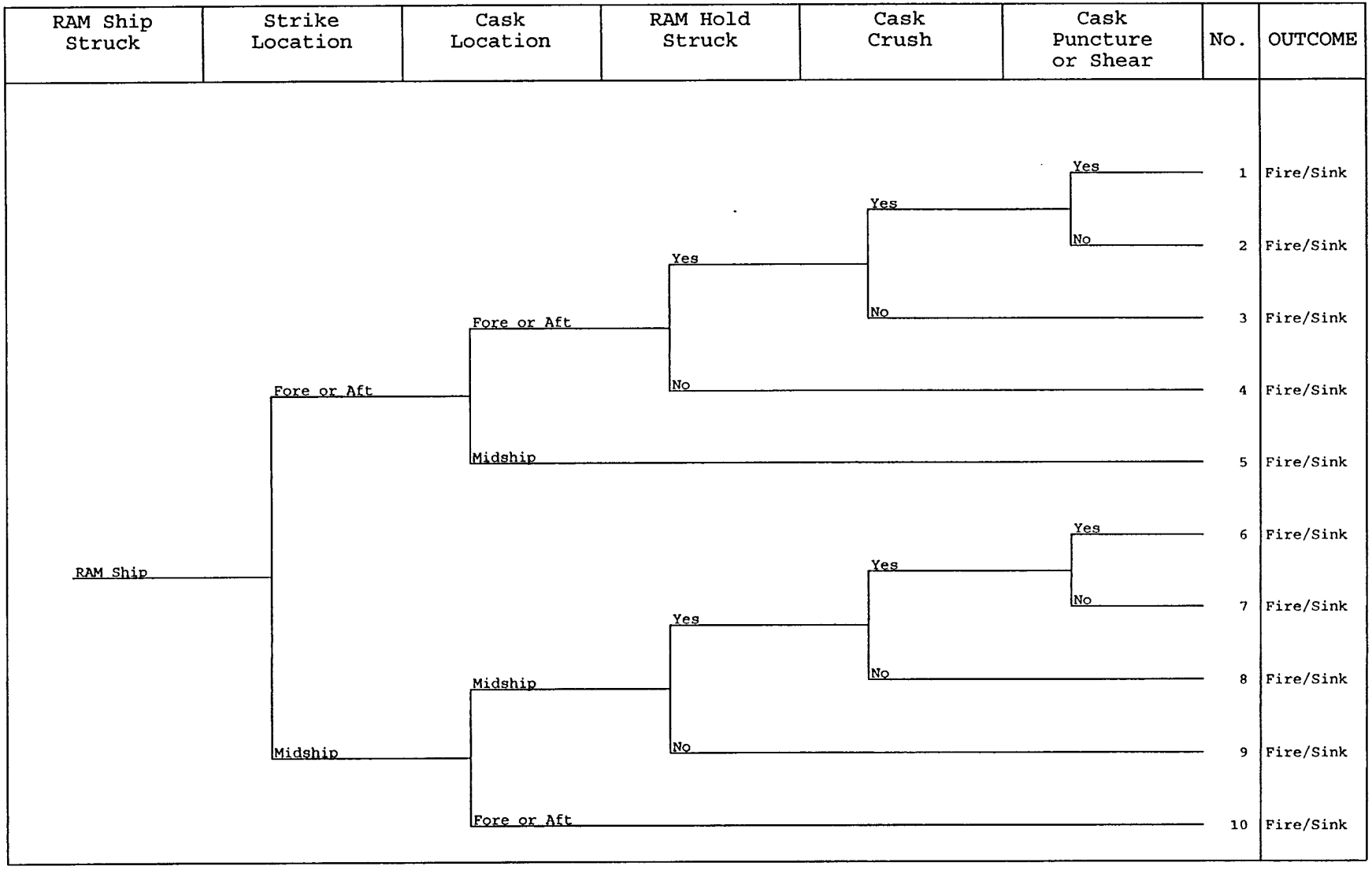

Figure 3-1b. RAM Ship Tree.

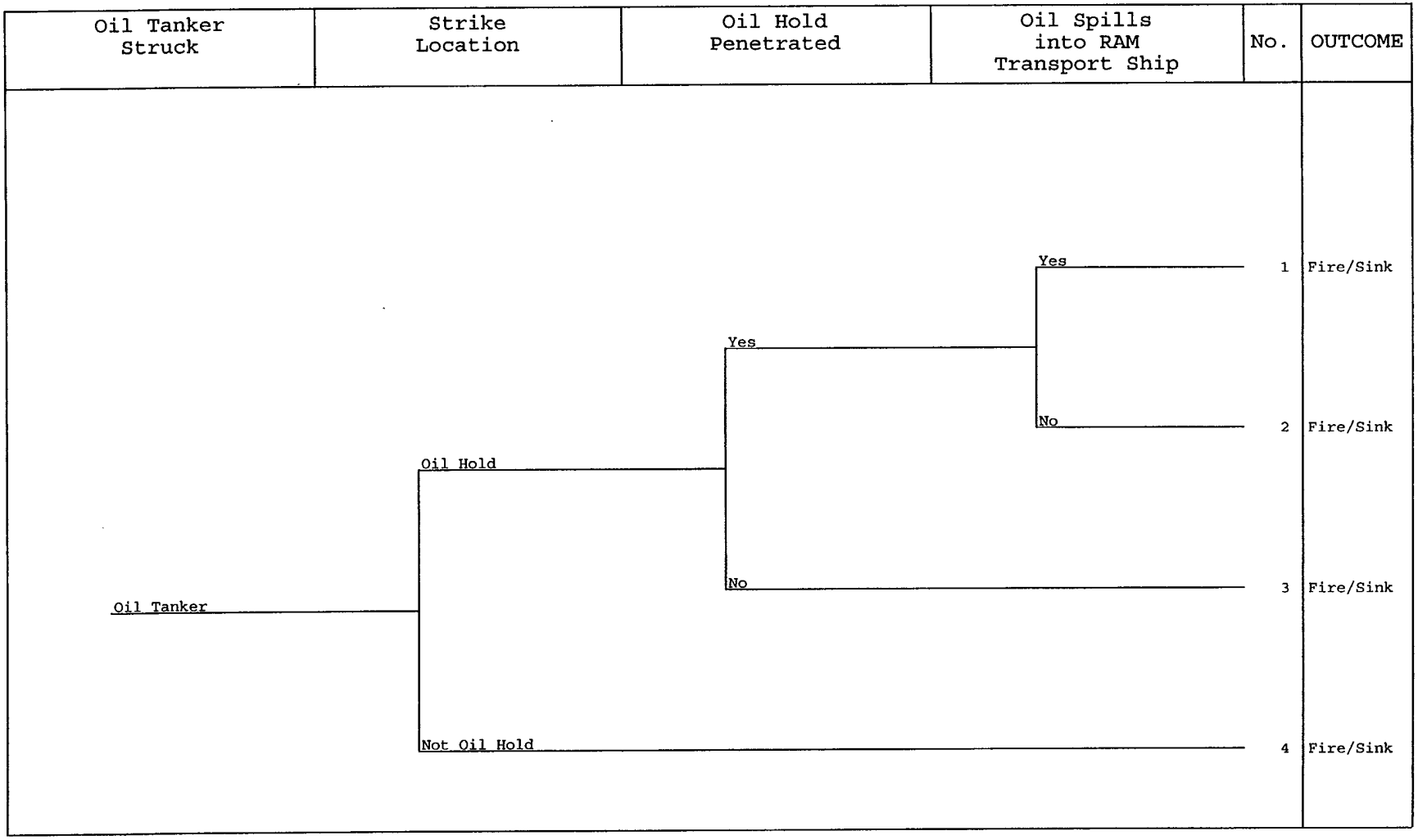

Figure 3-1c. Oil Tanker Tree.

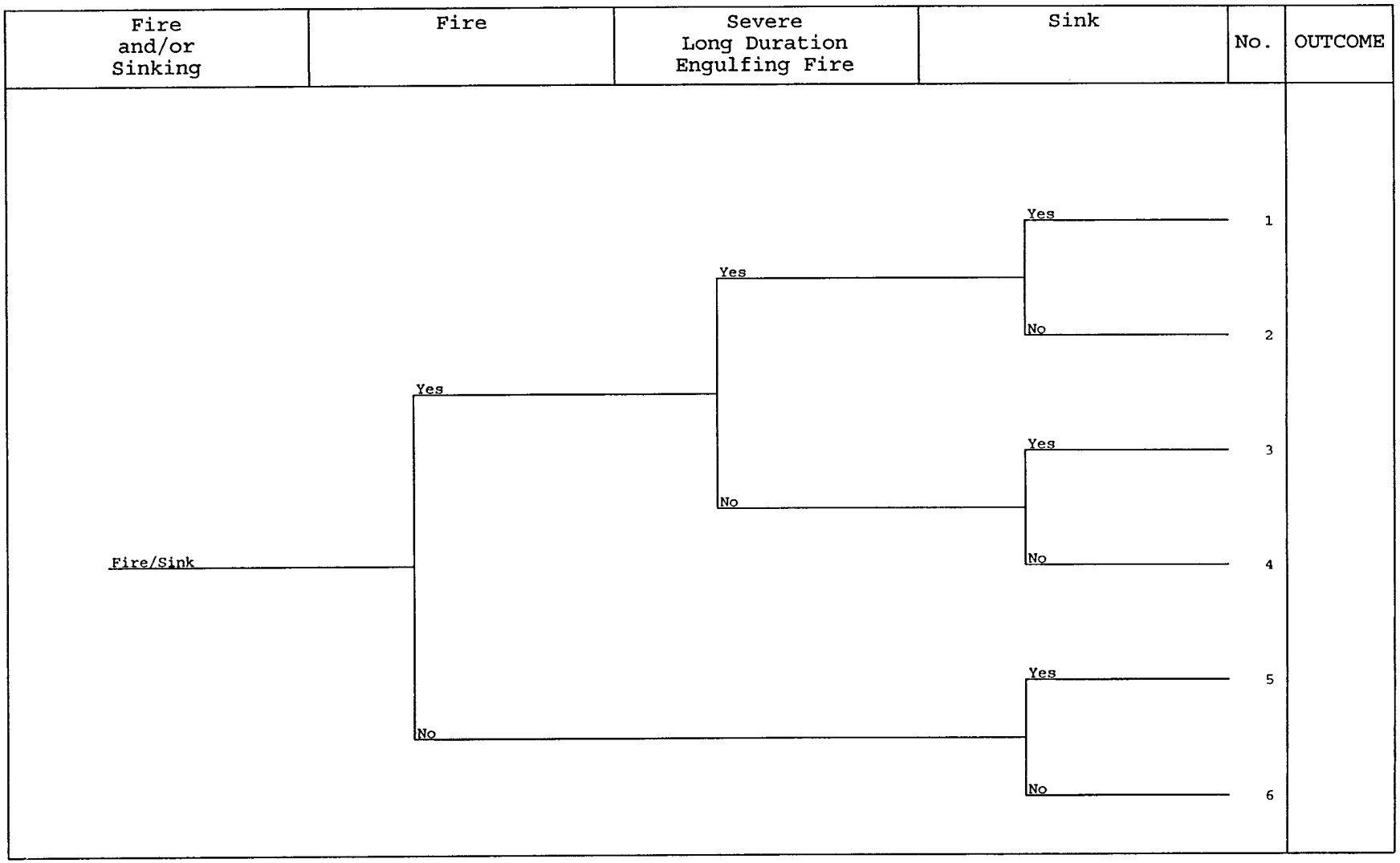

Figure 3-1d. Fire/Sink Tree.

4. ACCIDENT PROBABILITIES

Because severe transportation accidents (here ship accidents) are uncommon events, the probability (P_{STj}) that a transportation accident leads to the release of a radioactive source term of a specific composition and size can be formulated as the product of the probabilities of all of the events that must occur sequentially to cause the release of the specific source term. Thus,

$$P_{STj} = P_{Acc} \prod_{k=1}^{n} P_{jk} = P_{Acc} F_{Sev,j}$$

where P_{Acc} is the probability of the initiating event, here the ship accident, P_{jk} is the probability of one of the n events in the sequence of events initiated by the accident that culminates in the release of the j^{th} radioactive source term, and $F_{Sev,j}$ is the product of all of the events in the sequence that follow the initiating event. This section develops values for P_{Acc} for ship collisions and ship fires. Values for $F_{Sev,j}$ are usually constructed using event trees. This process is illustrated in Section 8.0 for a few important accident scenarios.

4.1 Casualty Data

Ship accident data is gathered by many organizations. Most review accident data principally in order to identify the causes of accidents. Several organizations enter accident data into databases. For this study, accident data gathered by the USCG, the U.S. National Transportation Safety Board (NTSB), and Lloyd's Maritime Information Services was examined in order to develop accident frequencies for ship collisions, ship fires, and ship collisions that lead to fires.

4.1.1 Data on Ship Accidents in U.S. Waters

Both the USCG and the NTSB investigate ship accidents and prepare reports that describe the accidents in considerable detail. Because the principal objective of these investigations is identification of the causes of the accident, so that similar accidents can be avoided in the future, the reports that document the findings of these investigations usually contain little information on accident severity. Specifically, damage to structures, whether caused by a collision or a fire, and the duration and intensity of fires are described briefly, if at all. Thus, although a significant number of USCG and NTSB reports were reviewed during the early stages of this study, none of the information in those reports proved to be useful for estimating the frequencies of ship collisions or ship fires. Data from the USCG Marine Safety Management System (MSMS) ship accident database was used to identify the locations of ship accidents that occurred in the approach waters to the port of New York. Collision and fire frequencies were developed entirely from data in the Lloyd's casualty database [1].

4.1.2 Worldwide Casualty Data: The Lloyd's Casualty File

Fifteen years of ship accident data covering the years 1979 to 1993 were purchased from Lloyd's Maritime Information Services and converted into a relational (RDBMS) format. The data, which constitutes a portion of the Lloyd's Casualty File [1], was supplied in electronic format. The data contained approximately 30,000 incident reports. Most of these incidents involved collisions with fixed structures and groundings. However, some 4,500 of these incidents involved collisions with other ships

(hereafter simply called ship collisions), collisions with other ships that led to ship fires, and ship fires not caused by a ship collision. Queries utilizing the SQL database programming language were then constructed to extract the data utilized in the analysis of ship fires, ship collisions, and ship collisions that led to fires.

4.1.2.1 STRUCTURE OF THE LLOYD'S CASUALTY FILE

Each incident in the Casualty File [1] consists of a sequence of up to 151 records where a record is a single line of data. Each record contains two fields, a nine-digit alphanumeric name followed by an extended 58 character data field. The first record in each entry in the Casualty File is always the incident number, the next 75 records report data for the first ship involved in the incident, and, for ship collisions, the second 75 records provide the same information for the second ship involved in the collision. Few if any entries in the Casualty File contain all of these records, and often, when a record is present, it contains no data (the alphanumeric name is present but the extended data field is empty). Our analysis used data from at most 41 of the 76 records. Table 4-1 identifies these records and lists their alphanumeric names.

Table 4-1. Casualty File Records Used in the Analysis of Accident Frequencies

Record	Lines	Alphanumeric Names
Vessel Identification Number	1	CAROLRNO
Vessel Description	4	
Ship Name		SHPNAME
Gross Tonnage		CAROGRT
Deadweight Tonnage		CARODWT
Ship Type		CAROSTYP
Incident Identification Number	1	CAROINNO
Incident Location	2	
Marsden Square		CAROMES
Environmental Location		CAROENVS
Incident Event Sequence	21	
Casualty Category		CAROGRP
Event		CAROEIOnm
Outcome		CAROEAOnm
Incident Description	12	PTEXTnm, CTEXTnm

The records used in this analysis are now described more fully.

Each ship in the Lloyd's database is identified by a unique 7-digit vessel identification number called the Lloyd's Registry Number. The alphanumeric name for this vessel identification number is CAROLRNO, where LRNO stands for Lloyd's Registry Number.

Up to fourteen characteristics of the vessel specified by the CAROLRNO number can be listed in the entry that describes a specific ship accident. Four of these ship characteristics were used in this analysis: the ship's name (SHPNAME), gross tonnage (CAROGWRT), deadweight tonnage (CARODWT), and ship type (CAROSTYP), e.g., freighter, passenger liner, liquefied natural gas or liquefied propane tanker.

A single, unique 7-digit Incident Number (the CAROINNO number) is assigned to all entries in the Casualty File that present data about a single incident. Thus, all of the entries in the casualty file that pertain to the same accident (incident) are supposed to have the same CAROINNO number. As is discussed below, submission of separate reports about the same incident by different Lloyd's agents appears to allow entries concerning the same incident to sometimes be identified by different CAROINNO numbers.

The location of each incident may be specified in three ways, by SIS Zone (CAROZNES field), by Marsden Square (CAROMES field), and by environmental location (CAROENVS field), e.g., at sea, in the restricted waters that lead to a port, or in the port. SIS zones are regions of the earth's oceans, for example, the Baltic Sea. Marsden squares are regions on the surface of the earth that are bounded by parallels and meridians spaced at 10° intervals starting from the intersection of the equator and the prime meridian [2]. There are 540, not 648, Marsden squares on the earth's surface (numbering ceases at 80° N and 70° S); the squares are numbered sequentially from 1 to 268 in the northern hemisphere and from 300 to 551 in the southern hemisphere with square 1 being the square that is immediately NW of the intersection of the equator and the prime meridian. Because they can be quite large, e.g., the north Pacific or the east African coast, SIS zones were usually not very useful and were rarely used by our analysis.

The structure of the Casualty File allows the events that constitute an incident to be specified. Specifically, the CAROGRP field allows the general character of the incident to be selected from the following list of incident types, each of which is identified by a 2-letter code: foundered, missing, fire/explosion, collision, contact, wrecked or stranded, war loss or damage during hostilities, hull/machinery damage, or other. In addition, the incident can be represented as a sequence of up to ten events that each have a general character (one of the nine incident types) and lead to a specific result (any of 99 different numbered outcomes).

The nature of the incident may be further described by 12 lines of text entered into the PTEXT and CTEXT fields. Thus, these fields can present information about the incident that cannot be specified by the codes used to describe the general character of the incident and of the incident's sequence of events and event outcomes. Information often presented in the text fields that was frequently used during these analyses included the latitude and longitude where the incident occurred (the accident location) or the identities of features near to the accident location such as cities, ports, lighthouses, or the names of other geographic features that could be found on maps. In addition, the text fields sometimes contained brief descriptions of the damage suffered by the vessels involved in the accident and thus some indication of accident severity.

4.1.2.2 PROBLEMS COUNTING SHIP COLLISION INCIDENTS

Searches of the Lloyd's Casualty file showed that ship collisions were not always described in only one incident file. Some incident files are duplicated; sometimes the same ship collision is documented in two incident files that have different incident (CAROINNO) numbers; and occasionally the same accident is documented in multiple incident files. When there were two different incident files for the same ship collision, usually each file contained the particulars for only one of the two ships involved in the collision. Multiple incident files for a single ship collision incident always described accidents that occurred in restricted waters (e.g., at an anchorage) or in a port. All of these accidents involved multiple collision events, such as a ship dragging an anchor during a storm and then colliding with other anchored ships, or a barge breaking free from its moorings and then bouncing off other barges and ships as it drifts downstream.

To avoid double counting of ship collisions, all of the incident files for a single accident had to be combined into a single incident file or all of the separate files that describe the same incident had to be flagged as being related. For collision events that involved several ships, but not collisions between all possible pairs of ships, determining the actual number of collisions was not always straightforward, even after the text fields in the separate incident files had all been read.

Accordingly, proper counting of incidents involved eliminating duplicate files, combining the records in separate files that describe a two-ship collision into a single file, and determining the actual number of collisions that occurred during multiple collision events reported in multiple files. Duplicate records for two-ship collisions were identified both by reading the text fields in incident files and by electronic searches that hunted for files that had the same incident (CAROINNO) number and same pair of ship registry (CAROLRNO) numbers. Ship collisions documented in multiple files were also identified and combined by electronic searches. When the same ship collision was documented in separate incident files, the data fields for each ship involved in the collision event were copied into one of the incident files for the accident and inactivated in the files from which they were copied (usually by setting the data fields in the copied files to null values). This was easy to do for two-ship collision events, as the first incident file usually contained empty fields for data about the second ship.

4.1.2.3 CONFIRMATION OF INCIDENT TYPE

Electronic searches were performed that compared the Casualty Category (CAROGRP event code) to the event outcome codes contained in the event sequence (CAROEAO codes). When the CAROGRP code indicated that an incident was a fire accident, CAROEAO event fields were sequentially scanned for codes that would confirm that the events that comprised the incident consisted of a fire by itself, a collision followed by a fire, some event other than a collision followed by a fire, or a fire followed by some other non-collision event. For collision incidents, event outcome (CAROEAO) codes were scanned to confirm that a ship collision had really occurred. When CAROEAO codes showed that the incident was a grounding and not a collision or that the object struck was a bridge, a wharf, or some other fixed object, then the CAROGRP code was reset so that the incident would not be counted as a ship collision. Finally, when the CAROGRP code for an incident identified the incident as a ship collision, confirmation of that designation was sought by scanning CAROEAO event fields to confirm that the incident consisted of a collision by itself, a collision followed by a fire, some event other than a collision followed by a collision, or a collision followed by some event other than a fire or another collision (these electronic searches and the reading of incident text fields showed that 19 incidents designated as ship collisions were, in fact, not ship collisions).

4.1.3 Number of Collision and Fire Incidents

Searches of the 15 years of accident data showed that the data contained 1,947 collision events, 702 of which occurred in ports, and 2,547 fire events, 975 of which occurred in ports. Only 50 of the 1,947 collision events led to fires, 39 fires resulted from collisions at sea, and 11 from collisions in ports. None of the 2,547 fire events involved collisions.

4.2 Accident Locations

The 15 years of data contained latitude and longitude coordinates for 758 of the collision events and for 812 of the fire events that occurred outside of port waters. The coordinates of these collision and fire

events were located on maps in a recent atlas [3] and the shortest distance from that location to shore was measured and converted to miles. Figures 4-1 and 4-2 present histograms of the distance from shore of these 758 collision and 812 fire events. Figure 4-1 shows that 90 percent of these collision events occurred within 60 miles of a coast. Although fire events also decrease as distance from shore increases, comparison of Figure 4-2 to Figure 4-1 shows that fire events are less likely to occur near to the shore and that the decrease of fire events with increase of distance from shore is much less than that found for collision events (e.g., the distance within which 90 percent of the fire events occurred is 300 rather than 60 miles). Figures 4-3 and 4-4 present the number of fire events and collision events that occurred in each of the 527 Marsden squares that contain ocean waters. Inspection of Figures 4-3 and 4-4 shows that fire events are more widely dispersed than collision events (169 squares contain at least 1 fire event while only 109 squares contain at least 1 collision event; 32 squares contain at least 10 fire events while only 20 squares contain at least 10 collision events). Finally, Figures 4-5, 4-6, and 4-7 plot the locations of collisions in three coastal regions: (1) the Inland Sea of Japan, (2) the approaches to the port of New York, and (3) the English Channel plus the southern portion of the North Sea.

The weak dependence of fire incidents on distance from shore probably is caused by greater sailing time in coastal waters. In addition, many of the 1,572 fire events that occurred outside of port waters involved cruise ships, which usually sail mainly in coastal waters. Because fire events appear to have only a weak dependence on distance from shore and occur in one-third of the Marsden squares that contain ocean waters, it seems likely that the frequency of fire events at sea depends principally on the time spent underway (sailing time outside of port waters). In contrast to fire events, inspection of Figures 4-1 and 4-4 through 4-7 suggests that the occurrence of ship collisions is strongly dependent on location, being much more frequent where ship traffic is high (e.g., in the 20 Marsden squares that each contain at least 10 collision events).

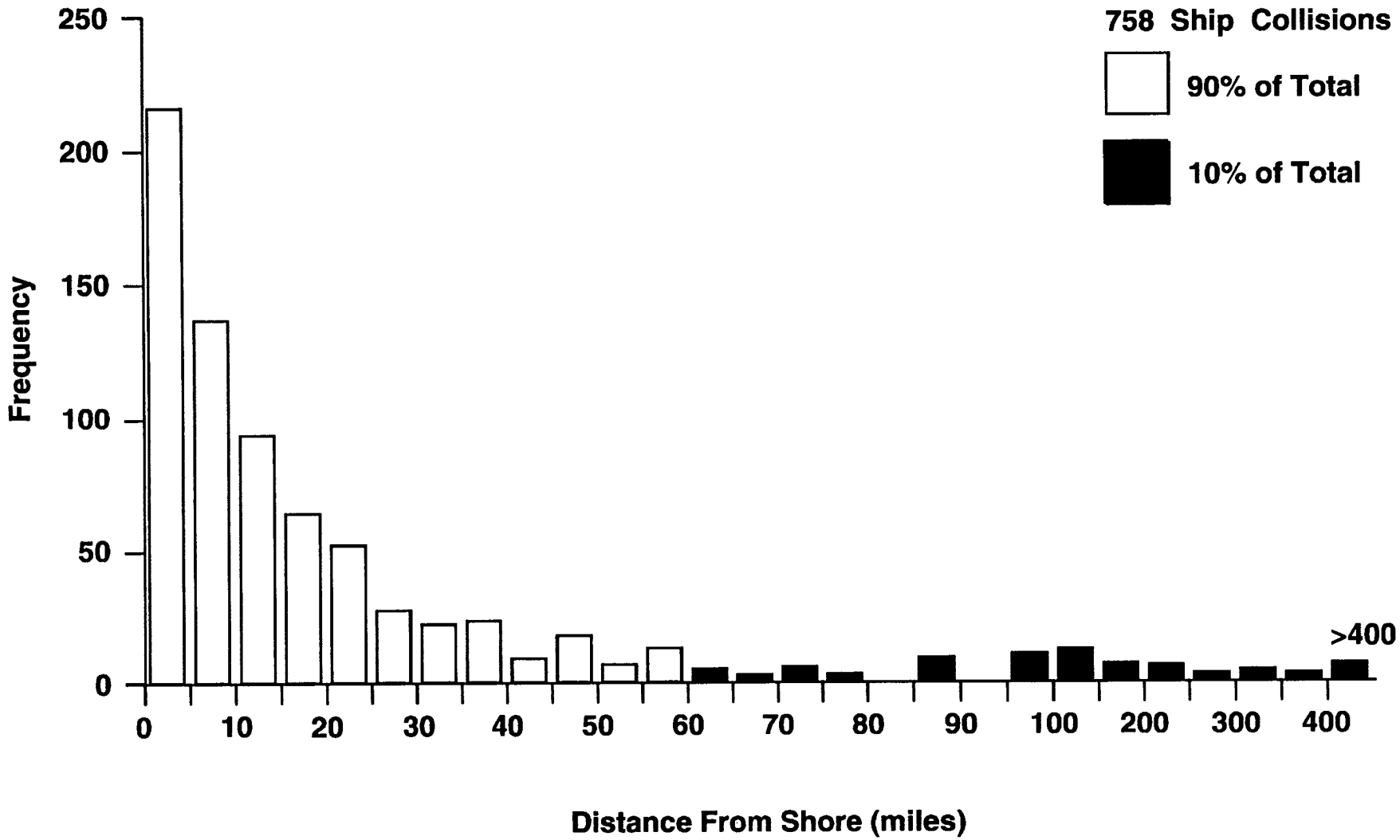

Figure 4-1. Histogram of Ship Collisions by Ranges of Distance From Shore for Ship Collisions That Occurred During the 15 Years From 1979 Through 1993.

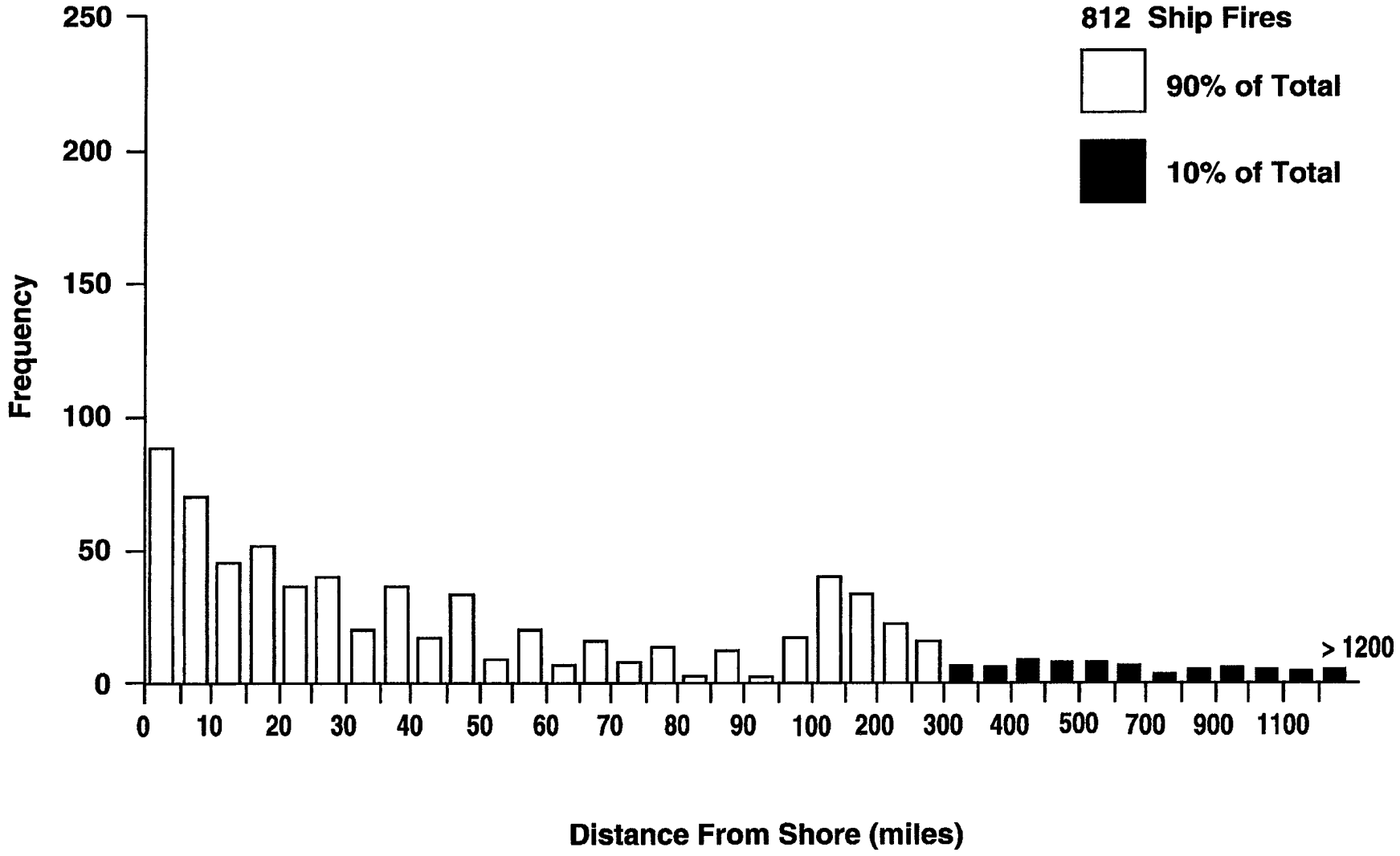

Figure 4-2. **Histogram of Ship Fires by Ranges of Distance From Shore for Ship Fires That Occurred During the 15 Years From 1979 Through 1993.**

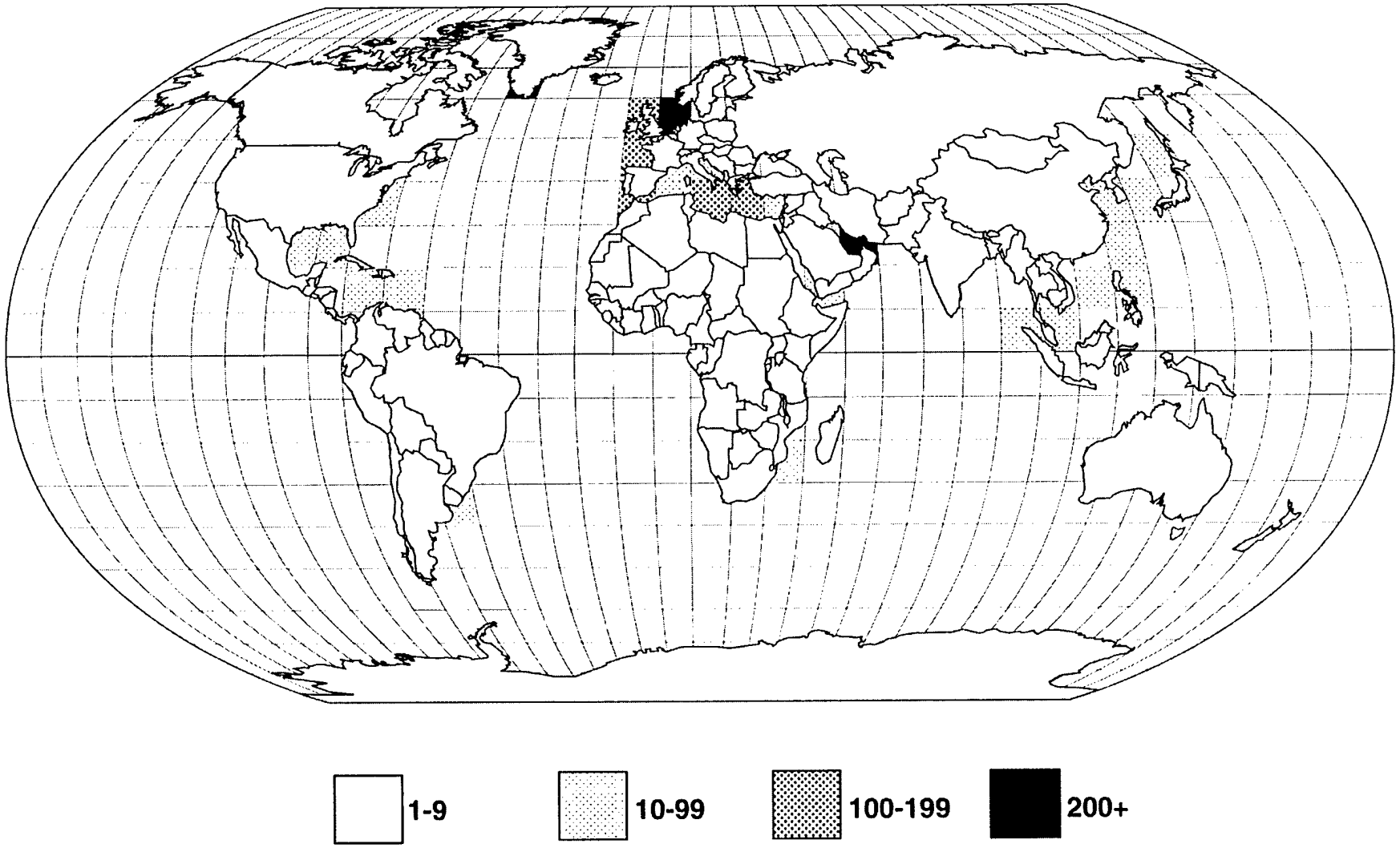

Figure 4-3. Number of Ship Fires That Occurred in the Indicated Marsden Squares for Ship Fires That Occurred During the 15 Years From 1979 Through 1993. (Marsden squares are regions on the surface of the earth bounded by meridians and parallels spaced at 10° intervals starting from the intersection of the prime meridian with the equator.)

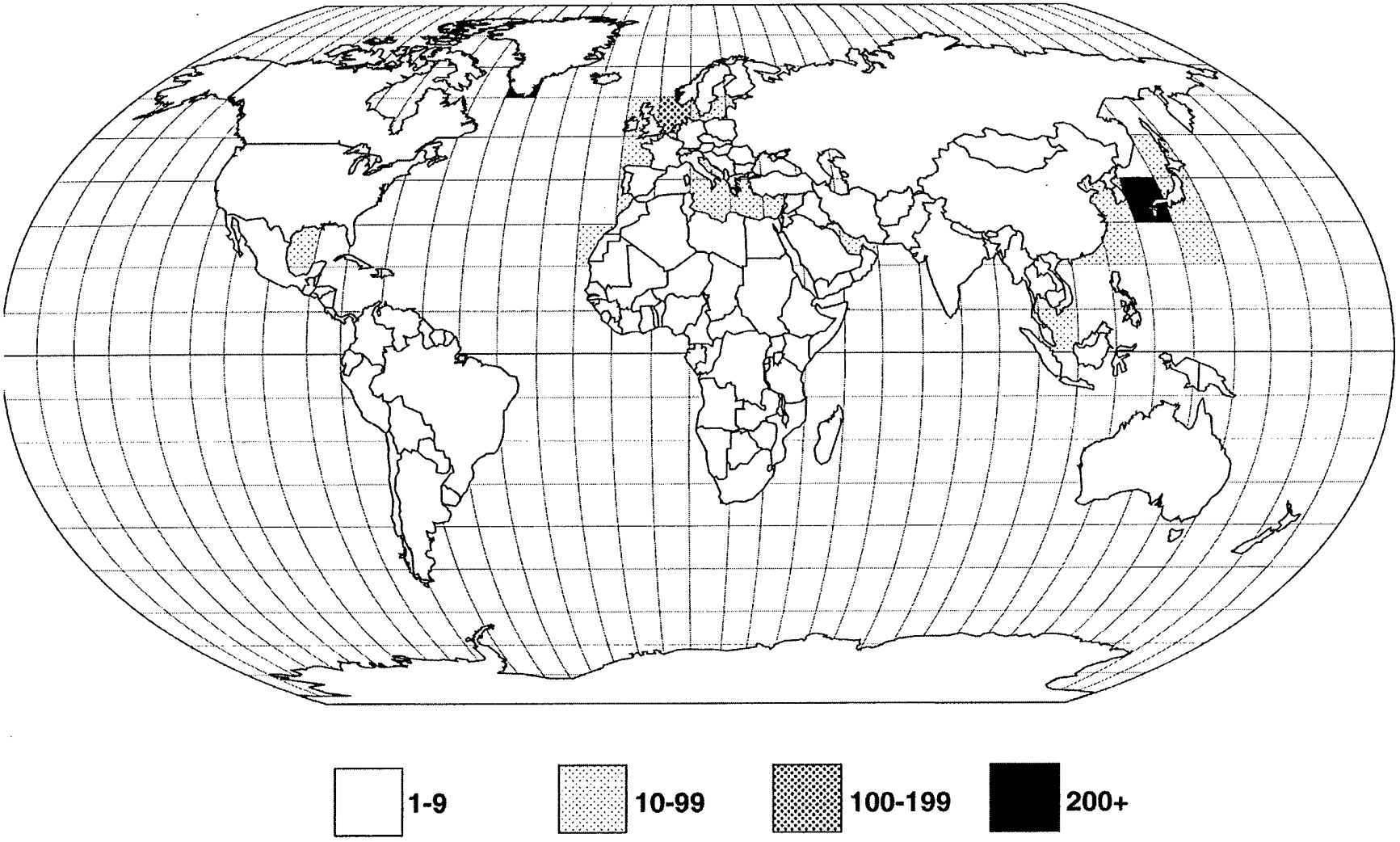

Figure 4-4. Number of Ship Collisions That Occurred in the Indicated Marsden Squares for Ship Collisions That Occurred During the 15 Years From 1979 Through 1993.

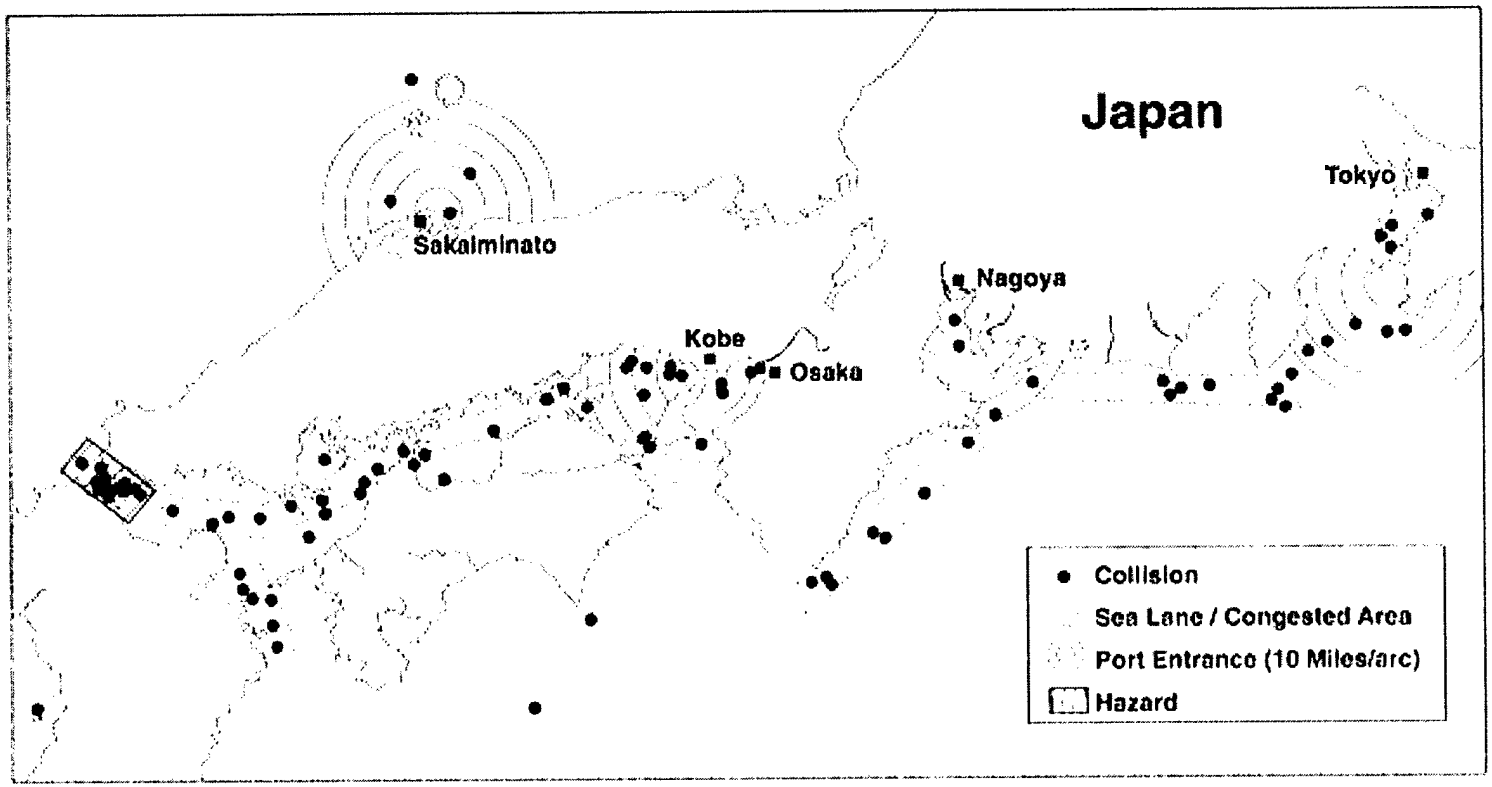

Figure 4-5. Locations of Ship Collisions in the Inland Sea of Japan for Collisions That Occurred During the Years 1979 Through 1993.

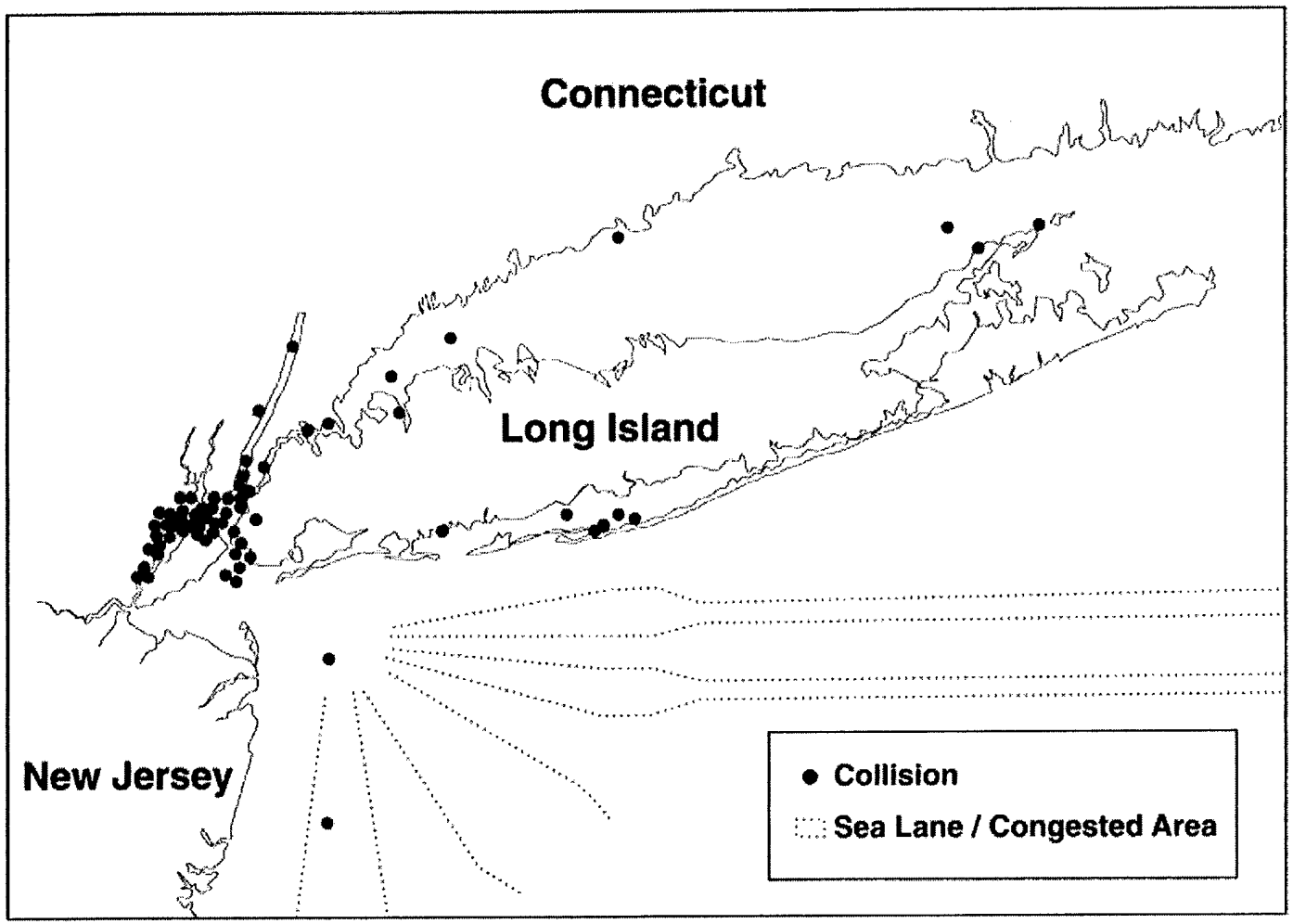

Figure 4-6. **Locations of Ship Collisions in the Approaches to the Port of New York for Collisions That Occurred During the Years 1979 Through 1993.**

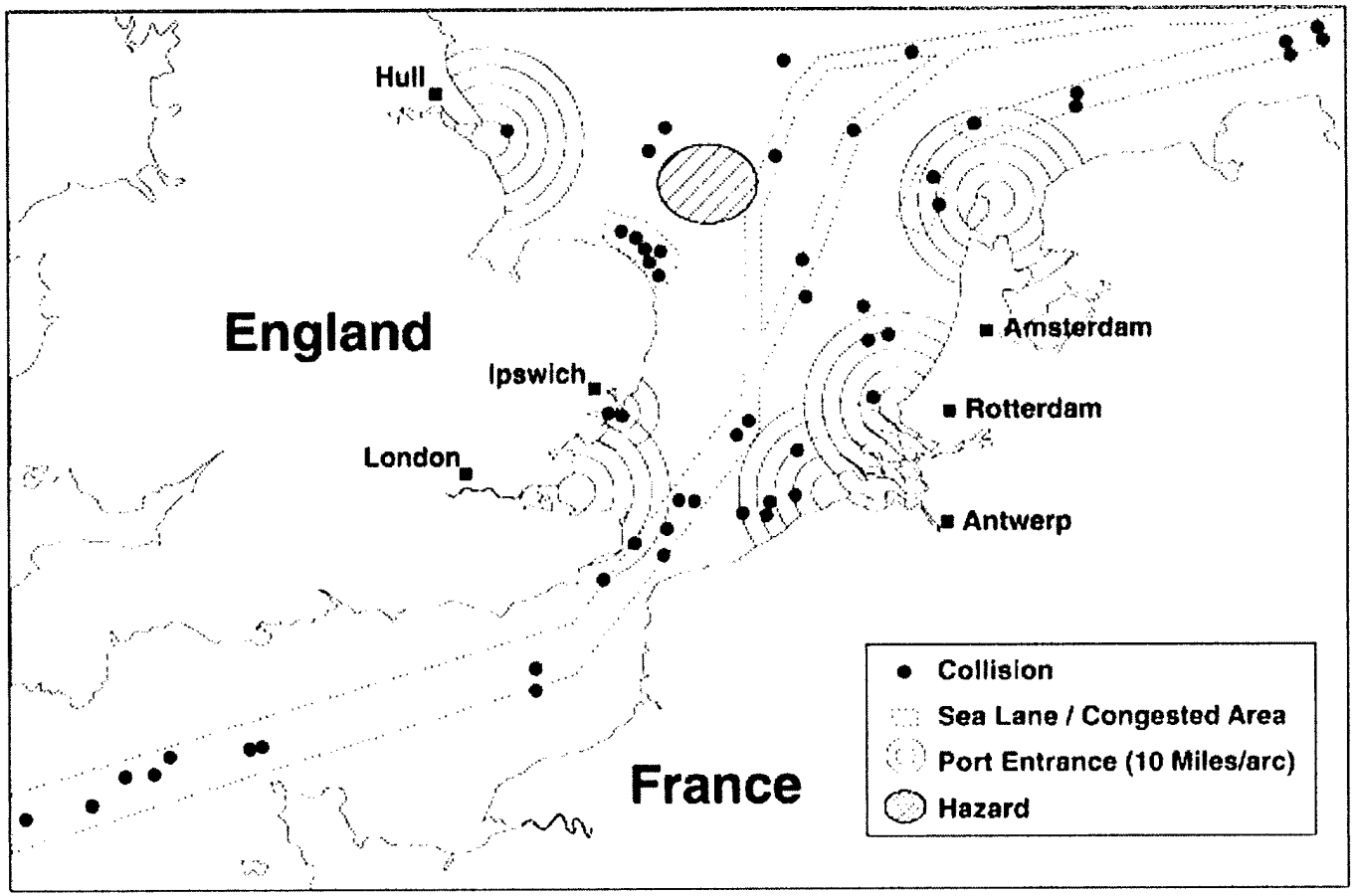

Figure 4-7. Locations of Ship Collisions in the English Channel and the Southern Portion of the North Sea for Collisions That Occurred During the Years 1979 Through 1993.

4.3 Congested Ocean Regions

We next attempted to quantify the qualitative conclusion that collision frequencies are location dependent, i.e., depend strongly on ship traffic densities in the regions sailed. To support this analysis, we divided the ocean surface into 21 regions, 19 congested regions that encompassed large parts of those Marsden squares that contained 10 or more ship collisions, and two catchall regions: all coastal waters (ocean waters ≤ 50 nautical miles from shore) not included in the 19 congested regions and the remaining ocean surface (i.e., the open oceans where a ship is sailing at sea). Table 4-2 presents the identities of the 19 congested regions for which we developed collision frequencies.

Table 4-2. Congested Ocean Regions

1.	Irish Sea	6.	Tyrrhenian Sea	11.	Persian Gulf, Gulf of Oman	16.	Sea of Japan, Korean Strait
2.	English Channel	7.	Adriatic Sea	12.	Approaches to Singapore	17.	Inland Sea of Japan
3.	North Sea	8.	Aegean Sea, Bosporus	13.	South China Sea, Taiwan Strait	18.	East Coast of Japan
4.	Baltic Sea	9.	Eastern Mediterranean	14.	East China Sea	19.	Western Gulf of Mexico
5.	Western Mediterranean	10.	Suez Canal, Red Sea, Gulf of Aden	15.	Yellow Sea		

Next, so that the number of nautical miles sailed per year in each of the 21 regions could be estimated, we purchased two non-contiguous years (1988 and 1993) of worldwide port call data from Lloyd's Maritime Information Services.

4.4 The Lloyd's Port Call Data

The two years of port call data was supplied in electronic form. Upon receipt, the data was converted into a relational (RDBMS) format. Searches then showed that the two years of port call data listed calls at 3,590 different ports, trips between almost 105,000 different pairs of ports (where a trip is a sailing from one port directly to another port without any intervening port calls), and 2,391,118 total trips.

4.4.1 Structure of the Port Call Data

Each year of Lloyd's Port Call Data consists of three tables titled, CLIENT_PLACE_MOVES, CLIENT_VESSELS, and CLIENT_PLACES. Each record in the CLIENT_PLACE_MOVES table describes a single port call by one vessel on a specific date. If the vessel made several calls to this port during the year, each call would be described in a separate record. Each record in the CLIENT_PLACE_MOVES table lists the unique identification numbers of the vessel (VESSEL_LLPNO field) and of the last port visited by the vessel (PREV_PLACE_IDNO field), the current port (PLACE_IDNO field), and the next port on the vessel's itinerary (NEXT_PLACE field). The vessel identification number is the vessel's Lloyd's Registry Number. Thus, the VESSEL_LLPNO number in the CLIENT_PLACE_MOVES table is the same as the CAROLRNO number in the Casualty File. The CLIENT_VESSELS table repeats most of the ship's particular fields that appear in the Casualty File,

including the vessel identification number (which here is entered into the LLPNO field), name (VSL_NAME field), deadweight tonnage (DWT field), and gross registered tonnage (GROSS_TONNAGE field). The CLIENT_PLACES table presents the name (PLACE_NAME field) and the geographic coordinates (LAT_DIR, LAT_DEGREES, LAT_MINUTES, LAT_SECONDS; LONG_DIR, LONG_DEGREES, LONG_MINUTES, LONG_SECONDS fields) of each port that appears in the CLIENT_PLACE_MOVES table. Coordinate fields in the CLIENT_PLACES table were empty for some ports. Occasionally, a place was a location (e.g., the North Atlantic) rather than a port.

4.4.2 Number of Trips Between Unique Pairs of Ports

Because ships don't always sail to the next port on their current itinerary, the number of trips sailed between unique port pairs was determined by counting the number of times a unique set of previous port (PREV_PLACE_IDNO field) and current port (PLACE_IDNO field) identification numbers appeared in the CLIENT_PLACE_MOVES tables for the years 1988 and 1993. Because trips sailed directly between a unique pair of ports can be sailed in either of two directions (e.g., London to Venice or Venice to London), for each unique pair of port identification numbers in the two years of port call data, a single ordering of the two identification numbers was selected, and whenever the reverse ordering was found, it was transposed. Counts of unique pairs of identification numbers then determined the number of sailings made during each year between each unique pair of ports, regardless of the direction the trip was sailed.

4.5 Region Sailing Distances

In order to calculate the number of nautical miles sailed in each ocean region per year, the sailing distance between each unique port pair had to be calculated and multiplied by the number of times this distance was sailed, and then this total distance had to be apportioned among those ocean regions exited, traversed, or entered when the route that connects each unique pair of ports is sailed. Apportionment of trip sailing distances among ocean regions required assigning each port that appeared in the two years of port call data to one of the 21 ocean regions, and then developing a way to estimate trip distances as none of the Lloyd's data files contained sailing distances.

4.5.1 Assignment of Ports to Regions

The two years of port call data lacked coordinates for many of the ports in the two data files. Coordinates for these ports were taken either from the port data in the Fairplay Encyclopaedia [4] or from a recent atlas [3]. Next, coordinates were specified for the vertices of irregular convex polygons that just encompassed the ocean waters of each of the 19 congested regions. The right hand rule for vectors [5] was now used to determine when the coordinates of a port fell within the boundaries of one of the 19 irregular convex polygons that each encompassed the ocean waters of one of the 19 congested regions (Addendum 4A presents the details of this analysis). Finally, all ports not assigned to a congested region by application of the right hand rule for vectors were assigned to the Coastal Waters region.

4.5.2 Trip Sailing Distances

Distance data for ocean voyages can be obtained from the Fairplay Encyclopaedia [4] and from Publication 151 of the U.S. Defense Mapping Agency [6]. Neither of these sources of distances between

ports can be automatically searched. As distances were needed for 105,000 different trips, a way to estimate trip distances had to be developed that could be implemented on a computer.

Initially, we tried to convert Publication 151 into an electronic format. To do this, we scanned the 200 pages in that publication into an electronic file and corrected by inspection the scanning errors and also the typos that were in the original document. Searches of the electronic form of Publication 151 then showed that for many ports the port name used in Publication 151 was not quite the same as the port name used in the Lloyd's port call data (e.g., Venezia in Publication 151 but Venice in the Lloyd's port call data, or Port Tampa in Publication 151 but just Tampa in Lloyd's). To permit trip distances in the electronic form of Publication 151 to be associated with port pairs in the Lloyd's port call data, wherever they differed, we substituted the Lloyd's port name for the Publication 151 port name for the same port. Finally, we counted the number of ports in Publication 151 and discovered that Publication 151 contains about 1,000 different ports while the Lloyd's port call data lists trips between about 3,500 different ports. Thus, for a very large number of port pairs, we either had no distance data (neither Publication 151 or the Fairplay Encyclopaedia contained the required distance) or the distance could only be obtained by a manual (Windows) search of the Fairplay Encyclopaedia. Because (1) many port names in the Lloyd's port call data could not be found in the Fairplay Encyclopaedia, (2) differences between port names in the Fairplay Encyclopaedia and port names in the Lloyd's data could not easily be identified and eliminated, and (3) even if they could have been eliminated, development of distances for a very large number of port pairs by manual searches of the Fairplay Encyclopaedia CD Rom was not practical, we were forced to develop our own method for calculating trip sailing distances.

4.5.2.1 TRIP DISTANCE ALGORITHM

The method selected was an extension of the distance algorithm used in Publication 151. Publication 151 defines 25 ocean junction points and specifies distances between these junction points and from ports to those junction points that lie nearest to the port. We defined the coordinates of an additional 24 junction points, all of which lie on the edges of the 19 congested regions identified in Table 4-2. Table 4-3 lists the coordinates of the 25 junction points taken from Publication 151 and the 24 additional junction points placed at the edges of congested regions. We then calculated the great circle distances from each of these additional junction points to all other nearby junction points, both those taken from Publication 151 and those chosen to define the edges of the 19 congested regions, and entered all of the distances between pairs of junction points into a lookup table. The method used to calculate great circle distances is described in Addendum 4B.

Trip distances were then calculated by a simple computer program as follows. For trips between ports in the same congested region or in coastal waters not separated by one of the 25 junction points defined in Publication 151, distances between the two ports were calculated as great circle distances. For all other trips, distances were calculated as the sum of the distances between the set of successive junction points (taken from the lookup table) that defined the minimum distance route from the departure port to the destination port, where the minimum distance route was identified using the Dijkstra shortest path algorithm [7], plus two additional great circle distances (the great circle distances from the departure port to the nearest junction point on the route and from the last junction point on the route to the destination port).

Figures 4-8 through 4-10 illustrate the strengths and weaknesses of the two methods used to calculate trip distances. Figures 4-8 and 4-9 show that great circle distances can significantly underestimate real sailing distances if the actual sailing route does not approximate a great circle route. Specifically, Figure 4-8 shows that the great circle distance from Rotterdam to Antwerp is 45 nautical miles and that

Table 4-3. Junction Points

No.	Identity	Latitude	Longitude
	Publication 151 Junction Points		
1	Bishop Rock, England	49°45' N	6°35' W
2	Cape Leeuwin, Australia	32°32' S	115°08' E
3	Cape of Good Hope, South Africa	34°22' S	18°23' E
4	Fastnet, Republic of Ireland	51°20' N	9°36' W
5	Grand Banks South	42°30' N	50°00' W
6	Honshu, Japan	35°00' N	140°30' E
7	Ile d'Ouessant, France	48°40' N	5°30' W
8	Inishtrahull, Republic of Ireland	55°25' N	7°30' W
9	Lombok Strait, Indonesia	8°50' S	115°43' E
10	Montreal, Canada	45°30' N	73°33' W
11	Nord-Ostee Kanal	54°22' N	10°09' E
12	Panama, Panama	8°53' N	79°31' W
13	Pentland Firth, Scotland	58°42' N	3°20' W
14	Port Said, Egypt	31°16' N	32°19' E
15	Punta Arenas, Chile	53°10' S	70°54' W
16	Singapore	1°16' N	103°50' E
17	Skagens Odde, Denmark	57°48' N	10°44' E
18	Strait of Gibraltar	35°57' N	5°45' W
19	Straits of Florida	24°25' N	83°00' W
20	Sunda Strait, Indonesia	6°04' S	105°50' E
21	Torres Strait, Australia	10°33' S	142°08' E
22	Tsugaru Kaikyo, Japan	41°30' N	140°40' E
23	Wetar Passage, Indonesia	8°19' S	127°27' E
24	Wilson Promontory, Australia	39°10' S	146°26' E
25	Yucatan Channel	21°50' N	85°03' W
	Additional Junction Points Located at Edges of Congested Regions		
26	Strait of Dover, Boundary between North Sea and English Channel	51°00' N	0°30' E
27	St. George's Channel, South Edge of Irish Sea	52°00' N	6°00' W
28	Eastern Edge of Alboran Sea, Eastern Edge of Western Mediterranean Region	37°00' N	0°00'
29	Northern Edge of Tyrrhenian Sea	43°00' N	10°00' E
30	Southwestern Edge of Tyrrhenian Sea	39°00' N	11°00' E
31	Southeastern Exit from Tyrrhenian Sea	37°30' N	16°00' E
32	Southern Edge of Adriatic Sea	40°00' N	19°00' E
33	Istanbul/Bosporus, Agean Sea/Bosporus Region	41°00' N	29°00' E
34	Western Edge of Sea of Crete, Agean Sea/Bosporus Region	36°00' N	23°00' E
35	Eastern Edge of Sea of Crete, Agean Sea/Bosporus Region	35°00' N	27°00' E
36	Western Edge of Eastern Mediterranean Region	33°00' N	30°00' E
37	Eastern Edge of Gulf of Aden, Suez Canal/Red Sea/Gulf of Aden Region	13°00' N	51°00' E
38	Eastern Edge of Gulf of Oman, Persian Gulf/Gulf of Oman Region	24°00' N	60°00' E
39	Northern Edge of Strait of Malacca, Approaches to Singapore Region	7°00' N	97°00' E
40	Northwestern Entrance to Java Sea, Approaches to Singapore Region	4°00' S	108°00' E
41	Southwestern Entrance to South China Sea, Approaches to Singapore Region	6°00' N	109°00' E
42	Eastern Edge of South China Sea/Strait of Taiwan Region	22°00' N	116°00' E
43	Northern Edge of Strait of Taiwan, South China Sea/Strait of Taiwan Region	26°00' N	121°00' E
44	Boundary between Yellow Sea and East China Sea	32°00' N	124°00' E
45	Eastern Edge of East China Sea	26°00' N	130°00' E
46	Korea Strait, Intersection of East China Sea, Sea of Japan/Korea Strait, and Inland Sea of Japan Regions	34°00' N	130°00' E
47	Southern Exit from Inland Sea of Japan	32°30' N	132°30' E
48	Eastern Exit from Inland Sea of Japan	33°00' N	135°00' E
49	Eastern Edge of Western Gulf of Mexico Region	24°00' N	87°00' W

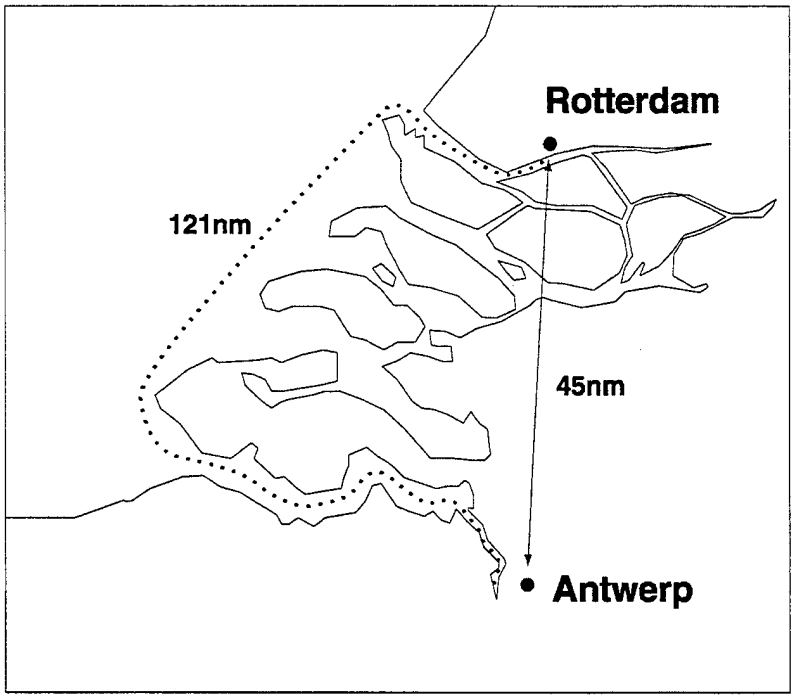

Figure 4-8. **Comparison of the Actual Sailing Distance (in Nautical Miles) From Rotterdam to Antwerp to the Great Circle Distance From Rotterdam to Antwerp.**

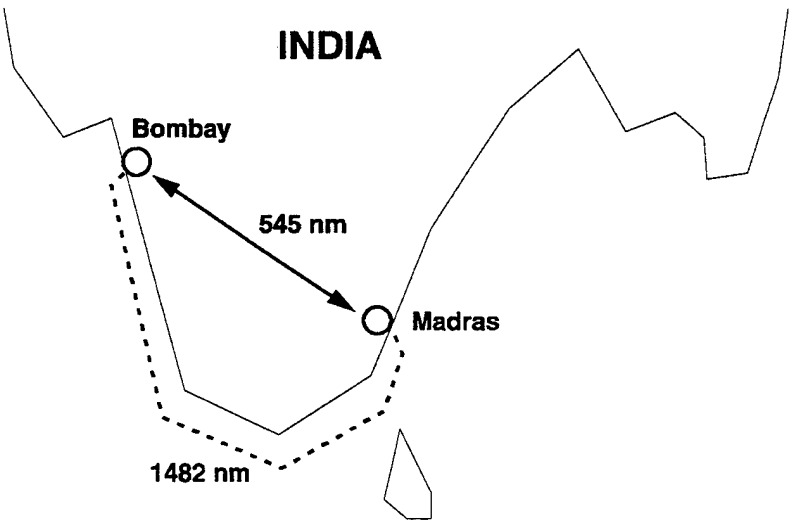

Figure 4-9. **Comparison of the Actual Sailing Distance (in Nautical Miles) From Bombay to Madras to the Great Circle Distance From Bombay to Madras.**

this distance is much smaller than the true sailing distance of 121 nautical miles because the true sailing route (down the Nieuwe Maas river to the North Sea, along the coast of the Netherlands to the Westerschelde and up the Westerschelde to Antwerp) deviates substantially from the great circle that connects the two ports. Figure 4-9 shows that the true sailing distance from Bombay to Madras around the horn of India is 1,482 nautical miles while the great circle distance across the horn is 545 nautical miles. Because great circle distances were used to approximate all trips between ports located in the same congested region, the use of great circle distances caused total sailing distances for many short trips sailed wholly in coastal waters or within a single congested region to be underestimated (on average by 10 to 30 percent).

Figure 4-10 shows how trip distances were calculated for routes that passed through one or more junction points. Figure 4-10 shows that the sailing distance for a trip from Rotterdam to Tunis was calculated as the sum of the two distances between the three junction points that define the sailing route (the junction points for the Ile d'Ouessant, the Strait of Gibraltar, and the eastern edge of the Western Mediterranean congested region) plus the great circle distances Rotterdam to the first junction point (the point at the Ile d'Ouessant) and from the last junction point (the point at the eastern edge of the Western Mediterranean congested region) to Tunis. The distance calculated by this method is 2,082 nautical miles which compares quite favorably to the sailing distance of 2,182 nautical miles given in Publication 151 [6]. Thus, for long trips that pass through several junction points, sailing distance is also underestimated (usually by 10 percent or less) because the great circle calculations can underestimate the sailing distances from the departure port to the nearest on-route junction point and from the last on-route junction point to the destination port.

The magnitude of this underestimate of sailing distances was investigated by comparing the distances calculated by our somewhat approximate methods to the sailing distances specified in the Fairplay Encyclopaedia for the set of the most sailed trips that accounted for 10 percent of the total distance sailed during the year 1988. The comparison showed that our approximate methods generally underestimated true sailing distances by less than 10 percent although occasionally by factors of as much as two.

4.5.2.2 APPORTIONMENT OF TRIP DISTANCES AMONG CONGESTED REGIONS

Placement of the additional 24 junction points at the edges of the 19 congested regions allowed trip distances to be apportioned between the congested regions, coastal waters, and the open ocean. Sailing distances in congested regions were calculated as great circle distances from a port in the region to a junction point at the edge of the region, when a trip began or ended in that region, or as the distance between two junction points located on the edges of the region, when the region was traversed. A sailing distance of 50 nautical miles was assigned to the coastal waters region whenever a departure or destination port was not located in one of the 19 congested regions. Finally, the balance of each trip sailing distance was assigned to the open ocean region.

Figures 4-11 through 4-17 illustrate how distance was apportioned to congested regions, coastal waters, and the open ocean (at sea). Figure 4-11 depicts a trip between a departure port and a destination port that are both located in the same region. For this case, all of the sailing distance is apportioned to the congested region in which the two ports are located. In addition, for some ports, a sailing distance of 50 nautical miles is also recorded as being sailed in the approach waters that surround the entrance to the port. This is done so that collision frequencies in the approach waters for these ports can be compared to the collision frequency of the region in which the port is located (see Section 4.7.3 below).

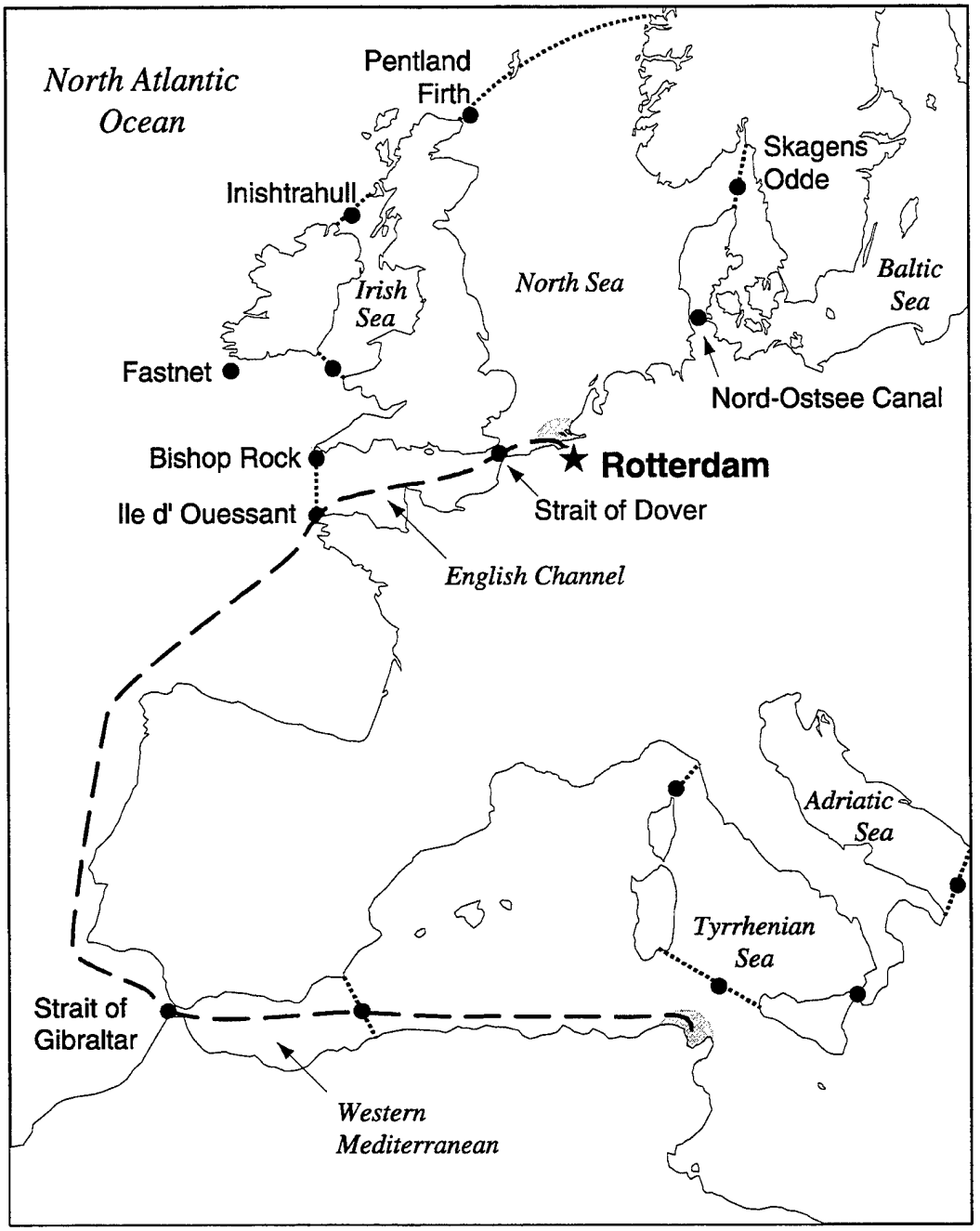

Figure 4-10. Sailing Route From Rotterdam to Tunis Showing the Congested Ocean Regions Traversed (North Sea, English Channel, and the Western Mediterranean) and the Four Junction Points (•) Passed When Sailing This Route (Strait of Dover, Ile d'Ouessant, Strait of Gibraltar, and the Eastern Edge of the Western Mediterranean Congested Region). Also shown are four congested regions (Baltic Sea, Irish Sea, Tyrrhenian Sea, and the Adriatic Sea) and eleven junction points (Nord-Ostee Canal, Skagens Odde, Pentland Firth, Inishtrahull, Fastnet, southern edge of the Irish Sea, Bishop Rock, three points on the edges of the Tyrrhenian Sea, and the southern edge of the Adriatic Sea) used in other distance calculations.

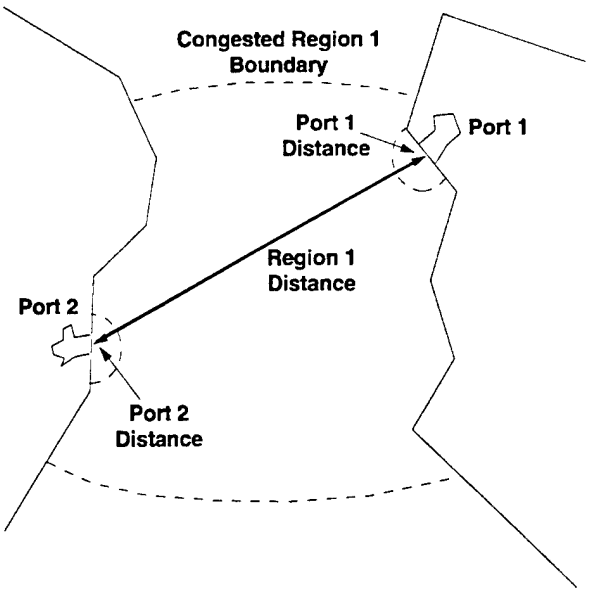

Figure 4-11. Trip Sailed Wholly Within a Single Congested Region.

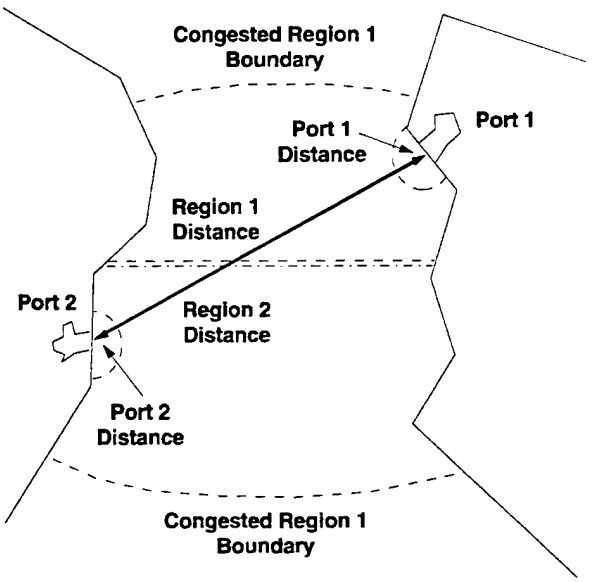

Figure 4-12. Trip Sailed Between Two Neighboring Congested Regions.

Figure 4-12 depicts a trip between departure and destination ports that are located in neighboring congested regions.

Because there is a junction point on the boundary that is shared by the two regions, the sailing distance in each region is separately calculated and then is assigned to the proper region. Again, the 50-nautical-mile sailing distance in port approach waters is recorded for some ports.

Figure 4-13 depicts a sailing route that crosses open ocean and then ends (or begins if the sailing direction is reversed) at a destination port located in a congested region. As there is a junction point where the route crosses into the congested region from the open ocean, the distance sailed in the region can again be calculated and assigned to the region that contains the destination port.

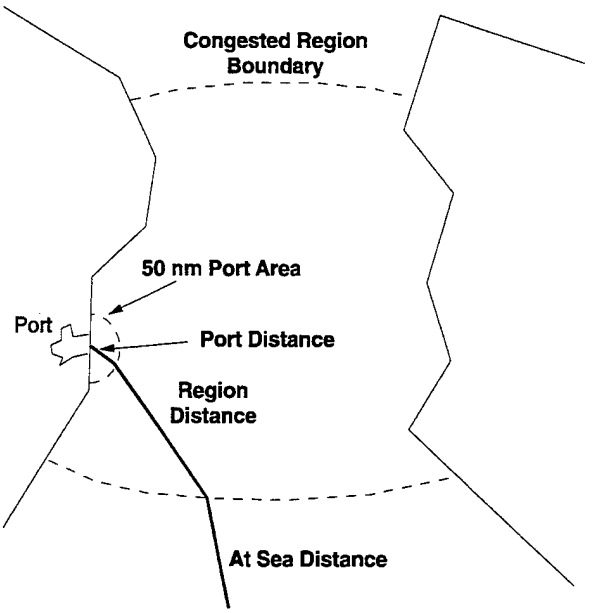

Figure 4-13. Trip that Ends (or Begins) in a Congested Region.

Figure 4-14 depicts a special case of a port located at the edge of a congested region. Here, the sailing distance to the region boundary may be less that 50 nautical miles, which means that if this port is one of the ports for which the frequency of collisions was calculated in the approach waters to the port, then the number of miles sailed in the port approach waters can be less than 50 nautical miles.

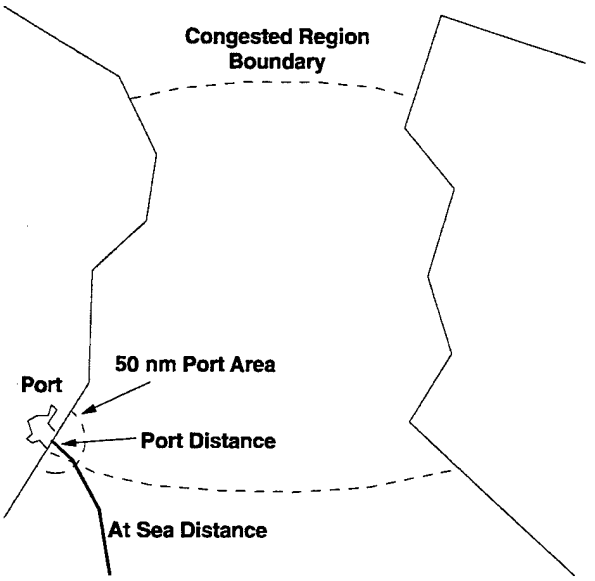

Figure 4-14. Port Located at the Edge of a Congested Region.

Figure 4-15 depicts a portion of a trip that passes through a congested region. As there is a junction point on each edge of the region, the distance between these two junction points is assigned to the congested region traversed by this trip sailing route.

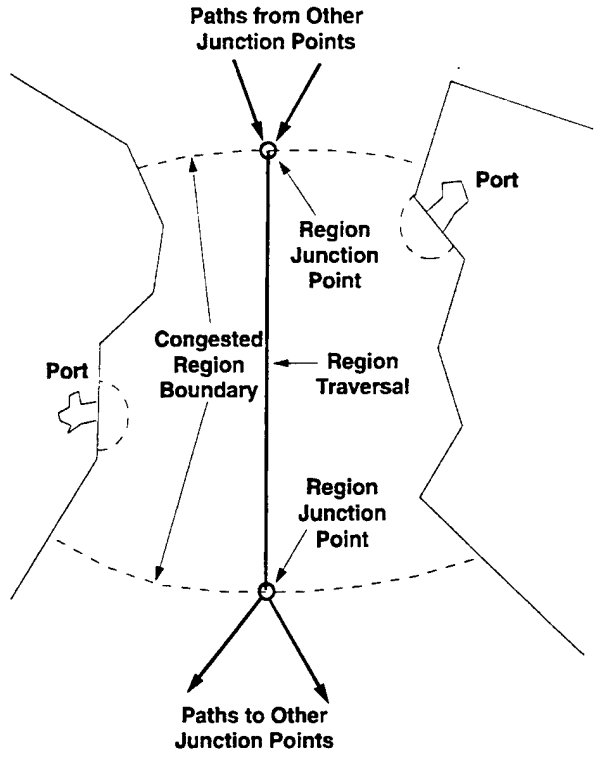

Figure 4-15. Trip That Passes Through a Congested Region.

Figure 4-16 depicts a trip that ends (or begins) at a port located in coastal waters. Because coastal waters are assumed to extend outward from shore for a distance of 50 nautical miles, when this trip distance is calculated, 50 nautical miles are automatically assigned to the coastal waters catchall region.

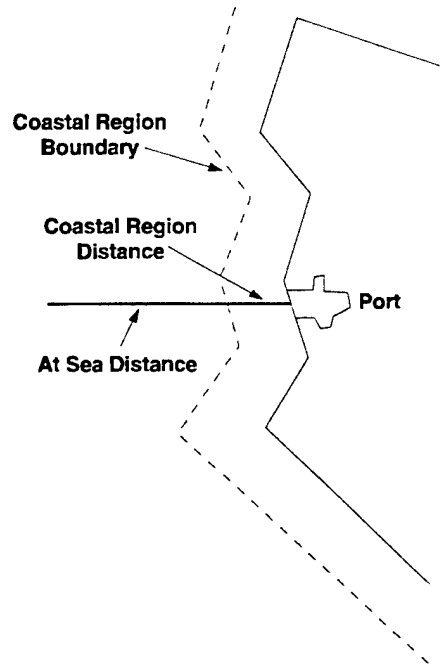

Figure 4-16. Trip That Ends at a Port Located in Coastal Waters.

Figure 4-17 depicts a trip sailed between two neighboring ports that both lie in coastal waters. Here the sailing distance between the ports is less than 100 nautical miles. Thus, the distance assigned to coastal waters is the actual sailing distance and, if collision frequencies are being calculated for the approach waters that lead to both ports, then the distance sailed in the approach waters of each port is half of the sailing distance between the two ports.

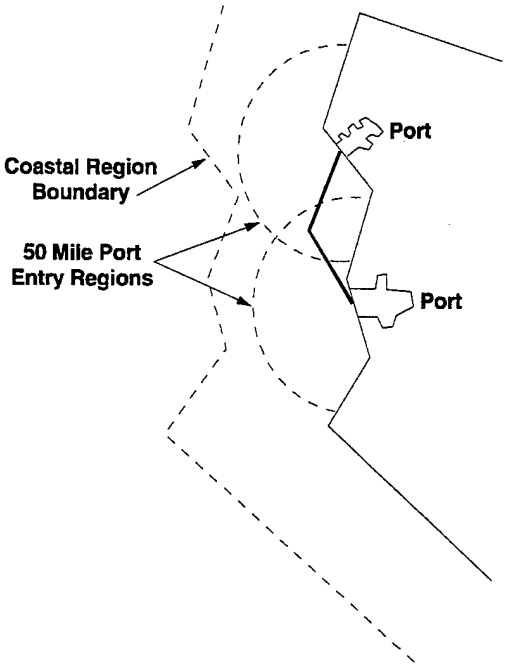

Figure 4-17. Trip Between Two Neighboring Ports Both Located in Coastal Waters.

Finally, for lengthy trips sailed down a coast, no attempt was made to decide whether more than 100 nautical miles was sailed in coastal waters. Instead, we assumed that the ship would be outside of coastal waters (more than 50 nautical miles offshore) as it sailed down the coast, and thus the total trip distance minus 100 nautical miles was assigned to the at sea (open ocean) catchall region.

4.6 Assignment of Ship Collisions to Regions

The number of ship collisions that occurred in each of the 19 congested regions, in coastal waters, in the open oceans, and in individual ports and port approach waters were determined by manual inspection of the text fields in the Lloyd's accident data that described each accident. Region assignments were straightforward when the text field contained accident coordinates. When coordinates were lacking, some combination of descriptive text that specified the identities of cities, geographic features (e.g., bays, islands), or structures (e.g., lighthouses) located near the accident site, and/or the identity of the Marsden square in which the accident occurred almost always allowed the accident to be assigned to one of the 19 congested regions, to coastal waters, to open ocean, or to a port or port approach waters. To assure that accidents were properly assigned to regions, ports, or port approach waters, all accident text fields were read by two different individuals and differences as to assignment were resolved by discussion. In fact, these procedures allowed all but eight of the 1,947 collisions to be assigned to a region, a port, or port approach waters. For these few cases, accident coordinates were not specified, the Marsden square (if specified) encompassed portions of at least two regions, and/or the description of the accident location in the text field was vague (e.g., off of Russia).

4.7 Sailing Distances, Number of Collisions, and Ship Collision Frequencies

Methods for assigning ship collisions to regions, ports, and port approach waters, and for estimating the number of nautical miles sailed in regions and port approach waters have now been described. The results obtained by applying these methods to the data in the Lloyd's Casualty File and port call data files are now presented.

4.7.1 Region Sailing Distances, Collisions, and Collision Frequencies

Table 4-4 presents the following data: (a) the distances sailed (d1988 and d1993) in each of the 21 ocean regions during the years 1988 and 1993, (b) the average of these two distances, (c) the number (N) of ship collisions that occurred in each region during the 15-year period from 1979 through 1993, and (d) the collision frequency per nautical mile sailed (F) in each region, where

$$F = [N/15]/[(d1988 + d1993)/2]$$

The calculation of F using this equation implicitly assumes that the port call data for the years 1988 and 1993 is not unlike the port call data for other years in the 15-year period from 1979 through 1993.

4.7.2 Port Collisions and Collision Frequencies

In order to examine the influence of port traffic on port collision frequencies, ports in the two years of Lloyd's port call data was divided into three groups: high traffic ports (13 ports), medium traffic ports (78 ports), and low traffic ports (3,499 ports). The division was based on the number of port calls to each port during the year 1988. During 1988, Singapore with 27,129 port calls was the world's busiest port. Somewhat arbitrarily, high traffic ports were then taken to be any port with more than 8,900 port calls during 1988 because 8,900 port calls per year is about one port call per hour; medium traffic ports, any port with 2,700 to 8,900 port calls during 1988; and low traffic ports, all ports with fewer than 2,700 port calls during 1988. Collision frequencies per port call were then calculated individually for all 13 high traffic ports and for 6 medium traffic ports, and calculated collectively for all high, all medium, and all low traffic ports. Table 4-5 presents these port collision frequencies.

4.7.3 Port Approach Water Sailing Distances, Collisions, and Collision Frequencies

Because Figures 4-5, 4-6, and 4-7 suggested that ship collisions often occur in port approach waters, we calculated collision frequencies in approach waters for 12 high traffic (not 13 because Europort and Rotterdam share the same approach waters) and 6 medium traffic ports. We did this by dividing the number of collisions that occurred each year within a radial distance of 50 miles of the entrance to the port by the number of nautical miles sailed during 1988 in the approach waters to the port. Table 4-6 presents the resulting collision frequencies in port approach waters for the 18 ports examined. At most ports, approach water mileage is less than the number of port calls at the port times 100 miles for two reasons. First, when a port is located within 50 miles of a region boundary, the distance to the boundary and not 50 miles was taken to be the distance sailed in approach waters; and second, distances less than 50 miles also occurred for short trips sailed entirely within approach waters.

Table 4-4. Distances Sailed, Ship Collisions, and Collision Frequencies for 21 Ocean Regions

Region	Distance Sailed (nautical miles)			Collisions 1979-1993	Collision Frequency (per nautical mile sailed)
	1988	1993	Average		
Irish Sea	2,829,048	2,683,242	2,756,145	7	1.7×10^{-7}
English Channel	21,879,012	20,497,594	21,188,303	33	1.0×10^{-7}
North Sea	48,945,873	46,676,760	47,811,317	134	1.9×10^{-7}
Baltic Sea	26,150,331	30,410,544	28,280,438	76	1.8×10^{-7}
Western Mediterranean	12,527,256	12,508,332	12,517,794	29	1.5×10^{-7}
Tyrrhenian Sea	4,713,083	5,163,556	4,938,320	8	1.1×10^{-7}
Adriatic Sea	8,847,482	9,216,251	9,031,867	11	8.1×10^{-8}
Agean Sea, Bosporus	6,979,278	7,521,944	7,250,611	59	5.4×10^{-7}
Eastern Mediterranean	9,717,480	11,511,423	10,614,452	21	1.3×10^{-7}
Suez Canal, Red Sea, Gulf of Aden	30,562,346	30,397,942	30,480,144	17	3.7×10^{-8}
Persian Gulf, Gulf of	6,123,288	9,272,603	7,697,946	17	1.5×10^{-7}
Approaches to	30,056,459	43,928,308	36,992,384	41	7.4×10^{-8}
South China Sea, Taiwan Strait	16,959,614	24,003,990	20,481,802	42	1.4×10^{-7}
East China Sea	24,138,006	32,718,462	28,428,234	34	8.0×10^{-8}
Yellow Sea	7,483,030	10,559,045	9,021,038	13	9.6×10^{-8}
Sea of Japan, Korean	6,223,109	7,748,095	6,985,602	35	3.3×10^{-7}
Inland Sea of Japan	12,440,950	14,106,520	13,273,735	193	9.7×10^{-7}
East Coast of Japan	4,169,250	4,497,723	4,333,487	120	1.9×10^{-6}
Western Gulf of Mexico	12,907,874	14,124,048	13,515,961	24	1.2×10^{-7}
Coastal Waters	80,737,497	97,489,242	89,113,370	253	1.9×10^{-7}

Table 4-5. Port Calls (1988) and Port Collision Frequencies (per port call)

Port	Port Collisions[1] (1979-1993)	Port Calls (1988)	Collision Frequency (per port call)
High Traffic Ports			
Antwerp	10	16,585	4.0×10^{-5}
Europort	2	9,772	1.4×10^{-5}
Gibraltar	1	13,991	4.8×10^{-6}
Hamburg	8	14,645	3.6×10^{-5}
Hong-Kong	7	14,216	3.3×10^{-5}
Istanbul	3	24,926	8.0×10^{-6}
Kobe	7	9,133	5.1×10^{-5}
Panama Canal	2	11,058	1.2×10^{-5}
Port Said	13	8,936	9.7×10^{-5}
Rotterdam	11	26,153	2.8×10^{-5}
Singapore	18	27,129	4.4×10^{-5}
Suez	3	9,742	2.1×10^{-5}
Yokohama	8	13,323	4.0×10^{-5}
All High Traffic	**93**	**199,609**	$\mathbf{3.1 \times 10^{-5}}$
Medium Traffic Ports			
Bangkok	2	3,889	3.4×10^{-5}
Barcelona	2	5,743	2.3×10^{-5}
Lisbon	2	3,984	3.4×10^{-5}
Los Angeles	0	6,587	0
Marseilles	2	4,238	3.2×10^{-5}
New York	12	5,144	1.6×10^{-4}
All Medium Traffic	**174**	**254,121**	$\mathbf{4.6 \times 10^{-5}}$
Low Traffic Ports			
All Low Traffic	**422**	**656,989**	$\mathbf{4.3 \times 10^{-5}}$

[1] Thirteen port collisions occurred in ports that did not appear in the two years of port call data.

Table 4-6. Collision Frequencies (per nautical mile sailed) in Port Approach Waters

Port	Approach Water Collisions (1979-1993)	Nautical Miles Sailed During 1988 in Port Approach Waters	Collision Frequency (per nautical mile sailed)
High Traffic Ports			
Antwerp	36	1,470,210	1.6×10^{-6}
Europort Rotterdam	13	738,293 2,173,195	3.0×10^{-7}
Gibraltar	16	975,902	1.1×10^{-6}
Hamburg	15	1,333,672	7.5×10^{-7}
Hong-Kong	18	1,334,660	9.0×10^{-7}
Istanbul	27	1,147,188	1.6×10^{-6}
Kobe	69	818,018	5.6×10^{-6}
Panama Canal	0	844,383	0
Port Said	7	455,898	1.0×10^{-6}
Singapore	19	2,396,264	5.3×10^{-7}
Suez	4	942,406	2.8×10^{-7}
Yokohama	30	1,015,232	2.0×10^{-6}
Medium Traffic Ports			
Bangkok	7	354,836	1.3×10^{-6}
Barcelona	0	546,995	0
Lisbon	2	365,270	3.7×10^{-7}
Los Angeles	0	636,501	0
Marseilles	2	402,842	3.3×10^{-7}
New York	0	494,651	0

4.7.4 LNG and LPG Tanker Sailing Distances and Collision Frequencies

No attempt was made during the general analysis of ship collisions to examine the possible dependence of collision frequencies on ship type or the degree of experience of the ship crew. Because many highly radioactive cargoes are shipped in purpose-built ships that have double hulls and unusually well-qualified crews, we determined the frequency of ship collisions per nautical mile sailed for one class of double-hulled ships, Liquefied Natural Gas (LNG) and Liquefied Propane Gas (LPG) tankers, that is usually sailed by experienced crews. As this type of ship is one of the ship types called out in Lloyd's databases, we could calculate the number of miles sailed by these tankers during the years 1988 and 1993 and the number of collisions that involved tankers during the period 1979 through 1993. Table 4-7 presents these results. For purposes of comparison, Table 4-7 also presents the same data for all ships. Inspection of Table 4-7 shows that the collision frequency per nautical mile sailed experienced by the general fleet is respectively about two times and five times larger than the collision frequencies per nautical mile sailed experienced by LPG and LNG tankers. Thus, one might expect collision frequencies per nautical mile sailed for purpose-built ships also to be at least two to five times lower than the collision frequency of the general fleet.

Table 4-7. Sailing Distances, Collisions, and Collision Frequencies for LNG and LPG Tankers

Tanker	Distance Sailed (nautical miles)			Collisions 1979-1993	Collision Frequency (per Nautical mile Sailed)
	1988	1993	Total		
LNG	4,080,851	5,439,253	9,520,104	1	1.4×10^{-8}
LPG	23,367,726	29,189,792	52,557,518	16	4.1×10^{-8}
All Ships	1,030,266,200	1,144,634,277	2,174,900,488	1,237	7.6×10^{-8}

4.8 Fire Frequencies

Because ship fires show little variation with ocean location and occur often only in Marsden squares that contain major oil fields (the North Sea and the Persian Gulf), we believe that fire frequencies need not be developed independently for each ocean region or for individual ports. Therefore, we calculated a fire frequency per nautical mile sailed and per port call. The fire frequency per nautical mile sailed is

$$\frac{1{,}572 \text{ nonport fires}/15 \text{ years}}{2{,}174{,}900{,}488 \text{ nautical miles sailed}/2 \text{ years}} = 9.6 \times 10^{-8} \text{ fires per nautical mile sailed}$$

and the fire frequency per port call is

$$\frac{975 \text{ port fires}/15 \text{ years}}{2{,}391{,}118 \text{ port calls}/2 \text{ years}} = 5.4 \times 10^{-5} \text{ fires per port call}$$

4.9 Discussion

Comparison of the collision frequencies presented in Table 4-6 for port approach waters to the collision frequencies presented in Table 4-4 for the region that contains each port shows that collision frequencies for port approach waters have values that are often significantly larger than the value for the region in which the port is located. Comparison of collision frequencies for port approach waters for ports located in coastal waters to the collision frequency for sailing in coastal waters shows that this relation is also true for ports located in coastal waters. Thus, because ship traffic densities are higher in port approach waters than in the region that contains the port being approached, values of collision frequencies in approach waters are also larger than the values observed for the ocean region that contains those approach waters. Inspection of the port collision frequencies presented in Table 4-5 shows that collision frequencies per port call are about the same for high, medium, and low traffic ports, possibly because ships are sailed more carefully or sailing is more carefully controlled in busier ports than in less busy ports.

Because a port call consists of a port entry and a port departure, a voyage that includes stops at two intermediate ports makes 3, not 4, port calls (sailing out of the departure port and into the destination port together constitute only one port call). Accordingly, because the probabilities presented in Tables 4-4 and 4-5 are all small, the probability of a ship collision during a voyage may be estimated for any sailing route as follows:

$$P_{SC,V} = 0.5 \quad P_{SC,Dep\,P} + \sum_i P_{SC,R_i} N_i + \sum_j P_{SC,P_j} + 0.5 \quad P_{SC,Des\,P}$$

where $P_{SC,V}$ is the probability that a ship collision occurs during the voyage, $P_{SC,Dep\,P}$ is the probability that a collision occurs during a full transit of the departure port, P_{SC,R_i} is the probability that a collision occurs while sailing a nautical mile in Region i, N_i is the number of nautical miles sailed in Region i, P_{SC,P_j} is the probability that a collision occurs during the transit of intermediate Port j, and $P_{SC,Dep\,P}$ is the probability that a collision occurs during a full transit of the destination port.

4.10 References

1. *Casualty File Manual.* Lloyd's Maritime Information Services, London, England, November 1991.

2. *Glossary of the Mapping Sciences.* American Society of Civil Engineers, New York, NY, 1994.

3. *Atlas of the World,* Revised Sixth Edition. National Geographic Society, Washington, DC, 1992.

4. *World Shipping Encyclopaedia.* Fairplay Publications Limited, Coulsdon, England, July 1995.

5. M. S. Milgram, "Does a Point Lie Inside a Polygon?," in *J. Comp. Phys.*, vol. 84, pp. 134–144, 1989.

6. *Distances Between Ports,* Publication 151, Seventh Edition. Defense Mapping Agency Hydrographic/Topographic Center, Bethesda, MD, 1993.

7. E. W. Dijkstra, "A Note on Two Problems in Connection with Graphs," in *Numerische Math.*, vol. 1, pp. 269–271, 1959.

4.11 Addenda

4.11.1 Addendum 4A. Assignment of Ports to Congested Regions Using the Right-Hand Rule for Vectors

Given that there are over 5,000 entries in the CLIENT_PLACES table defining the various ports in the Lloyd's ship movement database, a mechanical means had to be devised to assign the ports to one of the 21 regions defined for analysis. The CLIENT_PLACES table gives the location of each port by its latitude and longitude. Thus, port locations p are specified as

$$p = (\text{latitude, longitude})$$

where latitude and longitude are each a standard geographic coordinate

longitude = (long-hemisphere, degrees, minutes)
latitude = (lat-hemisphere, degrees, minutes)
long-hemisphere = North or South
lat-hemisphere = East or West

The specification of port locations by a latitude and a longitude is inconvenient for analytical purposes. The solution to this problem was to reencode the port locations as a vector

$$\hat{r} = (x, y, z)$$

where Figure 4-18 depicts the relations between the vector r and the point (x, y, z).

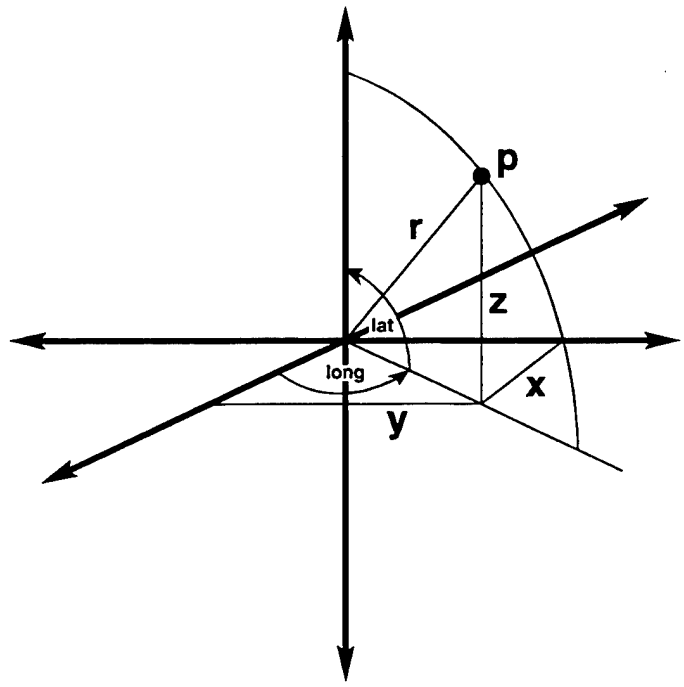

Figure 4-18. Coordinates of the Port Location p.

The coordinates of the vector r can be rationalized by applying the transformation

rational longitude = δ_o[longitude(hemisphere)] × [longitude(degrees)+longitude(minutes)/60]
rational latitude = δ_a [latitude(hemisphere)] × [latitude(degrees)+latitude(minutes)/60]

where

$$\delta_o = \begin{cases} 1, \text{if latitude (hemisphere)} = \text{North} \\ -1, \text{if latitude (hemisphere)} = \text{South} \end{cases}$$

$$\delta_\alpha = \begin{cases} 1, \text{if longitude (hemisphere)} = \text{East} \\ -1, \text{if longitude (hemisphere)} = \text{West} \end{cases}$$

and

$x = r \times cos\ (lat) \times cos\ (long)$
$y = r \times cos\ (lat) \times sin\ (long)$
$z = r \times sin\ (lat)$

Figures 4-19a and 4-19b depict the vector cross product and right-hand rule for vector cross products.

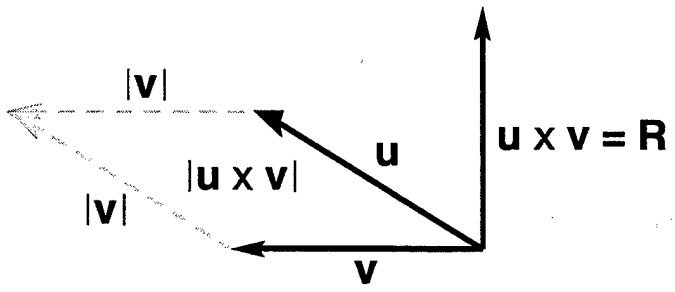

Figure 4-19a. Vector Cross Product.

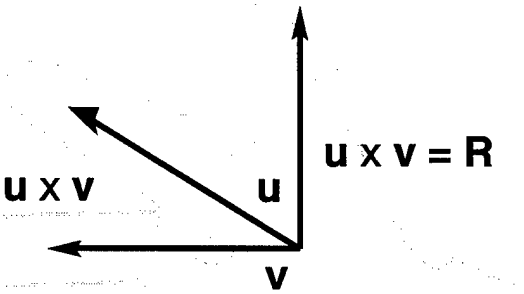

Figure 4-19b. Right-Hand Rule for Vector Cross Products.

We will take advantage of a property of the vector cross product. Specifically, the cross product will always be positive if the second vector in the product lies to the left of the first vector (i.e., the cross product vector will be perpendicular to the plane that contains the two vectors that enter the product and it will be directed upward). This is referred to as "the right-hand rule" because, as is shown above, when the index and middle fingers of a right hand are aligned respectively with the first and second vectors in a vector product and the thumb of the hand is extended, if the second vector lies to the left of the first vector, then the thumb will be pointing upwards and will be aligned with the cross product vector. Conversely, if the second vector lies to the right of the first vector, which causes the vector cross product to have a negative sign, then aligning the index and middle fingers as before will cause the extended thumb to point downwards, i.e., in the negative direction.

We will now describe how to take advantage of the right-hand rule to determine whether a point lies within a convex polygon. Consider an irregular convex polygon with five vertices labeled b_0 to b_{n-1}. As is shown in Figure 4-20, let p be a point that lies inside of the irregular convex polygon.

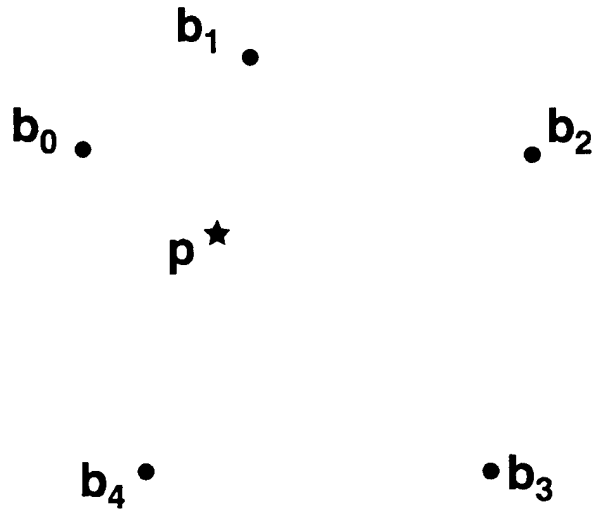

Figure 4-20. Vertices of a Convex Polygon That Contains the Point p.

The boundary of this irregular convex polygon is defined by computing the set of vectors

$$\bigcup_{i=0}^{n-1} b_{(i+1) \bmod n} - b_i$$

This is shown in Figure 4-21.

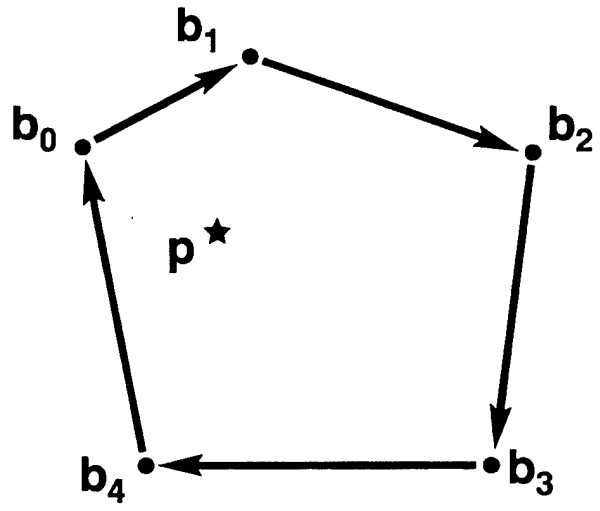

Figure 4-21. Set of Vectors That Bound the Complex Polygon Defined by the Vertices b_0....b_4.

Next, the set of vectors connecting each of the vertices of the convex irregular polygon to the point to be tested is computed

$$\bigcup_{i=1}^{n-1} p - b_i$$

This generates the dashed vectors shown in Figure 4-22 that connect the vertices of the convex polygon to the point p.

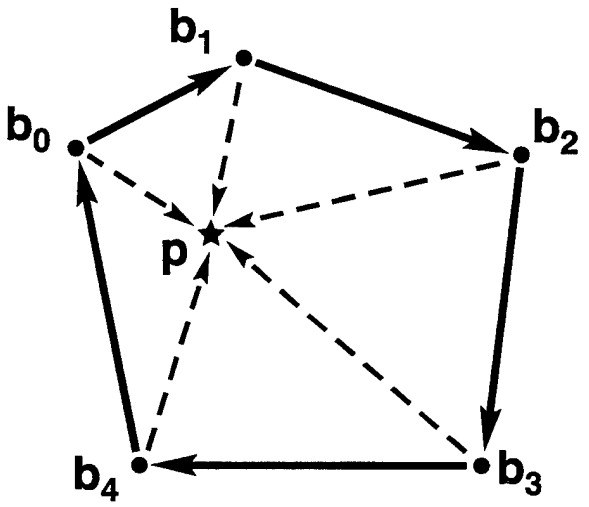

Figure 4-22. Convex Polygon With Vectors From Polygon Vertices to the Point to be Tested, Point p.

Now, the point p can be tested. The computation consists of testing the signs of the cross products $(b_i, b_{i+1}) \times (b_i, p)$ while moving in a clock-wise direction around the boundary of the irregular convex polygon. Mathematically, this is represented as

$$In(\{p_i\}, n) = \sum_{i=1}^{n-1} \delta \qquad [(p - b_i) \times (b_{(i+) \bmod n} - b_i)]$$

where

$$\delta(x) = \begin{cases} 1, x \geq 0 \\ 0, x < 0 \end{cases}$$

Thus the function *In*(...) returns the value n if the point p is inside the irregular convex polygon, and a value smaller than n (usually n-1) if the point lies outside the polygon. This formulation of the test includes points that are on the boundary as inside the polygon. To exclude the points on the boundary, the function d should be defined to return 0 if the value x is 0. When the point p lies inside of the polygon, all of the vector cross products will have the same sign and thus they will all point in the same direction. This case is depicted in Figure 4-23.

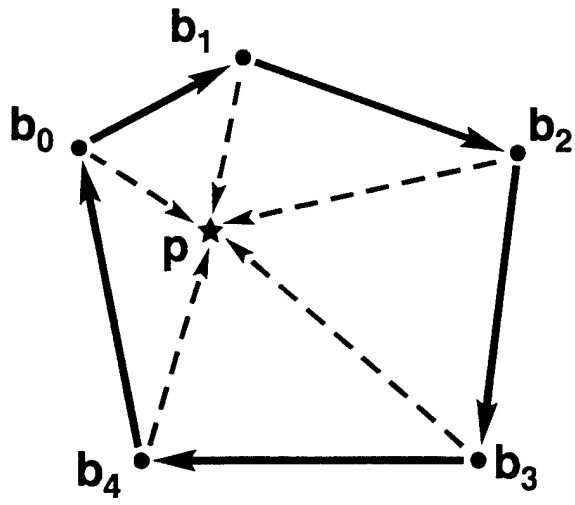

Figure 4-23. Cross Product Vectors for a Point That Lies Inside of the Convex Polygon Showing That All of the Vector Cross Products Have the Same Sign and Thus Point in the Same Direction. (Here all of the cross products are positive and thus all of the cross product vectors point upward.)

When the point p lies outside of the polygon, at least one of the cross product vectors will have a sign different from the sign of the other cross products. Figure 4-24 depicts the most common case where all but one of the cross product vectors have the same sign, here positive, and thus only one cross product vector points down.

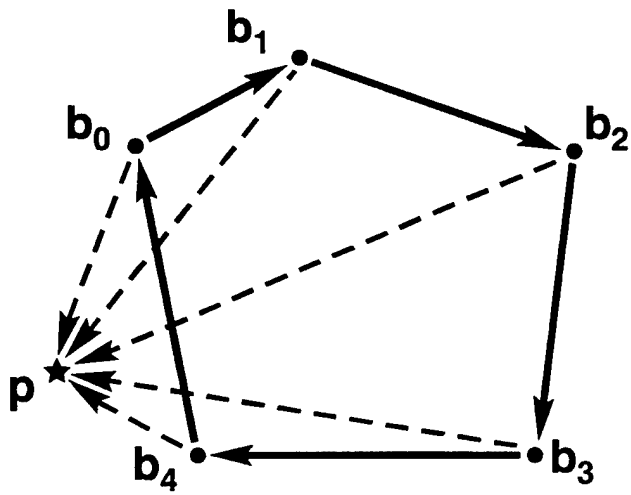

Figure 4-24. Cross Product Vectors for a Point That Lies Outside of the Convex Polygon Showing That One Cross Product Has a Negative Sign (Points Down).

4.11.2 Addendum 4B. Calculation of Great Circle Distances

Figure 4-25 depicts the great circle distance between to points, p_1 and p_2, that lie on the surface of a sphere.

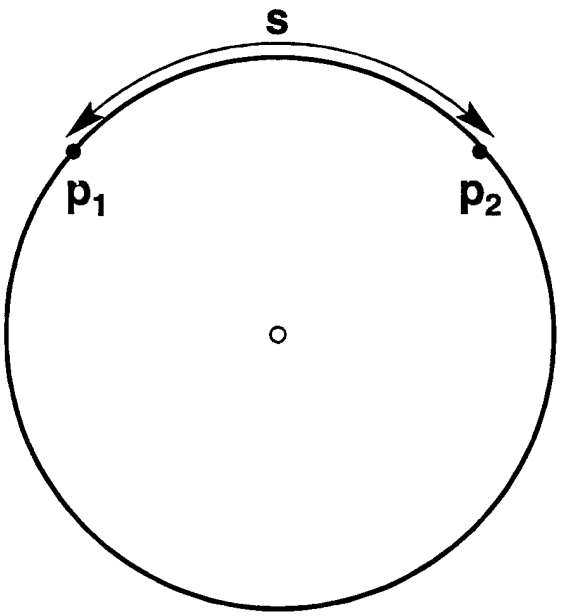

Figure 4-25. Great Circle Distance.

Figure 4-26 shows that the points p_1 and p_2 are connected not only by an arc of length s but also by a chord of length d.

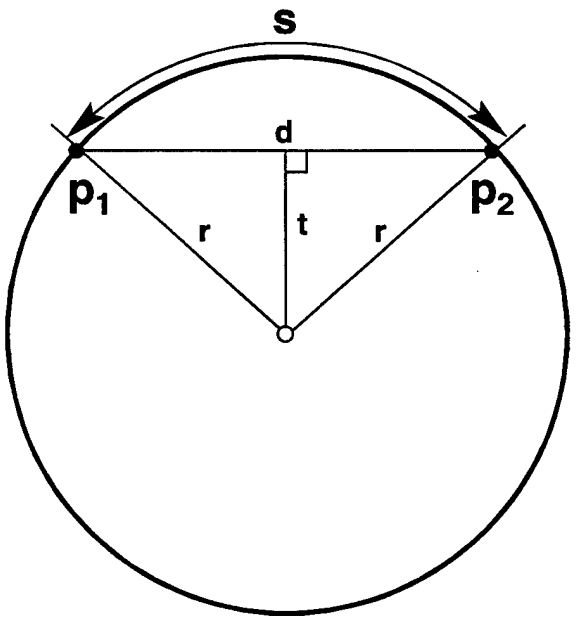

Figure 4-26. Great Circle Distance With Chord Connecting the Endpoints of the Great Circle Distance.

The distance d can then be determined via the standard vector equation

$$d = |p_1 - p_2| = \sqrt{(x_1 - x_2)^2 + (y_1 - y_2)^2 + (z_1 - z_2)^2}$$

where

$$\begin{aligned} x &= r \times cos\ (\text{lat}) \times cos\ (\text{long}) \\ y &= r \times cos\ (\text{lat}) \times sin\ (\text{long}) \\ z &= r \times sin\ (\text{lat}) \end{aligned}$$

and r is the radius of the earth (6,378 km = 3,444 nautical miles). Because r and d are both scalar quantities, the great circle distance s can be determined as

$$s = 2r\arcsin\left(\frac{d}{2r}\right)$$

For portability, it was decided to implement the great circle calculation method in a UNIX scripting language that did not support inverse trigonometric functions. Therefore, a numeric approximation of a great circle distance that didn't use inverse trigonometric functions was selected and implemented in a recursive scheme in order to obtain accurate estimates of sailing distances.

In order to compute the correct (but approximate) result without using the arcsin function, a set of algebraic relations that uses not only the length d of the chord that connects the points p_1 and p_2 but also the radius of the earth was defined and implemented in a recursive calculation. Figure 3 illustrates the basis of the recursive calculation. Figure 4-27 is a slight modification of Figure 2 that shows that the length of the arc s can be better approximated by using a larger number of shorter chords d'. Thus, for example, 2d' should be a better approximation of s than d.

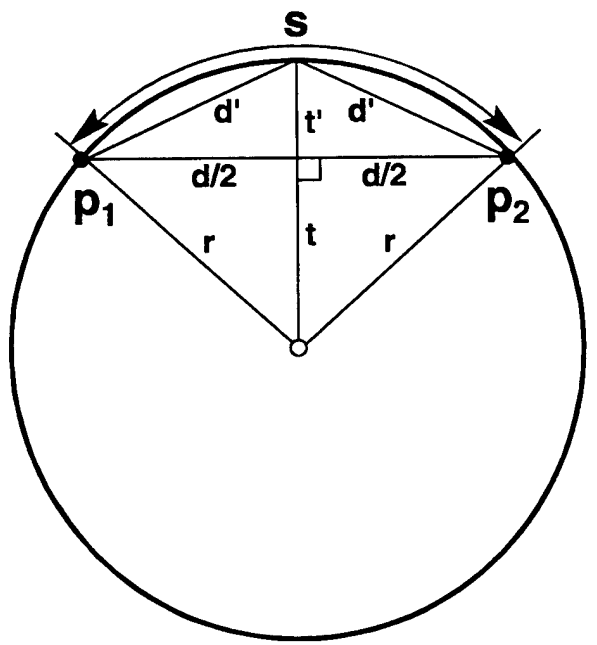

Figure 4-27. Depiction of Geometric Basis for the Recursive Great Circle Distance Calculation.

Solving for d' is done in three steps, once d is determined as above,

$$t = \sqrt{r^2 - (d/2)^2}$$

$$t' = r - t = r - \sqrt{r^2 - (d/2)^2}$$

$$d' = \sqrt{(t')^2 + (d/2)^2}$$

And, with a little algebra,

$$d' = r\sqrt{2 - 2\sqrt{1 - \frac{d^2}{4r^2}}}$$

Finally, by recursive substitution of d' for d, an estimate of the great circle distance of any accuracy can be obtained. For these analyses, the recursive process was terminated when $2^{n-1}d^n \cong 2^{n-2}d^{n-1}$ to eleven digits.

5. REPRESENTATIVE SHIPS AND SHIPPING PRACTICES

Spent nuclear fuel is shipped on four types of ships: small and large break-bulk freighters, container ships, and purpose-built ships. When spent nuclear fuel is transported in a Type B cask on one of these ships, the location of the cask, the way it is tied down, and the nature of the other cargo carried with the cask or in other ship holds all strongly influence the small chance that a ship collision and/or a ship fire will lead to failure of the Type B cask and release of radioactivity to the environment. An overview of representative ships and shipping practices for maritime transport of spent fuel is presented in this section; details of specific topics are presented in Appendix I.

5.1 IMO Ship Classes for Carriage of Radioactive Materials

On November 4, 1993, the International Maritime Organization (IMO) approved the Code for the Safe Carriage of Irradiated Nuclear Fuel (INF, the only material that is regulated by amount of radioactivity), Plutonium and High-Level Radioactive Waste in Flasks on Board Ships (Resolution A. 748 [18]). Under the Code, three classes of ships were established for transport of these materials:

> **Class INF 1**: Ships carrying such materials with an aggregate radioactivity less than 4,000 Terabecquerels (TBq, where a Bequerel is the unit of activity in the International System of Units that equals one disintegration per second and a Terabecquerel is 10^{12} Becquerels).
>
> **Class INF 2**: Ships carrying INF or high-level radioactive wastes with an aggregate amount of radioactivity less than 2×10^6 TBq, and ships carrying plutonium with an aggregate amount of radioactivity less than 2×10^5 TBq.
>
> **Class INF 3**: Ships carrying INF or high-level radioactive wastes and ships carrying plutonium with no restriction on the aggregate amounts of radioactivity in these materials.

5.2 Representative Ships

INF, also known as spent fuel, can be shipped on or aboard a variety of vessels. The following are examples of the different types of ships that Edlow International, a major shipper of RAM, has used to safely transport INF.

5.2.1 Charter Freighter

A charter freighter is a leased vessel that sails to a specified destination, with no intermediate ports of call. A charter vessel can be either a break-bulk or a container vessel. Morbihannaise et Nantaise de Navigation's *Bouguenais* is a charter freighter classified as an INF-2 vessel under the INF Code.

This vessel is 90 meters long and 16 meters wide. It has a dead weight of 4,800 metric tons and a maximum speed of 12.6 knots. Features complying with INF-2 standards include:

- Temperature control system linked to a powerful cargo cooling system
- Backup electrical systems
- Fire detection and protection systems
- Radiation protection equipment
- Radiation protection training for crew
- Standards for stability after damage
- Emergency shipping plans

Additional data about the *Bouguenais* and a type of roll-on/roll-off (Ro-Ro) vessel that has been used to transport RAM is presented in Appendix I, Part A, Charter Freighters.

5.2.2 Break-Bulk Freighter

A break-bulk freighter is a vessel in which both non-containerized goods and containerized goods can be shipped and that sails according to commercial schedule or the specifications of its charter. The *Marjorie Lykes* is a typical break-bulk freighter made of all steel construction with welded butts, seams and internals, with the exception of the seams, of the sheer and bilge strakes, which are double riveted.

The vessel has four cargo holds forward, crew and passenger accommodations amidship, No. 5. cargo hold, accommodations and machinery spaces with No. 6 cargo hold located aft. The vessel has a raised forecastle incorporating the No. 1 cargo hold and flush deck aft.

The vessel is equipped with electrically driven winches and derricks at the forward and after ends of all cargo holds. All vessel hatch covers are of the steel folding type hydraulically operated at the main, upper tween and lower tween deck levels, except for the main deck hatch covers for the No. 4 cargo hold, which are of the steel slab type secured by bolts and which may be lifted aside using the ship's gear. Propulsion is by means of cross compound steam turbines and double reduction gearing driving a single four-bladed propeller.

The specifications of the ship are as follows (a dual tonnage vessel):

- If draft is 27–07 or less, then gross ton. = 8,762.1; net ton. = 5,046.0
- If draft is 27–08 or deeper, then gross ton. = 11,891.61; net ton. = 7,780.0
- Light draft disp. = 8,719 at 12–08 draft; summer draft disp. = 22,892 at 30–01 1/8
- Summer dead weight tonnage = 14,172
- Suez Canal gross ton. = 12,890; net ton. = 11,727.8 (Danube rule = 9,988.23)
- Tropical fresh water draft = 31–04 5/8; Fresh water draft = 30–09 1/8
- Tropical zones draft = 30–08 5/8; Summer zones draft 30–01 1/8
- Winter zones draft = 29–05 5/8; Fresh water allowance = 8 inches
- Summer freeboard = 1108 & 1/4; Shaft horse power, normal–10,000
- Maximum commercial horse = 11,000; sea speed 80% normal shp 17.5 knots
- Propeller diameter (4 blades) = 21–00; propeller pitch = 21–06
- Speed factors: R.P.M. × 0.21299 = knots; knots × 1.1515= statute miles
- Length overall = 592–06 (180.6 meters)
- L.B.P.= 567–06 (172.97 meters)
- Breadth molded = 69–02 (21 meters)
- Depth molded = 41–07 (12.7 meters)
- Anchor chains = 150 fathoms × 2 & ¼ inch anchors (3) 10,250 lbs., ea.+ 4649.3 kg.
- Height above B.L.= 126–06 (38.6 meters)
- Bridge to bow = 335–00 (102.1 meters)
- Bridge to stern = 257–06 (78.5 meters)
- Booms (16) 15 tons × 57 feet long (17.4 meters)
- Booms (4) 35 tons × 67 feet long (20.4 meters)
- Boom (1) 60 tons × 65 feet long (19.8 meters)
- Towline (1) 130 fathoms × 1& 15/16 inch × 6 × 24 wire
- Lifeboat falls (2) 215 feet × ¾ inches (2) 245 feet × ¾ inches
- Bale cubic = 790,626 ft^3
- Grain cubic = 849,548 ft^3
- Fuel oil capacity = 19,081 BBLS (2,891 tons)
- Cargo oil tanks = 7,840 BBLS (1,078 tons)
- Mud ballast = 1,365 tons

Speeds Ahead: Maneuvering

Dead slow	= 10 rpm	= 2.13 knots
slow	= 20 rpm	= 4.26 knots
half	= 40 rpm	= 8.52 knots
full	= 60 rpm	= 12.78 knots

Speeds Astern: Maneuvering

Dead slow	= 10 rpm	= 1.07 knots
slow	= 20 rpm	= 2.13 knots
half	= 35 rpm	= 3.73 knots
full	= 50 rpm	= 5.33 knots

Astern power is 80% of rated ahead power.
Astern speed is 50% of rated ahead speed.
Prolonged astern power is 70% of rated ahead power.

Crash stop = 1,045 yards (959 meters) - 3 minutes 20 seconds
Turning circle: stbd: 1,013 yards (926 meters)
port: 810 yards (741 meters)

On Request:

15 rpm	= 3.19 knots
25 rpm	= 5.32 knots
30 rpm	= 6.39 knots
45 rpm	= 9.58 knots
50 rpm	= 10.65 knots
55 rpm	= 11.71 knots
65 rpm	= 13.94 knots
70 rpm	= 14.91 knots
75 rpm	= 15.79 knots

Full throttle maneuver without notice = 70 to 75 rpm. For any speed above full throttle, engine room will require a notice to slow down. The above speeds assume a clean hull and medium drafts.

Data on a second type of break-bulk freighter, which may meet either INF-1 or INF-2 requirements and has been used to transport RAM, is presented in Appendix I, Part B, Break-Bulk Freighters.

5.2.3 Container Ship

A container ship, either charter or commercial, is a vessel equipped with steel slots specially made to hold containers. Atlantic Container Line's (ACL) *Atlantic Compass* is a multi-purpose, single screw diesel driven, Ro-Ro container carrier intended for shipment of containers, block stowed general cargo, and all kinds of wheeled units (including heavy loads and cars and other vehicles with fuel in their tanks and batteries connected). Like all Ro-Ro vessels, the *Atlantic Compass* has a built-in ramp that is used for driving vehicles on and off of the ship (a pictures of a container ship with a Ro-Ro ramp is presented in Appendix I, Part C).

This vessel has a raked stem, bulbous bow, transom stern, semi-spade type rudder of streamlined form, fixed propeller, bow, and stern thrusters.

The vessel has an accommodation/cardeck superstructure and engine room located aft. Upper deck and tanktop are continuous; a transverse bulkhead divides the container cell part forward from the Ro-Ro part aft. In addition to the tank top, two Ro-Ro decks are arranged in the Ro-Ro part, the upper extending

from the stern door to the transverse bulkhead and the lower between the forward engine room bulkhead and the transverse bulkhead. Upper and lower Ro-Ro deck spaces are fitted with hoistable cardecks.

The decks are numbered from tanktop and upwards with Deck No. 1 (tank top) up to Deck No. 11 (Navigation Bridge Deck). Hoistable decks are designated 1A (in Ro-Ro Deck No. 1), 3A and 3B (lower and upper, respectively, in Ro-Ro Deck No. 3).

A superstructure deck house is arranged with wheel house/chart room on the upper level and two accommodation decks above a garage with fixed decks (Nos. 4 to 8 inclusive) for cars. Decks Nos. 4, 5 and 6 also are suitable for high-sided vehicles (HSV).

All cargo decks, including weather deck (No. 4) and inside accommodation decks, are without sheer and camber.

A double bottom is provided in the ship's holds and engine room; this double bottom is divided into ballast tanks and various other tanks. Ballast and fuel oil tanks are arranged in double shell along the ship sides. The fore peak tank is designed as ballast tank, the aft peak as cooling water tank for the stern tube. An anti-heeling system is arranged in WB tanks ST4, ST5, and ST6 (with a capacity of 3,200-ton cargo placed 7 meters from centerline).

The weather deck is arranged for stowage of 40-foot and 20-foot containers in fixed and movable cell guides (only two fixed 20-foot continuous cells). Under deck in the forward part are five container holds with cell guides. Hatches are covered with side rolling hatch covers.

Access to the Ro-Ro spaces in the after part, from and to the quay, is arranged via a wide angled ramp on starboard quarter. An internal permanent ramp system is provided between the stern door area and the various Ro-Ro and car/HSV-decks, including a center ramp to upper deck level and the garage.

The vessel complies with the following rules and regulations:

1. The Rules and Recommendations of the Swedish Board of Shipping and Navigation (including noise and hygienic limits on ships and requirements for one man on watch on the bridge) or corresponding Maritime Directorate as specified by the owner. If the Swedish limits are lower, then these are followed. British and French vessels comply with the equivalent British and French regulations.

2. The International Load Line Convention 1966, with amendment IMCO resolution A 231 (VII) 1971.

3. The International Convention SOLAS 1974 (IMCO 1975) with the London Protocol 1978.

4. The Government Marine Agency's Regulations relating to International Tonnage Measurement of ships together with Suez and Panama tonnage.

5. The International Tele-communication and Radio Regulations (Montreux 1965) and Annexes and Revisions (Geneva 1976).

6. The Suez Maritime Universal Company's Rules of Navigation.

7. The rules and regulations governing navigation of the Panama Canal and adjacent waters.

8. International Convention for the Prevention of Pollution from Ships 1973 with the London Protocol 1978, including Provisions for Sewage Disposal Plant.

9. International Regulations for the Prevention of Collisions at Sea (1972).

10. USCG Requirements for foreign flag vessels regularly calling at U.S. ports.

11. USCG and national rules for carriage of cars with up to five liters of fuel in their tanks and with batteries connected.

12. U.S. Department of Health, Rat Proofing, and Sanitation.

13. USCG Pollution Prevention (Vessels and Oil Transfer Facilities 1972).

14. USCG Marine Sanitation devices in Federal Register, 1975 (Volume 37, CFR Number 246).

15. Safety regulations for long shoring, U.S. Department of Labor.

16. The General Conference of the International Labor Organization, ILD 1974 (Convention 133).

17. The Canadian Department of Transport (Marine Safety).

18. Australian and New Zealand Safety Working and Harbor Regulations and Waterside Workers' Federation Requirements.

19. USCG requirements regarding stability (Volume 46, No. 93. 07 - 10).

20. Lloyd's Register of Shipping Code for lifting appliances in the marine environment.

21. U.K. Factories Act 1937 and 1948 and U.K. docks regulations 1934 (or equivalent for the vessel's country registration).

22. IEC - Electrical installation in ships (Publication 92).

23. MCO-m Resolution A 327 (IX) and A 325 to the extent that will be included in the amendments of SOLAS 1974.

5.2.4 Purpose-Built Ship

Purpose-built vessels are designed solely for the transportation of spent fuel and spent fuel byproduct material. Casks transported on these vessels may weigh in excess of 100 tons and far exceed the capacity of ocean containers. These vessels are fitted with special securement points for specific casks.

Pacific Nuclear Transport Limited (PNTL), a subsidiary of British Nuclear Fuels Limited (BNFL), owns five purpose-built ships. To adhere to the strict regulations that govern the business of transporting RAM, and to ensure the safety of all who come in contact with the nuclear fuel, BNFL and PNTL have built ships designed specifically for the transport of spent fuel.

PNTL provides transport service between Japan and Europe, a round trip of 33,000 miles, on its own fleet of five purpose-built ships. The ships on the Japan route are: The *Pacific Swan*, *Pacific Crane*, *Pacific Teal*, *Pacific Sandpiper* and *Pacific Pintail.*

Each PNTL ship is a 104-meter long, 4,500 ton, construction carrier made out of all welded steel. The hulls and upper decks have been specially strengthened to reduce collision damage. They are fitted with segregated cargo holds which are protected by double bottoms running from fore peak to after peak and side tanks running the full length of the cargo area. Special bow thrusters are installed at the front of the ships for easy maneuvering.

The twin screw motor vessel is powered by two diesel engines and is capable of sustained non-stop voyages with a full load of flasks of nuclear fuel stored in its holds. The main engines are capable of operating continuously on heavy oil fuel.

Heating is provided in all fuel oil double bottom tanks and daily service tanks because of the heavy density of the oil used. It is also necessary to arrange heaters in the fuel oil system so that its viscosity is reduced to that similar to diesel oil, before being injected into the engine. The viscosity is controlled by an automatic viscometer which governs the actual heat supplied to the final heater, thereby controlling the viscosity.

In order to provide the necessary electrical power for engine room auxiliary services and ship services, two 320 KW Deutz diesel generators are fitted, and each one is capable of supplying total power required when the vessel is operating at full power at sea. The other generator is, therefore, available for standby purposes.

In addition, in the forward diesel generating room two more generators are fitted: one 490 KW and the other 320 KW. These machines are principally for the purpose of supplying electrical power for the refrigeration machinery. These generators are connected directly to the refrigeration machinery switchboard, but can also be directed to ship supply if and when required.

The diesel engine of the 490 KW diesel generating set is also connected via pneumatic clutch and gearbox to the bow thruster drive. The diesel alternators are manufactured by Deutz, the smaller ones being type BA8M816 and the larger one being type BA12M816.

The ship design is not only based on but also exceeds the requirements of the IMO's "Code for the Construction and Equipment of Ships Carrying Dangerous Chemicals in Bulk." By far surpassing the criteria set by IMO, PNTL's vessels possess a stability far greater than other similar cargo vessels or tankers. These purpose-built ships and their 26 member crews have successfully carried nuclear materials over 15,000,000 miles with neither damage to a flask nor any breach of the containment.

Both the UK Department of Transport and the Lloyd's Register must approve the design and construction of the ships. Ships operating on the Japanese route also require clearance from the Japanese Ministry of Transport.

These ships are specially made to take great precautions for safety. For instance, the hulls of the ships are strengthened and in subdivided compartments to protect against collision impacts; watertight subdivisions give adequate reserve buoyancy; extra, high-standard firefighting equipment provides extra security. In addition, there is extensive duplication of machinery: equipment for navigation, communications and ship location (including satellite navigation equipment), cargo monitoring aids, and cooling systems in the holds provide back-up assurance in case of failure. The special features of the purpose-built ships allow for these ships to have greater maneuverability as well as increased margins of safety.

Safety is the primary concern constant in all stages of construction of the ships, as well as in the execution of the transport of the highly sensitive cargo. Therefore, the ships are equipped with a full range of firefighting, lifesaving, navigation, and communications equipment.

Levels of radiation are monitored continuously by the highest quality equipment. In addition, radiation shielding is installed to enhance crew safety. One safety measure for the protection from radiation on the purpose-built ships is the "clean room." It is set aside for the purpose of changing clothes and cleaning if necessary after a visit has been made to the holds when irradiated fuel is being carried. This room has holding bins for containing soiled clothing as well as washing and shower facilities. In addition, locker facilities are also provided for containing radiation monitoring equipment.

The firefighting equipment on board the ships is well in excess of what is required by the regulations set by the UK Merchant Shipping Regulations, 1980. The ships have two firefighting systems, each with redundant pumps at several locations including the engine room and the forward generator room. The systems, which are in accordance with the UK Department of Transportation regulations, are capable of completely flooding the cargo holds in order to suppress the fire, cool the cask, and provide additional radiation shielding. The holds and engine room are also fitted with carbon dioxide (CO_2) fire suppression systems.

To guarantee accurate navigation, the ships' equipment includes two radar sets, one with an automatic plotting aid and one anti-collision type; two echo sounders; a gyro compass and direction finder; satellite navigation equipment; an Omega navigation receiver; and a Decca navigator. This array of equipment provides for a highly reliable and precise navigation system.

The particular flasks that the ships are built to carry are also built with safety as a guide. The quality of the steel or steel and lead flasks, each weighing between 50 and 110 tons, is specially designed to carry INF. The Pacific route ships have a capacity of up to 28 flasks with a total load of 100 tons of irradiated fuel.

The PNTL purpose-built ships have made over 50 round trips between Europe and the far east carrying INF without radiological incident.

Attached as Appendix I, Part D, is a paper entitled *The Design of Ships for the Transport of Spent Nuclear Fuels* presented at the 1988 International Conference on Transportation for the Nuclear Industry in the United Kingdom, which provides additional technical information about PNTL purpose-built ships.

5.2.5 Charter Vessel Surveys

Prior to use of a charter vessel, Edlow International requires an independent marine survey of the proposed ship to ensure that all critical hull, engineering, operational, and maintenance procedures were acceptable for the carriage of the cargo. The marine surveyor inspects the vessel prior to signing of a charter agreement and performs inspections of the following systems:

- Watertight integrity (to check access hatches, cargo hold hatch covers, doors, vents, etc., and cargo oil tanks);
- Double bottom tanks;
- Anchors, windlasses, and cables;
- Cargo holds and securing arrangements are checked for general condition, cargo securement equipment, smoke detector, extractor fan and fire suppression systems;
- Machinery spaces such as propeller shaft tunnels, boiler casings, and burner registers are checked for cleanliness and leaktightness. Also checked are low pressure turbines, condenser tubes, the emergency bilge strumbox for the main sea water circulating pump, and the electrical system (main and emergency switchboards);
- Steering gear (port and starboard electro-hydraulic pumps tested separately); and
- Crew—the total complement of officers and crew—are checked for nationality.

Upon completion of the survey, the surveyor provides a recommendation as to the suitability of the vessel for the proposed charter. As part of the survey the following documents are also attached:

- Vessel details;
- Arrangement drawing of holds and tanks;
- Cargo stowage plan;
- Location of vessel at time of survey;

- American Bureau of Shipping Survey Status print-out (most recent copy for relevant vessel);
- Condition Survey Summary Report; and
- Photographs taken by the surveyor, showing general views of the vessel, and items which, in the opinion of the surveyor, require attention/repair to meet suitability requirements.

5.3 Shipping Practices

5.3.1 International Maritime Dangerous Goods Code

There are many regulations and standard practices involved in the transport of INF. Most regulations involved in INF shipments are stated in the International Maritime Dangerous Goods Code (IMDG). This code is based upon the principles of the International Atomic Energy Agency's (IAEA) Regulations for the Safe Transport of Radioactive Material, which establish standards of safety to provide an acceptable level of control of the radiation, criticality, and thermal hazards to persons, property, and the environment that are associated with the transport of RAM.

These regulations utilize the principles set forth in both the IAEA's Radiation Protection and the Safety of Radiation Sources, and the International Basic Safety Standards for Protection Against Ionizing Radiation and for the Safety of Radiation Sources," Safety Series No. 115, jointly sponsored by the FAO, IAEA, ILO, NEA/OECD, PAHO, and WHO. Thus compliance with these regulations is deemed to satisfy the principles of the International Basic Safety Standards in respect of transport.

5.3.2 Transport Index

The Transport Index (TI) is defined within the IMDG Code and is a method of determining appropriate course of action to take judging on the amount of radioactivity present in the material at hand. TI is a single number assigned to a package, overpack, tank, or freight container, which is used to provide control over both nuclear criticality safety and radiation exposure.

Use of the TI system makes it possible for packages, whether containing fissile materials or not, to be treated alike for transport purposes. It is used to facilitate stowage and segregation. It is also used to establish content limits on certain packages, overpacks, tanks, and freight containers; to establish categories for labeling; to determine whether transport under exclusive use shall be required; to establish mixing restrictions during transport under special arrangement and during storage in transit; and to define the number of packages allowed in a freight container or aboard a conveyance. TI limits for various types of freight are presented in Appendix I, Part E, Transport Index.

5.3.3 Spacing and Placement of Containers on Vessels

Containers carrying spent fuel are loaded on vessels depending on three factors: port destination, stowage requirements (listed in the IMDG Code), and specifications from Edlow International. The port destination is a variable because on a commercial vessel, the crew wants to move containers of spent fuel around as little as possible. Freight is moved as infrequently as possible, so it can be accessed when needed without obstructions.

IMDG Codes are not used when determining the placement of RAM relative to the sides and end of a vessel. However, for safety reasons, informal rules are practiced. For commercial break-bulk and chartered vessels in general, Edlow International specifies below deck storage, towards the middle of the ship. For commercially scheduled container vessels, Edlow International advises central slot location,

preferably near the bottom of the stack. Because it is considered unsafe, above deck placement is not suggested. Casks are usually placed parallel to each other along the length of the ship.

In spacing individual casks relative to each other and in determining the number of casks allowed in a given hold, the IMDG Code is used. The IMDG Code states "The consignment shall be so handled and stowed that the total sum of TIs in any individual group does not exceed 50, and that each group is handled and stowed so that the groups are separated from each other by at least 6 meters." Thus, casks are only individually separated if their TI exceeds 50 whereupon they are separated by at least 6 meters. Segregation requirements are discussed below in Section 5.3.5 and also in Appendix I, Part I, IMDG Segregation Requirements and Appendix I, Part J, DOT Segregation Requirements.

5.3.4 Securements and Lashings for Casks and Containers

Casks of spent fuel are placed in International Standards Organization (ISO) ocean containers (representative ocean containers are described in Appendix I, Part F, Ocean Containers), which are then secured onto the vessel. There are no regulations regarding the securements and lashings used in holding down casks to a ship. Thus, casks are treated as any other cargo in this regard. Depending on the vessel used for the shipment, a variety of securements may be employed. A container ship uses steel slots as part of a cell structure in which the container can slide and become secured. These are illustrated in Appendix I, Part G, Secured Cell Slots. A break-bulk ship uses steel lashing hooks, which are innate to the ship's design, that allow a container to become easily secured by incorporating the lashings with the lashing hooks. Examples of the various types of securements and lashings used to hold casks to a ship are presented in Appendix I, Part H, Securements and Lashings.

5.3.5 Spent Fuel Cask Segregation Requirements

Requirements for transporting RAM with other cargo are regulated by the IMDG Code in Class 7, Radioactive Materials, Section 4.2.3, p. 7017:

> Except in the case of shipment under special arrangement, mixing of packages of different kinds of radioactive material, including fissile materials, and mixing of different kinds of packages with different transport indices is permitted without specific competent authority approval. In the case of shipments under special arrangement, mixing shall not be permitted except as specifically authorized under the special arrangement.

These regulations do not prevent plutonium dioxide (PuO_2) and Vitrified High Level Waste (VHLW) from being shipped on vessels carrying other cargo. Further segregation requirements are listed in Class 7, Radioactive Materials, of the IMDG regulations Sections 4.5–5.0 (see Appendix I, Part I). Segregation requirements can also be seen in Section 176.83 of the DOT regulations (see Appendix I, Part J).

5.4 Shipping Costs

Approximate costs for trans-Atlantic shipment of spent fuel varies. The following are estimated costs for ocean freight of trans-Atlantic voyages on representative ships discussed in this section.

- Charter break-bulk: 160,000 USD
- Commercial container ship: 40,000 USD
- Purpose built: 800,000 USD
- INF2: 550,000 USD

These estimates are only for the ocean portion and do not include Edlow International costs for administration, permits and licenses, transport, cask rental, shipment of cask from shipping facility to ocean liner, or delivery to spent fuel destination once the vessel has docked.

5.5 IMO Special Consultative Meeting, March 4-6, 1996

In 1993, the Assembly of the IMO adopted by resolution (A.740) the Code for "The Safe Carriage of Irradiated Nuclear Fuel, Plutonium, and High-Level Wastes in Flasks on Board Ships." The assembly also adopted a recommendation that the code be kept under regular review and amended as necessary. In particular, the resolution requested that certain issues pertaining to the transport of the materials in question be considered, particularly the need for special routes, localization and salvage of packages, and emergency response.

A Special Consultative Meeting (SCM) of entities involved in the maritime transport of nuclear materials covered by the INF Code was held in London from March 4–6, 1996. The meeting was attended by approximately 100 delegates from 32 countries.

The main purpose of the meeting was to enable discussion of all aspects connected with the INF Code. The special meeting was arranged at the suggestion of the IMO Secretary General, Mr. William A. O'Neil, to enable all parties involved in or affected by INF transport to express their opinions and exchange ideas and viewpoints. The meeting did not make any recommendations but the technical papers presented and the questions and answers exchanged will be made available to governments so that recommendations for future activities can be formulated.

According to an IMO message dated March 7, 1996, the meeting discussed the following concerns:

- The adequacy of flask designs and tests. This is the responsibility of the IAEA and is under continuous review, particularly in the context of their coordinated research program.

- Route planning and the possibility of excluding ships carrying INF from particularly sensitive sea areas. Both items were considered by IMO's Sub-Committee on Safety of Navigation in July of 1996.

  The possibility of excluding ships from certain areas may also be considered by IMO's Marine Environmental Protection Committee (MEPC) and also the Legal Committee since it raises various issues concerning the freedom of navigation and rights under the United Nations Convention on the Law of the Sea (UNCLOS).

  The NAV sub-committee is also considering the possibility of shore based authority being able to track ships carrying INF.

- Emergency response arrangements. The International Convention on Oil Pollution Preparedness, Response and Co-operation (OPRC), 1990, is now in force and a working group is preparing guidelines for the development of plans for dealing with emergencies involving INF materials.

- Locating sunken ships or INF flasks. This matter has been considered by IMO subcommittees that have agreed that ships carrying INF can be continuously tracked and alarms given if containers are lost overboard, provided they are fitted with devices such as an acoustic transponder. The United Kingdom said that at least one ship is able to give off a signal that can be heard even if the ship sinks to a depth of 6,000 metres.

- Liability regimes. The International Convention on Liability and Compensation Damage in connection with the Carriage of Hazardous and Noxious Substances by Sea was agreed to by the IMO in 1996. The IAEA is addressing Liability Regimes during the current revision of the Paris

and Vienna Conventions which also deal with this subject.

- Environmental impact of accidents involving INF materials. It is proposed that this be referred to the Group of Experts on the Scientific Aspects of Marine Pollution (GESAMP) and perhaps also the United Nations Environment Program (UNEP).

- Notification of coastal states in the event of an accident. This is covered by existing regulations.

- The addition of other materials to the Code. This matter is to be conferred to a specialist group of the Subcommittee on Dangerous Goods, Solid Cargoes and Containers.

- Making the Code mandatory. Several delegations suggested that this be done. It was suggested that the issue be raised at the MSC, which has the authority to take action on such proposals.

The following presentations from the Special Consultative Meeting further illustrate the concerns expressed at that meeting. Appendix I, Part K, contains copies of these presentations.

- *Addressing Safety issues in the Sea Transport of Radioactive Materials*, presented by Edwin Lyman (on behalf of the Nuclear Control Institute)

- Presentation by the Solomon Islands

- Presentation by Argentina

- Presentation by Ireland

- *Ecological and Public Health Implications from Flasks lost at Sea*, presented by Sven P. Nielsen, Riso National Laboratory, Denmark

- *Applying the Precautionary Principle to Ocean Shipments of Radioactive Material*, presented by Jon M. Van Dyke, Nuclear Control Institute

- *Environmental Impact Assessment of Radioactive Materials during Sea Transportation: Case of Plutonium Released in the Ocean*, presented by Jean Christophe Niel, Institut de Protection et de Surete Nucleaire

6. PROBABILITY OF DEEP HULL PENETRATION

For a ship collision to damage a RAM cask carried on the struck ship, two things must happen. The RAM cask must be in the struck hold and penetration into that hold by the striking ship must be deep enough to damage the cask. Clearly, this can happen only during high-speed collisions. This section revalidates a correlation developed by Minorsky that correlates ship damage with the displacements of the ships involved in the collision, their speeds, and the collision angle. The correlation is then modified to allow collision penetration depths and the effects of cargo on cask damage to be estimated. Finally, the revalidated modified correlation is used to estimate the probability that ship collisions would damage a RAM cask carried aboard small and large break-bulk freighters.

6.1 Background

Ship collisions occur infrequently, and high speed collisions are rare. The IMO, which collects casualty reports from member countries when there is loss of life, severe pollution, or a declared total loss, includes only 21 collisions (for the latest reporting year) in their world-wide severe accident database [1]. In the United States, serious ship accidents are investigated by the NTSB. Of the 57 NTSB reports concerned specifically that collisions that were issued for the period 1972 through 1993, fewer than half involved collisions between two ships and only twelve quoted speeds over ten knots.

There exists, nevertheless, an extensive literature on various aspects of ship casualties [2]. This is due in part to the interest sparked during and after the decade of the 1950s, when there was wide concern about damage to onboard reactors in a then anticipated fleet of nuclear powered commercial vessels, subsequently never developed. More recently, the frequency and cost of oil spills from groundings of large tankers, among them the *Exxon-Valdez*, has spurred renewed interest in the study of marine accidents.

A few of these studies stand out as having particular significance. The earliest was written by V.U. Minorsky in 1959 [3]. He treated hydrodynamic forces during ship collisions through an added mass equal to 40 percent of the mass of the struck ship, and assumed the collisions were perfectly inelastic, which means that the collision causes the two ships to stick together forming a single object that has a well-defined terminal speed. The kinematics of inelastic collisions permit calculation of the reduction in total kinetic energy of the ships during the collision, and therefore implicitly allows the work done damaging ship structures to be calculated without the performance of detailed structural analyses.

Minorsky developed an empirical straight line correlation between the energy loss calculated from the inelastic collision assumption, and a resistance factor equal to the volume of steel in the structures damaged in the accident. To estimate that volume he considers,

1. Decks, flats, and the double bottom in both the struck and striking vessel.
2. Transverse bulkheads in the struck vessel when hit squarely.
3. Longitudinal bulkheads in the striking vessel.
4. The component in the direction of collision of the shell of the striking vessel.

Minorsky's resistance factor does not include the volumes of steel damaged in the shell plating (hull) of the struck ship or any other structures that lack depth in the direction of motion of the striking ship. Because the volume of steel in the shell of the struck ship is not included in Minorsky's resistance factor, the x-intercept of his correlation, the point where his regression line crosses the energy loss axis,

becomes a measure of the resistance of the struck ship's hull to penetration. Minorsky's value for this quantity was 121,900 tonne-(knot)^2, where a tonne is 1,000 kg = 2,200 lbs.

Shortly after the publication of Minorsky's paper, Gibbs and Cox Incorporated prepared a report for the U.S. Maritime Administration that contains a table, shown in Appendix 4-C, of the data collected by the U.S. Coast Guard concerning accidents up to 1958 [4]. Selected accidents from this table had been used by Minorsky, in advance of its publication, in developing his damage correlation. Gibbs and Cox also determined the volume of steel involved in these accidents, sometimes considering additional structures not treated by Minorsky.

This work was followed by a number of large-scale collision experiments performed in Japan by Akita [5, 6] and in Europe by Woisin [7, 8]. Akita [5, 6] presented a triangular damage model involving a non-deformable bow, in which the energy absorbed is proportional to the square of the depth of the observed penetration. The experiments in Japan and Europe in turn led to more detailed analysis models, for example, T. Hysing's hull penetration analysis [9], which determines load-penetration curves from membrane tension stresses and plastic buckling loads, and Martin Petersen's simulation of the dynamics in ship collisions [10].

Laboratory experiments on the fracture properties of the mild steel plate used in ship construction began at about the same time. Recently, Lu and Calladine used dimensional analysis to summarize a number of such experiments that involve the cutting of a plate by a wedge [11]. Wierzbicki and Thomas developed a formulation which agrees with Lu and Calladine, and gives a physical interpretation for the proportionality observed by Lu and Calladine between the (dimensionless) energy absorbed and (dimensionless) fracture length raised to a power [12]. Wierzbicki and Thomas have also applied their formulation to the prediction of grounding damage to double hull tankers [13].

Finite element analyses have been performed as well, beginning with the work of Chang et al. using ADINA [14]. Lenseling et al. use MSC DYNA in simulations that treated yaw and roll [15]. More recently, at Sandia National Laboratories, Porter and Ammerman used PRONTO3D to examine high-speed right angle impacts at the center bulkhead of an INF Class-2 freighter [16].

6.2 Roadmap

This section develops a probabalistic methodology for assessing the risk to spent fuel packages carried on two types of ships, a 1,050 TDW coastal freighter displacing 1,740 tonnes, and a 14,500 TDW general cargo vessel with a 22,243 tonne displacement. The following subsections discuss individual topics related to that methodology. Section 6.3 verifies Minorsky's correlation between the kinetic energy expended during a ship collision and his empirical resistance factor by reconsidering his original collisions. It further confirms his energy intercept, by applying the work of Lu and Calladine, and Wierzbicki and Thomas, to the estimation of hull damage energy for seven of his high energy collisions. In Section 6.4, new data is introduced from Marine Casualty reports published by the NTSB, and Minorsky's line is recalculated using the calculated hull damage energy as a constrained value for the intercept of the correlation. Section 6.5 derives a generalization of Akita's theoretical expression for the resistance factor and uses it to calculate the kinetic energy lost as a function of penetration depth during collisions. This is used with the updated Minorsky correlation to determine penetration depths into a small freighter and a larger general cargo vessel, when each is impacted by a number of ships having an empirically-based distribution of size, speed, and impact angle. Section 6.6 presents the probability of a striking ship reaching different depths of penetration into the struck ship for four cargo cases, and estimates the failure probability for an onboard spent fuel cask.

6.3 Minorsky's Correlation

In Minorsky's 1959 paper, he refers to data collected by the Coast Guard on 50 recent collisions, plus the *Stockholm–Andrea Doria* collision and two others that are only identified as tankers struck by passenger ships moving at high speed. From these 53 collisions, he selects 26 that have nearly right angled impacts, i.e., in the approximate range of 45° to 135°. For each, he calculates the energy loss during the collision and estimates a resistance factor related to the volume of steel structures damaged by the collision, not counting the side shell of the struck ship. As Figure 6-1 shows, when these two quantities are plotted as coordinates, the eight highest energy collisions and one representative low energy collision lie nearly on a straight line. In his paper, Minorsky notes that low-speed collisions generally fall above the line, which he attributes to a tendency on the part of ship's masters to under report their collision speed.

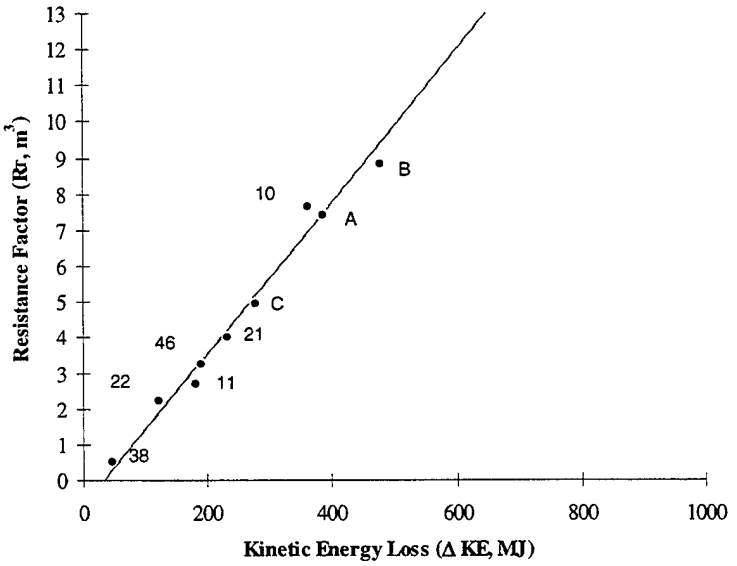

Figure 6-1. Minorsky's Original Correlation Plotted in SI Units.

6.3.1 Minorsky's Data Sources

Points on Minorsky's line are labeled #10, #11, #21, #22, #38, #46, and A, B, C. He mentions that one of the lettered points is the *Andria Doria–Stockholm* collision but does not further identify or give details about any of them. Since the relevant data was not published at the time of his paper, his work appears to lack independent reproducibility.

Appendix 4C of the Gibbs and Cox report [4] presents USCG data for ship accidents that occurred before the year 1958. Included are the names of the ships involved in the collision, their displacements at the time of the accident, and estimates of their speeds at impact, the impact angle, the penetration depth, and the height and width of damage at the hull. Entries in the appendix are sequentially numbered. Inspection of the appendix shows that Minorsky points and Appendix 4C entries identified by the same number have the same values for absorbed energy and damage volume. In this way, we determined that the six numbered points used in Minorsky's correlation of damage volume and absorbed energy represent the following six collisions:

#10 *Esso Greensboro–Esso Suez*	20 Apr 51	Gulf of Mexico
#11 *Tullahoma–P&T Adventurer*	4 Aug 51	North Pacific
#21 *Gulf Glow–Imperial Toronto*	4 Mar 52	Chesapeake Bay
#22 *Mojave–Prometed*	20 July 52	Atlantic Ocean
#38 *Catawba Ford–Hoegh Clair*	8 July 58	Pacific Ocean
#46 *David E Day–Marine Flier*	17 May 52	Pacific Ocean

Information relevant to these collisions is shown in SI units in Table 6-1.

Table 6-1. Information Abstracted From Gibbs & Cox [4]

Collision	Displacement (Tonne)	Speed (m/s)	Collision Angle (deg)	Damage Length (m)	Penetration Depth (m)	Damage Height (m)
Esso Greensboro	22,150	7.72	90	18.3	18.3	11.9
Esso Suez	19,813	7.72				
Tullahoma	22,252	5.14	90	6.10	7.62	11.9
P&T Adventurer	9,043	7.20				
Gulf Glow	22,252	0.00	65	6.10	11.6	12.2
Imperial Toronto	16,257	7.20				
Mojave	5,690	5.14	70	8.53	7.01	11.3
Prometed	16,257	7.20				
Catawba Ford	22,150	5.14	90	8.23	3.05	8.53
Hoegh Clair	6,706	4.11				
David E Day	8,840	8.38	55	10.7	5.18	14.6
Marine Flyer	20,728	8.49				

Minorsky's point B in Figure 6-1 was shown to be the *Andrea Doria–Stockholm* collision using data from a 1975 marine management symposium [17] and a textbook by William Hoffer [18].

#B *Andrea Doria–Stockholm*	25 July 56	Atlantic Ocean

Points A and C remain unidentified.

6.3.2 Kinetic Energy Loss

In perfectly inelastic collisions, the colliding objects couple and then move together with a single velocity after the collision. Minorsky assumed this model for his treatment of ship collisions, and by conservation of energy, he equates the kinetic energy lost during the event to the work done in damaging decks and structural members of the colliding vessels. He treats hydrodynamic forces through a virtual increase in the mass of the struck ship. His analysis is one-dimensional: the important motions take place transverse to the original direction of the struck ship and there is no consideration of roll, pitch, or yaw during the collision.

The work done in damaging structures during a collision is balanced by the kinetic energy lost, which is equal to the difference between the initial energy value for the striking ship, using the speed component perpendicular to the struck ship,

$$KE_{initial} = \frac{1}{2} MV^2 \sin^2\theta$$

and the final value for the merged system consisting of the striking ship, the struck ship, and the entrained water mass,

$$KE_{final} = \frac{1}{2}(M + m + dm)U^2$$

In these expressions, M is the displacement of the striking ship, m is the displacement of the struck ship, dm = 0.4 meter is the entrained water mass used to account for hydrodynamic forces, V is the speed of the striking ship, U is the terminal velocity of the system (the two ships after they become stuck together due to the collision), and θ is the collision angle (the angle between the initial directions of motion of the two ships).

The terminal velocity of the system, U, is found from momentum conservation

$$U = \frac{MV \quad \sin\theta}{M + m + dm}$$

Notice that the terminal velocity decreases when the mass of the struck ship increases, so that it is greater for smaller struck ships than for larger ones.

Combining these equations gives Minorsky's expression for the amount of kinetic energy (ΔKE) expended during the collision damaging ship structures

$$\Delta KE = \frac{M(m + dm)}{2(M + m + dm)} V \quad \sin^2\theta$$

Since this is also the amount of energy absorbed by damage to ship structures, it is important to understand how this quantity varies for different values of struck ship displacement. As is shown in Figure 6-2, for right-angle collisions of a 25,000-tonne striking ship moving at 5 meters per second with struck ships with displacements ranging up to 100,000 tonnes, direct calculation using the previous expression confirms that lost kinetic energy increases as the mass of the struck ship increases.

Because the amount of kinetic energy expended damaging ship structures increases with struck ship displacement, it follows that structural damage also increases with the mass of the struck ship. This is reasonable, but as a corollary it implies that *depth of penetration* during collisions is *smaller* for *lighter* struck ships, which might seem counter-intuitive.

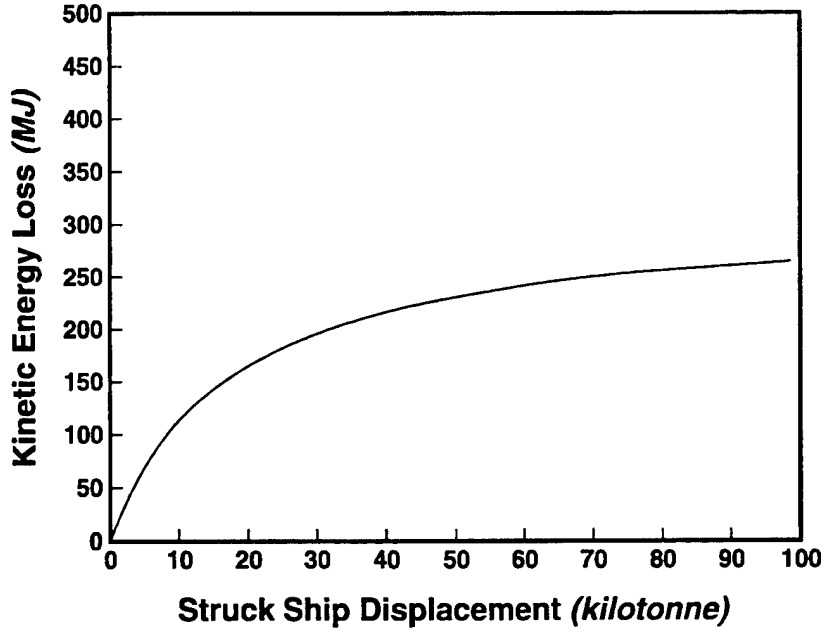

Figure 6-2. Variation of Absorbed Energy With Struck Ship Displacement for Right Angle Impacts by a 25,000-Tonne Striking Ship Moving at 5 Meters per Second.

6.3.3 The Collision Resistance Factor

Since collision resistance revolves essentially around the ability of structures to absorb energy, Minorsky considered only structural members having depth in the direction of collision. His resistance factor R_T can be written as

$$R_T = \sum_{i=1}^{N} P_i L_i t_i + \sum_{j=1}^{n} P_j L_j t_j$$

where the sums run over N members of the striking vessel and n members of the struck vessel and P denotes a penetration depth, L is a damage length, and t is a member thickness. The example resistance factor calculation in his paper uses only decks of the struck and striking ship, and 70 percent of the shell damage to the striking vessel. His paper mentions two other structures for which damage may be considered: transverse bulkheads (across the width of the struck ship) when hit squarely (edge-on), and longitudinal bulkheads (on the long axis) in the striking vessel.

6.3.4 Minorsky's Energy-Resistance Correlation

In his paper, Minorsky did not tabulate the values of the coordinates of the points that he plotted on his correlation. Therefore, in order to estimate the uncertainties in the slope and intercept of his correlation, coordinate values were determined by scaling from his plot. These values are presented in Table 6-2 for the nine points that enter his correlation. The points are identified with the same labels used in his paper, but the values are expressed in SI units.

Table 6-2. Coordinate Estimates for Nine Points that Enter Minorsky's Correlation

Point	Energy (MJ)	Resistance (m^3)
#10	360	7.65
#11	181	2.71
#21	227	4.01
#22	122	2.24
#38	46.7	0.47
#46	187	3.24
A	379	7.43
B	476	8.85
C	277	4.96

Minorsky used least squares regression analysis to obtain a formula for the linear relationship between kinetic energy loss (ΔKE) and collision resistance (R_T). His formula can be written in SI units as

$$\Delta KE\ [MJ] = 47.2\ R_T\ [m^3] + 32.7$$

Using the data in Table 6-2 and the program SIGMAPLOT [19], the standard error for the slope is found to be ± 2.4 MJ/m^3, while the corresponding standard error in the intercept is ± 13 MJ. Thus the slope is uncertain by ± 5 percent and the intercept by ± 40 percent.

6.3.5 Hull Penetration Energy

Because of the large uncertainty in Minorsky's intercept value, which accounts for damage to the shell of the struck ship, the energy absorbed due to shell damage was calculated directly and was then used to constraint the value of the intercept of Minorsky's correlation. To do this, it was assumed that the hull fails due to fracture driven by the prow of the striking ship, which because of the bow rake acts like a wedge driving downward through the plating from an initial region of penetration.

A number of experiments involving wedge-driven plate fracture were summarized by Lu and Calladine [11], who showed that in dimensionless form the work done by the wedge in these circumstances, $W/\sigma_y t^3$, is a function of the ratio l/t only, where l is the length of the cut, t is the thickness of the material, and σ_y is the material yield stress. From the data, they concluded the dimensionless work was nearly proportional to l/t raised to a power between 1.2 and 1.4, with proportionality constants in the range 0.9 to 3.5 depending on the material and test conditions. It was later shown analytically by Wierzbicki and Thomas [12] that an exponent value of 1.4 was preferred

$$\frac{W}{\sigma_y t^3} = C_1 \left(\frac{l}{t}\right)^{1.4}$$

They also showed that an expression could be derived for the constant C_1 in terms of a fracture parameter (the crack-opening displacement) and a friction coefficient

$$C_1 = 2.34 \mu^{0.4} \delta^{0.2}$$

where μ is the friction coefficient and δ is the crack-opening displacement. This expression is useful only when μ and δ are known quantities. For the present work, C_1 was set equal to the midpoint of the range of values reported by Lu and Caladine, namely 2.2.

The work done in damaging the struck ship hull was determined using this value of C_1 and the dimensionless work expression of Lu and Calladine, and Wierzbicki and Thomas. The values used for plate thickness and yield stress were 1.905 centimeters and 241 MPa, respectively. A damage height of 8.84 meters was used for the *Andria Doria*. Damage heights for the other six collisions were taken from Table 6-1. The resulting individual and average values for hull damage energy are shown in Table 6-3. All but one of the hull damage energies in this table fall within the 40% uncertainty estimated for Minorsky's intercept value (32.7 MJ ± 13.0 MJ).

Table 6-3. Hull Damage Energy for Seven High-Speed Ship Collisions

Collision		Damage Height (m)	Hull Damage Energy (MJ)
Esso Greensboro–Esso Suez	#10	11.9	30.2
Tullahoma–P&T Adventurer	#11	11.9	30.2
Gulf Glow–Imperial Toronto	#21	12.2	31.3
Mojave–Prometed	#22	11.3	28.1
Catawba Ford–Hoegh Clair	#38	8.53	18.9
David E Day–Marine Flyer	#46	14.6	40.2
Andria Doria–Stockholm	#B	8.84	19.9
Average Hull Damage Energy (MJ)			**28.4**

6.4 Verification of Minorsky's Equation

A number of high speed marine collisions have occurred since Minorsky's paper was published. Some of them can be included in Minorsky's correlation. Of 57 reports prepared by the National Transportation Safety Board for marine collisions in the period 1957 to 1993, only six describe two-ship collisions with impact angles in the range of 45° to 135° and collision speeds greater than ten knots, the kind of collisions which Minorsky found could be modeled by a linear correlation of damage volume with collision energy. The NTSB reports for some of these collisions did not contain all of the information required to calculate the values of the parameters that enter Minorsky's correlation, in particular ship displacements and penetration depths. ECO Inc. of Annapolis, Maryland, obtained the missing data from other sources or by estimation techniques [20]. ECO also supplied information for several other ship collisions for which NTSB reports were not available. Three of these other collisions meet the impact angle and speed criteria for entry into Minorsky's correlation. Data for the accidents reported by NTSB and the other three collisions described by ECO is shown below in Table 6-4.

Data was available for seven additional high-speed collisions. The names of the ships involved in these collisions and the reasons these collisions were not considered are:

Tien Chee–Roystonne Grange	Collision angle 40° (outside the 45°–135° range)
Candy Bar–Stolt Viking	Struck ship less than 500 tonne, aluminum hull
Cuyahoga–Santa Cruz II	Struck ship less than 500 tonne, collision angle 5°
Blackthorn–Capricorn	Collision angle 180°

Table 6-4. Data for High-Speed, Nearly Perpendicular Post-1970 Marine Accidents

Collision	Displacement (Tonnes)	Speed (m/s)	Collision Angle (deg)	Damage Length (m)	Penetration Depth (m)	Damage Height (m)
Oregon Standard	22,900	2.06	45	21.9	3.66	11.9
Arizona Standard	22,900	5.86				
Texanita	63,100	7.72	50	24.4	7.62	13.1
Oswego Guardian	112,000	8.23				
Esso Brussels	53,300	0.00	60	12.2	7.62	11.0
CV Sea Witch	27,100	7.97				
Regal Sword	35,300	6.17	60	45.7	6.10	7.62
Exxon Chester	37,200	5.14				
Trade Master	42,400	5.71	90	16.8	5.49	15.2
Pisces	31.600	5.92				
Hellenic Carrier	19,000	7.20	60	21.3	9.14	9.75
Lash Atlantico	45,300	9.26				
African Pioneer	18,900	7.72	45	24.4	9.14	10.1
Delta Norte	58,700	9.77				
Galvestonne	640	6.94	60	4.57	3.66	4.36
Atticos	17,500	5.40				
President Washingtonne	57,400	3.09	90	32.2	16.8	12.2
Hanjin Hongkong	28,200	5.14				

Sallee P–Coastal Transport	Struck ship less than 500 tonne
Harbel Tapper–Yankee	Striking ship less than 500 tonne
Camargue–Figaro	Collison angle 30°

The new collision data presented in Table 6-4 is pooled with the data in Table 1, and with a simplified version of Minorsky's resistance factor to recalculate Minorsky's correlation between energy loss and collision resistance. One simplification made was to assume there were no bulkheads involved in any of the identified events; another was to assume that all decks involved in any accident were penetrated to the same distance, which neglects the effect of bow rake. For all cases except the *Andria Doria*, the length of damage along the struck hull was assumed to be the same for all decks; for the *Andria Doria*, the damage is taken to follow an inverted triangular outline so the effective damage length is half the maximum value. All cases use the plate thickness value from the example in Minorsky's paper. With these simplifications, the resistance factor (volume of damaged steel) in the struck ship can be estimated as:

$$R_{\text{struck ship}} = nPLt$$

where n is the number of decks damaged in the struck ship, P is the depth of penetration into the struck ship, L is the horizontal length of damage, and t is the deck thickness used in Minorsky's example (0.83 inche = 0.021 meter). The penetration depths are shown in Tables 1 and 4 above. The values of n were estimated from the reported damage height and the type of struck ship; the specific values used for n are listed below in Table 6-5.

Table 6-5. Estimated Number of Decks Involved in High-Speed Accidents

Struck Ship - Striking Ship	Struck Ship Type	# Decks
Esso Greensboro–Esso Suez	T-2 Tanker	1
Tullahoma–P&T Adventurer	T-2 Tanker	2
Gulf Glow–Imperial Toronto	T-2 Tanker	2
David E Day–Marine Flyer	T-2 SE A1	2
Mojave–Prometed	Liberty	2
Andria Doria–Stockholm	Passenger	6
Catawba Ford–Hoegh Clair	T-2 Tanker	1
Oregon Standard–Arizona Standard	T-2 Tanker	1
Texanita–Oswego Guardian		3
Esso Brussels–CV Sea Witch	Container	4
Regal Sword–Exxon Chester	Bulk Carrier	1
Trade Master–Pisces	Bulk Carrier	3
Hellenic Carrier–Lash Atlantico	Freighter	2
African Pioneer–Delta Norte	Freighter	1
Galvestonne–Atticos	Bulk Carrier	1
President Washingtonne–Hanjin Hong Kong		1

For the striking ship, the example described in Minorsky's paper assumed a 5-foot (1.52 meter) high region of damage to the shell of the striking ship with a length that equaled the full penetration depth of the striking ship into the struck ship. The damage occurs at the level of the single deck in struck ship that was damaged by the collision. Minorsky took the projection of this damage in the direction of the collision, i.e., onto the center plane of the striking ship, as the contribution of damage to the striking ship to his resistance factor. Due to the bow angle of the striking ship, the projection of striking ship shell damage onto its center plane has a value equal to 70 percent of the actual damage to each outer shell of the striking ship. Thus, for the striking ship

$$R_{\text{striking ship}} = 1.4nHPt$$

Here the factor $1.4 = 2 \times 0.7$ accounts for the 70 percent projection factor applied to both sides of the striking ship, n is again the number of decks involved in the struck ship, H is 5 feet (1.52 meters), P is the penetration depth into the struck ship, and t is 0.6 inch (0.0152 meter), the side-shell thickness used in Minorsky's example. Table 6-6 shows the resulting values for resistance factor R and absorbed energy ΔKE for each of the 16 collisions used in the revalidation of Minorsky's correlation. In Table 6-6, the numbered points and point B are points that entered Minorsky's original correlation, and the lettered points are the new collisions that were added to see whether the correlation was sensitive to modern collisions.

With the energy intercept fixed at 28.4 MJ, the average value found in Section 6.3.5 for the work done penetrating (damaging) the shell of the struck ship, a least squares regression was used to find the slope of the best line through the expanded set of collision data. The regression value for the slope of this constrained linear correlation is 47.1 MJ/m^3, which is nearly the same as Minorsky's original slope (47.2 MJ/m^3). However, due to the greater spread in the extended set of collision data and the simplified

Table 6-6. High-Speed Marine Accident Coordinate Estimates

#	Struck Ship - Striking Ship	Kinetic Energy Loss (ΔKE, MJ)	Resistance Factor (R, m^3)
10	*Esso Greensboro–Esso Suez*	360	7.65
11	*Tullahoma–P&T Adventurer*	182	2.45
21	*Gulf Glow–Imperial Toronto*	227	3.73
22	*Mojave–Prometed*	122	2.98
38	*Catawba Ford–Hoegh Clair*	46.7	0.80
46	*David E Day–Marine Flyer*	187	2.67
B	*Andria Doria–Stockholm*	462	10.6
a	*Oregon Standard–Arizona Standard*	474	8.83
b	*Texanita–Oswego Guardian*	979	12.5
c	*Esso Brussels–CV Sea Witch*	210	6.07
d	*Regal Sword–Exxon Chester*	360	6.35
e	*Trade Master–Pisces*	539	8.82
f	*Hellenic Carrier–Lash Atlantico*	104	1.88
g	*Africa Pioneer–Delta Norte*	435	9.99
h	*Galvestonne–Atticos*	9.31	0.47
i	*President Washingtonne–Hanjin Hong Kong*	276	11.9

treatment used here in calculating collision resistance, the slope uncertainty is now ± 18.7 percent rather than ± 5 percent.

The regression line for the revalidated correlation is

$$\Delta KE\ [MJ] = 47.1\ R_T\ [m^3] + 28.4$$

The data points for the collisions tabulated in Table 6-6, and the constrained regression line fit to these points, are shown graphically in Figure 6-3.

Two points in Figure 6-3 have large deviations from the regression line. These are points b, the *Texanita–Oswego Guardian* collision, and i, the *President Washington–Hanjin Hong Kong* collision. There are two possible explanations for the large deviations of these points from the correlation line:

1. The simplified model used to find the resistance coordinate may not be applicable.
2. The data used to calculate the coordinates may contain relatively large errors.

At this time, it is not possible to decide between these possibilities. Since they deviate in opposite directions by approximately the same amount, the influence of these points on the regression fit tends to cancel. If in the future they were revised, either because better accident descriptions are obtained or a more detailed model is used for collision resistance, the stated uncertainty in the slope of the regression line would also decrease.

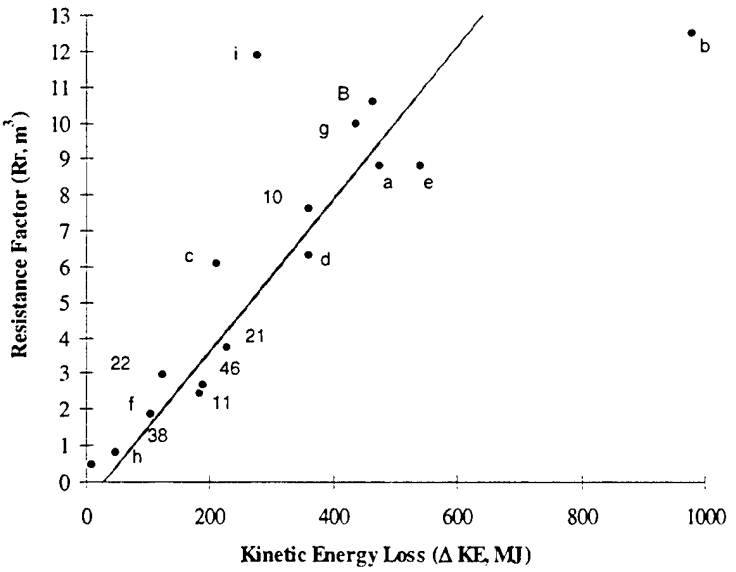

Figure 6-3. Energy Resistance Correlation for High-Speed Marine Collisions.

6.5 A Model for the Resistance Factor

To apply Minorsky's correlation of energy loss with the ship damage resistance factor to collisions that may occur sometime in the future, it is necessary to have a model for the resistance factor, i.e., an expression for the volume of steel damaged in the collision. This requires a relation between the penetration depth and damage length. The simplest supporting assumption is that the bow of the striking ship is approximately triangular and rigid, i.e., does not deform significantly during the collision.

An example of such a model was developed by Akita in his reports on large-scale experimental ship collisions [5, 6]. Akita assumed, discounting the motion of the struck ship, that in a perpendicular collision a rigid bow of half angle ϕ would create a triangular shaped damage region at each deck effected. The volume of steel damaged would equal the product of the steel thickness, the penetration depth, and half the damage length. In this case, however, the penetration depth and damage length are related by the equation

$$L = 2P \tan\phi$$

Therefore, there is a contribution to Minorsky's resistance factor equal to

$$R_T = \frac{1}{2} L \quad P \qquad t = P^2 t \tan\phi$$

This can be generalized to the case of non-right angle collisions by considering Figure 6-4. The area of triangle ABC is desired. The length of BD is the penetration P. Angle BDC is the collision angle θ and, following Akita, ϕ is the half angle at the bow (angle ABD). EF is denoted by b, the width of the collision bulkhead of the striking ship, and a coordinate system is set up with origin at the midpoint G of EF on the extension of BD.

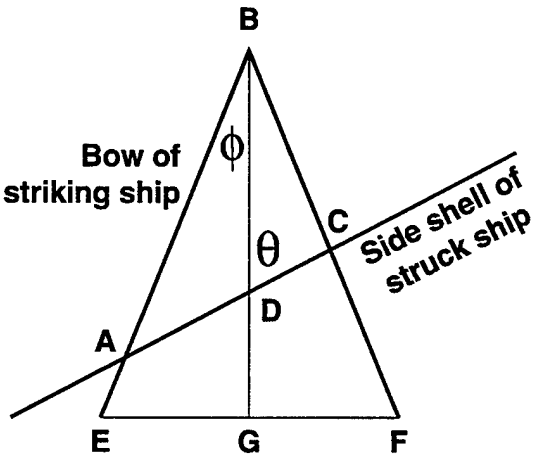

Figure 6-4. Penetration Geometry.

The line segments through AB, BC, and AC in Figure 6-4 have the following equations:

Line Segment	Equation
AB	$y_1 = [(b/2) + x]/\tan \phi$
BC	$y_2 = [(b/2) - x]/\tan \phi$
AC	$y_3 = x/\tan \theta + b/(2 \tan \phi) - P$

The x coordinate of point A is

$$x_L = -P/(1/\tan \phi - 1/\tan \theta)$$

and, similarly, the x coordinate of point C is

$$x_U = P/(1/\tan \phi + 1/\tan \theta)$$

With these definitions, the area of triangle ABD is found by integration from x_L to 0 of the height given by $(y_1 - y_3)$

$$\text{Area ABD} = \int_{x_L}^{0} (y_1 - y_3)\,dx$$

Similarly the area of triangle BCD is

$$\text{Area BCD} = \int_{0}^{x_U} (y_2 - y_3)\,dx$$

Substituting for y_1, y_2, and y_3 gives, after performing the integrals and combining terms

$$\text{Area ABC} = \frac{P^2 \tan \phi}{1 - (\tan^2 \phi / \tan^2 \theta)}$$

This result applies for $\phi < \theta$ and

$$P \le P_1 = \frac{b}{2}\left(\frac{1}{\tan\phi} - \frac{1}{\tan\theta}\right)$$

For somewhat deeper penetrations

$$P_1 \le P \le P_2 = \frac{b}{2}\left(\frac{1}{\tan\phi} + \frac{1}{\tan\theta}\right)$$

the lower limit of integration, X_L, changes to –b/2, with the following result for the collision area

$$\int_{-b/2}^{0}(y_1 - y_3)dx + \int_{0}^{X_U}(y_2 - y_3)dx = -\frac{b^2}{2}\left(\frac{1}{\tan\phi} - \frac{1}{\tan\theta}\right) + \frac{b}{2}P + \frac{P^2/\ 2}{\frac{1}{\tan\phi} + \frac{1}{\tan\theta}}$$

When $\theta < \phi$, shallow penetration will occur because now the corner (point A in Figure 6-5) rather than the leading edge (point B in Figure 6-5) of the bow of the striking ship will be the point that strikes the struck ship.

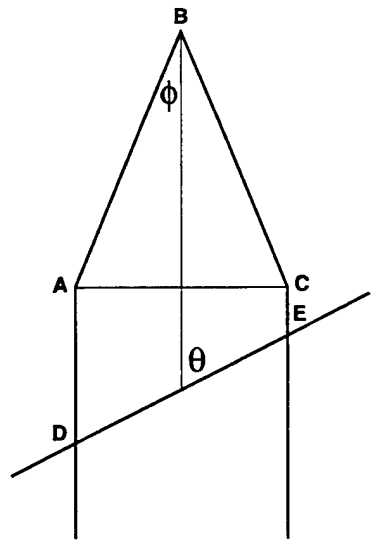

Figure 6-5. Deep Penetration Geometry.

For such collisions, $P_1 < P < 0$ and the collision area becomes

$$\int_{-b/2}^{X_L}(y_1 - y_3)dx = -\frac{b^2}{8}\left(\frac{1}{\tan\phi} - \frac{1}{\tan\theta}\right) + \frac{b}{2}P - \frac{P^2/\ 2}{\frac{1}{\tan\phi} - \frac{1}{\tan\theta}}$$

For penetrations beyond P_2, where the body of the striking ship has penetrated into the struck ship, as Figure 6-5 shows, the area becomes that of the triangular section ABC plus the quadrilateral ACED. In this case, the area is independent of θ.

The resistance factor related to this area is found by multiplying by the deck thickness to obtain a damage volume. The total resistance factor for the struck ship is the sum of similar terms for each deck, with allowance made for the effect of the rake angle of the striking ship. The rake angle α causes penetrations P_i for decks below the top of the damage region to be smaller than the maximum value P_0. Specifically, as Figure 6-6 shows, the penetration of lower decks is given by $P_i = P_0 - h_i/\tan \alpha$, where h_i is the distance the lower deck lies below the height at which maximum penetration occurs. If the deck has a hatch cover, no credit is taken for the resistance of the cover, and that portion of the intercepted area is discounted.

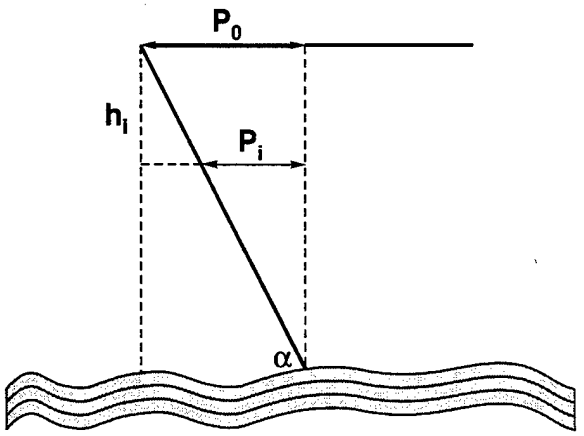

Figure 6-6. Lower Deck Penetration.

There is also a contribution to the total resistance from damage to the shell of the striking ship; in this sense, we are not using a completely rigid model for the bow. Here Minorsky's example calculation is followed by assuming that each deck struck by the penetrating bow of the striking ship produces a tear in the shell of the striking ship on both of its sides that has a length equal to the penetration distance of the striking ship bow into the struck ship and a height of 5 feet (1.52 meters). Minorsky's formula for the projection of this area in the direction of motion of the striking ship takes credit for only 70 percent of this damaged shell area. The contribution R_i from the i^{th} deck of the struck ship in damaging the hull of the striking ship is given by

$$R_i = 2(0.7)HP_it$$

where H = 5 feet (1.52 meters) is the damage height per deck, P_i is the penetration distance at the i^{th} deck of the struck ship, and t is the striking ship hull thickness, taken to be 0.6 inch (0.0152 meter).

6.6 Probabilistic Risk Analysis for a Small Coastal Freighter and a General Cargo Ship

The chance of damaging a radioactive material cask during a ship collision is examined for two break-bulk freighters, a 1,050-tonne TDW small coastal freighter and a larger 14,500-tonne TDW general cargo ship. Collision damage energy can be written as a function of penetration depth and collision angle by combining the resistance factors from Section 6.5 with the constrained least squares regression of Section 6.4. Similarly, when collision damage energy is equated to the kinetic energy loss for inelastic collisions, as in Section 6.3.2, it is related to the displacement of the ships, and the collision speed and impact angle. In principle then, we have a (non-linear) relationship among the variables which can be numerically solved for penetration depth when the following quantities, the ship displacements, impact

speed, beam width, and bow, rake, and collision angles are specified. Just that method is used below to numerically determine a probability distribution for penetration depth in marine accidents from probability distributions for striking ship displacement, collision speed, and impact angle. For each type of ship, generic values are used for beam width, bow half angle, bow rake angle, and displacement.

6.6.1 Deck Specifications

To apply the theoretical resistance factor to these two ships, several pieces of information are required, among them are the width, thickness, and distance below the main deck of all decks involved in a collision. This information is given in Tables 6-7a and 6-7b for both ships. Some decks are given a small width because no credit is taken for the resistance of hatch covers.

Table 6-7a. Deck Specifications for a Small Coastal Freighter

Deck #	Distance Below Main (meter)	Width (meter)	Thickness (meter)
1	0.00	1.25	0.008
2	1.68	0.75	0.007
3	2.91	0.75	0.007
4	4.77	10.0	0.010
5	5.90	10.0	0.009

Table 6-7b. Deck Specifications for a General Cargo Ship

Deck #	Distance below Main (meter)	Width (meter)	Thickness (meter)
1	0.00	2.50	0.019
2	3.33	2.50	0.019
3	6.67	2.50	0.019
4	10.0	2.50	0.019
5	12.9	25.0	0.019
6	14.2	25.0	0.019

6.6.2 The World Fleet

Information supplied by ECO Inc. suggests that the world merchant fleet at sizes above approximately 1,000 gross tonnes can be grouped into four types: tanker/bulker, general cargo, container ship, and passenger ship. These four types comprise, respectively, about 45 percent, 42.8 percent, 10.7 percent, and 1.5 percent of the fleet. The probabilistic analysis uses distributions of vessel displacement, collision speeds, and impact angles derived from a report by ORI Incorporated [21]. The distributions are presented in Tables 6-8a, 6-8b, and 6-8c. Collision angles are measured from the direction of the struck ship to the direction of the striking ship, which is the complement of the angle used by ORI. Angles are only specified for the first quadrant because the distribution is symmetric about 90 degrees.

Representative (generic) values for beam and bow angle based on general ship design practice can be associated with the ship displacements for each of the four ship types [20]. Table 6-9 shows the bow angles used for the different sizes and types of ships.

Representative values of the (maximum) beam were also developed for each ship type and size. They are tabulated in Table 6-10. The width at the collision bulkhead is taken to be half the beam value.

Table 6-8a. Conditional Accident Probability versus Displacement

Striking Ship Displacement (Tonne)	Probability of Occurrence
0 – 10,160	0.15
10,160 – 20,320	0.25
20,320 – 30,480	0.25
30,480 – 40,640	0.05
40,640 – 50,800	0.05
50,800 – 60,960	0.05
60,960 – 71,120	0.10
70,120 – 81,280	0.05
81,280 – above	0.05

Table 6-8b. Conditional Accident Probability versus Ship Speed

Speed (meters per second)	Probability of Occurrence
0 – 1.028	0.0448
1.028 – 2.058	0.2538
2.058 – 3.087	0.1045
3.087 – 4.115	0.1343
4.115 – 5.144	0.1343
5.144 – 6.173	0.0896
6.173 – 7.202	0.0746
7.202 – 8.231	0.0597
8.231 – 9.260	0.0746
9.260 – 10.29	0.0149
10.29 – 11.32	0.0149

Table 6-8c. Conditional Accident Probability versus Collision Angle

Collision Angle (degrees)	Probability of Occurrence
0 – 10	0.0434
10 – 20	0.0435
20 – 30	0.1303
30 – 40	0.0724
40 – 50	0.1015
50 – 60	0.1305
60 – 70	0.0725
70 – 80	0.1305
80 – 90	0.2754

Table 6-9. Representative Bow Half Angles for Ships of Different Size and Type

Displacement (Tonne)	Tanker/Bulker	General Cargo	Container Ship	Passenger
0 – 10,160	28	29	17	17
10,160 – 20,320	30	20	17	17
10,320 – 30,480	30	20	17	17
30,480 – 40,640	38	20	17	17
40,640 – 50,800	38	20	17	17
50,800 – 60,960	38	20	17	17
60,960 – 71,120	38	20	17	17
71,120 – 81,280	38	20	17	—
81,280 – above	38	20	17	—

Table 6-10. Representative Ship's Beam for Vessels of Different Size and Type

Displacement (Tonne)	Tanker/Bulker (meter)	General Cargo (meter)	Container Ship (meter)	Passenger (meter)
0 – 10,160	13	13	13	15
10,160 – 20,320	20	20	20	20
10,320 – 30,480	23	23	23	23
30,480 – 40,640	26	26	26	26
40,640 – 50,800	29	29	29	29
50,800 – 60,960	32	32	32	32
60,960 – 71,120	34	32	32	34
71,120 – 81,280	35	32	32	—
81,280 – above	38	32	32	—

6.6.3 Risk Calculations

Calculations of penetration depth, P, are here performed by solving an equation expressing conservation of energy. It is derived by replacing ΔKE in the revalidated Minorsky correlation that was developed using a constrained intercept with the expression for kinetic energy loss for inelastic collisions presented in Section 6.3, and adding a term that represents the work done compressing cargo

$$\frac{M(m+dm)}{2(M+m+dm)}V\sin^2\theta = \quad \Delta \quad KE = 47.1R_T(P) + 28.4 + W_{cargo}(P)$$

where R_T is the collision resistance factor of Section 6.4, and W_{cargo} is work done on the cargo.

The work done in cargo compression is zero until the inter-cargo space goes to zero, i.e., the cargo "goes solid." After that, W_{cargo} is taken proportional to the amount of compression in the direction of the collision. Following ORI [21], the energy expended compressing cargo is calculated using the equation

$$W_{cargo} = A\sigma(P - fB)$$

where A is the area of the surface compressing cargo (i.e., the effective surface area of the deformed bow of the striking ship), σ is the crush strength of the cargo, P is the penetration distance into the struck ship, f is the fraction of the width (beam) of the struck ship that is empty (i.e., the fraction of the space both within and between cargo along the beam of the struck ship that is not occupied by material), and B is the beam (width) of the struck ship. Thus, fB is the penetration distance that will use up all the empty space along the beam of the struck ship, A is the compressive force applied to the cargo after it goes solid, and P – fB is the distance over which that force acts. Again following ORI's development, the compressive surface area A is assumed to increase linearly with penetration depth P, the maximum compression surface area is assumed to equal one-third of the cross-sectional area of the striking ship at a distance back from its bow equal to one-tenth of its length (the usual location of the collision bulkhead), and this maximum is assumed to be attained when penetration distance is equal to the beam of the struck ship. This leads to the expression

$$A = (P/B)\ (1/3)\ H\ (L/10)\ 2\tan\phi$$

where H, L, and φ are respectively the height, length, and bow half-angle of the striking ship. Because cargo compression takes place over a small distance, P is approximated by fB (the position at which cargo compression starts) in the expression for A. For purposes of estimating W_{cargo}, we fixed the height of the compressed portion of the bow and the length and bow half-angle of the striking ship to the values used by ORI, respectively, 7.62 meters, 165.8 meters, and 26 degrees.

Substituting these values and combining the expressions above gives

$$W_{cargo} = 19.44\ f\ \sigma\ (P - fB)$$

where W_{cargo} is in MJ, σ is in MPa, and P and B are in m.

The energy conservation expression is an implicit non-linear relation between ship displacements, collision speed, collision angle, bow angle, rake angle, beam at the collision bulkhead, cargo characteristics, and the collision penetration depth. It was solved iteratively for penetration depth by Newtonne's method or in some cases by binary search. The calculation was repeated for each of the four

ship types for all combinations of displacement, speed and collision angle shown in Tables 6-8a, 6-8b, and 6-8c (intervals were represented by the value at their midpoint). In all, there were 3,366 calculations in a set. The results were binned in one-meter intervals to produce histograms of frequency versus penetration depth. The complete set of calculations was repeated for four cargo cases: none, light, medium, and heavy in which the cargo was characterized by different values of the one-dimensional packing fraction f, and crush strength as shown in Table 6-11.

Table 6-11. Cargo Model Characteristics

Cargo Type	1-D Packing Fraction	Crush Strength (MPa)
None	1.0	0.0
Light	0.6	6.8
Medium	0.2	34.5
Heavy	0.5	1500

The resulting distributions of penetration depth are shown for each cargo case in Table 6-12 for the 1,050-tonne TDW coastal freighter and in Table 6-13 for the 14,500-tonne TDW general cargo ship.

6.6.4 Loads on the Fuel Package During the Collision

Two mechanisms are considered by which damage to the contents of RAM packages on board the struck ship might occur. In the first mechanism, accelerations arising from the collision of the ships, if there is a lot of open space in the package interior, might damage the material inside the packages without directly failing the packages themselves. Because of the considerable openness of fuel assemblies, fuel rod flexibility, and the susceptibility of spacer grids to collapse, some spent nuclear fuel might be released to the cask interior in this way (plutonneium oxide powder in 6M-2R containers would not be subject to this kind of release). In the second mechanism, crushing of the package itself is the process by which the contents might be damaged.

6.6.4.1 LOADS DUE TO ACCELERATIONS

There are potential failure mechanisms for spent-fuel rods that can occur inside transportation casks subjected to large accelerations. The most significant is from the extension of prior-existing partial cracks in the cladding, which are known to exist as a combined result of irradiation, the chemical activity of fission products, and thermal cycling during the time the fuel is present in an operating nuclear reactor. Other forms of RAM (e.g., Pu containers) are not subject to these failures. The initiating event for such crack extension would be application of a pinch load at the crack site due to rod-to-rod impact or hard contact of the rod with the interior of the cask shell. Such severe impacts do not normally occur during spent fuel handling and transport. It was shown in Sanders et al. [22], however, that under accident conditions corresponding to a nine-meter drop onto an unyielding target, one of the regulatory tests, there is a small but significant probability (up to $\sim 10^{-4}$ per rod at 27°C ambient), either because of rod flexure or the collapse of fuel assembly spacer grids, that the applied loads would result in crack extension completely through the cladding wall. This would result in a pinhole crack or slit with subsequent rod depressurization and the release of radioactive gases and aerosols to the interior of the cask. Such impacts would also likely spall some cobalt-60 bearing iron oxides, called "CRUD," if the fuel rods or cask interior surfaces carried this form of external contamination [23, 24].

Table 6-12. Probability of Various Penetration Depths for Collisions with a Struck Ship Displacing 1,740 Tonnes for Four Cargo Cases, Conditional on the Occurrence of the Collision

Penetration (meter)	No Cargo	Light Cargo	Medium Cargo	Heavy Cargo
0.0	0.800	0.800	0.800	0.800
0.0 – 1.0	0.000	0.000	0.000	0.000
1.0 – 2.0	0.012	0.012	0.073	0.012
2.0 – 3.0	0.015	0.015	0.124	0.015
3.0 – 4.0	0.022	0.022	0.000	0.026
4.0 – 5.0	0.016	0.024	0.000	0.143
5.0 – 6.0	0.024	0.051	0.000	0.000
6.0 – 7.0	0.019	0.071	0.000	0.000
7.0 – 8.0	0.013	0.002	0.000	0.000
8.0 – 9.0	0.016	0.000	0.000	0.000
9.0 – 10.0	0.020	0.000	0.000	0.000
Beyond 10	0.040	0.000	0.000	0.000

Table 6-13. Probability of Various Penetration Depths for Collisions with a Struck Ship Displacing 22,234 Tonnes for Four Cargo Cases Conditional on the Occurrence of the Collision

Penetration (meter)	No Cargo	Light Cargo	Medium Cargo	Heavy Cargo
0.0	0.483	0.483	0.483	0.483
0.0 – 2.5	0.058	0.058	0.068	0.058
2.5 – 5.0	0.099	0.099	0.175	0.099
5.0 – 7.5	0.087	0.087	0.224	0.090
7.5 – 10.0	0.060	0.061	0.040	0.066
10.0 – 12.5	0.053	0.058	0.008	0.196
12.5 – 15.0	0.043	0.057	0.001	0.005
15.0 – 17.5	0.027	0.062	0.000	0.000
17.5 – 20.0	0.025	0.021	0.000	0.000
20.0 – 22.5	0.015	0.010	0.000	0.000
22.5 – 25.0	0.013	0.002	0.000	0.000
Beyond 25.	0.036	0.001	0.000	0.000

In this section, it is shown that the average acceleration experienced in ship collisions is very small, usually below 1 g. Since the impacts modeled by Sanders et al. for a nine-meter drop produce accelerations on the order of 100 g, it is concluded that ship collisions will not produce the loads required

to fail any fuel rods. The acceleration resulting in a ship collision is the time derivative of the transverse speed of the struck ship

$$a = \frac{dv}{dt} = \frac{dv}{dx}\frac{dx}{dt} = v\frac{dv}{dx}$$

Combining the conservation laws for momentum and energy yields a quadratic expression for the transverse speed of the struck ship during the collision, which can be solved for v

$$v = \frac{V_0 \sin\theta}{A} - \frac{1}{A}\sqrt{V_0^2 \sin^2\theta - \frac{2AW(x)}{m + dm}}$$

where $A = 1 + (m + dm)/M$, and $W(x)$ represents the work done during penetration of struck ship to the distance x. Equating $W(x)$ to the revalidated, modified Minorsky correlation and differentiating with respect to x leads to the following expression for the acceleration at x

$$a(x) = \frac{v(x)F(x)/(m + dm)}{\sqrt{V_0^2 \sin^2\theta - \frac{2AW(x)}{m + dm}}}$$

where

F(x) = dW(x)/dx
m = the displacement of the struck ship
dm = the mass of entrained water
V_0 = the component of the striking ship velocity transverse to the direction of motion of the struck ship
θ = the impact angle.

Notice that the acceleration peaks at the end of the collision. In this perfectly inelastic model, the acceleration has a vertical asymptote at the maximum distance of penetration; the average acceleration (a), however, remains small.

$$\langle a \rangle = \frac{\int_0^P a(x)dx}{\sqrt{P}} = \frac{V_0^2 \sin^2\theta}{2PA^2}$$

where P is the maximum penetration depth. This is an improper integral since $a(x)$ has a singularity at P. However, the integrand increases sufficiently slowly in the neighborhood of P, like $(P - x)^{-1/2}$, for the integral to converge. Average accelerations were presented in another report for each cargo case using the distributions of ship displacement, collision speed and impact angle presented in Section 6.5.1 above [25]. The largest average accelerations calculated for any set of input parameter values were always less than 1 m/s^2 for the no and light cargo cases, and less than 2 m/s^2 for the medium and heavy cargo cases. Because these accelerations are only a small fraction (about 1 percent) of the accelerations treated by Sanders et al. [22], the impact forces generated by ship collisions are not expected to damage the contents of any RAM transport casks carried on the struck ship.

6.6.4.2 CRUSH LOADS ON THE FUEL PACKAGE DURING THE COLLISION

A typical spent fuel package is the Pegase shipping cask, a transport cask of French design [26] that has been used for maritime shipments. It is a lead shielded truck cask, with a mass of 18.9 tonnes, a diameter of 1.875 meters, and a height of 2.239 meters. It has a body composed of two stainless steel shells built around a lead shield. It is designed to carry fuel or other radioactive material in baskets of differing design which fit into the cylindrical cavity of the cask. A detailed analysis of the mechanical response of the Pegase cask to crush forces is not available, however, it is similar in construction to the lead shielded truck cask analyzed by 2D finite element calculation in the study of Fisher et al. [27]. Their result is shown in Figure 6-7.

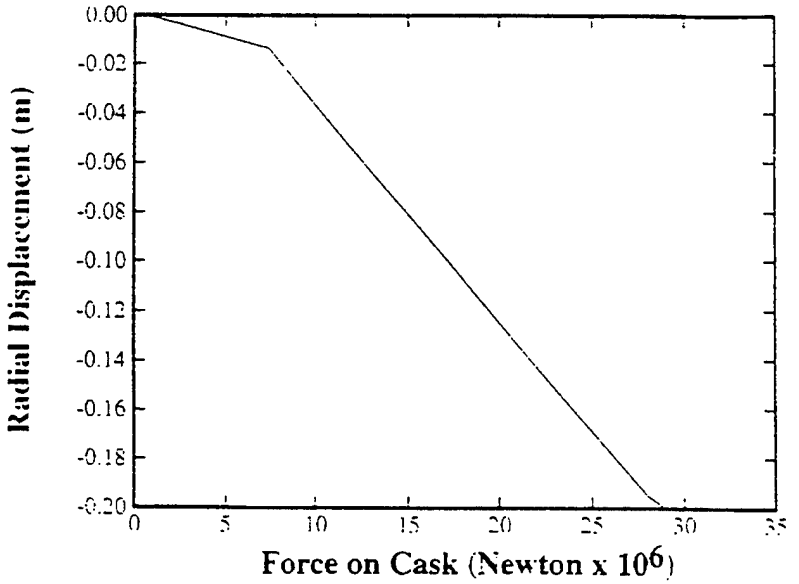

Figure 6-7. Generic Truck Cask Force Displacement Characteristics.

Fisher's curve is for static force versus deflection for sidewise loading of a truck cask that was 4.9 meters high, with a 0.133-meter-thick lead shield enclosed by an outer layer of stainless steel 0.0318 meter thick and an inner layer 0.0127 meter thick. Since his calculation is two-dimensional, however, it does not account for the extra rigidity provided to the cask body by the ends of the cask. Thus, it gives a conservative estimate of the axial displacements and is most applicable near the middle of the cask. Fisher's results show that it requires a load of about 8.9×10^6 Newtonnes to produce a deflection of the cask body of 0.0254 meter.

This deflection, 0.0254 meter, is judged to be a conservative estimate of the deflection that could occur without damage to the fuel. Said another way, a sidewise cask loading on a Pegase cask with a magnitude greater than or about 10^7 Newtonnes will probably result in some disruption of the fuel. Now the question is, can crush forces on the cask as high as 10 million Newtonnes be produced in a ship collision? To the extent that the homogeneous cargo models are applicable, the answer is yes. The one dimensional pinch force applied by the cargo in these models, after closeup, is approximately equal to

$$F_{cargo} = \sigma h d$$

where

σ = the cargo crush strength
hd = the cross sectional area of the cask

for the Pegase cask

$hd = 4.198\ m^2$

Thus the force in the light cargo case is about 30 million Newtonnes, and for the medium and heavy cargo cases, it is many times larger. These values so far exceed the cask damage threshold of approximately 10 million Newtonnes that damage to the fuel and cask can be expected unless these loads are relieved by the collapse of ship structures.

But if the cargo does not close up, because the penetration is shallow or there is no other cargo in the hold, the cask does not see this force. Then, unless the cask is within the penetration region of the striking ship, it will not be significantly affected.

Inside the penetration region, the cask can be crushed without the cargo going solid, even if there is no other cargo in the struck hold. Cask tiedowns are required, under United States regulatory practice, to withstand about 5 million Newtonnes of transverse force [28]. The difference between this value and the approximately 10 million Newtonnes required to produce a 0.0254-meter deflection in the cask wall of the generic cask is not considered significant since overdesign of the tiedowns is a possibility. Moreover, in ORI's opinion, the RAM cask could conceivably be restrained from sliding, even in an empty hold, after the tiedowns have failed [21], if a deck buckled up behind the cask and thus acted like an infinitely strong tiedown.

The preceding analysis indicates that there are two cases to consider for cask failure due to crush forces. In the first case, the penetration depth exceeds the cargo closeup distance (the penetration distance at which cargo compression causes the cargo in the hold to go solid about the cask); in the second case, the penetration distance exceeds the cask stowage location, that is, the cask location is overrun. Fuel damage and cask closure failure are possible for both types of events. For cask overrun, two subcases are possible, (1) cask tiedowns hold and overrun occurs when penetration reaches the initial stowage location of the cask; and (2) cask tiedowns fail and overrun occurs when penetration pushes the cask against the far shell of the hold.

Tables 6-14a through d present the probability of cask crush when the cask tiedowns hold and when they fail for two break-bulk freighters with displacements of 1,740 and 22,243 tonnes. The results presented in Tables 6-14a through d assume that the cask is stowed at the centerline of the RAM transport ship, with its height (length) oriented along the beam of the ship. Thus, overrun of the initial stowage location for the cask occurs at $b/2 - h/2$,where b is the beam of the RAM transport ship and h is the height of the spent fuel cask. The probability of cask overrun when tiedowns are assumed to hold is found by summing the penetration depth probabilities in Tables 6-12 and 6-13 beginning with the bin containing $b/2 - h/2$. The probability of cask overrun when tiedowns are assumed to fail is found by summing the penetration depth probabilities in Tables 6-12 and 6-13 beginning with the bin containing $b - h$. When the summations were performed, in order to avoid double counting, for collisions where both cask overrun and cargo closeup occur in the same bin, that is, at about the same penetration distance, the possibility of cask crush was charged to cask overrun.

The results for a 1,050 TDW freighter displacing 1,740 tonnes when the tiedowns hold are shown in Table 6-14a. With no or only light cargo present, there is about a 15.2 percent chance of cask failure due to cask overrun, given a collision that strikes the hold containing the cask. For heavy cargo, the chance

of cask overrun when the tiedowns hold is 14.7 percent. For the medium cargo case, cask overrun is not predicted to occur. Table 6-14c presents the results when tiedowns hold for the larger 14,500 TDW cargo vessel, displacing 22,243 tonnes. This table shows that this ship is more deeply penetrated because of its greater inertia and hydrodynamic drag, and that cask failure due to overrun can occur in all cargo cases except the medium cargo case: 17.4 percent for no cargo case, 17.1 percent for light cargo, 0.0 percent for medium cargo, and 13.1 percent for heavy cargo. Tables 6-14b and 6-14d, respectively, present the results for the 1,050 TDW freighter and 14,500 TDW cargo vessel when the cask tiedowns fail and sliding of the cask is not prevented by some obstruction, for example, upward buckling of the deck. These tables show that when tiedowns are assumed to fail, cask overrun is much less likely. Specifically, when tiedowns fail, overrun is never predicted if cargo is present in the hold and if no cargo is present, then cask overrun occurs only 7.9 percent of the time for the 1,050 TDW freighter and 4.8 percent of the time for the 14,500 TDW cargo vessel.

The cargo closeup distance is fb, where f is the packing fraction (fraction of space in the direction of the beam that is empty) and b is the beam of the ship. As with cask overrun, summing over the tail of the penetration depth distributions (Tables 6-12 and 6-13) beginning with the bin at fb, gives the estimated failure probability due to cargo closeup. The results are shown in the second row of the Tables 6-14a, b, c, and d. When tiedowns hold, for both the 1,050 TDW freighter and the 14,500 TDW cargo vessel, the probability that the cargo goes solid due to closeup around the cask are 0.0 percent for light and heavy cargo, and 12.4 percent and 27.4 percent respectively for medium cargo. When the tiedowns are assumed to fail, cargo closeup occurs for light, medium, and heavy cargo 9.6 percent, 27.4 percent, and 0.5 percent of the time for the 1,050 TDW freighter, and 7.3 percent, 12.4 percent, and 0.0 percent of the time for the 14,500 TDW cargo vessel.

Table 6-14a. Probability of Initiating a Cask Crush Event in the 1,740 Tonne (1,050 TDW) Freighter Given that a Collision has Occurred and Cask Tiedowns Hold

Event	No Cargo	Light Cargo	Medium Cargo	Heavy Cargo
Cask Overrun	0.152	0.152	0.000	0.147
Cargo Goes Solid	0.000	0.000	0.124	0.000
Total Probability	0.152	0.152	0.124	0.147

Table 6-14b. Probability of Initiating a Cask Crush Event in the 1,740 Tonne (1,050 TDW) Freighter Given that a Collision has Occurred and Cask Tiedowns Fail

Event	No Cargo	Light Cargo	Medium Cargo	Heavy Cargo
Cask Overrun	0.079	0.000	0.000	0.000
Cargo Goes Solid	0.000	0.073	0.124	0.000
Total Probability	0.079	0.073	0.124	0.000

Table 6-14c. Probability of Initiating a Cask Crush Event in the 22,243 Tonne (14,500 TDW) Freighter Given that a Collision has Occurred and Cask Tiedowns Hold

Event	No Cargo	Light Cargo	Medium Cargo	Heavy Cargo
Cask Overrun	0.174	0.171	0.000	0.131
Cargo Goes Solid	0.000	0.000	0.274	0.000
Total Probability	0.174	0.171	0.274	0.131

Table 6-14d. Probability of Initiating a Cask Crush Event in the 22,243 Tonne (14,500 TDW) Freighter Given that a Collision has Occurred and Cask Tiedowns Fail

Event	No Cargo	Light Cargo	Medium Cargo	Heavy Cargo
Cask Overrun	0.048	0.000	0.000	0.000
Cargo Goes Solid	0.000	0.096	0.274	0.005
Total Probability	0.048	0.096	0.274	0.005

6.7 References

1. *Casualty Statistics and Investigations: Database on Very Serious Casualties*, FSI 3/INF.8, IMO. International Maritime Organization, November 1994.

2. N. Jones, "Structural Aspects of Ship Collisions," in *Structural Crashworthiness*, N. Jones and T. Wierzbicki, Butterworths, London, England, 1983.

3. V. U. Minorsky, "An Analysis of Ship Collisions with Reference to Protection of Nuclear Power Plants," in *Journal of Ship Research*, October 1959.

4. *Criteria for Guidance in the Design of Nuclear Powered Merchant Ships*, Appendix 4-C. Gibbs & Cox Inc., New York, NY, May 1961.

5. Y. Akita et al., "Studies on Collision Protection Structures in Nuclear Powered Ships," in *Nuclear Engineering and Design*, vol. 19, 1972.

6. Y. Akita and K. Kitamura, "A Study on Collision by an Elastic Stem to a Side Structure of Ships," in *Transactions of Society of Naval Architecture of Japan*, vol. 131, 1972.

7. G. Woisin, "Die kollisionsversuche der GKSS," in *Jahrbuch STG*, vol. 70, 1976.

8. G. Woisin, "Die kollisionsversuche der GKSS," in *Schiff und Hafen*, vol. 20, 1977.

9. T. Hysing, *Impacts and Collisions Offshore, Progress Report No. 4, Analysis of Penetration of Hull*, VERITAS 78-433. Det Norske Veritas, July 1978.

10. Martin Petersen, "Dynamics of Ship Collisions," in *Ocean Engineering*, vol. 9, 1982.

11. G. Lu and C. R. Calladine, "On the Cutting of a Plate by a Wedge," in *International Journal of Mechanical Science*, vol. 32, 1990.

12. T. Wierzbicki and P. Thomas, "Closed-Form Solution for Wedge Cutting Force through Thin Metal Sheets," in *International Journal of Mechanical Science*, vol. 35, 1993.

13. P. Thomas and T. Wierzbicki, "Grounding Damage to Double Hull Tank Vessels," in *Proceedings of the Second International Offshore and Polar Engineering Conference*, San Francisco, CA, 1992.

14. P. Y. Chang et al., "A Rational Methodology for the Prediction of Structural Response due to Collisions of Ships," in *Transactions of SNAME*, vol. 88, 1980.

15. H. Lenselink et al., "Numerical Simulations of Ship Collisions," in *Proceedings of the Second International Offshore and Polar Engineering Conference*, San Francisco, CA, 1992.

16. V. L. Porter, "Structural Response and Evaluation of an INF Class 1 Freighter Impacted by Another Ship," Sandia National Laboratories memorandum to D. J. Ammerman, August 11, 1995.

17. *Proceedings of the National Symposium on Marine Transportation Management*, April–May 1975. College of Marine Studies, University of Delaware, November 1975.

18. W. Hoffer, *Saved! The Story of the Andrea Doria*, Summit Books, New York, NY, 1979.

19. J. Kuo, *SIGMAPLOT User Manual*, Revision SPM-1.1. Jandel Scientific Corporation, March 1993.

20. V. Keith, R. Heid, and R. Vann, *Technical Support for Risk Analysis and Shipment of Plutonneium by Sea*. ECO Inc., Annapolis, MD, November 1995.

21. *Hazardous Environments Experienced by Radioactive Material Packages Transported by Water*. ORI Incorporated, Silver Spring, MD, October 1980.

22. T. L. Sanders et al., *A Method for Determining the Spent-Fuel Contribution to Transport Cask Containment Requirements*, SAND90-2406. Sandia National Laboratories, Albuquerque, NM, 1992.

23. R. P. Sandoval et al., *Estimate of CRUD Contribution to Shipping Cask Containment Requirements*, SAND88-1358. Sandia National Laboratories, Albuquerque, NM, 1991.

24. T.L . Sanders et al., *A Methodology for Estimating the Residual Contamination Contribution to the Source Term in a Spent-Fuel Transport Cask*, SAND90-2407. Sandia National Laboratories, Albuquerque, NM, 1991.

25. J. Sprung et al., *Radiological Consequences of Ship Collisions That Might Occur in U.S. Ports During the Shipment of Foreign Research Reactor Spent Nuclear Fuel to the United Sates in Break-Bulk Freighters*, SAND96-0400. Sandia National Laboratories, Albuquerque, NM, 1996.

26. "Certificate of Approval of Package Design," F/007/B(U)-F D00. Ministry of Public Facilities, Housing, Territorial Development and Transportation, French Republic, May 1988.

27. L. E. Fisher et al., *Shipping Container Response to Sevcre Highway and Railway Accident Conditions*, NUREG/CR-4829. Lawrence Livermore National Laboratory, Livermore, CA, February 1987.

28. "Packaging and Transportation of Radioactive Material," U.S. Code of Federal Regulations, Title 10, Part 71, revised 1990.

7. PROBABILITY OF A SEVERE ENGULFING FIRE

Figure 7-1 presents a side view of the layout of the 14,500 TDW break-bulk freighter for which ship collision penetration depths were estimated using the revalidated, modified Minorsky correlation developed in Section 6.0.

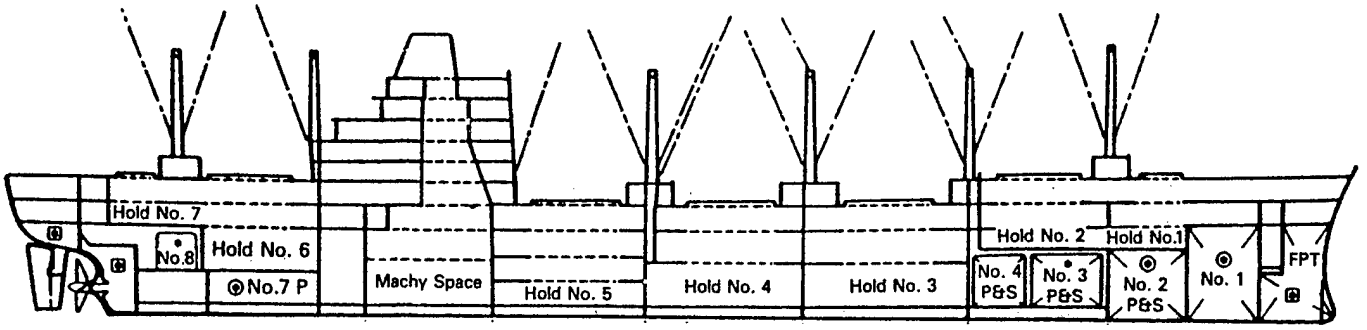

Figure 7-1. Side View of a 14,500 TDW Break-Bulk Freighter.

Figure 7-1 shows that a break-bulk freighter may be viewed as a set of holds (h) and decks (d) that define the locations (L_{hd}) of a set of compartments. For example, if superstructure is ignored, the machinery space is treated as a hold, and each hold is assumed to have four decks, then, as is shown in Figure 7-2, the break-bulk freighter examined using Minorsky's collision correlation can be represented as a 4 by 8 matrix of compartments.

Decks (d)								
4	L_{84}	L_{74}	L_{64}	L_{54}	L_{44}	L_{34}	L_{24}	L_{14}
3	L_{83}	L_{73}	L_{63}	L_{53}	L_{43}	L_{33}	L_{23}	L_{13}
2	L_{82}	L_{72}	L_{62}	L_{52}	L_{42}	L_{32}	L_{22}	L_{12}
1	L_{81}	L_{71}	L_{61}	L_{51}	L_{41}	L_{31}	L_{21}	L_{11}
	8	7	6	5	4	3	2	1
	Holds (h)							

Figure 7-2. Schematic Representation of the Holds and Spaces in a Break-Bulk Freighter.

7.1 Fire Spread Model

Consider a break-bulk freighter that is transporting RAM in a transportation cask. Suppose that the freighter is struck by another ship and that the prow of the striking ship penetrates Hold 3 of the RAM transport ship schematically depicted in Figure 7-2. Suppose further that the collision causes a fire in compartment L_{22} of the RAM transport ship, that spreads to compartment L_{31} by the path $L_{22} \rightarrow L_{32} \rightarrow L_{31}$. The probability that fire spread along this path leads to an engulfing fire in compartment L_{31} that damages the RAM transportation cask or its contents is given by

$$P_{Fire} = P_{System} P_{St,L_{22}} \left(P_F P_{O_2} P_{Ex}\right)_{L_{22}} \left(P_F P_{O_2} P_{Ex}\right)_{L_{32}} \left(P_F P_{O_2} P_{Ex}\right)_{L_{31}} P_{Csk,L_{31}} \quad (7.1)$$

where

P_{System} = the probability that the ship is equipped with a fire suppression system

$P_{St,L_{22}}$ = the probability that the fire starts in compartment L22

$P_{Csk,L_{31}}$ = the probability that the RAM cask is located in compartment L31

P_F = the probability required fuel is present in the indicated compartment Lhd

P_{O_2} = the probability required air is present in the indicated compartment Lhd

P_{Ex} = the probability that the fire suppression system in compartment L_{hd} doesn't operate

Thus, $(P_F P_{O_2} P_{Ex\,L})_{L_{22}}$ is the probability that the fire in compartment L_{22} is not extinguished by the operation of the fire suppression system and has enough of a good fuel and enough oxygen to place heat loads on the compartment walls that allow fire spread to compartment L_{32}. Similarly, $(P_F P_{O_2} P_{Ex\,L})_{L_{31}}$ is the probability that the fire in compartment L_{31} is not extinguished by the operation of the fire suppression system and has enough of a good fuel and enough oxygen to place damaging heat loads on the cask. Further, $P_F = P_{enough\,fuel} P_{good\,fuel}$ and $P_{Ex} = 1 - P_{Operate}$ where $P_{Operate}$ is the probability that the fire system operates in the indicated compartment.

If the RAM transport ship is not equipped with a fire suppression system, Eqn 7.1 is replaced by

$$P_{Fire} = (1 - P_{\text{System}}) P_{St,L_{22}} (P_F P_{O_2})_{L_{22}} (P_F P_{O_2})_{L_{32}} (P_F P_{O_2})_{L_{31}} P_{Csk,L_{31}} \tag{7.2}$$

where the terms $(P_F P_{O_2} P_{Ex})_{L_{hd}}$ have reduced to $(P_F P_{O_2})_{L_{hd}}$ because $P_{Ex} = 1 - P_{Operate} = 1$ since $P_{Operate} = 0$ as the ship is not equipped with a fire suppression system.

But the fire need not start in compartment L_{22} and the cask may not be stowed in compartment L_{31}. Summing over all possible fire start locations and fire spread paths yields a two-term equation that expresses the fact that the cask may be stowed in any compartment, that the fire may start in any compartment and spread to any other compartment, and that some break-bulk freighters are equipped with fire suppression systems (term one of Eqn 7.3) and some don't have fire suppression systems (term two of Eqn 7.3).

$$\begin{aligned} P_{Fire} = {} & P_{\text{System}} \sum_{\substack{\text{All Start} \\ \text{Locations} \\ \text{and Paths}}} P_{St,L_{hd}} \left[\prod_{\text{Path k}} (P_F P_{O_2} P_{Ex})_1 \ldots (P_F P_{O_2} P_{Ex})_{n_k} \right] P_{Csk,L_{hd}} \\ & + (1 - P_{\text{System}}) \sum_{\substack{\text{All Start} \\ \text{Locations} \\ \text{and Paths}}} P_{St,L_{hd}} \left[\prod_{\text{Path k}} (P_F P_{O_2})_1 \ldots \quad (P_F P_{O_2})_{n_k} \right] P_{Csk,L_{hd}} \end{aligned} \tag{7.3}$$

where

Path k = a sequence of compartments (e.g., L_{22}, L_{32}, L_{31}) of length n_k

n_k = the number of compartments on Path k,

$P_{St,L_{hd}}$ = the probability that the fire starts in the first compartment on Path k, and

$P_{Csk,L_{hd}}$ = the probability that the cask is located in the last compartment on Path k

If, as is likely, unique values of the probabilities $P_{St,L_{hd}}$, P_F, P_{O_2}, P_{Ex}, and $P_{Csk,L_{hd}}$ are not available for individual compartments, and therefore average values must be used, then

$$P_{Fire} = P_{St}P_{Csk}\left\{P_{\text{System}} \sum_k N_k \left(P_F P_{O_2} P_{Ex}\right)^{n_k} + \left(1 - P_{\text{System}}\right)\sum_k N_k \left(P_F P_{O_2}\right)^{n_k}\right\} \tag{7.4}$$

where

P_{St} and P_{Csk} = the respective probabilities that the fire starts and the cask is located in a random compartment

N_k = the number of paths of length n_k that connect a random fire start location through $n_k - 2$ intervening holds to a possible cask location

P_{System} = the probability that the ship is equipped with a fire suppression system

P_{Ex} = the probability that the fire system fails to operate in compartment L_{hd} when called upon

P_F and P_{O_2} = the probabilities that the compartment contains enough of a good fuel and enough air to support a fire of a size large enough and duration long enough to damage a RAM cask located in the compartment or to place heat loads on the compartment's walls that allow fire spread to a neighboring compartment.

7.2 Parameter Values

Fire spread on the break-bulk freighter depicted in Figure 7-1 for fires that occur in ports was examined by Sprung et al. [1] who estimated the following values for the probabilities that enter Eqn 7.4:

$$P_{enough\,fuel} = 0.95,\ P_{good\,fuel} = 0.9,\ P_{system} = 0.6,\ P_{operate} = 0.8, \text{ and } P_{O_2} = 0.17$$

where this value for P_{O_2} reflects the fraction of time that the hold and tween-deck covers of a break-bulk freighter are open for loading or unloading during a port call. As most ship collisions take place in ports or in the congested waterways that lead to major ports, this value is used here without attempting to adjust for the long periods of time at sea when hold covers are closed but during which ship collisions are quite improbable. Therefore,

$$\begin{aligned} P_F &= P_{\text{good fuel}}\, P_{\text{enough fuel}} = 0.95(0.9) = 0.86 \\ P_{Ex} &= 1 - P_{\text{Operate}} = 1 - 0.8 = 0.2 \\ P_F P_{O_2} &= 0.86(0.17) = 0.15 \\ P_F P_{O_2} P_{Ex} &= 0.86(0.17)(0.2) = 0.029 \end{aligned}$$

Fire spread paths are not likely to be contorted. For example, if a fire in compartment L_{22} places heat loads on the walls of that compartment large enough to initiate spread to compartment L_{23}, then it should also be able to spread to compartment L_{32}. Therefore, if fire spread from compartment L_{22} to compartment L_{32} by the path L_{22}, L_{23}, L_{33}, L_{32} is possible, then spread by the direct path L_{22}, L_{32} should also be possible and should be more probable.

If only minimum length fire spread paths are considered, then for each n_k, there is a single value for N_k. Specifically, for $n_k \geq 2$, $N_k = 4\left(\sum_i b_i - 1\right)$ where $\{b_i\}$ is the set of binomial coefficients obtained by expanding $(x+a)^{n_k-1}$ and the 4 accounts for the fact that, for an infinite matrix of compartments, for any value of n_k, there will always be four identical sets of compartments for the fire to spread to, one set in each of the four quadrants that border the compartment in which the fire starts. For example, for fire spread from compartment L_{32} by any path of length $n_k = 3$, there is only one path (L_{32}, L_{33}, L_{34}) to compartment L_{34}, but there are two paths (L_{32}, L_{33}, L_{43} and L_{32}, L_{42}, L_{43}) to compartment L_{43}. Thus, the number of fire spread paths from compartment L_{32} to compartments L_{34} and L_{43} is $[(1 + 2 + 1) - 1] = 3$, where 1, 2, and 1 are the binomial coefficients of a polynomial of order $n_k - 1 = 2$. But the same analysis applies to fire spread from compartment L_{32} to compartments L_{52} and L_{41} or to compartments L_{12} and L_{23} or to compartment L_{21} and the compartment that would be below compartment L_{31} if the freighter had five decks instead of four. Therefore, for a freighter with five decks (or for an infinite matrix of compartments), if $n_k = 3$, then $N_k = [4(1 + 2 + 1) - 1] = 12$. For the four deck freighter depicted in Figure 7-1, because there isn't a compartment below compartment L_{31}, the exact value of N_k for spread of fires that begin in compartment L_{32} along paths with lengths $n_k = 3$ is 11 rather than 12. Finally, Table 7-1 presents values for N_k, for the first six terms of the summations in Eqn 7.4, and for the sums of those terms.

Table 7-1. Values of N_k, Individual Terms, and Sums of Terms for Eqn 7.4 for an Infinite Matrix

n_k	N_k	$N_k\left(P_F P_{O_2}\right)^{n_k}$	$N_k\left(P_F P_{O_2} P_{Ex}\right)^{n_k}$
1	1	0.15000	0.02900000
2	4	0.09000	0.00336400
3	12	0.04050	0.00029267
4	28	0.01417	0.00001980
5	60	0.00456	0.00000123
6	124	0.00141	0.00000007
		$\sum_k N_k\left(P_F P_{O_2}\right)^{n_k} = 0.30064$	$\sum_k N_k\left(P_F P_{O_2} P_{Ex}\right)^{n_k} = 0.03267778$

The four-deck, eight-hold break-bulk freighter being considered here contains 32 compartments. Therefore, $P_{Csk} = 1/32 = 0.031$. As stated above in Section 4.1.3, the 15 years of Lloyds' collision data contains 702 port collisions, 11 of which lead to fires. Therefore, given that a collision has occurred, $P_{St} = 11/702 = 0.016$. Accordingly,

$$P_{Fire} = P_{St} P_{Csk}\left\{P_{\text{System}} \sum_k N_k\left(P_F P_{O_2} P_{Ex}\right)^{n_k} + \left(1 - P_{\text{System}}\right)\sum_k N_k\left(P_F P_{O_2}\right)^{n_k}\right\}$$

$$= 0.025(0.031)\{(0.6)(0.03) + (0.4)(0.3)\} = 7.0 \times 10^{-5}$$

which is more than an order of magnitude smaller than the value of 10^{-3} previously estimated by Sprung et al. [2] for the probability that a RAM transport cask will be subjected to a severe engulfing fire following a ship collision.

7.3 Air Availability

Because RAM casks are massive, only a large, long-duration, engulfing fire can place heat loads on the cask that threaten its integrity. In addition, although a relatively small fire situated close to a bulkhead can ignite combustible material situated just on the other side of the bulkhead, if the new fire is to propagate across the hold in which it starts or to damage a RAM cask located in that hold, it will have to become a large fire. Therefore, only large fires are believed to be able to cause fire spread or loss of integrity of a RAM cask.

To be large enough and to burn long enough to damage a RAM cask located in the same compartment, or to place heat loads on the compartment's walls that allow fire spread to neighboring compartments, an engulfing fire must not be oxygen-starved. The value of 0.17 assumed above for P_{O_2} was developed for a port call by a break-bulk freighter. It expresses the fraction of time that hold and tween-deck covers are off during a port transit. Thus, it assumes that if the hold and all tween-deck covers above the burning hold are off, loss of combustion gases from the burning hold due to buoyancy will draw enough fresh air into the hold so that the fire will burn at a rate little different from that of an open fire. Since a severe collision will open a hole in the side of the struck hold, it is possible that, if the two ships separate, as is usually the case, this hole will allow enough air to reach the fire to support unconstrained combustion in the struck hold even if the hold and tween-deck covers are in place.

Most combustible materials do not burn completely. Instead they release some combustible gases. Therefore, if a fire occurs in a compartment (e.g., the hold of a ship), these gases accumulate below the compartment ceiling. If these gases become hot enough, they will ignite and the fire will instantly involve the full volume that these gases occupy. This condition, which is called flashover, converts a somewhat localized fire burning on the floor of a compartment to a fire that involves the full extent of the compartment. Thus, fires that reach flashover are large, severe fires.

The energy release rate of a compartment fire that has attained flashover conditions is related to compartment and vent dimensions by the following equation [3]

$$\dot{Q}=620\left(\frac{k}{\delta}A_T A_o\sqrt{H_o}\right)^{1/2} \tag{7.5}$$

where

$\dot{Q}$ = the energy release rate of the fire;

k, δ, and A_T = the thermal conductivity, thickness, and surface area of the compartment walls; and

A_o and H_o = the area and height of the compartment vent, here the hole in the side of the ship hold caused by the collision.

Decks in the prototypical break-bulk freighter being considered here have the following dimensions and wall thicknesses: height, 10 feet; width, 82 feet; length, 68 feet; and wall thickness, 0.83 inches. Therefore, $A_T = 1.3 \times 10^3$ m^2 and $\delta = 2.1 \times 10^{-2}$meters. For carbon steel, k = 39.2 W m^{-1} K^{-1} at 800 K

[4]. If kerosene is used as a surrogate for bunker fuel and the engulfing fire is assumed to cover the entire floor of the hold, then, for free combustion (combustion not limited by the availability of air)

$$\dot{Q}=\Delta h_c \dot{m} A_F$$

where Δh_c = 43 MJ kg^{-1} and $\dot{m}$ = 0.04 kg m^{-2} s^{-1} are respectively the heat of combustion and the free mass burning rate of kerosene, A_F = 519 m^2 is the floor area of the compartment, and therefore, $\dot{Q}$ = 8.9 × 10^5 kJ s^{-1}. Substitution of the values specified for $\dot{Q}$, k, δ, and A_T allows Eqn 7.5 to be solved giving $A_o\sqrt{H_o}$ = 849 m$^{5/2}$. But $A_o = W_o H_o$ where W_o is the width of the hole in the side of the ship. Now, if it is assumed that the collision produces a gash in the side of the ship from the waterline to the main deck, then H_o = 6 meters, and thus W_o = 58 meters and A_o = 347 m^2.

Kerosene has an equivalent grey body flame temperature of 1480 K. For an engulfing fire, heat loads on compartment walls or on a RAM cask contained in the compartment would correspond to temperatures several hundred degrees lower than this flame temperature [5, 6], say 1200 to 1300 K. Since Eqn 7.5 was developed using an upper gas layer flashover temperature of 795 K, the size of the hole needed to attain a flashover temperature of 795 K is probably also a reasonable estimate of the size of the hole needed to support free burning (burning that is not limited by the rate at which oxygen can be supplied to the fire). Because a hole size of 347 m^2 is large compared to the sizes of holes usually produced by severe ship collisions (typically ~100 m^2), most ship collisions will not produce a hole that is large enough to support free burning of large amounts of combustibles in the struck hold unless the tween-deck covers and the hold cover of the struck hold are all open. Thus, the use of a value of 0.17 for P_{O_2} that reflects the time tween-deck and hold covers are removed during a port transit is believed to be reasonable.

7.4 Illustrative Applications

The preceding derivation assumed that the RAM transport ship may not be equipped with a fire suppression system, that the matrix of compartments is infinite in extent, and that fire start locations, collision locations, and cask locations are random. The impact of alternative assumptions on the value of P_{Fire} calculated above is now discussed. First, the effect of using a matrix of compartments of limited extent is examined for a 32 compartment break-bulk freighter. Second, the impact of assuming that collision, fire-start, and cask locations on the 32 compartment break-bulk freighter are correlated is examined. Third, values of P_{Fire} are calculated for transport of INF in two INF Class 2 ships (a 32 compartment break-bulk freighter and a smaller charter freighter), which are required by regulations to be equipped with fire suppression systems. Finally, because approximate input parameter values were used in all of the calculations presented in this section, the data needed to support development of more precise estimates of fire probabilities is summarized.

7.4.1 Limited Compartment Matrix

Use of binomial coefficients to derive values for N_k in Eqn 7.4 is strictly correct only for a matrix of compartments that is infinite in extent. Because the compartment matrix of a real ship will always be quite limited in extent, the resulting decrease in values of N_k needs to be examined to see whether it significantly affects the estimated value for P_{Fire}. N_k values can be developed by inspection for the 32-compartment matrix used above to represent a break-bulk freighter. Because the values of the

summations evaluated in the preceding table are largely set by the first three terms of each summation, only these three terms are reevaluated. The following table presents this reevaluation.

For fire spread paths that contain two compartments ($n_k = 2$), the 4 × 8 compartment matrix contains 12 compartments (L_{22} through L_{72} and L_{23} through L_{73}) that have all four of the fire spread path termini predicted by the binomial coefficient formula, 16 compartments (L_{21} through L_{71}, L_{24} through L_{74}, and L_{12}, L_{13}, L_{82}, and L_{83}) that have only three of the four termini predicted by the binomial coefficient formula, and four compartments (the corner compartments of the 4 × 8 matrix) that have only two of the four termini predicted by the binomial coefficient formula. An average number of termini (N_k value for an average compartment in the matrix) for fire spread paths that contain two compartments ($n_k = 2$) can be constructed as a weighted sum of the fraction of compartments in the matrix that have four, three, or two termini. Thus,

$$(12/32)\,(4) + (16/32)\,(3) + (4/32)\,(2) = [1/32][\,4(12) + 3(16) + 2(4)] = 3.25$$

where 3.25 is the N_k value for an average compartment in the 4 × 8 matrix for fire spread paths that contain two compartments. For $n_k = 3$, none of the compartments in the 4 × 8 matrix has all of the termini predicted by the binomial coefficient formula. If a weighted sum is constructed for fire spread paths that contain three compartments, Table 7-2 shows that a value of 7.75 is obtained for N_k for an average cell in the matrix. If the average cell N_k values of 1.00, 3.25, and 7.75 are divided by the values of N_k calculated for a compartment matrix of infinite extent, the resulting fractions can be used as weights to correct the values of the terms in the summations presented in Table 7-1 for a matrix of infinite extent.

Table 7-2. N_k Values for a 4 × 8 Matrix of Compartments

n_k	N_k	
	Infinite Matrix	**4 × 8 Matrix (average cell)**
1	1	1.00
2	4	[1/32][4(12) + 3(16) + 2(4)] = 3.25
3	12	[1/32][11(8) + 10(4) + 7(8) + 6(8) + 4(4)] = 7.75

Thus,

$$1(0.15) + (3.25/4)(0.09) + (7.75/12)(0.04) = 0.25$$

rather than the value of 0.3 calculated for an infinite matrix, and

$$1(0.0290) + (3.25/4)(0.0034) + (7.75/12)(0.0003) = 0.03$$

unchanged from the value computed for an infinite matrix.

If P_{Fire} is recalculated using these new values for the two summations in Eqn 7.4, a value of 5.6×10^{-5} is obtained instead of the value of 7.0×10^{-5} obtained assuming an infinite matrix. Accordingly, 6×10^{-5} seems a reasonable estimate for P_{Fire} for a general break-bulk freighter (one that may not be equipped with a fire suppression system), provided that collision locations and fire start locations are not correlated.

7.4.2 Fire Location Correlated to Collision Location

If a ship collision initiates a fire on the struck ship, the compartment where the fire starts may not, as was assumed above, start on any deck in any hold of the struck ship (that is, in any compartment on the matrix). Instead, fire start may be limited to holds near the struck hold. Suppose that the chance of a fire starting is significant only in the struck hold or in the two holds immediately adjacent to the struck hold (the holds on either side of the struck hold). In addition, assume that the struck hold has at least three holds on either side of it. Then, if the RAM cask is located in the struck hold, a value for P_{Fire} can be estimated for fire paths that contain one, two, or three compartments (n_k = 1, 2, or 3) by using path dependent values for P_{Csk} to recalculate the values for P_{Fire} that were calculated in Section 7.4.2 for a limited compartment matrix.

For fire paths that contain only one compartment (n_k = 1), the chance that the fire starts and therefore also terminates in a compartment in the struck hold is 4/12 = 0.333. Thus, P_{Csk} = 0.333 for the first term in each of the two summations in Eqn 7.4.

For fire paths that contain two compartments (n_k = 2), the chance (average value of P_{Csk} for this term) that the neighboring compartment to which the fire spreads contains the RAM cask is

$$(2/12)\ (2/4) + (4/12)\ (1/4) + (6/12)\ (1/3) = 0.333$$

because two of the twelve compartments in the three holds where fire start is significant have four neighboring compartments of which only two are in the struck hold; four have four neighboring compartments of which only one is in the struck hold; and six have three neighboring compartments of which only one is in the struck hold. Thus, P_{Csk} = 0.333 for the second term in each of the two summations in Eqn 7.4.

For fire paths that contain three compartments (n_k = 3), a similar analysis yields the following expression:

$$(2/12)\ (1/7) + (4/12)\ (2/7) + (6/12)\ (1/5) = 0.219$$

Thus, P_{Csk} = 0.219 for the third term in each of the two summations in Eqn 7.4.

If P_{Fire} is recalculated assuming that the striking ship strikes the RAM hold, that the fire starts in either the struck hold or in one of the two holds immediately adjacent to that hold, and that P_{Csk} values are path dependent, then

$$P_{Fire} = P_{St}\left\{P_{\text{System}}\sum_k P_{Csk,n_k} N_k \left(P_F P_{O_2} P_{Ex}\right)^{n_k} + \left(1 - P_{\text{System}}\right)\sum_k P_{Csk,n_k} N_k \left(P_F P_{O_2}\right)^{n_k}\right\}$$

$$= 0.016\{0.6[(0.333)\ (1)\ (0.15) + (0.333)\ (3.25/4)\ (0.09) + (0.219)\ (7.75/12)\ (0.04)]$$

$$+ 0.4[(0.333)\ (1)\ (0.029) + (0.333)\ (3.25/4)\ (0.0034) + (0.219)\ (7.75/12)\ (0.003)\}$$

$$= 7.7 \times 10^{-5}$$

If the RAM hold is struck and the probability of fire start is significant only in the struck hold, then $P_{Fire} = 1.1 \times 10^{-4}$. Thus, for break-bulk freighters carrying combustible cargo (e.g., wood, plastics, etc.) that may or may not be equipped with a fire suppression system, $10^{-4} > P_{Fire} > 5 \times 10^{-5}$.

7.4.3 INF Class 2 Break-Bulk Freighter

Regulations require that INF Class 2 ships be equipped with a fire suppression system. If the value for P_{Fire} for a 32-compartment break-bulk freighter calculated using Eqn 7.4 is recalculated assuming that the ship is equipped with a fire suppression system, the second term in Eqn 7.4 vanishes as $P_{System} = 1$ and therefore $1 - P_{System} = 0$. Accordingly, for a break-bulk freighter serving as an INF Class 2 ship, $P_{Fire} = 0.016(0.031)\{(1.0)(0.03) + (0.0)(0.3)\} = 1.5 \times 10^{-5}$, which is smaller by a factor of 0.2 than the value estimated for break-bulk freighters that may or may not be equipped with fire suppression systems.

7.4.4 INF Class 2 Charter Freighter

RAM casks are frequently shipped in charter freighters, for example the *Marsis*. For purposes of fire spread, the *Marsis* may be viewed as a three hold, one deck matrix, where one hold, the stern hold, is the equipment hold (the hold that contains the ship's engines) and the other two holds are cargo holds, only one of which will be used if only one cask is being shipped. Because the freighter has only three holds, fire spread paths are short and few in number. When used to transport a RAM cask, a charter freighter usually carries no other cargo. Thus, the only time a combustible material is present in a cargo holds is when the ship collision breaches the fuel tank in the double bottom of the that cargo hold releasing bunker or diesel fuel into the hold.

A value for P_{Fire} for a charter freighter like the *Marsis* can be estimated using Eqn 7.3 for collisions that strike one of the two cargo holds and thus might fail the cask if it is stowed in the struck hold. The estimate is developed assuming that any collision may initiate a fire in the engine compartment, but that only a collision with a cargo hold can initiate or allow a fire to spread through that hold because the fuel tank in the double bottom of a cargo hold is unlikely to be breached if that hold is not directly struck. Accordingly,

$$P_{Fire} = \frac{1}{3} P_{System} P_{St} \left[\left(P_F P_{O_2} P_{Ex}\right)_{L_3} \left(P_F P_{O_2} P_{Ex}\right)_{L_2} + \left(P_F P_{O_2} P_{Ex}\right)_{L_2} + \left(P_F P_{O_2} P_{Ex}\right)_{L_1} \right]$$

where the first term in the brackets represents a collision with hold 2 (compartment L_2) that initiates a fire in the engine hold (compartment L_3) that spreads to hold 2, the second term represents a collision with hold 2 that initiates a fire in hold 2, and the third term represents a collision with hold 1 that initiates a fire in hold 1. When the first cargo hold (compartment L_1) is struck, fire spread from the engine compartment through the second cargo hold to the first cargo hold is neglected, because the double bottom of the second cargo hold should not have been failed by the collision and thus there will be nothing combustible in the second cargo hold to support fire spread through that hold. Collisions with the engine compartment are also neglected because these collisions are not expected to fail the double bottom bunker fuel tank in either of the two cargo holds and thus fire start in the cargo holds or fire spread from the engine compartment to these holds are both very unlikely. Finally, the leading 1/3 expresses the fact that a collision with any of the three holds is equally likely.

The Minorsky calculations described in Section 6.0 indicate that the small mass (5 ktons) of typical charter freighters means that, if struck by another ship, only one time in ten will the hull of the charter freighter be penetrated. However, because almost all collisions (9 of every 11) that penetrate the hull of a charter freighter will also lead to deep enough penetration to breach the double bottom of the struck hold, when the cargo hold of a charter freighter is struck, for that hold, $P_F = (1/10)(9/11) \approx 0.1$. Of course, for the engine compartment, $P_F = 1.0$.

INF Class 2 regulations specify that a charter freighter carrying a RAM cask must be equipped with a fire suppression system. Therefore, $P_{System} = 1.0$ and $P_{Ex} = 0.2$, where P_{Ex} is the probability that the system fails to operate when called upon. Now, if $P_{S_i} = 0.016$ and $P_{O_2} = 0.5$ because while in port hold covers will be off perhaps half of the time [1], then

$$P_{Fire} = (0.33)(1.0)(0.016)\{[(1.0)(0.5)(0.2)][(0.1)(0.5)(0.2)]$$

$$+ [(0.1)(0.5)(0.2)] + [(0.1)(0.5)(0.2)]\} = 5.3 \times 10^{-5}$$

for port fires on small break-bulk freighters initiated by collisions.

7.4.5 Data Requirements for More Precise Estimates of P_{Fire}

The preceding estimates of P_{Fire} values were developed using approximate values for P_{O_2} and P_F where $P_F = P_{enough\,fuel} P_{good\,fuel}$. Better estimates of P_{Fire} can be made if better values can be developed for P_{O_2}, $P_{enough\,fuel}$, and $P_{good\,fuel}$. Oxygen availability depends on air availability which depends on the size of the openings (ventilation shafts, bulkhead doors, holes produced by the ship collision) in a hold and the fraction of time that each hole is open on average. The types and amounts of cargo required to support a fire that burns hot enough and long enough to allow the fire to spread to a neighboring hold or to threaten a cask colocated with the fire can be estimated using a compartment fire model and the combustion characteristics and typical shipment quantities of the various types of cargo transported on freighters. Thus, the ship and cargo data and fire models required to support the development of more precise values for P_{O_2}, $P_{enough\,fuel}$, and $P_{good\,fuel}$ are all available.

7.5 References

1. J. L. Sprung et al., *Radiological Consequences of Ship Collisions that Might Occur in U.S. Ports during the Shipment of Foreign Research Reactor spent Nuclear Fuel to the United States in Break-Bulk Freighters*, SAND96-0400, p. 53. Sandia National Laboratories, Albuquerque, NM, August 1996.

2. Ibid., p. 56.

3. W. D. Walton and P. H. Thomas, "Estimating Temperatures in Compartment Fires," in *SFPE Handbook of Fire Protection Engineering*, p. 2-28. P. J. DiNenno, ed., National Fire Protection Association, Quincy Massachusetts, 1988.

4. F.P. Incropera and D. P. DeWitt, *Fundamentals of Heat Transfer*, p. 764. Wiley, New York, NY, 1981.

5. J. J. Gregory et al., "Thermal Measurements in Large Pool Fires," in *J. Heat Transfer*, vol. 111, p. 446, 1989.

6. M. E. Schneider and L. A. Kent, "Measurements of Gas Velocities and Temperatures in a Large Open Pool Fire," in *Fire Technology*, vol. 25, p. 37, 1989.

8. SCENARIO PROBABILITIES

8.1 Probability Expressions

Event trees that illustrate important ship accident scenarios were presented in Section 3.0. The development of ship accident probabilities in Section 4.0, of hull penetration probabilities in Section 6.0, and of fire spread probabilities in Section 7.0 allows probabilities to be estimated for all of the branch points that define several important scenario paths through ship accident space. Specifically, branch point probabilities can be estimated (1) for a ship collision where the RAM transport ship is the struck ship and the RAM cask fails due to crush, puncture, or shear, and (2) for the extension (branch) of this scenario that leads to a severe fire that engulfs the RAM cask, but not to the sinking of the RAM transport ship.

Inspection of Figures 3-1 through 3-4 allows the events along these scenario paths to be identified. These events are listed in Table 8-1.

Table 8-1. Scenario Event Probabilities

Event	Probability
A ship collision occurs	$P_{collision}$
The RAM ship is the struck ship	$P_{RAM\ ship\ struck}$
The strike location is midship	$P_{strike/midship}$
The RAM cask location is midship	$P_{cask/midship}$
The RAM hold is struck	$P_{RAM\ hold\ struck}$
Cask crush occurs	P_{crush}
Cask puncture or shear occurs	$P_{puncture/shear}$
A fire starts on the RAM ship, spreads to the RAM hold, engulfs the cask, and then burns hot enough and long enough to increase radioactive release from the failed cask	$P_{severe\ engulfing\ fire}$
The RAM ship sinks	P_{sink}

In Section 4.0, the probability of an accident leading to the release of a particular source term (P_{STj}) was formulated as follows:

$$P_{STj} = P_{Acc}\prod_{k=1}^{n} P_{jk} = P_{Acc}F_{Sev,j}$$

where P_{Acc} is the probability of the initiating event, here a ship collision, P_{jk} is the probability of one of the n events in the sequence of events initiated by the accident that culminates in the release of the j^{th} radioactive source term, and $F_{Sev,j}$ is the product of the probabilities of all of the events in the sequence that follow the initiating event.

Source term probabilities, P_{STj}, are usually formulated in this way because accident statistics (e.g., P_{Acc}) depend on transport mode and on the route traveled, while accident severities, given that a transportation accident has occurred, depend on the accident progression that follows the initiating event. Thus, P_{Acc} gives the probability of a class of initiating events, here a ship collision, and $F_{Sev,j}$ gives the

probability that the set of ensuing events leads to a particular final accident state characterized by a set of conditions (mechanical and thermal loads) that will cause the release of radioactive source term j.

By combining probabilities listed in the Table 8-1, expressions for the probabilities of the following severe accident scenarios can be constructed:

> **First Scenario:** the RAM transport ship is struck by another ship, the RAM hold is the struck hold, and bow penetration by the striking ship is deep enough to cause the RAM cask to fail due to crush, but not so deep that the RAM ship sinks.
>
> **Second Scenario:** the RAM transport ship is struck by another ship, the RAM hold is the struck hold, bow penetration by the striking ship is deep enough to cause the RAM cask to fail first due to crush and then due to puncture or shear, but not so deep that the RAM ship sinks; the collision leads to a fire, the fire spreads to the RAM hold, and upon reaching the RAM hold engulfs the RAM cask and burns hot enough and long enough to substantially increase release of radioactivity from the RAM cask to the environment; however, the fire does not cause the RAM transport ship to sink.

Let the probability of the radioactive release produced by the first scenario be $P_{\text{release/collision only}}$ and that of the second scenario be $P_{\text{release/collision + fire}}$. Then, inspection of Table 8-1 leads to the following expressions for these two scenario probabilities:

$$\begin{aligned} P_{\text{release/collision only}} &= P_{\text{collision}}\, P_{\text{RAM ship struck}}\, P_{\text{strike/midship}}\, P_{\text{cask/midship}}\, P_{\text{RAM hold struck}}\, P_{\text{crush}} \\ &= P_{\text{collision}}\, F_{\text{severity/ collision only}} \end{aligned} \tag{8.1}$$

where

$$F_{\text{severity/ collision only}} = P_{\text{RAM ship struck}}\, P_{\text{strike/midship}}\, P_{\text{cask/midship}}\, P_{\text{RAM hold struck}}\, P_{\text{crush}} \tag{8.2}$$

and

$$\begin{aligned} P_{\text{release/collision + fire}} &= P_{\text{collision}}\, P_{\text{RAM ship struck}}\, P_{\text{strike/midship}}\, P_{\text{cask/midship}}\, P_{\text{RAM hold struck}}\, P_{\text{crush}} \\ &\times P_{\text{puncture/shear}}\, P_{\text{severe engulfing fire}}\, (1.0 - P_{\text{sink}}) \\ &= P_{\text{collision}}\, F_{\text{severity/ collision + fire}} \end{aligned} \tag{8.3}$$

where

$$\begin{aligned} F_{\text{severity/ collision + fire}} &= P_{\text{RAM ship struck}}\, P_{\text{strike/midship}}\, P_{\text{cask/midship}}\, P_{\text{RAM hold struck}}\, P_{\text{crush}} \\ &\times P_{\text{puncture/shear}}\, P_{\text{severe engulfing fire}}\, (1.0 - P_{\text{sink}}) \end{aligned} \tag{8.4}$$

The remainder of this section develops estimates for the probabilities that enter these expressions and uses them to calculate values for $F_{\text{severity/ collision only}}$ and $P_{\text{release/collision only}}$ and for $F_{\text{severity/ collision + fire}}$ and $P_{\text{release/collision + fire}}$.

8.2 Event Probabilities

8.2.1 Probabilities Developed from Ship Accident Data

The probability of a ship collision depends on the route sailed. Here, for purposes of illustration, transport of a spent fuel cask from Charleston, South Carolina, directly (i.e., without stops at any intermediate ports) to Cherbourg, France, for conversion to mixed oxide fuel, is hypothesized. The probability that the RAM transport ship will be involved in a collision while sailing this route can be calculated using the following expression that was developed in Section 4.0,

$$P_{SC,V} = 0.5\,P_{SC,\,Dep\,P} + \sum_i P_{SC,R_i} N_i + \sum_j P_{SC,P_j} + 0.5\,P_{SC,\,Des\,P}$$

where

$P_{SC,\,V}$ = the probability that a ship collision occurs during the voyage
$P_{SC,\,Dep\,P}$ = the probability that a collision occurs during a full transit of the departure port
$P_{SC,\,R_i}$ = the probability that a collision occurs while sailing a nautical mile in Region I
N_i = the number of nautical miles sailed in Region I
$P_{SC,\,P_j}$ = the probability that a collision occurs during the transit of intermediate Port j
$P_{SC,\,Dep\,P}$ = the probability that a collision occurs during a full transit of the destination port

The hypothesized sailing route requires sailing out of Charleston harbor through coastal waters to the open ocean, across the Atlantic to the English Channel, and finally through the English Channel into the Port of Cherbourg. Publication 151, Distances Between Ports [R], gives the sailing distance from Charleston to Bishop Rock, the entrance to the English Channel, as 3,375 nautical miles, and from Bishop Rock to Cherbourg as 197 nautical miles. Lloyd's port call data suggests that both Charleston (1,592 port calls in 1988) and Cherbourg (183 port calls in 1988) are low traffic ports. Table 4.6, Port Calls (1988) and Port Collision Frequencies (per port call), states that the probability of a ship collision per port call at a low traffic port is 4.3×10^{-5}. Therefore, $P_{SC,\,Dep\,P} = P_{SC,\,Dep\,P} = 4.3 \times 10^{-5}$. Table 4.5, Distances Sailed, Ship Collisions, and Collision Frequencies for 21 Ocean Regions, gives the following values for the probabilities of a ship collision per nautical mile sailed in Coastal Waters, the Open Ocean, and the English Channel: 1.9×10^{-7}, 6.8×10^{-9}, 1.0×10^{-7}, respectively. Therefore, as the first 50 nautical miles of this hypothetical voyage are sailed in coastal waters,

$$P_{collision} = P_{SC,V} = 0.5(4.3 \times 10^{-5}) + (1.9 \times 10^{-7})(50) + (6.8 \times 10^{-9})(3375 - 50) + (1.0 \times 10^{-7})(197) + 0.5(4.3 \times 10^{-5}) = 9.5 \times 10^{-5}$$

and the probabilities of a ship collision occurring while sailing out to sea, across the Atlantic, in the English Channel, and in the harbors of Charleston or Cherbourg are 9.5×10^{-6}, 2.3×10^{-5}, 2.0×10^{-5}, and 2.2×10^{-5}, respectively. Thus, each leg of this hypothetical voyage has a ship collision probability of approximately 10^{-5} and the total voyage has a ship collision probability of approximately 10^{-4}.

8.2.2 Strike Location and Cask Stowage Location Probabilities

Because Type B spent fuel casks are both heavy and large, they are usually stowed on the centerline of the RAM transport ship. To minimize the chance of damage during a collision, stowage in a midship

hold is preferred unless the schedule for loading and unloading of other cargo necessitates stowage of other cargo along the centerline of the midship holds. Here, the more likely stowage situation is assumed, stowage of the spent fuel Type B cask on the ship centerline in a midship hold.

Type B RAM casks are transported by sea (1) in small break-bulk freighters that are chartered specifically to carry the RAM casks, and thus carry no other cargo, (2) in larger break-bulk freighters that carry other cargo and therefore may make intermediate stops at other ports besides the RAM shipment departure and destination ports, (3) in container ships, and (4) in purpose-built ships. This illustrative analysis considers transport of a single Type B spent fuel cask on a small chartered break-bulk freighter that is carrying no other cargo, and on a larger break-bulk freighter that is carrying other cargo.

The small chartered break-bulk freighter considered here is a four-deck, two-hold ship with a length of 215 feet and a loaded displacement of 1,740 tons. The larger break-bulk freighter considered here is a five-deck, seven-hold ship with a length of 579 feet and a loaded displacement of 23,500 tons. Figure 7.1 presents a side view of this ship. If the machinery space in each ship is treated as an additional hold, then the charter freighter may be viewed as a three-hold ship which has a single cargo hold midship, and the larger break-bulk freighter may be viewed as an eight-hold ship that has three cargo holds midship.

Values are now estimated for the following probabilities for each of these two ships:

$P_{\text{RAM ship struck}}$ = the probability that the RAM ship is the struck ship

$P_{\text{strike/midship}}$ = the probability that the strike location is midship

$P_{\text{cask/midship}}$ = the probability that the cask is stowed in a midship hold

$P_{\text{RAM hold struck}}$ = the probability that the midship hold where the RAM cask is stowed is struck

Although ship size is likely to influence the probability that a ship is involved in a ship collision and also the chance that the ship is the striking or the struck ship, because data on ship collisions at this level of detail is not available and was not developed during this study, for these illustrative analyses, it is assumed that the probability that the RAM transport ship is the struck ship, is 0.5. Thus, $P_{\text{RAM ship struck}} = 0.5$.

Lloyd's casualty data suggests that bow-to-bow and bow-to-stern collisions are somewhat more probable than bow-to-midship collisions. Mostly likely this bias reflects attempts by the captain of the striking ship to turn and thereby avoid the impending collision. As the bias is small, here it will be assumed that the probability of striking a given section of a ship (a single hold or one hold in a set of neighboring holds) is equal to the length of the section divided by the length of the ship. Because for both of these ships the machinery space is about as long as the length of an average hold, for the charter freighter $P_{\text{strike/midship}} = 1/3 = 0.33$ and for the larger break-bulk freighter $P_{\text{strike/midship}} = 3/8 = 0.38$. Further, because for this illustrative calculation stowage of the RAM cask in a midship hold is being assumed, $P_{\text{cask/midship}} = 1.0$. And because the small charter freighter has only one midship cargo hold while the larger break-bulk freighter has three, the probability that a midship collision actually strikes the RAM hold, $P_{\text{RAM hold struck}} = 1.0$ for the small charter freighter and 0.33 for the larger break-bulk freighter.

8.2.3 Crush Probability

In Section 6.6.4.1, it was concluded that ship speeds are far too low to damage a RAM cask due to impact forces. Therefore, if a ship collision damages a RAM cask, the damage must occur by crush,

puncture, or shear. The probability that a collision with the RAM hold leads to cask failure due to the application of crush forces to the RAM cask is given by the following expression

$$P_{crush} = (P_{cask\ overrun} + P_{cargo\ closeup})\ (1.0 - P_{relief}) \quad (8.5)$$

where $P_{cask\ overrun}$ is the probability that, given a collision with the RAM hold, the penetrating bow of the striking ship penetrates deeply enough into the RAM hold to overrun the position where the cask is stowed, $P_{cargo\ closeup}$ is the probability that the penetrating bow consumes all of the empty horizontal space in the struck hold by compressing cargo stowed in that hold about the cask, and P_{relief} is the probability that collapse of ship structures (the bulkheads or the far wall of the struck hold) relieves the forces applied to the cask by cask overrun or cargo closeup.

Values for $P_{cask\ overrun}$ and for $P_{cargo\ closeup}$ were developed in Section 6.6.3 for the small charter freighter and for the larger break-bulk freighter being considered here. Table 8-2 summarizes the relevant values. Three types of cargo were examined for the larger break-bulk freighter, light cargo (palletized cargo in boxes), medium cargo (palletized cargo in wooden crates), and heavy cargo (heavy machinery). Because the charter freighter is assumed to carry no other cargo besides the RAM cask, for the charter freighter values are presented only for $P_{cask\ overrun}$.

In Table 8-2, the sum of the probabilities for cask overrun and cargo goes solid provides a reasonable, conservative estimate of the probability that the cask will be subjected to crush forces. The estimate is conservative because, if the width of the collision bulkhead of the striking ship is substantially smaller than the width of the hold in the struck ship in which the RAM cask is stowed, then the penetrating bow of the striking ship may miss the cask, when the hold contains only the cask, or may not compress cargo efficiently about the cask, when the hold contains other cargo. Thus, for the small charter freighter, $P_{cask\ overrun} + P_{cargo\ closeup} = 0.15$, and for the larger break-bulk freighter, $P_{cask\ overrun} + P_{cargo\ closeup} = 0.5$, because most cargo shipped in break-bulk freighters is now containerized and thus should behave more like crates than boxes.

Table 8-2. Probabilities of Cask Overrun and Cargo Closeup during Ship Collisions

Collision Result	Charter Freighter	Break-Bulk Freighter			
		Cargo Type			
	None	None	Light	Medium	Heavy
Shell Penetration	0.200	0.563	0.563	0.563	0.563
Cask Overrun	0.144	0.238	0.049	0.000	0.000
Cargo Goes Solid	0.000	0.000	0.187	0.458	0.236
Overrun + Solid	0.144	0.238	0.235	0.458	0.236

Whether cask crush occurs, given cask overrun or cargo closeup about the cask, depends on how these crush forces are relieved. Because cask tiedowns are deliberately designed to fail when they are subjected to forces smaller than those required to inflict significant damage upon a Type B cask, should the cask be overrun during a ship collision by the advancing bow of the striking ship, the tie downs would fail before significant cask damage occurred allowing the cask to be pushed across the hold in which it is stowed until it reaches the far wall of the ship or until further cargo compression consumes the remaining empty horizontal space in the hold. At that moment, crush forces are being exerted on the cask, on any cargo present in the hold, and on the far wall and the fore and aft bulkheads of the hold.

How these crush forces are relieved is determined by the strength of the cask in comparison to the strengths of the shell of the ship (the far wall of the hold) and of the fore and aft bulkheads of the hold.

Finite element calculations that model the behavior during a ship collision of a cask stowed in an empty hold indicate [1] that, should cask overrun cause the cask to be pushed up against the far wall of the hold in which it is stowed, the crush forces will be relieved by pushing the cask through that wall into the sea. As hold bulkheads are usually not as strong as the shell of the ship, should the cask be pushed up against a bulkhead, or should cargo compression apply crush forces to both the cask and a bulkhead, failure of the bulkhead and not the cask is expected. Therefore, during the collision, collapse of ship structures into some unusual configuration (e.g., upward buckling of the hold floor behind the cask to a degree sufficient to prevent shoving of the cask across the hold) must occur if the cask is to be subjected to crush forces that won't be relieved by collapse of some other ship structure. Because neither data nor modeling results are available from which to estimate the probability that ship structures will collapse, it is here assumed that, in four of every five collisions, collapse of ship structures will relieve any crush forces experienced by the cask before those forces can damage the cask. Thus, $P_{relief} = 0.8$. Finally, substituting the values estimated for $P_{cask\ overrun} + P_{cargo\ closeup}$ and P_{relief} into Eqn 8.5 yields the following estimates for P_{crush}:

Ship	$P_{crush} = (P_{cask\ overrun} + P_{cargo\ closeup})\ (1.0 - P_{relief})$
Charter Freighter	$P_{crush} = (0.15)(1.0 - 0.8) = 0.03$
Break-Bulk Freighter	$P_{crush} = (0.5)(1.0 - 0.8) = 0.1$

8.2.4 Probability of Puncture or Shear

During a collision, tearing of ship structures might produce some pointed or sharp-edged objects that, if properly oriented, could be pushed against the cask causing the cask to fail by puncture or shear, provided the cask is unable to move when struck by the pointed or sharp-edged object. As was the case with crush, because of the strength of Type B spent fuel casks, an unusual configuration of collapsed ship structures must be produced during the collision if the cask is to fail by puncture or shear. Most likely, to inflict cask damage by puncture or shear, the collapsing ship structures must not only produce an unusually sturdy pointed or sharp-edged object that is oriented properly, but also must trap the cask between collapsed structures in a way that subjects it to crush forces, prevents relief of forces by shifting of the cask, and thus allows a puncture or shear failure to occur. Otherwise, when struck by the pointed or sharp object, puncture or shear would not be expected. Instead the cask would be expected to be pushed across the hold until all available horizontal space had been used up whereupon the crush, puncture, and/or shear forces would be relieved by collapse of some other ship structure, and not by collapse or damage of cask structures. Therefore, most of the time, formation of pointed or sharp-edged objects by the tearing of ship structures is not expected to lead to cask failure by puncture or shear. Nevertheless, puncture or shear is at least conceivable during some collisions that lead to cask failure by crush. In the absence of data or modeling results, it is here assumed that one crush failure in five also leads to a second cask failure due to puncture or shear. Accordingly, $P_{puncture/shear} = 0.2$.

8.2.5 Probability of a Severe Engulfing Fire

In Section 7.0, a simple probabilistic model of fire spread in a break-bulk freighter was developed. In Section 7.4, the probability, $P_{severe\ engulfing\ fire}$, that a collision causes a fire on a charter freighter or a larger break-bulk freighter that spreads to the RAM hold and there engulfs the RAM cask and burns hot enough and long enough to significantly increase radioactive release was estimated to be $P_{severe\ engulfing\ fire} = 6.0 \times 10^{-5}$ for the charter freighter and 2.0×10^{-5} for the larger break-bulk freighter.

8.2.6 Probability that the Fire Causes the RAM Ship to Sink

Should a collision lead to a severe engulfing fire, because RAM casks are massive, the fire must burn vigorously for several hours to raise cask temperatures high enough to increase the release of radioactive materials, say by vaporization of slightly volatile inorganic species such as CsI, CsOH, or RuO_4. Therefore, if the ship sinks before the cask reaches temperatures of concern, the sinking will prevent the release of volatile inorganics and will decrease release caused by thermal expansion of cask gases due to heating by the fire.

The 15 years of Lloyd's Casualty data analyzed during this study contained 1,947 collisions. Only seven of these collisions led first to fires and then to sinkings. Therefore, the conditional probability of a sinking given a collision that leads to a fire is $P_{sink} = 3.6 \times 10^{-3}$.

8.3 Estimated Values for Severity Fractions and Scenario Probabilities

Table 8-3 summarizes the estimates made above for the probabilities that enter Eqns 8.1 through 8.4.

Table 8-3. Values of Scenario Event Probabilities

Event	Probability	Value	
		Charter Freighter	Break-Bulk Freighter
A ship collision occurs while sailing from Charleston to Cherbourg	$P_{collision}$	9.5×10^{-5}	9.5×10^{-5}
The RAM ship is the struck ship	$P_{RAM\ ship\ struck}$	0.5	0.5
The strike location is midship	$P_{strike/midship}$	0.33	0.38
The RAM cask location is midship	$P_{cask/midship}$	1.0	1.0
The RAM hold is struck	$P_{RAM\ hold\ struck}$	1.0	0.33
Cask crush occurs	P_{crush}	0.03	0.1
Cask puncture or shear occurs	$P_{puncture/shear}$	0.2	0.2
A fire starts on the RAM ship, spreads to the RAM hold, engulfs the cask, and then burns hot enough and long enough to increase radioactive release from the failed cask	$P_{severe\ engulfing\ fire}$	6.0×10^{-5}	2.0×10^{-5}
The RAM ship sinks	P_{sink}	3.6×10^{-3}	3.6×10^{-3}

Substitution of these values into Eqns 8.1 through 8.4 yields estimates for the probabilities of the two hypothetical illustrative scenarios posed at the beginning of this section. These estimates are presented in Table 8-4.

Inspection of Table 8-4 shows that, while making a transatlantic voyage, the chance that a break-bulk freighter that is carrying a RAM cask will be involved in a ship collision is about 10^{-4}. Given that a collision occurs, the chance that the freighter is the struck ship, that the hold that is struck is the hold where the RAM cask is stowed, and that the struck hold is penetrated deeply enough to cause the seal of the RAM cask to fail is less than or approximately 10^{-2}. Given that seal failure occurs, the chance that the collision also leads to a second cask failure due to puncture or shear and to a fire that spreads to the RAM hold and there burns hot enough and long enough to significantly increase release of radioactivity

Table 8-4. Values of Collision Probabilities, Severity Fractions, and Scenario Probabilities for a Transatlantic Voyage from Charleston, South Carolina, to Cherbourg, France

Scenario	Cask Failure	Probability or Severity Fraction	Value	
			Charter Freighter	Break-Bulk Freighter
Severe Collision Only	Seal Failure	$P_{collision}$	9.5×10^{-5}	9.5×10^{-5}
		$F_{severity/collision\ only}$	5.0×10^{-3}	6.3×10^{-3}
		$P_{release/collision\ only}$	4.7×10^{-7}	6.0×10^{-7}
Very Severe Collision plus a Severe Fire	Seal Failure plus Puncture or Shear Failure	$P_{collision}$	9.5×10^{-5}	9.5×10^{-5}
		$F_{severity/\ collision\ +\ fire}$	5.9×10^{-8}	2.5×10^{-8}
		$P_{release/collision\ +\ fire}$	5.6×10^{-12}	2.4×10^{-12}

from the cask is less than or approximately 10^{-5}. Finally, because the collision-only accident analyzed is the least severe accident expected to cause cask failure, while the double failure, collision-plus-fire accident is probably about as severe an accident as is at all credible, the range of these results, 10^{-6} to 10^{-11}, represents the likely range for the chance that a severe ship accident (severe collisions with or without severe fires) leads to the release of radioactivity from a Type B spent fuel cask during a transatlantic crossing.

8.4 References

1. D. J. Ammerman and J. S. Ludwigsen, "Crush Loadings to Radioactive Material Transportation Packages during Ship Collisions." (Submitted for publication to *Intl. J. Radioactive Materials Transportation.*)

9. SOURCE TERMS

If a ship collision or fire damages a RAM cask being transported on the ship, radioactive vapors and/or aerosols could be released from the cask to the environment. The magnitude M_i of the release of radioactive specie i is usually estimated as the product of three quantities, the inventory I_i of species i in the cask, the fraction f_{ICi} of that inventory that is released from the radioactive material being carried in the cask to the atmosphere of the cask, and the fraction f_{CEi} of the amount released to the cask atmosphere that escapes from the cask to the environment. Thus, the magnitude M of the total release is given by

$$M = \sum_i M_i = \sum_i I_i f_{ICi} f_{CEi}$$

Cask inventories for specie i may be precisely calculated using a number of codes, for example, ORIGEN [1]. Values for f_{ICi} are usually based on the experiments of Lorenz [2] which measured the release of radioactive vapors and aerosols from spent fuel rods. Wilmot [3] suggested a value of 0.05 for f_{CEi} for vapors and aerosols. As this value was the result of expert judgement, the Modal Study [4] chose to assume that $f_{CEi} = 1.0$, an assumption that probably was quite conservative.

For this study, MELCOR calculations were performed in order to estimate values for f_{CEi} for a range of cask failures and failure conditions. MELCOR is a compartment code that implements a full suite of thermal-hydraulic and fission product transport processes [5]. For this study, release of radioactive gases, vapors, and aerosols from spent power reactor fuel carried in a transnuclear TN-125 cask [6] was examined for a range of accident conditions. Specifically, the dependence of f_{CEi} values on the size of the cask failure and the temperature of the cask was investigated by an extensive series of MELCOR calculations. The size of the hole in the cask was used as a surrogate for the magnitude of the mechanical damage done to the cask by the ship collision. The temperature of the cask was used as a surrogate for the effects of a ship hold fire on the cask and its contents.

The input to these MELCOR calculations and the results of these calculations are summarized in this section. The calculations are fully described in Appendix IV, Cask-to-Environment Release Fractions.

9.1 MELCOR Input

MELCOR calculations require specification of the thermal and hydraulic properties of the system being examined, here the TN-125 shipping cask [6] and its Westinghouse fuel assemblies. Thus, the cask had to be represented as a set of compartments connected by flow paths, and the thermal response of the walls of these compartments also had to be specified so that the effects of an engulfing fire on the temperature of cask and its contents (spent fuel assemblies and the basket that holds the assemblies) could be calculated. In addition, the amount of each radioactive aerosol and gas that is released into the cask atmosphere due to failure of fuel rods during the hypothetical ship collision and/or fire also had to be specified. This input data is summarized in Sections 9.1.1 through 9.1.6.

9.1.1 The TN-125 Cask

The cylindrical carbon steel shell of the TN-125 cask is 6 feet long and has an outer diameter of 4 feet. The shell is clad with stainless steel and is surrounded by a 4-inch thick hydrogenous resin layer that functions as a neutron shield. The cask is capped by a lid that is 14 inches thick. Cask cooling is provided by approximately 60,000 nickel-chromium fins that are attached to the cask shell and protrude

through the neutron shield layer. Each fin is 13 inches long and has 15 in^2 of surface that is exposed to the air. Each TN-125 cask holds 12 Westinghouse 15 × 15 fuel rod assemblies in a basket that has 12 square fuel assembly lodgements with 0.75 feet sides. The basket is divided into four quadrants that are separated by a cross-shaped channel centered on the cask axis. The vertical spacer plates that support the walls of the lodgements and the cross channel are tied together by four horizontal tie rods. There is a 1 to 2 mm gap between the basket and the cask shell. When filled with 12 fuel assemblies, the cask has a free volume of 2.68 m^3. During transportation, this free volume is normally filled to 0.05 MPa (0.5 atm) with dry air or nitrogen.

9.1.2 Westinghouse Fuel

Each 15 × 15 Westinghouse fuel assembly contains 204 Zircaloy fuel rods. Each rod has an 0.422-inch outer diameter and an active fuel length of 144 inches. When loaded with fresh uranium dioxide fuel pellets, each rod has a free volume of about 34 cm^3. Cladding creep and fuel swelling during reactor operation converts this free volume into an internal network of voids and cracks dispersed through the interior of each pellet. During normal transport, decay heating of the fuel and the rods heats the helium rod fill gas to 538°C which pressurizes each rod to about 20 MPa (200 bars).

9.1.3 Cask Hydraulics

In order to model the flow of gases from failed rods into the cask, within the cask, and out of the cask through hypothetical cask failures, the cask was divided into eight compartments that are interconnected by eight flow paths. Table 9-1 identifies the eight compartments and lists the free space in and the initial gas temperature of each compartment. Table 9-2 lists the properties of the eight flow paths that interconnect the eight cask compartments and also of the hypothetical flow paths through the failed rod cladding (total over all failed rods) and through the failed cask seal to the environment (one large failure and one small failure, each examined separately) that were assumed to be caused by the ship collision and/or fire. The location of these compartments and flow paths is depicted schematically in Figure 9-1. Figure 9-1 shows: that the free volume of the 12 basket lodgements is modeled as a stack of five compartments numbered V1 through V5, that the lumped flow path that models the rod failure flow paths is numbered F0, that this flow path connects the failed rods to the middle compartment (compartment V5) of the stack of five compartments that represent the free volume of the basket lodgements, and that the seal failure flow path is numbered F9.

9.1.4 Cask Thermal Properties

The temperatures of the cask atmosphere and of internal cask surfaces strongly influence gas flow and fission product transport within the TN-125 cask. For example, cask pressurization and depressurization, aerosol agglomeration and transport, and the evaporation and condensation of fission product vapors (e.g., CsOH, CsI, TeO) are all temperature dependent processes. Thus, in order to model gas flow and fission product transport inside of the TN-125 cask, it was necessary to model heat transport through and between major cask structures and between the cask and the environment.

The heat transport processes which needed to be modeled included:

- Heat exchange between the cooling fins and the ambient environment during normal operation including heating by solar insolation,

Table 9-1. Compartments Used to Model the TN-125 Cask

Identifier	Volume Description	Volume (m^3)	Initial Temperature (°C)
V1	Fuel Lodgment - Upper Section	0.325	477
V2	Fuel Lodgment - Upper Mid Section	0.325	477
V3	Fuel Lodgment - Center Section	0.325	477
V4	Fuel Lodgment - Lower Mid Section	0.325	477
V5	Fuel Lodgment - Bottom Section	0.325	477
V6	Lower Cask Region	0.230	165
V7	Basket Center Space (Cross)	0.591	279
V8	Upper Cask Region	0.233	165

Table 9-2. TN-125 Cask Flow Paths

Identifier	Pathway Description	Flow Area (m^2)	Form Loss Coefficient	Friction Term	Flow Resistance (m^{-4})
F0	Fuel Rod Ruptures	6.88×10^{-4}	2400	5244	8.1×10^{9}
F1	Exit from Fuel Lodgments into Cask Upper Region	0.398	1.5	0.48	6.3
F2, F3, F4, F5	Intermediate Lodgment Pathways	0.398	2.4	0.96	10.6
F6	Entrance to Fuel Lodgments from Bottom Region	0.398	1.5	0.48	6.3
F7	Entrance to Cross from Cask Bottom Region	0.189	200	0.64	2820
F8	Exit From Cross into Cask Upper Region	0.189	200	0.64	2820
F9-S	Small Cask Seal Leak	4×10^{-6}	5	7	3.8×10^{11}
F9-L	Large Cask Seal Leak	1×10^{-4}	5	7	6.0×10^{8}

- Heating of these fins by a hypothetical fully engulfing pool fire,
- Heat conduction through the fins, the resin layer, and the steel shell of the cask,
- Heat transport through the gap between the steel shell of the cask and the basket,
- Heat conduction through the basket,
- Heat transport through the gap between the basket lodgment walls and the fuel assemblies,
- Heat transport within the fuel assemblies,
- Convective heat transport between the fuel rods and the lodgment gases, and
- Heat transport to structures in the end regions of the cask.

Accordingly, thermal models were constructed for three heat structures, the cask, the cask basket, and the fuel assemblies carried in the basket, and models of heat transfer between the fuel and the basket, between the basket and the cask, and between the cask and the environment were also developed.

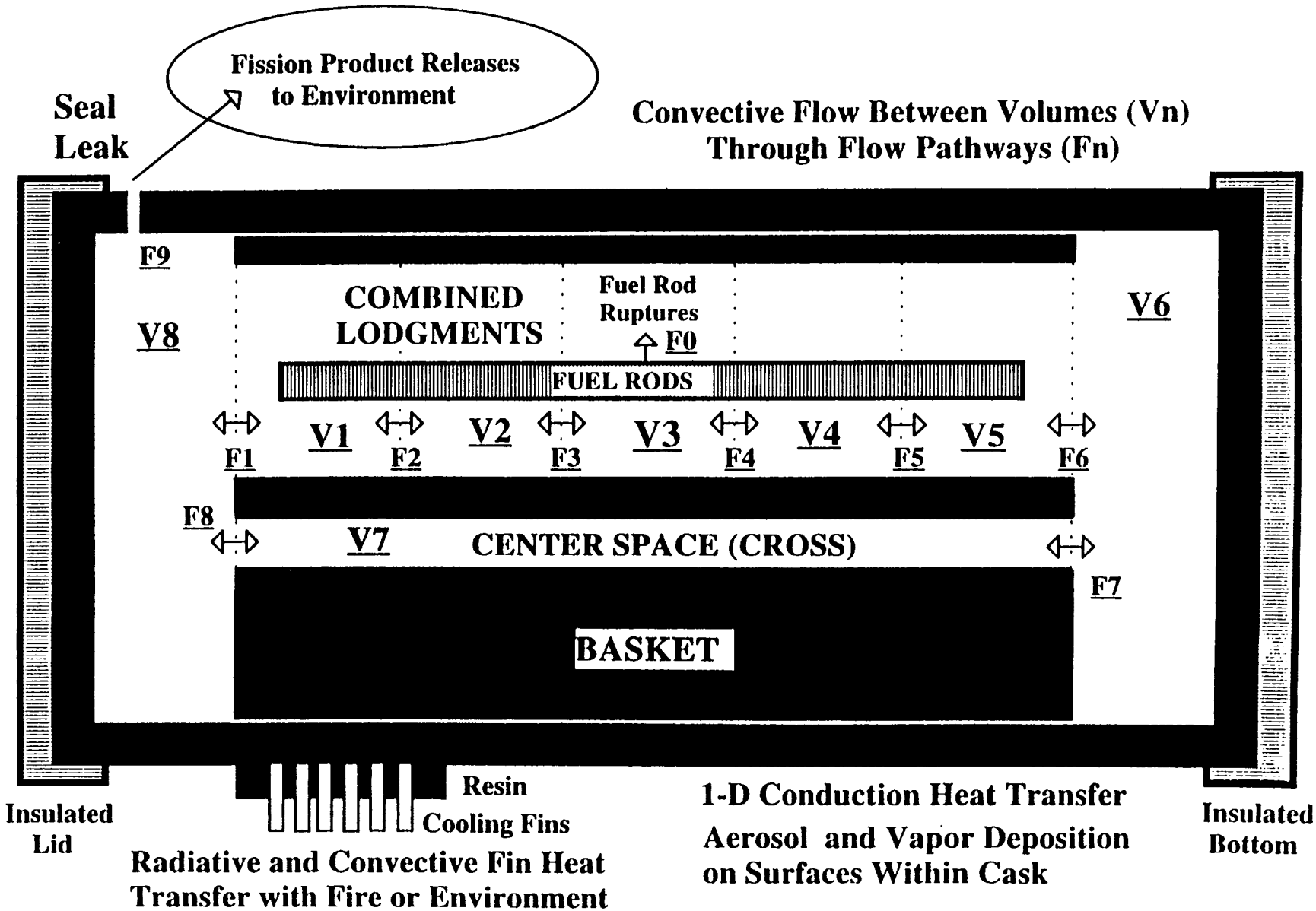

Figure 9-1. TN12 Shipping Cask Hydraulic Model.

One-dimensional models of heat conduction through structures and of convective and radiative heat transfer between the surfaces of these structures and the atmospheres that surround them are implemented in the MELCOR code [5]. Other heat transport processes, such as surface-to-surface radiative heat transfer can be modeled indirectly by implementing appropriate equations using MELCOR's unique control function logic [5] and applying the computed heat fluxes to the affected structures using the surface boundary conditions selected for those structures.

Several important assumptions were made during the development of the heat structure and heat transport models, a number of assumptions and modeling choices were made. These include:

- The cask cooling fins and resin layer were modeled as equivalent one-dimensional heat conducting cylinders,
- The resin is inert, although it can char during a fire,
- The cask shell along the length of the basket was modeled as a one-dimensional symmetric cylinder that had a uniform diameter and wall thickness along its entire shell length,
- Axial heat conduction in cask heat structures was neglected except for conduction through the steel shell of the cask to its end regions (the cask lid and bottom),
- Heat loss from the cask through the cask lid and bottom was neglected, because of the low thermal conductivity of the balsa wood impact limiters that protect the ends of the cask,
- The impact limiters are not seriously damaged during ship collisions,
- The cask-to-basket radial gap was assumed to have a constant width of 0.135 mm (the value specified in the cask Safety Analysis Report (SAR) [6] for normal operating conditions),
- The basket was modeled as an equivalent one-dimensional heat conducting cylinder,
- Because the basket thermal conductivity is high, all of the twelve fuel assemblies carried in the basket behave identically regardless of their locations within the basket,
- The fuel assemblies were modeled as one-dimensional cylinders,
- Fuel assemblies properties were developed by homogenizing the properties of individual fuel components (the fuel cladding and pellets),
- Because properties for casks filled with nitrogen were not readily available, homogenized fuel properties for assemblies shipped in helium were used rather than properties for assemblies shipped in nitrogen,
- The decay heat power of the fuel carried in the cask contents was assumed to be 120 kW, the maximum rated value for the cask,
- The decay power was uniformly distributed along the length of the fuel rods,
- Decay heat is dissipated from the cask entirely through the cask's cooling fins, and
- Gamma radiation heat transport was neglected.

The TN-125 cask thermal model is shown schematically in Figure 9-2. Each submodel is now briefly described. Details of the specific submodels (equations and parameter values) are presented in Appendix IV.

9.1.4.1 ENVIRONMENTAL CONDITIONS FOR NORMAL TRANSPORT

Ambient conditions were defined as follows: temperature = 38°C, pressure = 1.0 standard atmosphere, and solar insolation = 1354 Wm^{-2} applied uniformly to the tips of all of the cask fins which together had a surface area of 31.24 m^2.

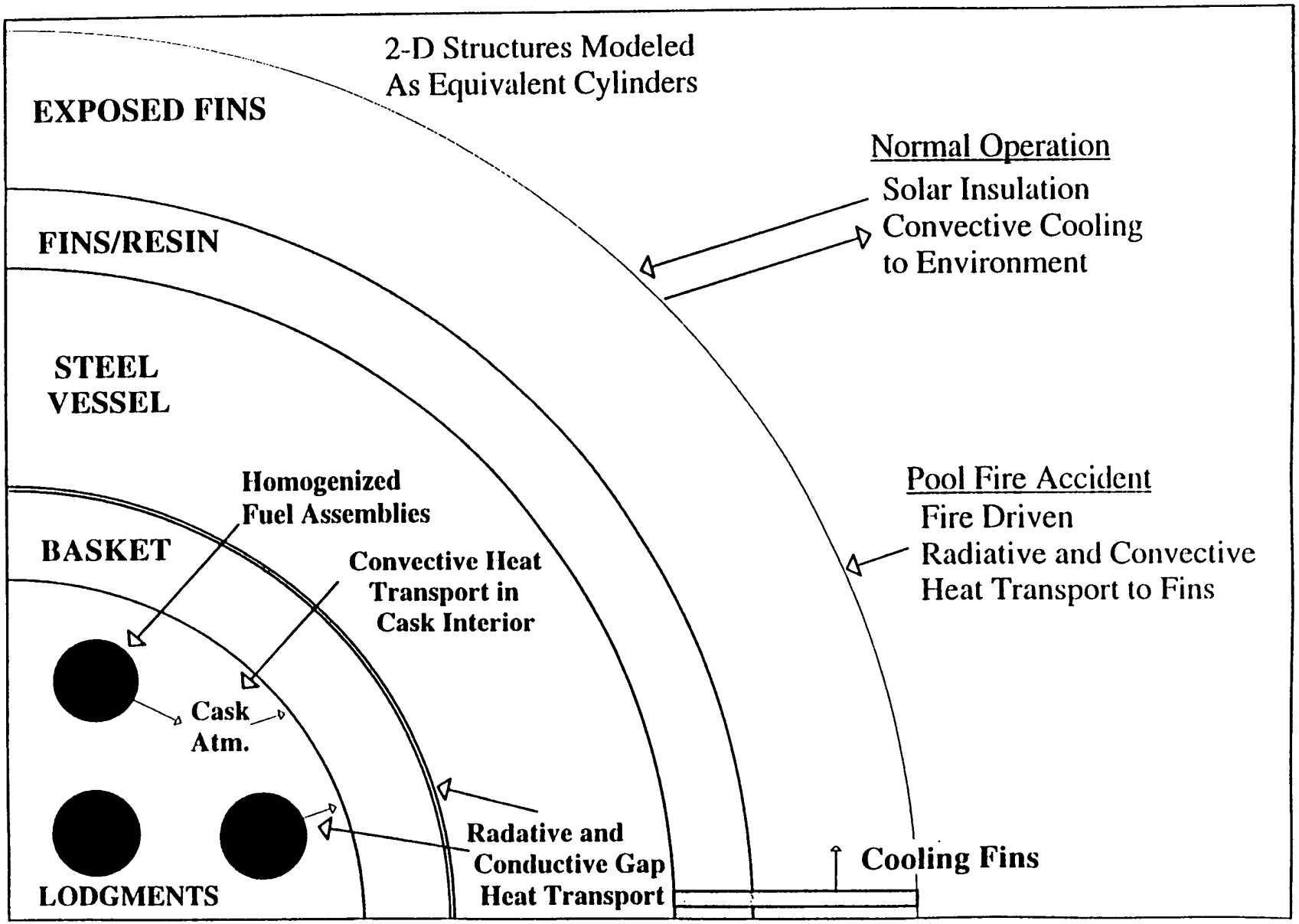

Figure 9-2. TN12 Shipping Cask Thermal Model.

9.1.4.2 ENGULFING POOL FIRE

The development of the pool fire was not modeled. Instead attainment of fully-developed fire conditions characterized by a constant average fire temperature was assumed. Two average fire temperatures were examined, 800 and 1200°C. The heat flux produced by fully-developed fires having these average flame temperatures was calculated using an experimental correlation based on measured heat fluxes from pool fires to large cylindrical calorimeters [7].

9.1.4.3 COOLING FINS AND RESIN LAYER

The exposed portions of the casks cooling fins, and the resin layer and the portions of the fins embedded in that layer, were both modeled as a one-dimensional cylindrical heat structures. During normal transport, cask cooling occurs by conduction of heat through the fins and transfer from the fins to the ambient atmosphere primarily by convection and secondarily by radiation. When engulfed by a pool fire, cask heating occurs predominantly by radiative heat transfer to the fin tips. The thermal properties of the two cylindrical heat structures were given values (1) that caused the amount of heat conducted through the layers to match the measured amount conducted through the fins under normal transport conditions, and (2) that made the two cylindrical heat structures together have a heat capacitance equal to that measured for the fins and the resin layer.

9.1.4.4 CASK SHELL-TO-BASKET GAP

The TN-125 cask SAR states that under normal operating conditions the width of the gap between the steel cask shell and the aluminum basket is 0.135 mm. Although expansion of the basket when heated by a fire would decrease this gap width, the value of 0.135 mm was used both for normal transport conditions and for engulfing fire conditions. Heat transport across this gap occurs by conduction, convection, and radiation with conduction dominating under normal transport conditions. Gap gases were assumed to have thermal properties identical to those of nitrogen gas. Because heat transfer from gap gases to the gases in the lid and bottom regions of the cask was small, it was neglected. The effects of turbulence in the gap gases and of pressurization of those gases on heat transport through gap gases were also neglected.

9.1.4.5 BASKET

The basket is divided into four quadrants by the axial cross-shaped channel that spans its entire length. Each quadrant contains three lodgements for fuel assemblies, which are located at two different distances from the circumference of the basket. Two-dimensional modeling of a similar basket that contained 21 lodgements has shown that the temperatures of fuel assemblies in inner lodgements are quite similar to those of assemblies located in outer lodgements [8]. This suggests that radial heat conduction through basket structures is much more rapid than heat transport across the fuel-basket gap or across the basket-cask shell gap. Since this should also be true for the TN-125 basket with its 12 lodgements, the TN-125 basket was modeled as a one-dimensional equivalent cylinder having an average density of 3318 kg m^{-3}, and the temperatures of the 12 fuel assemblies transported in the basket were assumed to be the same.

9.1.4.6 BASKET-FUEL GAP

Because the basket-to-fuel gap is about 46 times larger than the basket-to-cask shell gap, heat transfer across the basket-fuel gap is dominated by radiation rather than conduction with convection being relatively unimportant except during rod depressurization. Although convection was not important for heat transport across the fuel-basket gap, it did control the temperature of the gases in this gap.

9.1.4.7 FUEL ASSEMBLIES

Each Westinghouse 15 × 15 PWR fuel assembly holds 204 fuel rods. Heat transport along rods is driven by conduction. Heat transport between rods occurs directly by radiative transport and indirectly by conduction through the gases that surround the rods. Circulation of these gases also causes some heat to be transported between rods by convection. Because decay heating raises the rods to elevated temperatures, heat transfer between rods is principally driven by radiation. Because rod-to-rod conductive and radiative heat transport was computationally intractable, fuel assemblies were modeled as homogenized equivalent cylinders with densities and temperature dependent heat capacities chosen such that the homogenized cylinder had a mass and heat capacitance equal to that of a real assembly. An effective thermal conductivity for the homogenized cylinder was derived using a two-dimensional finite element thermal analysis code able to model rod-to-rod heat transport. The temperature dependence of the density, specific heat capacity, and thermal conductivity of the homogenized fuel were taken from the literature [8]. Values for assemblies immersed in helium rather than nitrogen were used because values for nitrogen were not readily available. Use of homogenized properties for fuel assemblies immersed in helium rather than in nitrogen overpredicted conductive transport between rods. Because heat transport between rods is dominated by radiation, the magnitude of the overprediction was probably no more than a factor of two.

9.1.4.8 CONVECTIVE HEAT TRANSPORT TO LODGEMENT GASES

The homogenized cylinders used to represent the fuel assemblies transported in the TN-125 cask had surface areas that were substantially smaller than the surface area of the 204 rods carried in each real assembly. Therefore, MELCOR's convective heat transport models underpredicted convective heat transfer from the 12 fuel assembly heat structures to the gases that contacted those structures. As fission product vapor transport depends strongly on gas temperatures, this underprediction was of concern.

In order to properly model convective heat transfer from fuel rods to lodgement gases, MELCOR's convective heat transfer models were disabled for fuel assembly heat structures and were replaced with a model that was implemented via MELCOR's control function logic and used a surface area equal to the active fuel cladding surface area of the 204 rods carried in a single assembly. The replacement convective heat transfer model assumed (1) that variation of rod surface temperatures with rod length could be neglected because decay heating of rods caused rod surface temperatures to be quite similar over the length of the rods, (2) that radial heat transfer caused the surface temperatures of individual rods to depend strongly on their location within a fuel assembly, and (3) that lodgement gas temperatures varied significantly along the axial length of the lodgement.

Division of lodgement volumes into five axial subvolumes (volumes V1 through V5 in Figure 9-1) allowed the variation of gas temperatures along the length of the lodgements to be modeled. The effect the radial variation of rod surface temperatures within a fuel assembly on convective heat transfer was modeled by allocating the surface area of the rods in an assembly to nine radial regions and calculating a

different surface temperature for the rods in each radial region. This was done by dividing the equivalent cylinder that represented each fuel assembly into nine concentric, cylindrical shells. Convective heat transfer between each shell and the gases that contacted that shell was then calculated separately for each of the five axial lodgement gas volumes.

9.1.4.9 CONVECTIVE HEAT TRANSFER TO THE GASES IN THE CROSS VOLUME

Convective heat transfer from basket surfaces to cross volume gases would also have been underpredicted if referenced to the surface area of the equivalent cylinder used to model radial heat transfer through the basket and from the basket to neighboring heat structures. Therefore, as was done for the fuel assemblies, for convective heat transfer from the spent fuel basket to cross gases, MELCOR's convective heat transfer models were disabled and replaced by a model implemented via control functions that used the actual surface area of cross internal surfaces and the actual temperature difference between these surfaces and the bulk temperature of cross volume gases.

9.1.4.10 CONDUCTIVE HEAT TRANSPORT TO CASK END STRUCTURES

Because the cask lid and bottom were surrounded by wood impact limiters that also insulated these cask structures, axial heat transfer to these structures had little effect on the transfer of heat between the cask and the environment. However, the temperature of the internal surfaces of cask end structures (the cask lid, bottom, and the top and bottom parts of the cask shell that were not next to active fuel) did strongly influence the deposition of fission product vapors onto these heat structures and thus the retention of fission product vapors by the cask. Therefore, axial conduction of heat through the cask shell-to-shell end regions and from shell end regions to the cask lid and bottom was modeled by making conduction proportional to both the cross-sectional area of the cask shell and to the temperature difference between either the center of the cask shell and the ends of the cask shell or the ends of the cask shell and the cask lid and bottom. Loss of heat from end structures to the environment was set to zero to reflect the insulating effect of the cask impact limiters.

9.1.4.11 VALIDATION OF THE CASK FIN COOLING MODEL

As reported in the SAR for the TN-125 cask [6], Transnuclear, Inc., built a full-scale test model of a 0.513-meter axial section of the finned zone of the TN-125 cask to verify the thermal performance of the fins. The steel shell of the cask was simulated by two concentric shells of mild steel separated by a 3 mm thick cement layer. The shell was equipped with cooling fins identical to those on a real TN-125 cask. The ends of the model were capped by drums packed with glass wool to provide insulation. Because heat loss through the drums was insignificant, heat loss from the model cask section occurred almost exclusively through its fins. The full-scale cask section was heated by evenly spaced electrical heaters mounted inside the shell of the test section, 10 mm from its inner surface. The 14,700 watts delivered to the heaters during the test of the thermal performance of the fins equaled the decay power of a fully loaded TN-125 cask. During the test, the model was oriented with its cylindrical axis parallel to the ground.

This fin heat dissipation test was simulated with the MELCOR code using only the thermal model of the cask shell, resin layer, and fins. Power was introduced to the calculation as a heat source to the cask's internal atmosphere. The computed fin temperatures were then compared to the experimental temperatures to validate the cooling fin model.

The test apparatus was cooled by ambient air, which flowed around the circumference of the cask up over its fins. This flow was driven by natural convection, which forced air to flow around and through the fins from the underside to the topside of the test apparatus. Since the air was cooler when passing over the lower fins, then when passing over the upper fins, the resulting experimental temperatures were not symmetrical around the circumference of the test apparatus. Therefore, the results of the MELCOR calculations were compared to the average of the experimental temperatures measured around the circumference of the test section.

The effective fin convective heat transfer coefficient used in the MELCOR calculations was adjusted to obtain the best fit to the experimental data. Figure 9-3 shows that the use of a value of 2.8 $Wm^{-2}K^{-1}$ for this effective heat transfer coefficient provided excellent agreement with the test temperature data. Moreover, this value is quite close to the value of 2.5 $Wm^{-2}K^{-1}$ that was derived in the SAR from the experimental data. The calculated fin temperatures were found to decrease about 1.8K for each 0.1 $Wm^{-2}K^{-1}$ increase in the effective convective heat transfer coefficient. Figure 9-3 shows that the largest deviation between the experimental results and the MELCOR predictions was at the fin tips where MELCOR predicted a 5°C higher temperature than the SAR reported. The SAR reported an average fin tip temperature of 80°C. However, within uncertainties, the measured temperature distribution around the test section experimental apparatus was also consistent with the average temperature of 85°C predicted by the MELCOR model. In addition, the uncertainty in the test results was probably significantly larger than the difference between the MELCOR results and the test results.

Because the fin heat dissipation benchmark calculation demonstrated that the cask shell thermal models closely replicated the thermal behavior of the test cask, when the effective convective heat transfer coefficient of the cask fins was set to 2.8 $Wm^{-2}K^{-1}$, this value used in all subsequent calculations that that didn't involve a fire. During fire scenarios, heat transfer from the fire to the cask fins was dominated by radiative heat transfer to the fin tips and then conductive heat transfer through the fins to the steel shell of the cask. Therefore, although this benchmark calculation did not model radiative heat transfer to the cask fins, it does show that heat transfer from the fins to the cask shell is appropriately modeled.

9.1.4.12 VALIDATION OF THE CASK THERMAL MODEL FOR NORMAL OPERATING CONDITIONS

The full MELCOR thermal model for the TN-125 shipping cask was run in a steady state mode until model parameters, especially temperatures, achieved their steady state values for normal transport conditions. Table 9-3 compares radiative, conductive, and convective heat transport across cask gaps and from the cask to the environment for normal transport conditions.

The TN-125 SAR [6] contains estimates of steady state normal operating temperatures along a mid-cask cross section. The steady state temperatures computed by MELCOR were compared to these SAR temperatures as a validation of the full MELCOR thermal model of the TN-125 cask. Tables 9-4 and 9-5 present the results of this comparison. Table 9-4 presents temperatures at specific radial locations in the cask; Table 9-5 presents temperature differences across cask components.

Both the MELCOR and the SAR calculations assumed an ambient temperature of 38°C and a constant decay heat power of 120 kW. Table 9-4 shows that the component temperatures computed by MELCOR were in good agreement with those presented in the SAR (ΔT = 3 to 8°C) for the cask shell, basket, and lodgment walls, and total cask gases. As the fin, resin, and shell temperatures predicted by MELCOR were all slightly higher than those given in the SAR, the MELCOR model appears to be slightly less efficient at cooling the cask than the SAR model. In contrast to the good agreement for the fins, resin

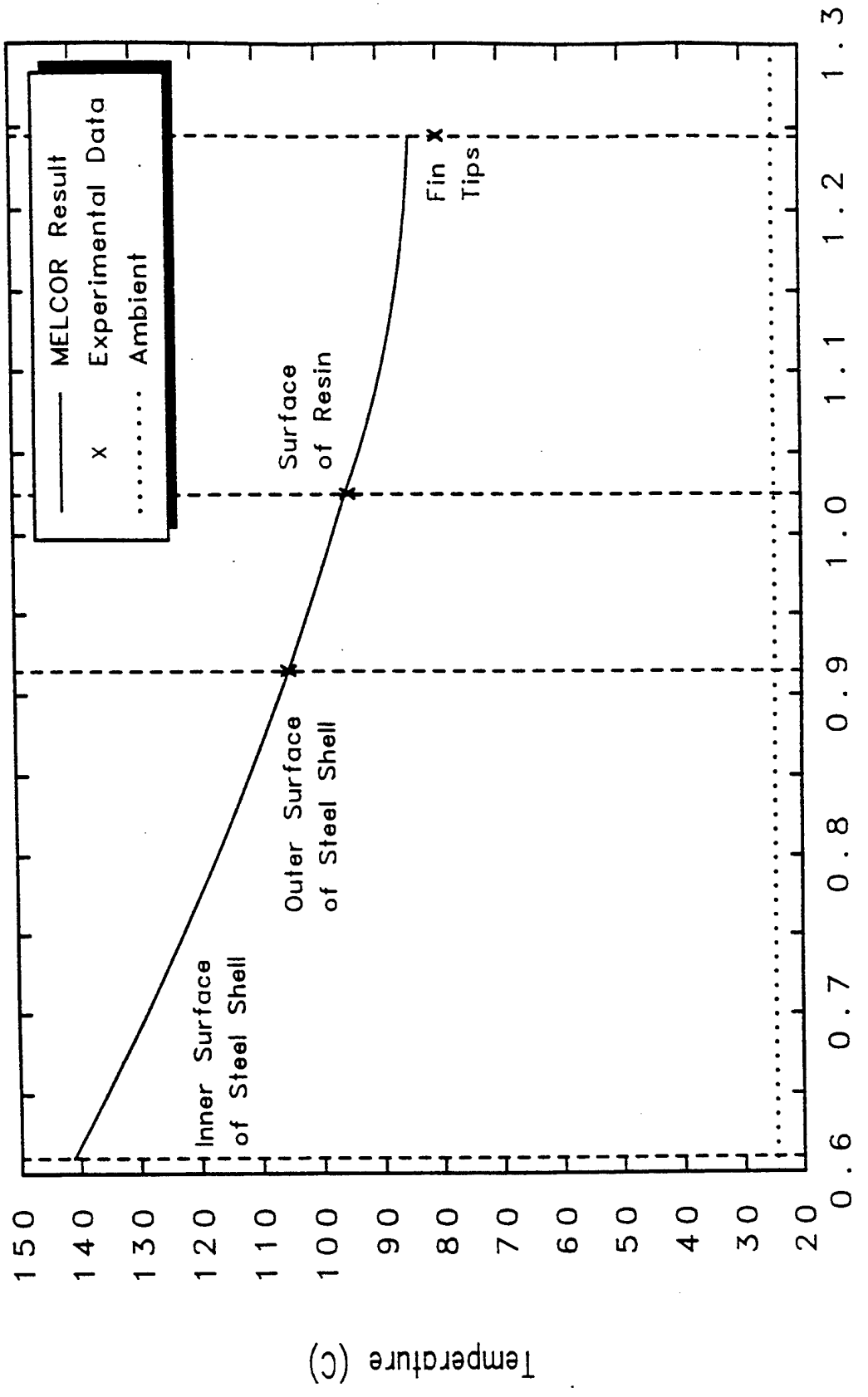

Figure 9-3. MELCOR Model Steady-State Fin Benchmark.

Table 9-3. Relative Importance of Heat Transport Processes During Normal Transport Conditions

Heat Transport Process	Heat Transported from Cask, kW		
	Spent Fuel to Basket Gap	Basket to Steel Shell Gap	Cask Exterior to Environment
Radiative Heat Transport	91.7	3.9	23.6
Conductive Heat Transport	28.1	116.1	0
Convective Heat Transport	0.2	0.04	38.7
Solar Insolation	0	0	–42.3
Total	120	120	120

Table 9-4. Comparison MELCOR and SAR Normal Transport Temperatures

Location	Temperatures (°C)		
	MELCOR	SAR	Difference
Ambient	38	38	0
Tip of Fins	121	116	5
Resin Surface	130	124	6
Outer Steel Shell	140	134	6
Inner Steel Shell	193	188	5
Outer Basket	219	216	3
Lodgment Walls	279	275	4
Outer Fuel	376	421	– 45
Inner Fuel	569	518	51
Lodgment Gases	443	472	– 29
All Cask Gases	359	367	– 8

Table 9-5. Comparison MELCOR and SAR Normal Transport Temperature Differences

Component	Temperature Differences Across Components (°C)		
	MELCOR	SAR	Ratio
Fin Tips-to-Environment	83	78	1.06
Exposed Fins	9	8	1.13
Resin Layer	10	10	1.00
Steel Shell	53	54	0.98
Steel Shell-to-Basket Gap	26	28	0.93
Basket	60	59	1.02
Basket-to-Spent Fuel Gap	97	146	0.66
Fuel Assemblies	193	97	1.99
Total	531	480	1.11

layer, and cask shell, the temperatures predicted by MELCOR for outer and inner fuel differed substantially from the temperatures given in the SAR ($\Delta T = -45$ and 51°C, respectively). Consistent with this result, the MELCOR prediction of the temperature of lodgement gases is 29°C lower than the SAR prediction.

Table 9-5 shows that both the MELCOR model and the SAR predict quite similar temperatures differences across cask components for all cask components except the basket-to-spent fuel gap and the fuel assemblies for which temperature difference ratios of 0.66 and 1.99 were obtained. The SAR calculation overpredicted the temperature required to drive the 120 kW of power across the gap between the outer fuel rods and the lodgment walls for two reasons. First, the SAR calculation did not include conductive heat transport through the nitrogen gas which, in the MELCOR calculation, accounted for 23 percent of the heat transport across this gap. Second, the SAR calculation used an emissivity of 0.55 for the fuel whereas the MELCOR calculation used 0.8. Both used 0.55 for the emissivity of the lodgment walls. The SAR emissivity of 0.55 rather than 0.8 for fuel results in about a 20 percent reduction in radiative heat transport for the same surface temperatures. Since the spent fuel emissivity of 0.8 is a measured value for typical PWR spent fuel [8] and conductive heat transport through the gas was significant, the outer fuel temperature calculated by MELCOR is believed to be more valid than the SAR temperature.

The MELCOR input model predicted an inner fuel temperature that was 51°C hotter than the temperature reported in the SAR despite the fact the outer temperature predicted by MELCOR was 45°C colder than the SAR temperature. Thus, the MELCOR calculation predicted a temperature drop across a fuel assembly of 193°C rather than the 97°C drop reported in the SAR. This difference results from different assumptions about the emissivity of fuel and about the efficiency of rod-to-rod radiative heat transport. Specifically, the MELCOR calculation, in agreement with measured data for PWR fuel [8], assumed a value of 0.8 rather than 0.55 for the emissivity of fuel, and, as is proper, restricted rod-to-rod radiative heat transfer to rod pairs separated by no more than four rod pitches instead of allowing radiative heat transfer between all pairs of rods in a fuel assembly. Thus, the MELCOR result is believed to be superior to the SAR result. This conclusion was checked by estimating the temperature difference from the center to the edge of a fuel assembly using a textbook equation [9]. Since this calculation gave a temperature difference of 192.5°C, which agrees well with the MELCOR result, the MELCOR result is believed to be validated.

9.1.5 Fuel Rod Depressurization

Transport of aerosols and fission product vapors from failed fuel rods through the cask to the environment by gas flows released into the cask by rod failure and vented from the cask by cask failure provide the dominant pathway for release of radioactive species during transportation accidents. Thus, fuel rod depressurization had to be reasonably modeled if radionuclide release fractions were to be estimated with any precision.

In fresh fuel, rod depressurization occurs by gas flow through the fuel-cladding gap to the location of the rod failure. But irradiation causes fuel pellets to crack and swell and cladding to creep down onto the pellets contained within the clad. These physical and dimensional changes cause the fuel-cladding gap in aged irradiated fuel to be converted into a network of cracks and voids inside of the pellets. Thus, depressurization gas flows in aged fuel must reach the rod failure location by flowing through the internal network of cracks produced by irradiation rather than through the fuel-cladding gap that was present when the fuel was fresh. The resistance of this network of cracks to gas flow depends on the spectrum of crack widths and shapes, and on the effective length of the flow path to the failure location,

which because of the tortuosity of the crack network is likely to be significantly longer than the linear distance along the clad to the failure location. In addition, plugging of cracks in this network by fuel fines entrained in the gas flows may diminish subsequent flows and thus fission product release.

Rod depressurization times depend not only on depressurization flow rates but also on the location of the rod failure. For example, because 40 percent of the gas volume of a rod is located in its upper plenum, rod failure near the top of the rod rather than near its bottom leads to more rapid depressurization because most of the rod gas has a relatively short flow path to the failure location.

Failure of the pressurized PWR fuel rods transported in the TN-125 cask was assumed to be caused either by collision forces or by overpressurization due to a fire that engulfs the cask. Rod failure test results suggest that typical rod failures have lengths no greater than 1 cm and cross-sectional areas of about 2 mm^2 [8]. Although neither collision forces nor the thermal loads of an engulfing fire are likely to fail all of the 2,448 rods carried in a fully loaded TN-125 cask, because many rods are likely to fail, we conservatively assumed the failure of all of the rods in the cask.

Because the likely mode of cask failure is seal failure, cask depressurization is unlikely to be rapid. Since cask depressurization is expected to be significantly slower than rod depressurization, the rod depressurization model did not need to be extremely precise. Thus, a simple model was constructed. The model treated gas flow from all of the failed fuel rods as a single equivalent flow. The model was developed from limited data using engineering judgment, and after development, was refined by performing trial calculations. The model consists of one control volume that represents the combined gas volume within all the failed rods and one flow path that simulates the friction and form losses of a typical crack network. The model assumes that all rod gases must flow through the same flow resistance, which is obviously not the case since the gases are distributed throughout the crack network within the pellets in the rod.

The parameters of the fuel rod depressurization flow model are listed in Table 9-6 for both an irradiated spent fuel rod, where depressurization flow is through a network of cracks in the irradiated pellets, and for a new unirradiated fuel rod, where depressurization flow is through the fuel cladding gap. The parameter values for irradiated fuel were based on new fuel design parameters from the Zion Updated Final Safety Analysis Report (UFSAR) [10], on scaling of the cracks and cladding gaps shown in pictures of spent fuel cross sections [Figures I-12 and I-13 of Reference 8], and on engineering judgment.

Several assumptions were required to complete this model. Whereas, the cross-sectional flow area of a new fuel rod was taken to be the cross-sectional area of the fuel-cladding gap, the cross-sectional flow area of a spent fuel rod was taken to be bounded by the sum of the cross-sectional areas of the individual cracks in a pellet. Since many of these cracks effectively dead end and many of the cracks are too narrow to support significant flow, the effective flow area of a spent fuel rod must be significantly reduced from that of a new fuel rod. Based on the pictures of spent fuel pellets, an effective flow area of 10 percent of the original fuel-cladding gap area was used in the rod depressurization model; and the effective flow path length was estimated to be 50 percent longer than the linear geometric length of the fuel. The flow hydraulic diameter was based on flow through cracks with an effective width of 10 percent of the cladding thickness; a form loss coefficient of 10 was applied to flow through each of 240 fuel pellets in a rod; and the surface roughness of the flow path was taken to be 25 percent of the average crack width because the height of the bumps on crack walls were about this large. Finally, the size of the cladding rupture was assumed not to add any additional flow resistance. The combined effect of these assumptions caused the total flow resistance for old fuel to be 430 times larger than the flow resistance of new fuel.

Table 9-6. Fuel Rod Depressurization Flow Parameters

Parameter	Units	New Fuel	Irradiated and Fragmented Fuel	Assumptions and Comments for Modeling Irradiated Fuel
Gas Volume	m^3	0.0833	0.0833 (2448 rods)	34 cm^3/rod
Gas Pressure	MPa	17.1	20	At 538°C (1000°F)
Flow Area	m^2	6.88×10^{-3} (Fuel-Clad Gap)	6.878×10^{-4} (2448 rods)	Effective Area for Irradiated Fuel = 10% of New Fuel Gap Area
Length of Flow	m	3.66 (Active Fuel Length)	5.49	Effective Flow Length = 150% of Active Fuel Length
Hydraulic Diameter	m	1.9×10^{-4} (Fuel-Clad Gap)	1.2×10^{-4}	Effective Width of Crack Flow Pathways = 10% of Clad Thickness
Form Loss Coefficient		2	2400	K = 10 for each of the 240 fuel pellets in a rod
Surface Roughness	m	1.5×10^{-5}	1.5×10^{-5}	25% of Crack Width
Roughness/Diameter		0.081	0.125	
Friction Factor		0.093	0.118	
Friction Loss Coefficient		1776	5244	
Total Loss Coefficient		1787	7644	
Flow Resistance	m^{-4}	1.88×10^{7}	8.08×10^{9}	Ratio = 430

Rod depressurization times and helium flow velocities through the hole in the failed rod for fuel rods that contain fresh and spent fuel as calculated using the fuel rod depressurization model are shown in Figures 9-4 and 9-5. The results shown were calculated assuming that the cask had not failed and that all of the 2,448 fuel rods had failed simultaneously. As modeled, full depressurization of a spent fuel rod takes about 3 minutes, whereas a new fuel rod depressurizes in a few seconds.

9.1.6 Release and Transport of Radionuclides

Estimation of the cask-to-environment release fractions for fission products requires the modeling of (1) fission product release from fuel pellets through failed fuel rods to the cask atmosphere, (2) the gas borne transport of fission products from the region of the cask where they are released (usually volume V3 in Figure 9-1) to the lid region of the cask (volume V8 in Figure 9-1) and from that region through the failed seal to the environment, and (3) the deposition of fission products onto cask internal surfaces that lie along the several gas transport paths that connect the rod regions to the lid region. Because some fission products (noble gases) transport as non-condensable gases, some as condensable vapors (CsOH, CsI, TeO), and others as aerosols (fuel fines), the release, transport in the gas phase, and deposition to internal cask surfaces of all of these species had to be modeled. Because aerosol agglomeration strongly influences the rate of deposition of aerosols to surfaces, agglomeration of gas borne aerosols also had to be modeled.

The MELCOR code was provided input data for one noble gas (Kr), for three fission product vapors (CsOH, CsI, and TeO), and for fuel fines. For Kr, only the size of the accident source term had to be

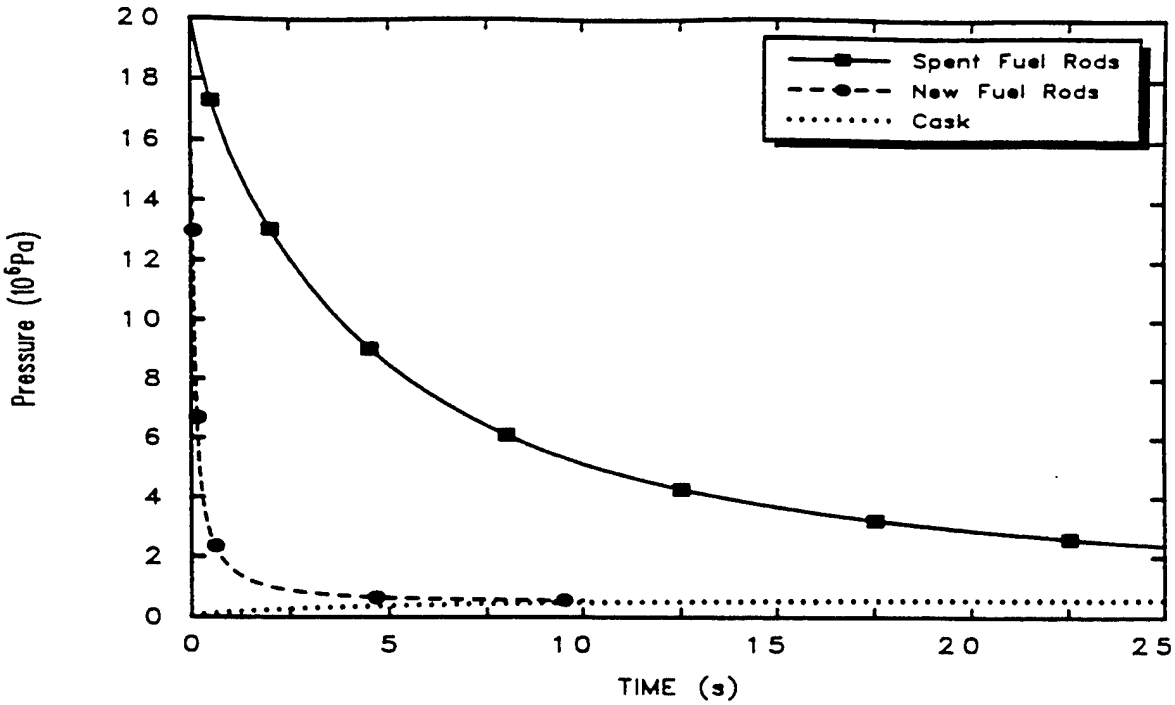

Figure 9-4. Fuel Rod Depressurization.

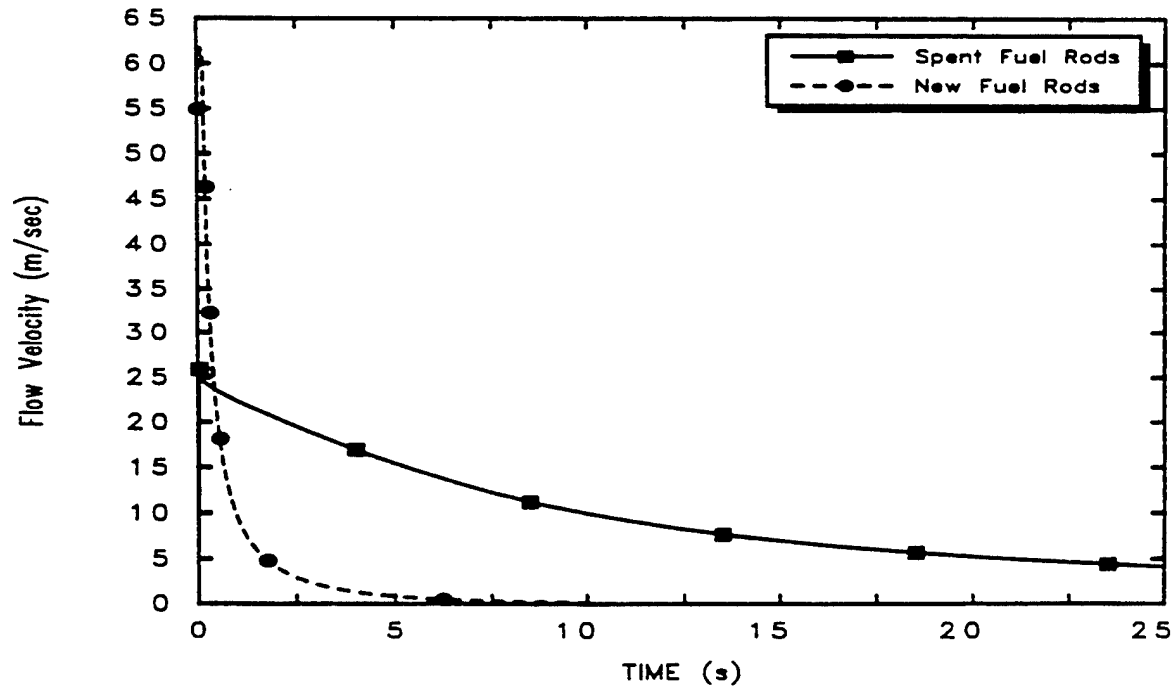

Figure 9-5. Fuel Rod Helium Flow Velocity.

provided. For the three fission product vapors, both source term magnitudes and vapor pressure curves [11] were required. For fuel fines, the mass of fines released as particles, the size distribution of those particles, and the values of the parameters that control the agglomeration and deposition of particles had to be specified.

9.1.6.1 RELEASE FRACTIONS FOR FUEL FINES

Experiments conducted by Lorenz [2] indicate that the release fraction for fuel fines from spent fuel not subjected to crush or impact forces is 3×10^{-5}. Although collision forces may produce additional fuel fines, the conversion of the pellet-cladding gap volume in fresh fuel into internal pore and crack volume in spent fuel means that only those fines generated at crack surfaces will be able to escape from the spent fuel pellets. Because the initial fuel-cladding gap has a volume that equals about 4 percent of the volume of the fuel pellets when fresh, conversion of this volume to a network of internal pores and cracks means that about 4 percent of the fuel fines produced by collision forces will be located on surfaces connected to the internal network of cracks in the spent fuel. In addition, only pellets located near fuel rod spacers are likely to experience forces large enough to cause fragmentation. Therefore, if only 20 percent of the pellets in a rod experience collision forces large enough to produce additional fracturing of fuel, if these forces fracture 2 percent of the mass of the affected pellets, and if 4 percent of these fines escape from the pellet, then the release fraction for fuel fines from rods subjected to collision forces will be $2 \times 10^{-4} = 3 \times 10^{-5} + 0.2 \times 0.02 \times 0.04$. As the upper bound release fraction for aerosols from rods, failed by the detonation of explosives on their surface, is about 1×10^{-3}, the value of 2×10^{-4} for the release fraction for fuel fines for collision accidents is approximately the geometric mean of the range defined by the Lorenz release fraction for fuel not subjected to additional accident forces and the release fraction for release of fines from fuel subjected to the force of an explosion.

9.1.6.2 SOURCE TERMS

Because MELCOR's fission product release models are implemented inside of a complicated model of the meltdown of a reactor core, they could not be used to drive the release of fission product vapors from spent fuel during transportation accidents that led to fires. Although in principle, vapor release models could have been implemented using MELCOR's control function logic, this was not done. Instead, for scenarios that involved collisions, and thus additional fracturing of fuel which would be expected to enhance the release of vapors, 1.0 gram quantities of Kr, CsOH, CsI, and TeO were sourced from the fuel rods into the cask either at a constant rate for 100 seconds or at a rate that was proportional to the rate of release of helium from the failed fuel rods. For any scenario that didn't involve additional fracturing of fuel (fire only scenarios), 0.15 grams of each of these vapor species was released, again either at a constant rate for 100 seconds or at a rate proportional to the rate of release of helium. Use of a value of 0.15 g for the amounts of Kr, CsOH, CsI, and TeO released during accident scenarios not subject to fuel fracturing causes the ratio of the amount of a fission product species released without fuel fracturing to the amount released with fuel fracturing to be the same for noble gases and vapors as it is for aerosols. That is, the ratio of the mass of gaseous species released for scenarios without and with additional fracturing is the same as the ratio of aerosol release fractions for these two scenarios (i.e., $0.15\ g/1.0\ g = 3 \times 10 \times^{5}/2 \times 10^{-4}$). This is appropriate if additional fracturing of fuel enhances release of gases and vapors because gaseous species can escape more easily from the fuel fines produced by fracturing than from the bulk mass of fuel pellets.

Table 9-7 presents the masses of the species released by the two source terms examined during this study. Accident scenarios that led to additional fuel fracturing used the source term in the third column of Table 9-7. Fire scenarios that didn't involve collisions used the source term in the second column of the table.

Table 9-7. Radionuclide Source Terms

Specie	Accident Scenarios without Fuel Fragmentation	Accident Scenarios with Fuel Fragmentation
Kr	0.15 gm	1 gm
CsOH	0.15 gm	1 gm
CsI	0.15 gm	1 gm
TeO	0.15 gm	1 gm
Fuel Fines	0.1833 kg (3×10^{-5} of total fuel mass)	1.222 kg (2×10^{-4} of total fuel mass)

9.1.6.3 AEROSOL PROPERTIES

A log-normal size distribution with a mass median diameter of 2 μm and a geometric standard deviation of 2.5 was assumed [8] for the fuel fines released from failed rods to the interior of the cask. A sensitivity study of these distribution parameters showed that the results of this study were little affected by the initial shape assumed for the distribution of fuel fines.

The aerosol agglomeration and deposition models implemented in the MELCOR code treat gravitational, diffusive, and turbulent agglomeration and gravitational, diffusive, and thermophoretic deposition. In order to treat these processes, MELCOR's agglomeration and deposition models require that values be specified for the following aerosol parameters: particle density, particle shape correction factors, particle slip and sticking coefficients, the turbulent energy dissipation rate, the gas-to-particle thermal conductivity ratio, the thermal accommodation coefficient, and the diffusive boundary layer thickness. The values used for these parameters are listed in Table 9-8. Use of values of 1.0 for the particle shape factors causes both agglomeration and deposition of particles to be underestimated and thus particle release fractions to be overestimated. As they should, the values selected for these parameters cause diffusive processes to dominate the agglomeration and deposition of small particles, and gravitational processes to dominate the agglomeration and deposition of large particles.

9.1.6.4 DEPOSITION SURFACES

The use of simple one-dimensional heat structures (e.g., equivalent cylinders) to model the complex geometries of the cask basket and fuel assemblies caused the areas of these surfaces to be significantly underestimated. In addition, especially for fuel rods, the temperatures of the many surfaces in the real cask structure (e.g., a fuel assembly) varied over a wide range which meant that the condensation and evaporation of vapors from these surfaces would have been poorly modeled using the surface area and temperature of the simple one-dimensional heat transport model. As the simplified heat transport models had their parameter values adjusted to produce heat flow between the spent fuel and the environment that closely matched test results for the TN-125 cask, this simplification did not adversely affect the modeling of heat transport. However, because both aerosol and fission product vapor deposition to surfaces are

Table 9-8. Values of MELCOR Aerosol Parameters

Parameter	Value
Nominal Density of Aerosol Particles	10500 kg/m^3
Aerosol Dynamic Shape Factor	1.0
Aerosol Coagulation Shape Factor	1.0
Particle Slip Coefficient	1.257
Particle Sticking Coefficient	1.0
Turbulent Dissipation Rate	0.001 m^2/s^3
Gas to Particle Thermal Conductivity Ratio	0.008
Thermal Accommodation Coefficient	1.0
Diffusion Boundary Layer Thickness	1×10^{-5} m

quite sensitive to surface area and surface temperature, the heat structures that were wholly adequate for the calculation of heat transport were quite inadequate for the calculation of fission product deposition.

The MELCOR code allows heat structures to be specified as active or inactive for the purposes of calculating fission product deposition. This feature allowed the heat structures that were constructed to model heat transport to be inactivated for fission product deposition. Fission product deposition was then modeled using a set of thermally passive heat structures that had surface areas and temperatures that closely approximated those of the real structures they represented. Because each structure was a thin plate with a high thermal conductivity and a low heat capacity, none of these thermally passive deposition heat structures stored a significant quantity of heat. Thus, each structure provided a surface with an area and a temperature that closely matched those of the real structure that it represented without having any significant effect on the flow of heat from the fuel in the cask through cask internal structures and the cask shell to the environment.

Forty-five passive heat structures, nine structures in each of the five lodgement control volumes (volumes V1 through V5 in Figure 9-1), were used to model fuel rod deposition surface areas. The surface temperature of each of the nine structures in one of the five lodgement volumes were equated to the midpoint temperature of one of the nine concentric shells that comprise the equivalent cylinder used to fuel assembly heat transport. All 45 of these surfaces were modeled as vertical surfaces. Thus, deposition of aerosols onto these surfaces by gravitational settling was neglected.

Fifteen passive heat structures, three structures in each of the five lodgement control volumes, were used to model lodgement deposition surfaces. The surface temperature of each of these passive heat structures was equated to the temperature of the inner surface of the equivalent cylinder that was used to model the basket of the TN-125. In each lodgement volume, one of the three passive heat structures was modeled as a ceiling (i.e., the deposition surface was facing downward), one was modeled as a wall, and one as a floor. Only the floor was active for gravitational deposition of aerosols.

Five passive heat structures were used to model the deposition surfaces of the cross volume in the basket of the TN-125 cask (volume V7 in Figure 9-1). Three of these surfaces (one ceiling, one wall, and one floor) modeled the sides of the cross volume. The two remaining structures (both walls) modeled the basket spacer plates and tie rods. The surface temperature of each of these passive heat structures was equated to the temperature of the inner surface of the equivalent cylinder that was used to model the basket of the TN-125 cask.

The cask lid and bottom were each modeled by two passive heat structures, one large wall and one small floor. The floor accounted for the curvature of the cask lid and bottom which allowed deposition of aerosol to these structures by gravitational settling. The surface temperatures of each of these four passive heat structures were equated to the temperature of the inner surfaces of the active heat structures that represented the cask lid and bottom.

Table 9-9 summarizes the orientations and surface areas of the passive heat structures used to model aerosol and fission product deposition to cask surfaces.

Table 9-9. Radionuclide Deposition Surface Areas

Component	Surface Areas by Orientation (m^2)			
	Horizontal Ceiling	Vertical Wall	Horizontal Floor	Total
Fuel Rod Cladding	0	301.6	0	301.6
Lodgment Walls	10.9	21.8	10.9	43.6
Top Lid End	0	1.6	0.2	1.8
Center Cross Space	4.8	26.7	4.8	36.3
Basket-Shell Gap	0	0	0	0
Bottom End	0	1.8	0.2	2.0
Total	15.7	353.5	16.1	385.3

9.2 Accident Scenarios, Sensitivity Studies, and Results

Three severe accident scenarios were investigated using the MELCOR TN-125 cask input model described in the preceding sections. The three accident scenarios studied were a fire without a collision, a collision without a fire, and a collision that causes a fire. Principal scenario characteristics are presented in Table 9-10. Each of the scenarios in Table 9-10 was examined twice, once assuming that the size of the cask seal failure was 4 mm^2 and once assuming that it was 100 mm^2. In addition, sensitivity studies were performed to reveal the effect of the values of the following parameters: cask seal failure area, rod-to-cask release fraction for fuel fines, fraction of rods failed by the collision, axial location of the rod failures, mass of gaseous species released to the cask, initial aerosol size distribution, and diffusion boundary layer thickness.

9.2.1 Accident Scenario Results

Table 9-11 presents, for rod helium and for the five radioactive species that were sourced into the cask from the failed rods at a rate proportional to the rate of introduction of rod helium, the fraction of the mass of the species that was released from the cask to the environment (cask-to-environment release fraction, f_{CEi}). Release fraction values are presented for fuel fines (UO_2 and non-volatile radionuclides), for four radioactive species that at least sometimes transport as gases (Kr, CsOH, CsI, and TeO), and for He (the rod pressurization gas). Because fission product species that remain in the solid phase throughout the course of an accident scenario (e.g., oxides of Co, Sr, and Ce) transport only as constituents of fuel fines, their cask retention fractions are identical to those calculated for the fuel fines.

Table 9-10. Accident Scenarios Studied

Accident Scenario	Fire Conditions	Rod/Cask Failure Time	Fuel Release Fraction From Rods To Cask
Collision Without a Fire	No Fire	At Collision	2×10^{-4} (Collision Induced Fragmentation)
Collision With a Fire	3 Hours 1200°C	At Collision	2×10^{-4} (Collision Induced Fragmentation)
Fire Without a Collision	3 Hours 1200°C	4 Hours After Start of Fire	3×10^{-5} (Lorenz Value, No Fragmentation)

Table 9-11. Accident Scenario Cask-to-Environment Release Fractions

Accident Scenario	Leak Area (mm^2)	Cask-to-Environment Release Fractions					
		He	Kr	CsOH	CsI	TeO	Fuel Fines
Collision Without a Fire	4	8.1×10^{-1}	8.1×10^{-1}	1.4×10^{-3}	5.0×10^{-3}	4.2×10^{-2}	5.3×10^{-2}
	100	8.1×10^{-1}	8.1×10^{-1}	2.3×10^{-1}	2.5×10^{-1}	3.1×10^{-1}	3.9×10^{-1}
Collision With a Fire	4	8.6×10^{-1}	8.6×10^{-1}	6.7×10^{-3}	1.1×10^{-2}	4.4×10^{-2}	5.4×10^{-2}
	100	8.6×10^{-1}	8.6×10^{-1}	2.7×10^{-1}	2.8×10^{-1}	3.3×10^{-1}	4.2×10^{-1}
Fire Without a Collision	4	8.6×10^{-1}	8.6×10^{-1}	3.8×10^{-1}	3.9×10^{-1}	3.9×10^{-1}	7.8×10^{-2}
	100	8.6×10^{-1}	8.6×10^{-1}	6.5×10^{-1}	7.0×10^{-1}	7.4×10^{-1}	4.3×10^{-1}

Inspection of Table 9-11 shows that cask-to-environment release fractions have the following ranges for non-condensable gases, condensable vapors, and particulates:

- 0.81 to 0.86 for non-condensable vapors (He, Kr)
- 1.4×10^{-3} to 0.70 for condensable vapors (CsOH, CsI, TeO)
- 0.042 to 0.74 for particulates (fuel fines)

Thus, use of a value of 1.0 for cask-to-environment release fractions, as was done in the Modal Study [4], is slightly conservative for noble gases regardless of the nature of the accident (collision without a fire, collision with a fire, fire without a collision). For fission product vapors and fuel fines, the use of a release fraction value of 1.0 is somewhat conservative (large by factors of 1.4 to 4.4) for severe accidents that cause large cask failures with areas of about 100 mm^2, more conservative (large by factors of 2.6 to 13) for fires without collisions that cause seal failures with areas of about 4 mm^2, and quite conservative (large by factors of 19 to 700) for collision accidents that cause seal failures with leak areas of order 4 mm^2 regardless of whether the accident initiates a fire.

Table 9-11 shows, as would be expected, that for each accident scenario the cask-to-environment release fractions for He and Kr are identical. Table 9-11 also shows that the cask-to-environment release fraction for non-condensable gases has values of 0.81 and 0.86, respectively, for collision-only scenarios and for scenarios that involve fires. For collision-only scenarios, release of non-condensable gases should be determined by the fraction of the cask gases expelled to the environment by cask depressurization. Because rod failure pressurizes the TN-12 cask to 5 atmospheres, blowdown to atmospheric pressure should cause the cask-to-environment release fraction for non-condensable gases to have a value of 0.8. Thus, the calculated value of 0.81 is in excellent agreement with the value predicted by release from the cask driven solely by cask depressurization. For scenarios that involve fires, the final

size of the cask-to-environment release fraction is determined by the fraction of the gases released to the cask that are driven from the cask first by relief of pressure and then by gas expansion caused by heating of the cask by the fire. Because rod failure pressurizes the cask to about 5 atmospheres while fire heating raises the temperature of cask gases from about 450 to 750°C, ideal gas behavior predicts a cask-to-environment release fraction of about

$$0.88 = [(P_{peak} - P_{final})/P_{peak}]_{depressurization} + [P_{final}/P_{peak}]_{depressurization}[(P_{heating} - P_{final})/P_{final}]_{heating}$$
$$= [1 - P_{final}/P_{peak}] + [P_{final}/P_{peak}][T_{peak}/T_{initial} - 1] = [1-1/5] + [1/5][1023/723 - 1]$$

in good agreement with the calculated result of 0.86 for scenarios that involve fires.

Deposition of particles and condensable vapors onto interior cask surfaces should increase as cask depressurization time increases, because slower cask depressurization means that more time is available for deposition. Because cask depressurization times were much slower for scenarios with 4 mm^2 leak areas (about 1.75 hours) than for scenarios with 100 mm^2 leak areas (about 10 minutes), retention of condensable vapors and particles should be substantially greater for the 4 mm^2 scenarios than for the 100 mm^2 scenarios. In agreement with this prediction, inspection of Table 9-11 shows that cask-to-environment release fractions for condensable vapors and particles for the collision-only and the collision-plus-fire scenarios with 100 mm^2 leak areas are about ten times larger than they are for the same scenarios with 4 mm^2 leak areas. For the fire scenarios without a collision, the dependence on failure area is smaller, especially for condensable vapors because now, when the fuel rods fail, all cask interior surfaces are at elevated temperatures and remain at these temperatures throughout the depressurization time period even when depressurization takes place through a small 4 mm^2 cask failure. For collision scenarios with 100 mm^2 leak areas, cask-to-environment release fractions for fission product vapors and fuel fines are all about the same (values of 0.23–0.74), because for these scenarios there isn't time for vapors to condense on cold surfaces. Instead, when vapors condense during these scenarios, they do so mainly onto fuel fine particles, which causes condensable vapors and fuel fines to have similar release fractions for these scenarios.

Table 9-11 shows that, even though CsOH is more volatile than CsI, its cask-to-environment release fractions always have values smaller that those of CsI. Although this seems counterintuitive, it is expected, because vapor deposition to a cold surface is much more efficient than particle deposition onto the same surface. Therefore, whenever there is a cold deposition surface along a vapor's escape path from the rods, through the cask, to the environment, cask-to-environment release fractions will be smaller for vapors that condense to form particles than for vapors that don't. Because CsI is less volatile than CsOH, CsI vapors will form particles by gas-to-particle conversion or by condensing onto existing particles more rapidly than CsOH vapors and thus, during transport through the cask, CsI will deposit onto cold surfaces less efficiently than CsOH. Of course, when deposition times are short, as they are for the scenarios with 100 mm^2 failure areas, cask-to-environment release fractions for CsOH are only slightly smaller (4 to 9 percent) than those for CsI, while when deposition times are long, as they are for scenarios with 4 mm^2 leak areas, cask-to-environment release fractions for CsI are significantly larger (1.5 to 3.5 times larger) than those of CsOH, whenever there is a cold surface along the vapors transport path through the cask. Because all cask surfaces are at elevated temperatures when the fuel rods fail due to burst rupture during fire-only scenarios, for these scenarios, cask-to-environment release fractions for CsOH and CsI are quite similar and change only slightly with cask failure area.

The addition of a fire to the collision scenario increases release of fission product vapors, especially CsOH, the most volatile vapor examined, but less than one might expect. This is because a fire following a collision must enhance release of condensed vapors by causing the vapors to evaporate from the surfaces on which they have deposited and then transporting them from the cask by expansion of cask

gases due to heating by the fire. But this process is inefficient because at hydrocarbon fire temperatures, none of the vapors examined is highly volatile and uneven heating of internal cask structures means that there is always a surface somewhere in the cask that is cool enough to allow vapors to recondense on it (e.g., the cask bottom and lid).

Evaporation of vapors from one cask surface and condensation onto a second surface is illustrated by the results presented in Tables 9-12 and 9-13. For each fission product species sourced into the cask during the collision-only and the collision-plus-fire scenarios with 4 mm^2 seal leak areas, these tables present the mass fractions of these species for each of their possible physical forms (vapors, aerosols) and final location. Because MELCOR allows vapors to condense on aerosols, the final locations of fission product species also illustrates the effect on transport of fission product vapors of condensation onto cold surfaces and of condensation onto aerosol surfaces.

Because Kr is a non-condensable gas, it appears in Tables 9-12 and 9-13 in only two final locations, gasborne in the cask and outside the cask. Because UO_2 transports only as particles of fuel fines, it appears in these tables only as an aerosol. Because CsOH, CsI and TeO can condense on aerosols, they can be present in the gas phase and on surfaces both as vapors and as aerosols (that is as a vapor condensed onto an aerosol).

Comparison of Tables 9-12 and 9-13 shows that addition of a fire to a collision accident has no effect on the transport and release of UO_2 (fuel fines), as neither the locations nor the masses of fuel fines in these locations are changed by the fire. Because of its low volatility, transport and release of the TeO are also little affected by the fire; some TeO revaporizes from fuel and lodgement surfaces and then either recondenses on other cask surfaces or escapes from the cask which slightly increases the fraction of TeO released to the environment from 0.14 to 0.15. Addition of a fire, also slightly increases the release of Kr from the cask to the environment (the fraction of Kr released from the cask to the environment increases from 0.89 to 0.92). Because they are significantly volatile at fire temperatures, CsOH and CsI revaporize from both aerosol and cask surfaces and then recondense on cooler cask surfaces (note that MELCOR tracks condensation of vapors onto gasborne aerosols but not onto aerosols that reside on surfaces).

Table 9-12. Final Locations of Fission Product Species for the Collision Only Scenario (4 mm^2 leak area)

Location	Fuel and Lodgement Surfaces			Other Cask Surfaces			Gasborne in the Cask			Outside the Cask
Form	Aerosol	Vapor	Both	Aerosol	Vapor	Both	Aerosol	Vapor	Both	Both
Specie	Fraction of Each Specie in Each Location									
Kr	0.0	0.0	0.0	0.0	0.0	0.0	0.0	0.111	0.111	0.889
CsOH	0.767	0.228	0.995	0.00091	0.00332	0.00423	0.0	0.0	0.0	0.000557
CsI	0.840	0.154	0.994	0.00316	0.00150	0.00466	0.0	0.0	0.0	0.00128
TeO	0.932	0.032	0.964	0.0192	0.00266	0.0219	0.0	0.0	0.0	0.0142
UO_2	0.943	0.0	0.943	0.0406	0.0	0.0406	0.0	0.0	0.0	0.0165

Table 9-13. Final Locations of Fission Product Species for the Collision Plus Fire Scenario (4 mm^2 leak area)

Location	Fuel and Lodgement Surfaces			Other Cask Surfaces			Gasborne in the Cask			Outside the Cask
Form	Aerosol	Vapor	Both	Aerosol	Vapor	Both	Aerosol	Vapor	Both	Both
Specie	Fraction of Each Specie in Each Location									
Kr	0.0	0.0	0.0	0.0	0.0	0.0	0.0	0.0816	0.0816	0.918
CsOH	0.0	0.850	0.850	0.0669	0.00094	0.0679	0.0014	0.0757	0.0771	0.00448
CsI	0.0	0.938	0.938	0.0472	0.00037	0.0476	0.0002	0.0097	0.0099	0.00434
TeO	0.860	0.096	0.956	0.00003	0.00458	0.0046	0.0	0.00003	0.00003	0.0149
UO_2	0.943	0.0	0.943	0.0406	0.0	0.0406	0.0	0.0	0.0	0.0167

Thus, because they are volatile at fire temperatures, the locations of CsOH and CsI inside of the cask change significantly (revaporization from fuel and lodgement surfaces followed by recondensation onto other cooler cask surfaces is significant), but the fraction of each of these vapors that remains in the cask is little changed (the fractions of CsOH and CsI retained in the cask both decrease slightly from 0.999 and to 0.995). Thus, Tables 9-12 and 9-13 show that a fire that follows a collision has little or no effect on the transport of non-condensable gases (Kr) and particles (fuel fines), while causing vapors volatile at fire temperatures (CsOH and CsI) to move from hotter to cooler cask interior surfaces without significantly increasing their release from the cask to the environment.

9.2.2 Sensitivity Study Results

The following parameter sensitivity studies were conducted using the collision-only accident scenario. All of the other studies but one (the study that varied the area of the seal leak) assumed a seal leak area of 4 mm^2. Two of these sensitivity studies, the studies that varied the rod-to-cask release fraction for fuel fines and the size of the cask failure area, introduced fission products into the cask at a rate that was proportional to the rate of introduction of the helium rod pressurization gas. For all of the other sensitivity studies, fission product species were sourced into the cask at a constant rate for 100 seconds.

- **Mass of Volatile Fission Products Released from Rods.** Variation of the mass of each fission product specie released from the failed rods to the cask over the range 10^{-3} g to 10^{3} g hardly affected the cask retention fractions for these species (increases or decreases of one percent or less).

- **Rod-to-Cask Release Fraction for Fuel Fines.** Variation of this fraction over the range 10^{-5} (the lower bound from Lorenz results for fuel not subject to crush or impact) to 10^{-3} (the upper bound from rod failure tests using shaped charges) caused the fraction of fuel fines retained by the cask to decrease from 0.975 to 0.925.

- **Fraction of Rods that Fail.** Variation of this fraction over the range 0.1 to 1.0 caused the fraction of fuel fines retained by the cask to decrease from 1.0 to 0.984.

- **Rod Failure Location.** Moving the location of the rod failures from the bottom lodgement volume to the top lodgement volume caused the fraction of fuel fines retained by the cask to decrease from 0.99 to 0.93.

- **Aerosol Size Distribution.** Variation of the mass median diameter and standard deviation of the initial size distribution of fuel fines respectively over the ranges, 1 to 3 microns and 2.5 to 6.0, caused the fraction of fuel fines retained by the cask to vary over the range 0.979 to 0.987.

- **Size of the Cask Seal Failure.** As is shown in Figure 9-6, variation of the cross-sectional area of the seal failure during the collision-only accident scenario from 0.1 mm^2 to 1.0 cm^2 had no effect on the fraction of Kr released from the cask (the fraction remained constant at 0.8), but large effects on the fractions of vapors and aerosols released from the cask. Specifically, cask-to-environment release fractions for aerosols (fuel fines and TeO which transports during the collision-only scenario as an aerosol) increased from 2×10^{-3} to 0.65, and condensable vapor (CsOH and CsI) release fractions increased from about 6×10^{-5} to 0.5.

Thus, release of radioactive species from the cask to the environment is only slightly affected by the amounts of the species released to the cask from the failed rods, by the number of rods that failed, by the rod location, or by the initial size distribution of the fuel fines released from the rods, but is strongly affected by the size of the seal failure as this controls the time required to depressurize the cask and thus the time available for deposition of particles and vapors onto cask interior surfaces. When this time is long (small cask leak area), release fractions for condensable vapors and particles will be very small. When this time is short (large cask leak area), release fractions for condensable vapors and particles will be quite large although still significantly smaller than one.

9.3 Summary

A realistic model of a TN-125 cask was constructed and its thermal behavior was shown to well approximate the results of experiments and calculations presented in the SAR for that cask. The model was used to evaluate the size of cask-to-environment release fractions for non-condensable gases (Kr), condensable vapors (CsOH, CsI, and TeO), and particles (fuel fines). Cask-to-environment release fractions depend principally on the length of time required for cask depressurization after failure of the spent fuel rods carried in the cask by the mechanical or thermal loads generated by collisions and/or fires. For condensable vapors and particles, cask-to-environment release fractions are very small when depressurization times are long and increase substantially as depressurization times shorten. For particles, the geometric mean of the calculated range for this parameter of 0.002 to 0.65 is 0.036, which agrees well with Wilmot's estimate of 0.05 and is 28 times smaller than the Modal Study's very conservative estimate of 1.0. A fire following a collision was shown to have little impact on cask-to-environment release fractions, principally causing vapors to evaporate from surfaces that become hot and then to recondense on other interior cask surfaces that remain cool. When rod and cask failures are caused by an engulfing fire, cask-to-environment release fractions increase significantly as heating of the cask by the fire significantly decreases vapor condensation inside of the cask as there are substantially fewer cool surfaces available to condense upon.

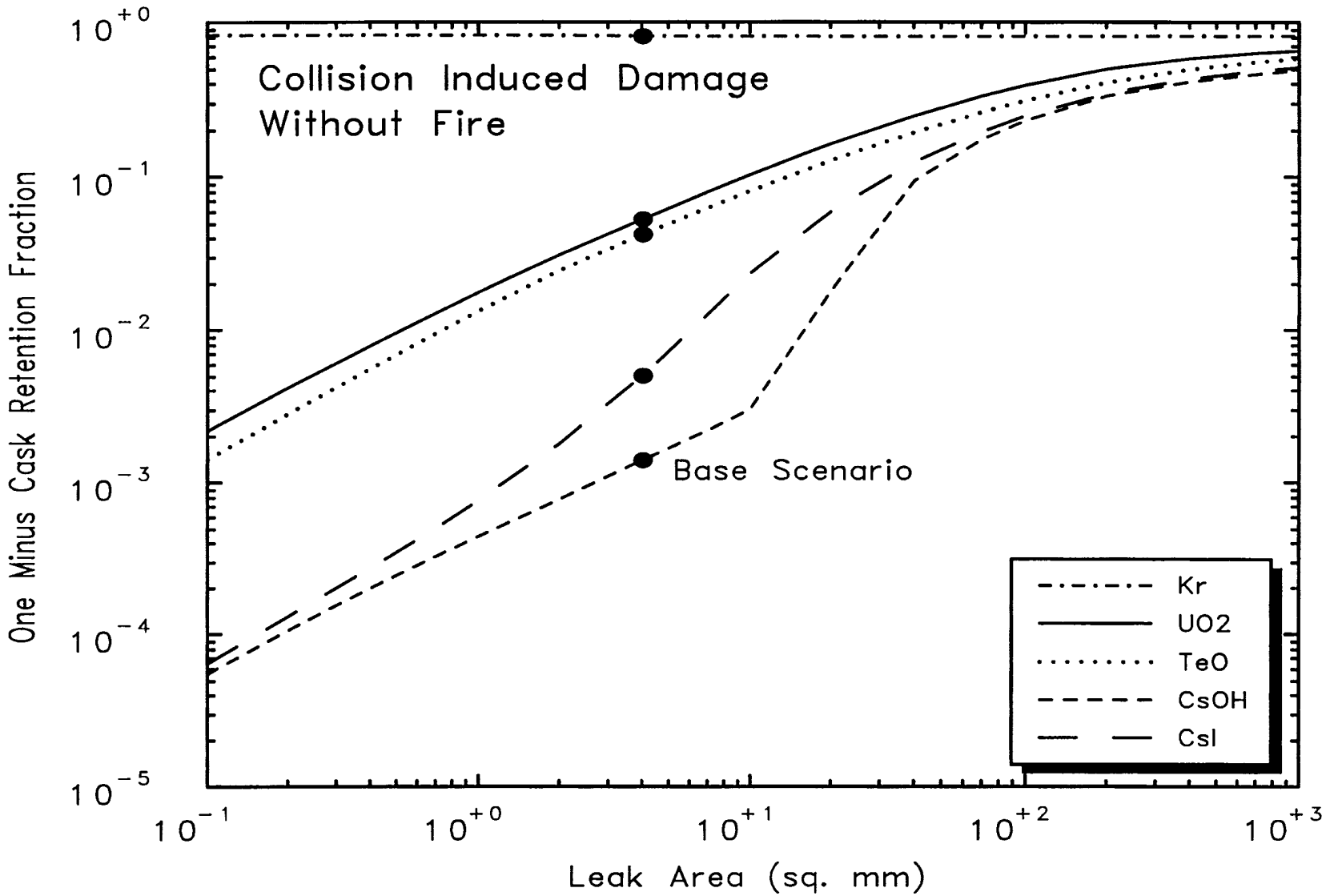

Figure 9-6. Cask Seal Failure Size Sensitivity.

9.4 References

1. A. G. Croff, *ORIGEN2 — A Revised and Updated Version of the Oak Ridge Isotope Generation and Depletion Code*, ORNL-5621. Oak Ridge National Laboratory, Oak Ridge, TN, July 1980.

2. R. A. Lorenz et al., *Fission Product Release from Highly LWR Irradiated Fuel*, NUREG/CR-0722. Oak Ridge National Laboratory, Oak Ridge, TN, February 1980.

3. E. L. Wilmot, *Transportation Accident Scenarios for Commercial Spent Fuel*, SAND80-2124. Sandia National Laboratories, Albuquerque, NM, July 1984.

4. L. E. Fischer, et. al., *Shipping Container Response to Severe Highway and Railway Accident Conditions*, NUREG/CR-4829, UCID-20733. February 1987.

5. R. M. Summers et al., *MELCOR 1.8.0: A Computer Code for Nuclear Reactor Severe Accident Source Term and Risk Assessment Analyses*, NUREG/CR-5531, SAND90-0364. Sandia National Laboratories, Albuquerque, NM, January 1991.

6. *TN-12 Safety Analysis Report*, Revision 1, Transnuclear, Inc., April 30, 1979.

7. N. R. Keltner, W. Gill, and L. A. Kent, "Simulating Fuel Spill Fires Under the Wing of an Aircraft," in *Fourth International Symposium on Fire Safety Science*, Ottawa, Canada, June 1994.

8. T. L. Sanders, et. al., *A Method for Determining the Spent-Fuel Contribution to Transport Cask Containment Requirements*, SAND90-2406. Sandia National Laboratories, Albuquerque, NM, November 1992.

9. J. P. Holman, *Heat Transfer*, Second Edition. McGraw-Hill Book Company, 1963.

10. *Zion Station Updated Final Safety Analysis Report*. Commonwealth Edison Company, June 1992.

11. *Fission Product Transport in Degraded Core Accidents*, IDCOR 11.3 Report, p. 15. Impell Corporation, 1983.

10. ILLUSTRATIVE CONSEQUENCE CALCULATIONS

Should a ship transporting spent fuel in a Type B cask be involved in a ship collision that is severe enough to cause the failure of the cask, release of some radioactive materials from the cask to the environment would be expected to occur. Transport of these radioactive materials from the sea to land would then cause population along the overland transport path to be exposed to radiation. In addition, deposition of radioactivity onto the ocean surface would lead to the entry of radioactivity into marine food pathways, whereupon harvesting of contaminated marine foods would subject the people who consume those contaminated foods to ingestion doses.

The radiological consequences of a release of radioactive materials to the environment are estimated using consequence codes. Which code is used depends on the circumstances of the release. When release occurs at a known location, a site specific consequence code, for example the MACCS code [1, 2], is used to estimate the radiation exposures that might be incurred by the population that surrounds the release location. If the release might take place at any of a large number of locations along a transportation route, then a transportation code, for example RADTRAN [3], is used to estimate radiation exposures. If the release takes place in the open ocean far from land, then a marine food pathways code, for example MARINRAD [5], is used to estimate population doses as it is expected almost all of the radioactivity released to the atmosphere from the failed cask will deposit onto the ocean surface before reaching the shore and thus that no significant quantity of radioactivity will reach land due to windborne transport.

This section describes illustrative consequence calculations performed using the MACCS, RADTRAN, and MARINRAD consequence codes. The illustrative calculations model a ship accident that occurs in a port at a known location, a ship accident that occurs while sailing a coastal route at a distance from shore of several tens of miles, and a ship accident that occurs in the open ocean way out to sea during a transocean voyage.

Radiological accident consequences depend principally upon (1) the size of the radioactive release, (2) the degree to which the release is diluted during transport to the locations where population exposures occur or where radioactive species enter food pathways, (3) the size of the populations exposed to radiation as a result of the release, and (4) the effectiveness of any short- or long-term responses (evacuation, sheltering, relocation, decontamination) taken to mitigate the exposures. As the consequence calculations presented here are only intended to illustrate the use of consequence codes to model transportation accident consequences and the likely magnitudes of several important consequence measures (population doses, radiation induced cancer fatalities) attributable to the radioactive release caused by the accident, the input used in these calculations will only be summarized, rather than presented in full.

10.1 Consequence Codes

The MACCS code [1, 2] was developed by Sandia for the U.S. Nuclear Regulatory Commission (NRC). The code was originally developed to model the radiological consequences of nuclear power plant accidents. Thus, MACCS models radioactive releases that occur at a known location (for example, an accident prone location along a transportation route) and requires as input detailed population and weather data for the accident site. MACCS calculations normally use (1) one year of hourly weather data (wind speed, rain rate, atmospheric stability) recorded at a weather station located at or near the hypothetical accident site (at least in the same meteorological region), and (2) a real population distribution constructed from census data on a polar coordinate, compass sector grid centered on the

accident site that has a number of radial intervals that cover the radial distance interval from 0 to 50 miles.

The RADTRAN code [3, 4] was developed by Sandia, Version 1 for the NRC and later versions for the U.S. Department of Energy. The code models the radiological consequences of the transport of radioactive materials, both the exposures that will occur if the transport occurs without incident, and the exposures that may occur should the transport vehicle be involved in an accident while en route. Because accidents might occur at any point along the transport route, RADTRAN divides the transport route into segments (links) and uses a uniform population density and constant meteorological conditions (windspeed and atmospheric stability) to represent the population and weather characteristics of each route segment. The use by RADTRAN of a uniform population density to represent the population along each route segment means that RADTRAN cannot directly model a route segment that has a near-field region that is devoid of population, as is the case when a ship is sailing a coastal route at a distance of several tens of miles from shore. In Section 10.4.1 below, a way to meaningfully model a coastal ship route with RADTRAN is described, validated, and then illustratively applied in Section 10.4.2 to the transport of spent fuel from New London, Connecticut, to Charleston, South Carolina.

The MARINRAD code [5] was developed by Sandia for DOE. The code models radiation exposures that result from the introduction of radioactive materials into the oceans. The ocean regions considered are represented as a series of compartments. Movement of water, waterborne radioactive materials, and marine organisms (e.g., fish) between compartments is modeled. Within compartments, movement of radioactivity from the water onto sediments and into marine food chains is modeled. Also modeled are the population doses that result from the entry of radioactivity into marine food chains.

10.2 Source Terms

For transportation accidents, the amount of radionuclide i released to the environment (M_{STi}) is the product of the inventory (I_i) of that radionuclide in the transport cask and the fraction of that inventory (F_i) that is released to the environment from the failed cask. Because release usually occurs in two stages, first from the radioactive material to the cask interior and then from the cask interior to the environment, the overall release fraction F_i can be represented as a product of two release fractions, F_{mci} and F_{cei}, where F_{mci} is the release fraction for radionuclide i from the radioactive material to the cask interior and F_{cei} is the release fraction for that radionuclide from the cask interior to the environment. Thus, the accident source term (M_{ST}) is given by

$$M_{ST} = \sum_i M_{STi} = \sum_i I_i F_i = \sum_i I_i F_{mci} F_{cei}$$

The illustrative consequence calculations described below all assumed transport of spent fuel in a TN-125 cask. Table 10-1 presents the TN-125 cask inventory that was used in each of the consequence calculations.

Release fractions are usually specified for groups of chemical elements (e.g., noble gases, condensable vapors, and particulates) that are expected to behave similarly, especially during release from the radioactive material to the cask interior and transport through the cask to the environment. The inventory presented in Table 10-1 contains nuclides of 18 different elements. Fourteen of these elements

Table 10-1. TN-125 Cask Inventory

Radionuclide	Inventory (Bq)	Radionuclide	Inventory (Bq)
CO-58	3.64E+10	CS-136	9.40E-10
CO-60	1.71E+15	CS-137	2.12E+16
KR-85	1.73E+15	BA-140	7.33E-09
SR-89	6.89E+10	LA-140	8.43E-09
SR-90	1.52E+16	CE-141	3.11E+07
Y-90	1.52E+16	CE-144	2.02E+16
Y-91	7.07E+11	PR-143	2.07E-07
ZR-95	2.99E+12	ND-147	2.58E-13
NB-95	6.65E+12	NP-239	3.73E+12
RU-103	1.69E+09	PU-238	5.47E+14
RU-106	1.60E+16	PU-239	6.81E+13
TE-127	3.54E+12	PU-240	1.03E+14
TE-127M	3.62E+12	PU-241	2.24E+16
TE-129	1.28E+06	AM-241	1.34E+14
TE-129M	1.96E+06	CM-242	6.97E+13
CS-134	1.35E+16	CM-244	4.03E+14

will be released and will transport only as components of fuel fires. Therefore, they are assigned to the Particulate chemical element class. One additional element, Co, is also expected to be released as a constituent of particles. However, because these particles are formed from the chemical deposits that form on the surface of fuel rods during reactor operation, they are assigned to a separate chemical element class, termed CRUD [6]. One element in the inventory, Kr, will always transport as a gas and therefore is assigned to the Noble Gases chemical element class. Finally, two elements in the inventory, Cs and Ru, may be released from spent fuel as vapors during fire accident scenarios that heat the fuel to elevated temperatures. During fire scenarios that heat the spent fuel to temperatures above 800°C, where both CsI and CsOH have significant vapor pressures, Cs will be released as either CsI(g), if the spent fuel contains I, or as CsOH(g), if the fuel doesn't contain I. In addition, if spent fuel is exposed to air while hot, Ru that is present in the fuel as involatile RuO_2 will be oxidized to, and will be released and will transport as, RuO_4 vapor. Thus, because Cs and Ru have unique high temperature chemistries, they are each assigned to a separate chemical element class, Cs to the Cesium and Ru to the Ruthenium chemical element classes.

Values of release fractions (F_i where $F_i = F_{mci}\ F_{cei}$) are estimated for two accident scenarios, the single failure (1 hole), collision-only scenario and the double failure (2 holes), collision-plus-fire scenario for which probabilities were developed in Section 8.0. The development of estimates for the values of cask-to-environment release fractions (F_{cei}) is described in Appendix IV and summarized in Section 9.0 of this report. For the collision-only scenario, a seal failure with a cross-sectional area of 2 mm^2 is assumed. Figure 26 in Appendix IV shows that a 2 mm^2 leak produces a cask-to-environment release fraction of 1×10^{-2}. For the collision-plus-fire scenario, two cask failures are assumed, seal failure plus a puncture or shear failure.

Estimates of the fractions of the radionuclides in spent fuel that are released to the cask cavity during transportation accidents that don't involve fires (values of F_{mci}) were taken from Wilmot [7]. Release

fractions for Cs and Ru for release from spent fuel to the cask interior due to vaporization during fire accidents were taken from Sprung et al. [8]. Release fractions for CRUD from fuel rod surfaces to the cask interior were based on estimates of CRUD spallation fractions under accident conditions developed by Sandoval et al. [6]. Because the collision-plus-fire scenario is assumed to involve a double failure, it is also assumed that uneven heating of the cask will cause a significant flow through the failed cask of combustion gases, that contain enough air to oxidize involatile RuO_2 to somewhat volatile RuO_4. Therefore, for the collision-plus-fire scenarios, $F_{cei} = 1.0$ for all species, because the flow of combustion gases plus entrained air through the cask is assumed to transport all species released to the cask interior from the cask to the environment. Table 10-2 presents the estimated release fraction values used to calculate consequences for the collision-only and the collision-plus-fire scenarios that lead to release of radioactivity from the cask into the atmosphere.

Table 10-2. Release Fractions

Chemical Element Class		Scenario					
Name	Symbol	Collision-Only (1 hole)			Collision-plus-Fire (2 holes)		
		F_{mci}	F_{cei}	F_i	F_{mci}	F_{cei}	F_i
Noble Gases	Kr	0.2	0.8	0.16	0.2	1.0	0.2
CRUD	Co	0.3	1×10^{-2}	3×10^{-3}	0.3	1.0	0.3
Cesium	Cs	2×10^{-6}	1×10^{-2}	2×10^{-8}	1.6×10^{-3}	1.0	1.6×10^{-3}
Ruthenium	Ru	2×10^{-6}	1×10^{-2}	2×10^{-8}	1.6×10^{-6}	1.0	1.6×10^{-6}
Particulates	Part	2×10^{-6}	1×10^{-2}	2×10^{-8}	2×10^{-6}	1.0	2×10^{-6}

10.3 Port Accidents (MACCS Calculations)

Illustrative port accident consequence calculations for release of radioactivity into the atmosphere were performed using the MACCS code for two ports, Charleston, South Carolina, and Newark (the Port of Elizabeth), New Jersey. For both ports, the consequences were calculated for two source terms, the source terms for the collision-only (1 hole) accident and for the collision-plus-fire (2 hole) accident. A channel accident location was assumed for both ports, because ship speeds in the neighborhood of docks (≤7 knots) are usually too low to produce significant damage even if a collision were to occur, while speeds in major harbor channels may be as high as 15 knots, high enough to produce significant damage although significantly lower than open ocean sailing speeds (15–25 knots).

Each consequence calculation used the inventory presented in Table 10-1 and the release fractions presented in Table 10-2. Charleston was assumed to be the departure port for a TN-125 spent fuel cask being transported in a small charter freighter. Newark was assumed to be an intermediate port stop for a break-bulk freighter carrying other cargo in addition to the TN-125 cask. The Charleston calculations used one year of variable meteorological data recorded at the Charleston National Weather Service Station. The Newark calculations used one year of variable meteorological data recorded at the New York National Weather Service Station. All of the calculations used population distributions constructed for another study [9] from 1990 census data using POPSEC90 [R]. No short term emergency response actions (evacuation, sheltering) were assumed to take place. Post-accident relocation of population from and decontamination and/or condemnation of significantly contaminated property was assumed to take place.

Table 10-3 presents the results (expected values for population dose and cancer fatalities predicted to be caused by the radiation exposures that follow the hypothetical accidents) of these illustrative MACCS consequence calculations. All of the results were calculated for the distance range 0 to 50 miles and for the 50-year period that immediately follows the accident. Several comments are appropriate. First, none of the calculations predicted the occurrence of any acute fatalities or acute injuries (e.g., prodromal vomiting).

Table 10-3. MACCS Predictions of Population Dose and Cancer Fatalities Among the Population Exposed to Radiation as a Result of the Hypothetical Port Accidents During the First 50 Years that Follow the Accident

Site	Source Term	Probability (per port call)	Population Dose (Sv)	Cancer Fatalities
Charleston	Collision-Only (1 hole)	1.1×10^{-7}	63	3
	Collision-plus-Fire (2 holes)	1.3×10^{-12}	699	30
Newark	Collision-Only (1 hole)	1.0×10^{-6}	857	37
	Collision-plus-Fire (2 holes)	4.0×10^{-12}	23,700	1020

Second, the source term probabilities are the product of the probability that a ship collision occurs while transiting the port ($P_{accident}$) and the severity fraction ($F_{severity}$) for the particular source term. Thus, Table 4.6 shows that $P_{accident} = 0.5(4.3 \times 10^{-5})$ for Charleston (the port accident probability for a full port transit is halved as only a departure occurs), and $P_{accident} = 1.6 \times 10^{-4}$ for ship collisions in New York City ports (e.g., Newark); and Table 8.4 shows that $F_{severity} = 5.0 \times 10^{-3}$ for the collision-only (1 hole) accident and 5.9×10^{-8} for the collision-plus-fire (2 hole) accident for a charter freighter, and 6.3×10^{-3} for the collision-only (1 hole) accident and 2.5×10^{-8} for the collision-plus-fire (2 hole) accident for a break-bulk freighter.

Third, because some of the predicted consequences (especially the number of cancer fatalities predicted for the collision-plus-fire accident at the Newark port) seem large, these predicted consequences need to be placed in context by comparing them to normal background radiation doses and to the normal incidence of cancer fatalities. The 0-to-50 mile populations of the average sector in the compass sector population distributions that surround the Charleston and Newark ports are 3.5×10^4 and 1.0×10^6, respectively. Thus, the radioactive plume released to the environment at each accident site might expose about this many people to radiation should the hypothetical accidents ever occur. During the first 50 years following the hypothetical accidents, each individual in the exposed population would normally receive a dose of 0.18 Sv (3.6×10^{-3} Sv per year [R]) from cosmic rays, terrestrial sources, and medical x-rays. Thus, the total population that might be exposed to radiation as a result of the accident would normally receive during the first 50 years after the accident a dose of 6,300 Sv at Charleston and 180,000 Sv at Newark. Accordingly, the population doses that might be caused by the hypothetical accidents are small in comparison to then background radiation doses that will normally be experienced by these populations.

Radiation induced cancer fatalities usually occur in an exposed population about 20 to 40 years after the exposure takes place. Thus, the cancer fatality rate among the population that might be exposed to radiation should the hypothetical collision-plus-fire accident occur in the Newark port would be on average 1,020/20 years = 51 cancer fatalities per year. As the rate would not be constant, assume that the rate is four times above the average (200 per year) in the years when more people die from cancers induced by the radiation doses received as a result of the hypothetical accident. But the normal incidence

of cancer fatalities in the general population is 200 cancer fatalities per hundred thousand people [R]. Therefore, the normal rate of cancer fatalities among the one million people at Newark who might be exposed to radiation by the hypothetical accident is 2,000 deaths per year, which is ten times greater than the rate predicted for the extremely improbable collision-plus-fire accident, which has a probability of 4.0×10^{-12} per port transit at Newark. Thus, the 1,020 cancer fatalities predicted at Newark for this improbable, nearly incredible, ship accident would probably not be capable of detection by the best of epidemiological studies, especially given the fact that the cancer fatality models implemented in MACCS are linear, no-threshold models that most likely significantly overpredict cancer fatalities at the low doses and dose rates that would be characteristic of the exposures that these hypothetical accidents might cause.

10.4 Coastal Routes (RADTRAN Calculations)

10.4.1 Plume Dispersion

The RADTRAN code does not contain an atmospheric plume dispersion model. Instead, a set of plume isopleth areas calculated externally using some appropriate dispersion model is input to the code. The set of isopleth areas may be calculated using any dispersion model. The RADTRAN calculations described here used sets of 18 isopleths that were calculated using a Gaussian plume model. Each isopleth has the shape of an elongated tear drop. As a group, the isopleths form a set of nested tear drops that have the pointed tops of each drop centered on the release point for the radioactive plume, that is, on the location of the RAM cask at the hypothesized time of the transportation accident. RADTRAN can use either one set of isopleths calculated using average weather conditions typical of the hypothetical accident location, or six sets of isopleths, one for each of the six Pasquill-Gifford atmospheric stability classes. When six sets of Pasquill-Gifford isopleths are used, the consequences calculated using each set of isopleths are summed, weighting the individual results by the frequency of occurrence in the region where the hypothetical accident is assumed to occur of each Pasquill-Gifford atmospheric stability class.

Table 10-4 presents the set of 18 isopleths used for the illustrative RADTRAN calculations described below in Section 10.4.3.

Inspection of Table 10-4 shows that the eighteenth isopleth has a downwind length of 75.2 miles. Thus, the standard RADTRAN calculation will calculate radiation doses and consequences for population located as far away from the accident location as 75.2 miles. Should consequence estimates be desired for a shorter impact distance, the desired result can be obtained by deleting from the isopleth table all isopleths that extend to downwind distances further than the desired impact distance. Because of the elongated shape of the isopleths, most of the area that is neglected by removal of an isopleth lies beyond the downwind endpoint of the next longest isopleth. Accordingly, performing a RADTRAN calculation using only the first 17 isopleths in Table 10-4 would produce consequences that have an impact distance somewhat smaller than 55.9 miles. The impact distance would be less that 55.9 miles because removal of the eighteenth isopleth from the table deletes not only all area beyond 55.9 miles but also all area inside of 55.9 miles that lies between the outlines of the seventeenth and eighteenth isopleths. Thus, if consequences with a 50-mile impact distance are desired (i.e., a 0-to-50 mile calculation), the standard isopleth table should be used with the eighteenth isopleth deleted. If consequences with a 20-mile impact distance are desired (i.e., a 0-to-20 mile calculation), the standard isopleth table should be used with the sixteenth, seventeenth, and eighteenth isopleths deleted.

Table 10-4. Isopleth Areas and Downwind Lengths for the Set of 18 Isopleths Calculated Using a Gaussian Plume Model and National Average US Weather

Isopleth	Area (km^2)	Downwind Length (mi)
1	4.59×10^{-4}	0.0208
2	1.53×10^{-3}	0.0423
3	3.94×10^{-3}	0.0652
4	1.25×10^{-2}	0.152
5	3.04×10^{-2}	0.229
6	6.85×10^{-2}	0.349
7	1.76×10^{-1}	0.634
8	4.45×10^{-1}	1.01
9	8.59×10^{-1}	1.44
10	2.55	2.65
11	4.45	3.40
12	1.03×10^{1}	6.90
13	2.16×10^{1}	8.14
14	5.52×10^{1}	13.2
15	1.77×10^{2}	25.2
16	4.89×10^{2}	43.5
17	8.12×10^{2}	55.9
18	1.35×10^{3}	75.2

10.4.2 Modeling an Empty Near-Field Region with RADTRAN

The population along a transportation route segment that might be exposed to radiation, if a vehicle carrying radioactive material were to be involved in a transportation accident, is input to the RADTRAN code by specifying the average population density along the route segment. If the route segment has a near-field region that is devoid of population, as is the case when a ship is sailing a coastal route at a distance of several tens of miles from shore, RADTRAN can not directly model the empty near-field region. Because RADTRAN assumes that population density along each route segment is uniform, by differencing two RADTRAN calculations that use the same population densities, but applying them to different outward distances from the route, a near-field region that is devoid of population can be modeled. For example, assume that a ship is sailing a coastal route at a distance of 30 miles from shore and that the average population density in the region that extends inland 20 miles from the shoreline is 2.6 people per square kilometer. Then, by subtracting the results of a 0-to-30 mile RADTRAN calculation from the results of a 0-to-50 mile RADTRAN calculation, the results for the 30-to-50 mile distance interval, the interval that extends inland 20 miles from the shoreline and has a population density of 2.6 people per square kilometer, can be obtained.

To confirm that a near-field region that is devoid of population can be modeled by differencing two RADTRAN calculations, results of differencing two RADTRAN calculations were compared to the results of a MACCS calculation that directly used a population distribution that was empty from 0 to

30 miles. Specifically, a MACCS calculation was performed that modeled the release of a radioactive source term from Buxton, North Carolina. Buxton was selected as the accident location for three reasons: first, because Buxton is located on the outer banks at a distance of 30 miles from the North Carolina shoreline; second, because a National Weather Service Station is located at Buxton; and third, because a MACCS meteorology file (one year of hourly readings of wind speed, rain rate, and atmospheric stability), constructed from Buxton National Weather Service data, was available for the Buxton site.

Accordingly, a MACCS polar coordinate, compass sector, population distribution centered on Buxton was constructed using POPSEC90 [R]. This population distribution had ten downwind distance intervals which had the following outer radii: 1, 2, 3, 4, 5, 10, 20, 30, 40, and 50 miles. Next, all populated intervals with outer radii of 30 miles or less had their calculated populations set to zero. This removed the population of the outer banks from the population distribution and reduced the population in the distribution to the population located within 20 miles of the North Carolina coastline and also within 50 miles of Buxton. Table 10-5 presents this population distribution.

Table 10-5. Compass Sector Distribution of Population on the North Carolina Coast Located within 50 Miles of Buxton, North Carolina

Distance	N	NNE	NE	ENE	E	ESE	SE	SSE	S	SSW	SW	WSW	W	WNW	NW	NNW
0-30 mi	0	0	0	0	0	0	0	0	0	0	0	0	0	0	0	0
30-40 mi	851	0	0	0	0	0	0	0	0	0	0	0	70	1948	5	191
40-50 mi	4036	0	0	0	0	0	0	0	0	0	0	316	124	1394	361	3472

Next, the land areas of the 11 populated elements of this distribution were estimated. The average population density of the 11 populated elements was then calculated by dividing the total population of the 11 elements by the sum of their estimated areas. The resulting average population density was thus estimated to be 2.6 people per square kilometer. Finally, the data in the MACCS meteorology file for Buxton was used to construct an annual wind rose for the Buxton site and the annual frequency of occurrence of the six Pasquill-Gifford atmospheric stability classes A through F. Tables 10-6 and 10-7, respectively, present the wind rose and the frequencies of occurrence of Pasquill-Gifford stability classes developed by these analyses.

Table 10-6. Annual Wind Rose for the Buxton, North Carolina, Site (frequency with which the wind blows from the site toward the specified direction)

Direction	N	NNE	NE	ENE	E	ESE	SE	SSE
Frequency	0.0702	0.0999	0.1083	0.0607	0.0282	0.0200	0.0255	0.0201
Direction	S	SSW	SW	WSW	W	WNW	NW	NNW
Frequency	0.0650	0.0884	0.1152	0.0749	0.0421	0.0422	0.0458	0.0936

Table 10-7. Annual Frequency of Occurrence of Pasquill-Gifford Atmospheric Stability Classes A Through F at Buxton, North Carolina

Class	A	B	C	D	E	F
Frequency	0.0008	0.0352	0.1113	0.5906	0.1495	0.1126

Finally, one MACCS calculation and two RADTRAN calculations, one 0-to-30 mile calculation and one 0-to-50 mile calculation, were performed. All of the calculations used the TN-125 cask inventory presented in Table 10-1. The radionuclides in this inventory were assigned to the following four chemical element groups, Noble Gases, Cesium, Ruthenium, and Particulates (CRUD release was neglected), which had the following release fractions for release from failed fuel rods to the environment: 0.1, 9.0×10^{-4}, 1.0×10^{-6}, and 5.0×10^{-8}, respectively.

The MACCS calculation used the population distribution presented in Table 10-5 and one year of hourly meteorological data recorded at the National Weather Service Station located at Buxton, North Carolina. Results for single variable meteorology weather trials that assumed the wind was blowing in a given compass direction were summed using the wind rose frequencies presented in Table 10-6 as weights. Because MACCS calculates results for all 16 compass sectors, including those sectors that are devoid of population, MACCS usually calculates consequences only when the wind is blowing into a compass sector that contains population (because plumes can be broader than a single compass sector, sometimes MACCS calculates consequences when the wind blows into a sector that is devoid of population, because that sector lies next to a sector that contains population). Inspection of Table 10-6 shows that the fraction of time when the wind blows from Buxton toward the six compass sectors that contain population, the WSW, W, WNW, NW, NNW, and N compass sectors, is 0.3688. Therefore, the fraction of MACCS single weather sequence trials that yielded consequences was about 0.37.

Each RADTRAN calculation consisted of six constant meteorology calculations, one for each of the six Pasquill-Gifford atmospheric stability classes. Both RADTRAN calculations assumed a downwind population density of 2.6 people per square kilometer. Each calculation produced an average annual result by summing the results for the six separate constant meteorology calculations using the annual frequencies of occurrence for the six Pasquill-Gifford atmospheric stability classes given in Table 10-6 as weights. By subtracting the 0-to-30 mile RADTRAN results from the 0-to-50 miles RADTRAN results, the 30-to-50 mile RADTRAN results were obtained. Because RADTRAN uses a uniform population distribution that has no dependence on compass direction (doesn't reflect the presence of ocean), the 30-to-50 mile results must be multiplied by 0.37 in order to obtain a result directly comparable to the MACCS result. Table 10-8 compares the RADTRAN population dose for the 30-to-50 mile distance interval multiplied by 0.37 to the population dose obtained by the MACCS calculation.

Table 10-8. Comparison of the Population Dose calculated by RADTRAN for a Hypothetical Ship Collision that Occurs While Sailing a Coastal Route along the North Carolina Coast 30 Miles Out to Sea with the population Dose Calculated by MACCS for an Accident Location 30 Miles from the North Carolina Coast

Code	30 to 50 Mile Population Dose (person-rem)
RADTRAN	16.4
MACCS	32.0

Table 10-8 shows that the population dose calculated by MACCS, using a 0-to-50 mile population distribution that is devoid of population from 0 to 30 miles, is twice the population dose calculated by RADTRAN for the 30-to-50 mile region after multiplying the RADTRAN 30-to-50 mile result by 0.37 in order to correct for compass sectors that contain only ocean and thus are devoid of population. For the following reasons, the RADTRAN and MACCS population doses would not be expected to differ by much less than a factor of two: first, because the two codes use atmospheric dispersion data calculated

using different Gaussian dispersion models; second, because the 0.37 correction factor is too small since some MACCS weather trials where the wind is blowing into an unpopulated compass sector still yield population dose by exposing population in neighboring compass sectors to the radioactive plume; third, because the codes do not use identical dosimetric models; and fourth, because the precision of these consequence calculations is no more than a factor of two to three. Thus, the fact that MACCS predicts a population dose only twice that predicted by RADTRAN shows that differencing two RADTRAN calculations yields a reasonable estimate of the dose to the population of a transportation route segment that contains a near-field region that is devoid of population.

10.4.3 New London to Charleston Coastal Route

This section describes illustrative RADTRAN calculations that develop an estimate of the consequences of a transportation accident that might occur while spent power reactor fuel is transported in a TN-125 cask from New London, Connecticut, around Long Island and then down the coast to Charleston, South Carolina, on an ocean going barge sailing at a distance of approximately 25 miles from the coast. The calculations used the inventory presented in Table 10-1, the release fractions presented in Table 10-2, and the isopleth areas presented in Table 10-4. The calculation used three aggregate route segments, one urban, one suburban, and one rural segment. The lengths and average populations densities of these three aggregate route segments were calculated using the HIGHWAY code and the following coastal highway route: State Highway 27 from Montauk Point on Long Island to New York City; US 9 from New York City through Cape May, New Jersey, and Lewes, Delaware, to US 13; US 13 to Norfolk, Virginia; and US 17 from Norfolk, Virginia, to Charleston, South Carolina. Table 10-9 presents the lengths and population densities of the aggregate urban, suburban, and rural route segments used in these calculations.

Table 10-9. Aggregate Route Segment Lengths and Population Densities

Segment	Urban	Suburban	Rural
Length (km)	133	415	902
Population Density (people per km^2)	2780	386	13.5

Two sets of RADTRAN calculations were performed. The first set used the release fractions specified in Table 10-2 for the collision-only (1 hole) accident scenario and the second set used the release fractions specified in that table for the collision-plus-fire (2 holes) accident scenario. Thus, as was done for the illustrative port accident calculations performed using the MACCS code, results were developed for two accident scenarios that bound the expected range of severe ship accidents. Each set of RADTRAN calculations consisted of two individual RADTRAN calculations. The first calculation used the full set of isopleths presented in Table 10-4 and the second calculation deleted from that set of isopleths, isopleths sixteen, seventeen, and eighteen. Thus, the first calculation in each set was a 0-to-75 mile calculation and the second was a 0-to-25 mile calculation. Then, by differencing the results of these two calculations, the 25-mile wide, near-field open ocean region between the barge and the shoreline was subtracted from the results of the standard RADTRAN calculations, thereby obtaining an estimate of the consequences that occurred in the 25-to-75 mile distance range, which comprises the first 50 miles of land next to the shoreline.

Table 10-10 presents the results of these RADTRAN calculations. Specifically, Table 10-10 presents for each source term and each distance range, the 50-year population dose estimated by RADTRAN for each of the three aggregate route segments used in these calculations. Finally, the table presents the results

Table 10-10. Fifty-Year Population Doses (Sv) Calculated by RADTRAN for Three Distance Ranges for the New London to Charleston Coastal Shipping Route

Source Term	Collision-Only (1 hole)			Collision-plus-Fire (2 holes)		
Route Segment	Urban	Suburban	Rural	Urban	Suburban	Rural
0-to-75 miles	1110	255	8.9	106,000	24,400	855
0-to-25 miles	795	183	6.4	72,900	16,700	586
25-to-75 miles	315	72	2.5	33,100	7,700	269

obtained for the 25-to-75 mile distance range, i.e., for the onshore population along the sailing route, by differencing the results obtained for the 0-to-75 and 0-to-25 mile distance ranges.

Inspection of Table 10-10 shows that deposition of radioactive materials, onto the surface of the 25-mile-wide region of ocean between the barge sailing route and the shoreline, reduces the estimated population dose by a factor of about three. Thus, correcting for the presence of a near-field region that is devoid of population produces a significant reduction in estimated population dose. Of course, some of the radioactivity that deposits onto the ocean surface will eventually cause population dose as a result of its incorporation into marine foodstuffs, harvesting of these foodstuffs by commercial fishing, and distribution of the harvested marine foods through the commercial food distribution system. Because these doses reach population through the commercial food distribution system, as is discussed in the next section, individual doses will always be very small, well below normal background exposures, and thus of little significance.

Because the 50-year population dose of 33,100 Sv predicted for the collision-plus-fire accident scenario, when the accident occurs while the barge is sailing along the urban segment of the coastal route, seems large, this result needs to be further discussed. Inspection of Table 10-4 shows that the 33,100 Sv dose is incurred by population located inside of the eighteenth isopleth but downwind of the fifteenth isopleth. Table 10-4 shows that isopleths 18 and 15 have respective areas of 1,350 and 177 km^2. Table 10-9 shows that the population density along the urban aggregate route segment is 2,780 people per square kilometer. Therefore, the number of people exposed to radiation as a result of the hypothesized ship collision is about

$$3.3 \times 10^6 \text{ people} = 2780 \text{ people km}^{-2} (1350 \text{ km}^2 - 177 \text{ km}^2)$$

Because normal individual background radiation doses are about 3.6×10^{-3} Sv per year, the 50-year population dose that would normally be incurred as a result of background radiation by the 3.3×10^6 people who might be directly exposed to some additional radiation as a result of the ship accident is about

$$5.9 \times 10^5 \text{ Sv} = (3.3 \times 10^6 \text{ people}) (3.6 \times 10^{-3} \text{ Sv yr}^{-1}) (50 \text{ yrs})$$

which is about 20 times larger than the 33,100 Sv population dose predicted for the collision-plus-fire (2 holes) ship accident scenario should that accident occident occur while sailing off of an urban area. Thus, even an unusually long epidemiological study of a large portion of the exposed population would not be expected to be able to detect the radiological effects of the radiation exposures that might result from this accident scenario.

Finally, the population dose predicted for the collision-plus-fire ship accident scenario is not only small, it is also most improbable. Table 10-9 shows that the length of the urban aggregate route segment is 133 km = 71.8 nautical miles and Table 4.4 shows that the probability of a ship collision per nautical mile sailed is about 1.9×10^{-7} when sailing in coastal waters. Therefore, the probability that the barge that is carrying the TN-125 cask will be struck while sailing near an urbanized stretch of coastline while en route from New London to Charleston is approximately

$$6.8 \times 10^{-6} = (0.5)\ (71.8 \text{ nautical miles})\ (1.9 \times 10^{-7} \text{ collisions per nautical mile sailed})$$

where the factor of 0.5 corrects for the fact only about half of the time will the barge be struck during the hypothetical collision (the other half of the time, the tug pulling the barge will be the striking ship).

Table 8.3 shows that, for a small ship (a charter freighter with a loaded displacement of 1,740 tonnes), the probability that the collision leads to a double (2 hole) failure of the cask is about

$$6 \times 10^{-3} = P_{crush}\ P_{puncture/shear} = (0.03)\ (0.2)$$

Since the probability of a double cask failure given a collision is 6×10^{-3}, the probability that the collision will both occur and also lead to a double (2 hole) failure of the cask is about $4.1 \times 10^{-8} = (6.8 \times 10^{-6})\ (6 \times 10^{-3})$.

Since the barge carries no fuel and no cargo in addition to the RAM cask, the collision can lead to a large, long-duration engulfing fire only if the striking ship is a tanker and then only if the collision is severe enough to fail both the tanker's collision bulkhead and also its forward oil hold. Given that less than half of the ships in the world fleet are tankers or bulkers and that only a most severe collision of a tanker with a barge can fail the tanker's collision bulkhead (say 4 of every 100 collisions), and assuming that the world fleet contains roughly equal numbers of tankers and bulkers, then the probability that the collision leads to a long-lasting oil fire that engulfs the barge is something like (probably much less than) $10^{-2} = (1/2)\ (1/2)\ (0.04)$. Accordingly, the probability that the barge is struck during the voyage from New London to Charleston, while sailing off of an urban area, and that the collision leads to a double failure of the cask and also to a large long-duration oil fire, that engulfs the barge and thus the cask, is estimated to be something like $4 \times 10^{-10} = (6.8 \times 10^{-6})\ (6 \times 10^{-3})\ (10^{-2})$. Thus, not only are the radiological consequences of this most severe collision-plus-fire accident unlikely to be capable of epidemiological detection, but also the probability that this accident occurs during voyage from New London to Charleston is so small that its occurrence is almost not credible.

10.5 Accidents at SEA (MARINRAD Calculations)

If a ship collision were to culminate in the loss into the ocean of a RAM package, eventually, whether failed during the accident or later due to corrosion, radioactivity would be released into the ocean from the failed package. Over time, transport of this radioactivity back to man would subject many people to small radiation exposures due to ingestion of aquatic foods, consumption of desalinized water and sea salt, inhalation of sea spray, exposure to shore sediments, and/or immersion in ocean water. The transport processes that cause these radiation exposures are all modeled by the MARINRAD code system [5].

MARINRAD is a system of three FORTRAN computer codes: MARRAD, MAROUT, and ADJOINT, where MARRAD and MAROUT model ocean transport and ADJOINT allows sensitivity studies to be performed. These codes were developed by The Analytical Sciences Corporation (TASC)

for the Sub-Seabed Disposal Program conducted by Sandia during the 1970s and 1980s. As a part of the SeaRAM Program, MARRAD and MAROUT were ported to a Hewlett-Packard Unix workstation, a test problem developed by the Sub-Seabed Disposal Program that exercises MARRAD was successfully rerun, and an example calculation was performed in which a TN-12 cask loaded with PWR spent fuel, having a burnup of 35 GWD/MTIHM, is lost in the Labrador region of the Atlantic ocean. The following sections discuss the example calculation.

10.5.1 The Source Term

The total amount of activity released into the ocean is the product of the fuel burnup and the mass of initial heavy metal in the fuel. For this example, that mass was calculated as the product of 0.606 MTIHM per assembly times the payload of 12 assemblies carried by a TN-12 cask, for a total of 7.27 MTIHM. This represents 254 GWD of activity, or, in the units used in MARRAD, 232 Mwe-yrs of activity, where a 33.3% thermal-to-electric conversion efficiency has been assumed.

MARRAD has a number of source term options, among them a model for the direct release to an ocean compartment of a collection of radionuclides specified from an ORIGEN inventory file with concentration in units of curies per Mwe-yr. This is the option that was used for the example calculation. Figure 10-1 shows a graph of the time profile of the release for three assumed values of the nuclide leaching time constant, τ. Leaching is assumed to begin at t = 1 yr, which means that the fuel pellets are one year out of the reactor when first exposed to sea water (Note that over time, each case will produce the same total release!).

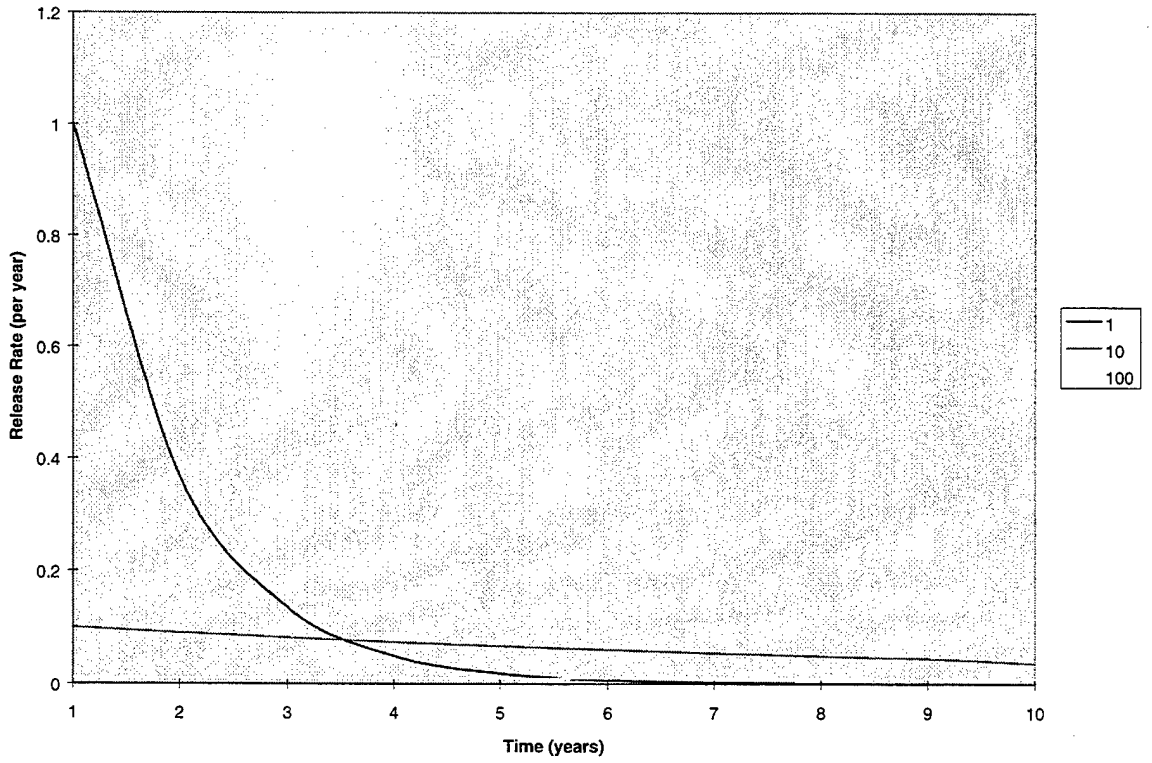

Figure 10-1. Fractional Release Rate vs. Time.

10.5.2 The Ocean Model

The 19 compartment ocean model used in the NARES Abyssal Plain radioactive seabed waste disposal assessment [10], was also used for the example calculation. The release point, however, was moved from compartment 1 (the ocean bottom above the hypothesized seabed disposal site) to compartment 9 (the top-Labrador ocean compartment that contains the upper waters of the North Atlantic off of Eastern Canada and Greenland). As this compartment contains the Grand Banks, release of radioactivity into the top-Labrador ocean compartment simulates release into a major fishing region of the ocean. Figure 10-2 shows a schematic (not to scale) of the 19 compartments in the ocean model used in the example calculation. The flows, indicated by arrows in the figure, are in sverdrups (1.0×10^6 cubic meters per second). Radionuclide transport between compartments takes place by advection and diffusion according to the systems model described in Reference 5. The Site or Benthic Mixing Layer, and the Mesoscale and Gyre compartments refer to regions near the NARES sub-seabed site, not the release location used in this example calculation. Loss mechanisms included in the systems model are sedimentation, diffusive deposition, and burial in ocean sediments.

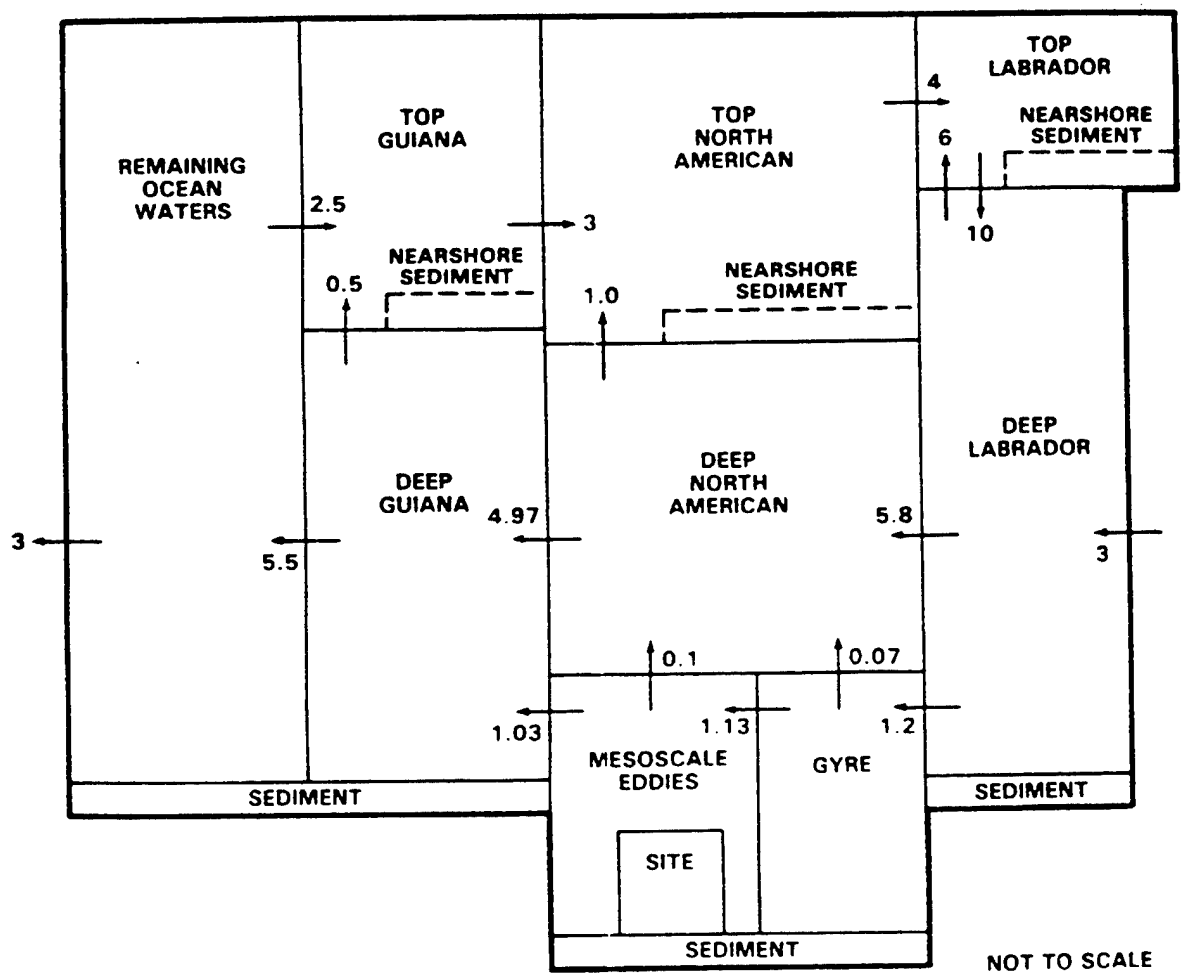

Figure 10-2. The NARES 19 Compartment Ocean Model.

10.5.3 Pathways to Man

MARINRAD calculates dose to an average individual by considering the ingestion of aquatic foods, consumption of desalinized water and sea salt, inhalation of spray, exposure to shore sediments and immersion in ocean water. Aquatic foods are divided into seven groups: fish, crustaceans, mollusks, seaweed, plankton, and two levels of predation referred to as J and K predators. Thus, J predators consume K predators that consume level L species (e.g., larval fish, crustaceans, mollusks, seaweed, and plankton). At both the J and K predator levels, there may be up to five different species. The dose for the various pathways is calculated by multiplying together a usage factor U, a concentration factor CF calculated within MARRAD, a path dependent multiplier M which accounts for differences in units, and an effective dose equivalent E, each of which may depend on the pathway.

10.5.3.1 USAGE FACTORS

When all of the usage factors for a pathway are zero, that pathway is effectively removed. All of the usage factors for the deep water compartments in Table 10-11 have been assumed to be zero because they are believed to have no direct contribution to maritime foods. Usage factors from the NARES sub-seabed site evaluation are built into the code in routine GETUF in MAROUT. For this example calculation, the default usage factors were overridden in the input through namelist OVRLST to produce the usage shown in Table 10-11 for each pathway and all compartments. The units are kg/yr except for the inhalation pathways, which are in cubic meters per hour, and the exposure pathways, which are in hours per year. The market basket for consumption of fish, crustacean, mollusk, and seaweed assumed in the example calculation is that of an Average Adult Frenchman [11].

10.5.3.2 CONCENTRATION FACTORS

MARRAD computes the concentration of each radionuclide in each pathway by multiplying the concentration factor (CF) values, obtained by solving the transport equations for the ocean model as driven by the source term for that nuclide, by the concentration of the nuclide in the compartment, as a function of time. The FISH pathway, which can include biological concentration due to predation, begins with the CF0 values from MARRAD for level L ocean species. These, in turn, contribute to the concentration factors (CF1) for the predators at predator level K, through coefficients that involve the predator biomass, its ingestion rate, the fraction of a nuclide adsorbed through the predator's gut, the biological turnover rate per year of the nuclide for that predator, and consumption fractions. Finally, the CF0 and CF1 values are combined through a second and similar level of coefficients (CF2) specific to the J predator level. Table 10-12 lists the prey level CF0 concentration factors, which are given as default values in the MARRAD portion of the MARINRAD code.

It was necessary to include in the MARRAD input, several factors involved in computing the CF1 and CF2 predator level concentration factors. Four of these were taken to be nuclide independent:

The ingestion rate of predators in kg per year	2.74
The biomass of predators in the compartment in kg	1.0
The fraction of predators K consumed by predator J	0.1
The fraction of prey consumed by predators	0.1

Table 10-11. Usage Factors for the Labrador Example Calculation

a. Ocean Compartments

Pathway	Compartment									
	Ben Mix Layer	Meso-scale	Gyre	Deep N America	Deep Guiana	World Ocean	Top Guiana	Top N America	Top Labrador	Deep Labrador
Fish						8.4	8.4	8.4	8.4	
Crustacean						4	4	4	4	
Mollusk						4.6	4.6	4.6	4.6	
Seaweed						0.4	0.4	0.4	0.4	
Plankton										
Fish Pred K1						2.23	2.23	2.23	2.23	
Fish Pred K2										
Fish Pred K3										
Fish Pred K4										
Fish Pred K5										
Fish Pred J1						22.3	22.3	22.3	22.3	
Fish Pred J2										
Fish Pred J3										
Fish Pred J4										
Fish Pred J5										
Desal Water						0.37	0.37	0.37	0.37	
Sea Salt						1.8	1.8	1.8	1.8	
Inhale Sed										
Inhale Water						0.000024	0.000024	0.000024	0.000024	
Swim Expose						300	300	300	300	
Shore Expose										

b. Sediment Compartments

PATHWAY	COMPARTMENT								
	Ben Mix Layer Sediment	Mesoscale Sediment	Gyre Sediment	Deep Labrador Sediment	Deep Guiana Sediment	World Ocean Sediment	Top Guina Sediment	Top N Ameica Sediment	Top Labrador Sediment
Fish									
Crustacean									
Mollusk									
Seaweed									
Plankton									
Fish Pred K1									
Fish Pred K2									
Fish Pred K3									
Fish Pred K4									
Fish Pred K5									
Fish Pred J1									
Fish Pred J2									
Fish Pred J3									
Fish Pred J4									
Fish Pred J5									
Desal Water									
Sea Salt									
Inhale Sed						8.0E-7	8.0E-7	8.0E-7	8.0E-7
Inhale Water									
Swim Expose									
Shore Expose						1000.	1000.	1000.	1000.

Table 10-12. PREY Level Concentration Factors (CF0)

ISO-TOPE	FISH	CRUST-ACEAN	MOL-LUSC	SEA WEED	PLANK-TON	DESAL WATER	SEA SALT	INH SED	INH WATER	SWIM EXP	SHORE EXP
AM243	0.01	0.2	2.0	20.0	2.0	1.0	1.0	1.0	1000.	1.0	1.0
AM241	0.01	0.2	2.0	20.0	2.0	1.0	1.0	1.0	1000.	1.0	1.0
PU240	0.04	12.0	0.36	0.7	12.0	1.0	1.0	1.0	1000.	1.0	1.0
PU239	0.04	12.0	0.36	0.7	12.0	1.0	1.0	1.0	1000.	1.0	1.0
PU238	0.04	12.0	0.36	0.7	12.0	1.0	1.0	1.0	1000.	1.0	1.0
NP237	0.01	0.02	0.014	1.0	2.0	1.0	1.0	1.0	1000.	1.0	1.0
U238	0.0001	0.01	0.01	0.7	0.005	1.0	1.0	1.0	1000.	1.0	1.0
U235	0.0001	0.01	0.01	0.7	0.005	1.0	1.0	1.0	1000.	1.0	1.0
U234	0.0001	0.01	0.01	0.7	0.005	1.0	1.0	1.0	1000.	1.0	1.0
U233	0.0001	0.01	0.01	0.7	0.005	1.0	1.0	1.0	1000.	1.0	1.0
PA231	0.02	0.01	0.01	0.1	1.0	1.0	1.0	1.0	1000.	1.0	1.0
TH232	1.0	1.0	1.0	1.3	10.0	1.0	1.0	1.0	1000.	1.0	1.0
TH230	1.0	1.0	1.0	1.3	10.	1.0	1.0	1.0	1000.	1.0	1.0
TH229	1.0	1.0	1.0	1.3	10.	1.0	1.0	1.0	1000.	1.0	1.0
AC227	0.03	1.0	1.0	1.0	10.	1.0	1.0	1.0	1000.	1.0	1.0
RA228	0.1	0.025	0.0024	0.07	0.005	1.0	1.0	1.0	1000.	1.0	1.0
RA226	0.1	0.025	0.0024	0.07	0.005	1.0	1.0	1.0	1000.	1.0	1.0
PO210	7.0	75.	20.	1.0	20.0	1.0	1.0	1.0	1000.	1.0	1.0
PB210	0.3	0.95	0.7	1.0	1.2	1.0	1.0	1.0	1000.	1.0	1.0
EU154	0.1	1.0	1.0	1.0	10.0	1.0	1.0	1.0	1000.	1.0	1.0
SM151	0.1	1.0	1.0	1.0	3.0	1.0	1.0	1.0	1000.	1.0	1.0
CS137	0.08	9.0	0.9	0.06	0.7	1.0	1.0	1.0	1000.	1.0	1.0
CS135	0.08	9.0	0.9	0.06	0.7	1.0	1.0	1.0	1000.	1.0	1.0
I129	0.01	0.1	0.1	1.0	1.0	1.0	1.0	1.0	1000.	1.0	1.0
SN126	1.0	0.3	0.1	0.1	1.0	1.0	1.0	1.0	1000.	1.0	1.0
PD107	0.3	0.3	0.3	1.0	1.0	1.0	1.0	1.0	1000.	1.0	1.0
TC99	0.09	0.25	0.2	1.5	1.0	1.0	1.0	1.0	1000.	1.0	1.0
NB93m	0.001	0.1	1.0	0.5	1.0	1.0	1.0	1.0	1000.	1.0	1.0
ZR93	0.001	0.1	1.0	0.5	10.0	1.0	1.0	1.0	1000.	1.0	1.0
SR90	0.02	0.015	0.16	0.035	0.056	1.0	1.0	1.0	1000.	1.0	1.0
SE79	0.1	1.0	1.0	1.0	10.0	1.0	1.0	1.0	1000.	1.0	1.0
NI59	0.5	0.1	0.1	0.5	1.0	1.0	1.0	1.0	1000.	1.0	1.0
C14	5.0	4.0	5.0	0.4	0.3	1.0	1.0	1.0	1000.	1.0	1.0
NP239	0.01	0.2	2.0	20.0	2.0	1.0	1.0	1.0	1000.	1.0	1.0
AC225	1.0	1.0	1.0	1.3	10.0	1.0	1.0	1.0	1000.	1.0	1.0
RA225	1.0	1.0	1.0	1.3	10.0	1.0	1.0	1.0	1000.	1.0	1.0
RA223	0.03	1.0	1.0	1.0	10.0	1.0	1.0	1.0	1000.	1.0	1.0
SB126	1.0	0.3	0.1	0.1	1.0	1.0	1.0	1.0	1000.	1.0	1.0
Y90	0.01	0.015	0.16	0.035	0.56	1.0	1.0	1.0	1000.	1.0	1.0
CM244	0.01	0.2	2.0	2.0	2.0	1.0	1.0	1.0	1000.	1.0	1.0
CM242	0.01	0.2	2.0	2.0	2.0	1.0	1.0	1.0	1000.	1.0	1.0
PU241	0.04	12.0	0.36	0.7	12.0	1.0	1.0	1.0	1000.	1.0	1.0
PM147	0.1	1.0	1.0	1.0	1.0	1.0	1.0	1.0	1000.	1.0	1.0
CE144	0.01	1.0	1.0	1.0	1.0	1.0	1.0	1.0	1000.	1.0	1.0
CS134	0.08	9.0	0.9	0.06	0.7	1.0	1.0	1.0	1000.	1.0	1.0
RU106	0.001	0.6	2.0	2.0	1.0	1.0	1.0	1.0	1000.	1.0	1.0
NB95	0.001	0.1	1.0	0.5	1.0	1.0	1.0	1. 0	1000.	1.0	1.0
ZR95	0.001	0.1	1.0	0.5	10.	1.0	1.0	1.0	1000.	,1.0	1.0
Y91	0.01	0.15	0.16	0.035	0.56	1.0	1.0	1.0	1000.	1.0	1.0
SR89	0.01	0.15	0.16	0.035	0.56	1.0	1.0	1.0	1000.	1.0	1.0
AM242m	0.01	0.2	2.0	20.0	2.0	1.0	1.0	1.0	1000.	1.0	1.0
PU242	0.04	12.	0.36	0.7	12.0	1.0	1.0	1.0	1000.	1.0	1.0
U236	0.0001	0.01	0.01	0.7	0.005	1.0	1.0	1.0	1000.	1.0	1.0

There are observations which place the ratio of ingestion rate to predator biomass in the range 2.74 to 3.52 kg per year (see Reference 12, page 48). For this example, the predators were all given a 1 kg mass, which implies 2.74 to 3.52 kg per year for the ingestion rate; 2.74 kg per year was the value used.

Two other input factors, known to vary among different nuclides, are the fraction of a nuclide adsorbed in the predator gut and the biological turnover rate for the nuclide in the predator. When this example was performed, the only data known to be available for these factors was that of Table C.2-2 of Reference 12, so, in most cases, conservative values are assumed (1.0 or 0.33 for nuclide adsorption and 0.23 for turnover rate.) The specific values input for the calculation are shown below in Table 10-13. Note that the nuclides in this table follow a different order from that in Table 10-12; this is due to a code execution requirement that, in the input, daughter nuclides are listed after their parents.

Table 10-13. Assumed Predator Nuclide Adsorption and Biological Turnover Rates

Nuclide	Gut Adsorption	Biological Turnover	Nuclide	Gut Adsorption	Biological Turnover
AM243	0.33	0.23	CS135	1.00	1.20
AM242m	0.33	0.23	I129	1.00	7.20
CM245	0.33	0.23	SN126	1.00	7.20
AM241	0.33	0.23	PD107	1.00	0.23
CM244	0.33	0.23	TC99	1.00	5.50
PU240	0.33	0.23	ZR93	1.00	0.23
PU239	0.33	0.23	NB93m	1.00	0.23
PU238	0.33	0.23	SR90	1.00	2.30
NP237	0.33	0.23	SE79	1.00	23.0
U238	0.33	0.23	CE144	0.33	0.23
U235	0.33	0.23	CS134	1.00	42.2
U234	0.33	0.23	RU106	1.00	0.23
U233	0.33	0.23	NB95	1.00	0.23
PA231	0.33	0.23	ZR95	1.00	0.23
U236	0.33	0.23	Y91	1.00	0.23
TH232	0.33	0.23	SR89	1.00	0.23
TH230	0.33	0.23	PU242	0.33	0.23
TH229	0.33	0.23	NI59	1.00	0.23
AC227	0.33	0.23	C14	1.00	0.23
RA228	0.33	0.23	NP239	0.33	0.23
RA226	0.33	0.23	RA225	1.00	0.23
PB210	1.00	0.23	AC225	0.33	0.23
PO210	1.00	8.40	RA223	1.00	0.23
EU154	0.33	0.23	SB126	1.00	0.23
SM151	0.33	0.23	Y90	1.00	2.3
CS137	1.00	1.20	PU241	0.33	0.23

10.5.4 Average Individual Dose

The usage factors presented in Table 10-12 were used by MAROUT to calculate the average individual doses presented in Figures 10-3 through 10-6. Results are presented for consumption from the Top Labrador compartment (where the accident that leads to loss of the RAM package into the ocean is hypothesized to occur), the Top North America compartment, the Top Guiana compartment, and the World Ocean compartment. Three cases are presented for each compartment; in the first case, all nuclides have an e-folding time τ of 1 year (nuclide release time period of about 3 years); in the second case, Cesium isotopes, because of their high solubility in water, still have $\tau = 1$ year but, because of their relative insolubility in water, all other isotopes have $\tau = 10$ years (nuclide release time period of about 30 years); and in the final case, Cesium isotopes again have $\tau = 1$ year but now all other isotopes have $\tau = 100$ years (nuclide release time period of about 300 years).

10.5.5 Discussion of Results

While there is no available data on the leaching of elements from spent fuel pellets immersed in brine, and the cask enclosure will inhibit their mixing with compartment waters, the values of τ chosen for these calculations are thought to span the possible range of e-folding times for the release of most radionuclides. Thus, in each of the preceding charts, it is the region between the curves (i.e., the range of the doses) that is of interest, rather than any specific dose value on any of the three curves.

With this in mind, we conclude from Figure 10-3 that a maritime accident in the Labrador region of the north Atlantic Ocean that released the source term described above in Section 10.5.1 could produce a peak average individual dose of about 60-to-180 millirem per year about five years after the accident due to consumption of marine foods harvested from this compartment. The annual dose would rapidly decrease and after 50 years would be about 10-to-50 millirem per year. After 100 years, it would be about 1-to-40 millirem per year and would continue to decline. As these yearly individual doses are all smaller than the 360 millirem average annual dose that an average individual receives from natural (e.g., cosmic rays, radon, terrestrial radionuclides) and routine man-made (e.g., medical X-rays) sources of radiation, they are not expected to significantly increase the incidence of radiological health effects.

The variation of individual dose with time is different in the other compartments. The Gulf Stream is a strong current in the top of the eastern Atlantic which flows from the Top Guina compartment, through the Top North American compartment into the Top Labrador compartment. The predominant back-linkage between the Top Labrador and Top North America compartments is through deep-water currents beneath them, which run counter to the direction of the Gulf Stream. This, in turn, will dilute the nuclide concentrations and delay their appearance. As seen in Figure 10-4, the average individual dose would peak no sooner than 20 years after the accident and may, if the important nuclides are released slowly, take more than a century. The peak annual individual dose values are not expected to exceed 5 millirem per year from this compartment; though not shown in the graph, the peak value calculated for the curve with $\tau = 100$ years is 5.3 millirem and occurs at about 150 years after the accident.

Other parts of the ocean follow the same trend. The computed peak value in the Top Guiana compartment ranges between 0.64 millirem at 90 years (for the curve with $\tau = 1$ year) and 2.1 millirem at 200 years (for the curve with $\tau = 100$ years). For the World Ocean compartment, the annual dose is between 0.05 millirem at 300 years (for the curve with $\tau = 1$ year) and 0.19 millirem at 500 years (for the curve with $\tau = 100$ years).

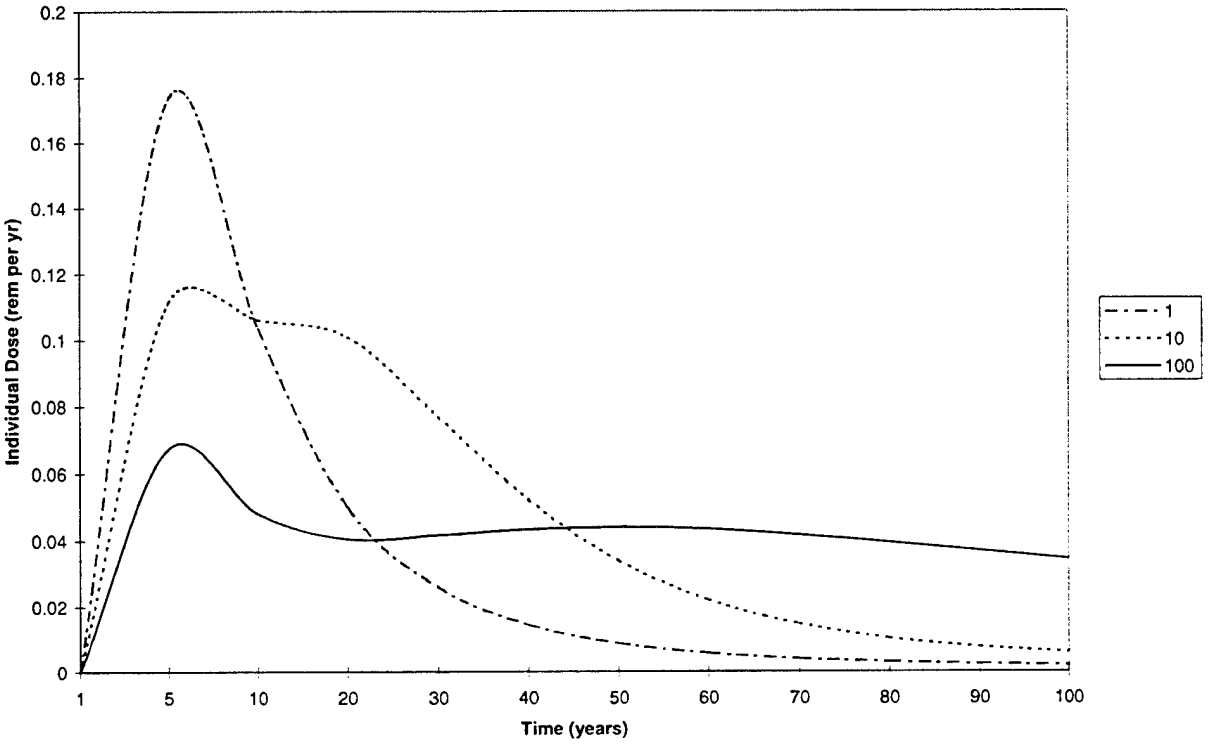

Figure 10-3. Average Individual Dose From the Top Labrador Compartment.

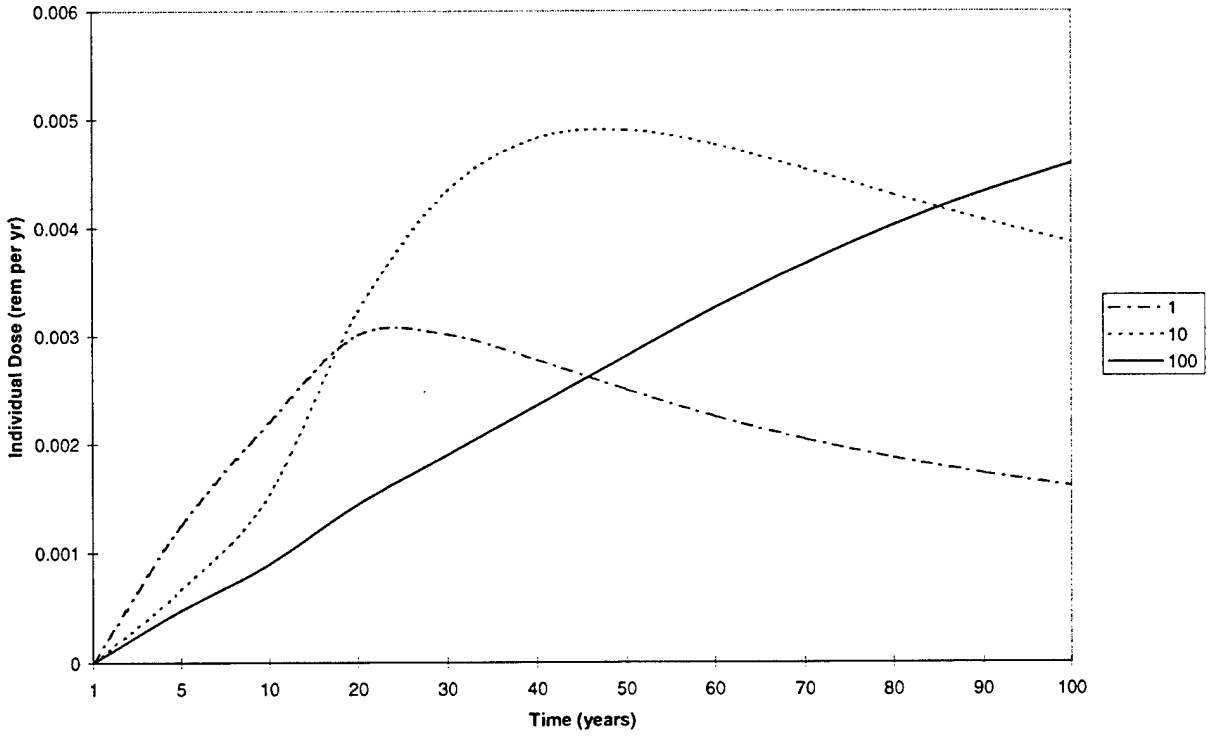

Figure 10-4. Average Individual Dose From the Top North American Compartment.

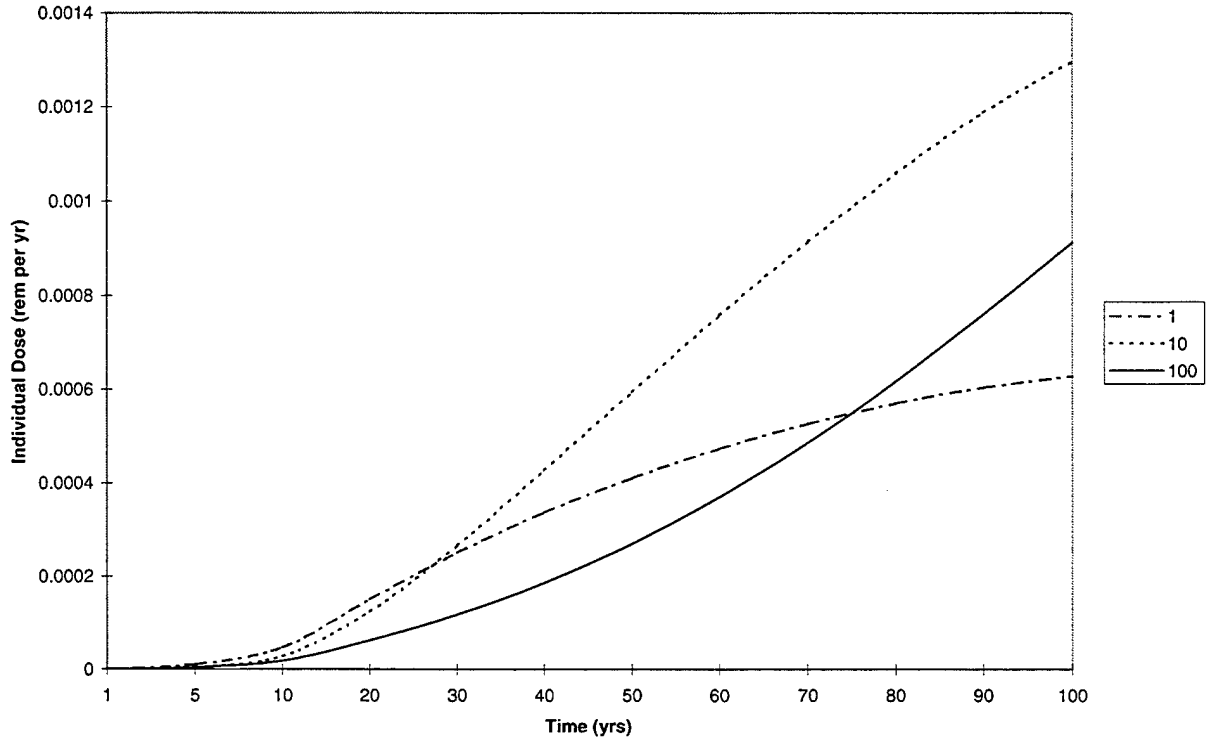

Figure 10-5. Average Individual Dose From the Top Guiana Compartment.

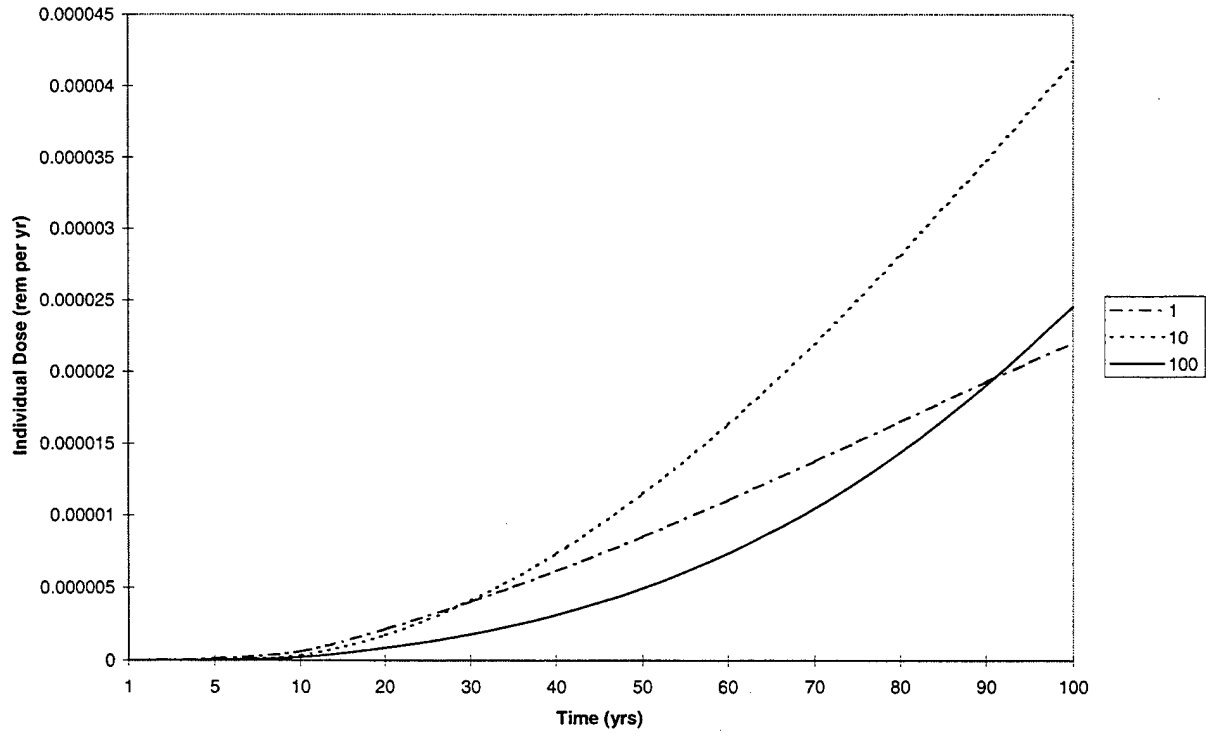

Figure 10-6. Average Individual Dose From the World Ocean Compartment.

The world wide, 50-year integrated population dose predicted by MARINRAD for the loss of 12 PWR assemblies into the Top Labrador compartment is 63 million person-rem for $\tau = 1$ year and 54 million person-rem for $\tau = 100$ years. Assuming stochastic effects produce 5×10^{-4} latent cancer fatalities per person-rem, this implies an excess cancer fatality rate of 5 to 6 thousand cases per year, worldwide. This result, while large, is not significant relative to the yearly worldwide cancer fatality rate of approximately 6 million cancer fatalities per year.

Finally, since in this analysis there were no compartments specifically located in the eastern or southern Atlantic (these waters were all lumped into the World Ocean compartment), these results are not directly applicable to the ocean waters off the European, African, or South American coasts.

10.6 Discussion

The illustrative consequence calculations described in this section have one result in common. They all predict doses that are very small when compared to the average annual dose normally incurred by individuals due to exposure to natural (e.g., comic rays, radon, terrestrial radionuclides) or routine man-made (e.g., medical X-rays) sources of radiation. Thus, these illustrative calculations suggest that the radiological consequences that might result if a ship transporting a Type B package were involved in a severe maritime accident are not of great concern.

10.7 References

1. D. I. Chanin et al., *MELCOR Accident Consequence Code System (MACCS), Volume I: User's Guide*, NUREG/CR-4691. Sandia National Laboratories, Albuquerque, NM, February 1990.

2. H. N. Jow et al., *MELCOR Accident Consequence Code System (MACCS), Volume II: Model Description*, NUREG/CR-4691. Sandia National Laboratories, Albuquerque, NM, February 1990.

3. K. S. Neuhauser and F. L. Kanipe, *RADTRAN 4, Volume II: Technical Manual*, SAND89-2370. Sandia National Laboratories, Albuquerque, NM, May 1994.

4. K. S. Neuhauser and F. L. Kanipe, *RADTRAN 4, Volume III: User Guide*, SAND89-2370. Sandia National Laboratories, Albuquerque, NM, January 1992.

5. D. A. Ensminger, C. M. Koplik, and J. Y. Nalbandian, *Users Guide to Marinrad IV: Model for Assessing the Consequences of Release of Radioactive Material into the Oceans*, SAND87-7067. Sandia National Laboratories, Albuquerque, NM, September 1987.

6. R. P. Sandoval et al., *Estimate of CRUD Contribution to Shipping Cask Containment Requirements*, SAND88-1358. Sandia National Laboratories, Albuquerque, NM, January 1991.

7. E. L. Wilmot, *Transportation Accident Scenarios for Commercial Spent Fuel*, SAND80-2124. Sandia National Laboratories, Albuquerque, NM, July 1984.

8. J. L. Sprung et al., *Radiological Consequences of Ship collision that Might Occur in U.S. Ports During the Shipment of Foreign Research Reactor Spent Nuclear Fuel to the U.S. in Break-Bulk Freighters*, SAND96-0400. Sandia National Laboratories, Albuquerque, NM, August 1996.

9. S. L. Humphreys et al., *SECPOP90: Sector Population, Land Fraction, and Economic Estimation Program*, NUREG/CR-6525. Sandia National Laboratories, Albuquerque, NM, March 1997.

10. M. F. Kaplan and C. M. Koplik, *Preliminary Post-Emplacement Safety Analysis of the Subseabed Disposal of High-Level Nuclear Waste*, SAND83-7106. Sandia National Laboratories, Albuquerque, NM, March 1984.

11. *The Radiation Exposure of the Population of the European Community from Radioactivity in North European Marine Waters Project 'Marina'*, RP47, EUR12483. European Commission, 1990.

12. M. F. Kaplan and R. D. Klett, *Biological and Physical Oceanographic Sensitivity Analyses for Subseabed Disposal of High-Level Waste*, SAND83-7107. Sandia National Laboratories, Albuquerque, NM, November 1984.

11. DISCUSSION AND CONCLUSIONS

The first three sections of this report:

- Presented the reasons for reexamining the risks associated with the maritime transport of radioactive materials (Section 1),
- Outlined how transportation accident risks are calculated (Section 2), and
- Developed illustrative ship accident event trees (Section 3).

Next, the frequencies of ship fires and ship collisions per nautical mile sailed were examined in Section 4.0. That examination suggested that the frequency of ship collisions depends on ship traffic density and thus on the region of the ocean in which the ship is sailing, while the frequency of ship fires depends only on sailing time or sailing distance, but not on ship traffic density and thus is independent of the ocean region in which the ship is sailing. This analysis also suggested that the frequencies of ship collisions in port waters has only a weak dependence on port traffic.

After reviewing representative ships and shipping practices in Section 5.0, in Section 6.0, Minorsky's correlation of ship collision damage with collision energies was revalidated, modified to allow collision penetration distances to be predicted, and illustratively applied to a small- and a medium-sized break-bulk freighter. Assuming that the hold in which the RAM cask is stowed is struck, this analysis suggested that for small ships only about one collision in six will penetrate deeply enough to apply crush forces to the cask, and that for large ships penetration will be deep enough in one or two collisions out of four to apply crush forces to the cask. Because Minorsky's correlation does not determine whether crush forces are relieved by collapse of cask or ship structures, prediction that penetration is deep enough to subject a cask to crush forces does not mean that the cask has been failed by those forces. In fact, the finite element ship collision calculations performed by the mechanical subtask of the SeaRAM program indicate that, if a cask is subjected to crush forces during a ship collision, these forces will most likely be relieved by collapse of ship structures rather than cask structures.

In Section 7.0, a probabilistic fire spread model was developed and illustratively applied to a small- and a medium-sized break-bulk freighter. The analysis suggested that fire start in or spread to the hold in which the RAM cask is stowed is unlikely. It also indicated that, should a fire start in or spread to the hold where the RAM cask is stowed, then ingress of air at a rate sufficient to support free burning of a good fuel in that hold can only take place through a large opening, which means that the collision must have produced a large hole in the wall of the hold that isn't blocked by the damaged prow of the striking ship, or enough bulkhead doors, ventilation shafts, and/or hold covers must be open to allow unrestricted flow of air into the hold to the fire.

In Section 8.0, the probabilities of two ship accidents that bound the likely range of ship accidents severe enough to fail a RAM cask were estimated for trans-Atlantic voyages of small- and medium-sized break-bulk freighters. The two accidents were examined: (1) a ship collision that results in a small failure of the RAM cask seal, and (2) a much more severe accident that produces a double cask failure (both a seal failure and a shear or puncture failure) and also a fire that spreads to the hold where the cask is stowed, engulfs the cask, and burns long enough and hot enough to significantly enhance the release of radioactivity from the cask. This analysis showed that the probability of the first accident occurring during a trans-Atlantic voyage was about 5×10^{-7}, and that the probability of the second accident occurring during the same voyage was about 5×10^{-12}.

MELCOR calculations that examined the release of radioactivity from the interior of a TN-125 cask to the environment were described in Section 9.0. Those calculations showed that the cask-to-

environment release fraction (R_{ce}) for particles and also for condensable vapors increases as the size (cross-sectional area, A_c) of the cask failure increases. For particles, Log R_{ce} increases linearly with Log A_c. Release increases as failure area increases because increasing failure area increases the rate of cask depressurization which decreases the time available for particles and condensable vapors to deposit onto cask interior surfaces. So, faster cask depressurization means less retention of radioactive species by the cask. For small seal failures (failures with areas of 1 mm^2 or less), these calculations indicate that the size of the cask-to-environment release fraction will be ≤ 0.01.

Illustrative consequence calculations, performed using the MACCS, RADTRAN, and MARINRAD consequence codes, were described in Section 10.0. These calculations examined port accidents, accidents that might occur while sailing a coastal route, and accidents that occur out to sea. The calculations used source terms developed for the two limiting accidents for which probabilities of occurrence were estimated in Section 8.0. These calculations showed that even the limiting upper bound accident, the accident that leads to a double cask failure and an engulfing, hot, long-duration fire, produces 50-year population doses at least an order-of-magnitude smaller than the 50-year background radiation doses that the population exposed to radiation as a result of the ship accident would normally receive.

Given the preceding, the principal conclusions of this study are:

- Ship collisions depend on ship traffic density and thus on the region of the ocean in which a ship is sailing, fires don't.
- Ship collisions are unlikely to damage a RAM cask, because collision forces will be relieved by collapse of ship structures, not cask structures.
- Fires aren't likely to start in the RAM hold; if a fire starts elsewhere on the ship, its spread to the RAM hold is not probable; and, even if a fire spreads to the RAM hold, lack of fuel or air will usually prevent the fire from there burning hot enough and long enough to significantly increase the release of radioactivity from the RAM cask.
- Most radioactive materials released to the interior of the RAM cask will deposit on interior cask surfaces; so cask retention fractions are large and cask-to-environment release fractions are small.
- Consequently, the risks of maritime transport of RAM are very small.

UNLIMITED RELEASE DISTRIBUTION

1 United States Department of Energy
Office of Scientific & Technical Information
Attn: DOE/OSTI-4500-R74, UC722
Oak Ridge, TN 37830

1 United States Department of Energy
Attn: J. Sweeney, GC-51
1000 Independence SW
Washington, DC 20585

1 United States Department of Energy
Attn: C. Head, EM-60
1000 Independence SW
Washington, DC 20585

1 United States Department of Energy
Attn: D. Huizenga, EM-60
1000 Independence SW
Washington, DC 20585

1 United States Department of Energy
Attn: K. Chacey, EM-67
1000 Independence SW
Washington, DC 20585

3 United States Department of Energy
Attn: M. Keane, EM-76
K. Kelkenberg, EM-47
M. Wangler, EM-76
19901 Germantown Road
Germantown, MD 20874-1290

3 United States Department of Energy
Attn: J. Williams, RW-51
W. Lake, RW-45
C. Kouts, RW-45
Washington, DC 20545

6 United States Department of Energy
Albuquerque Operations Office
Albuquerque Headquarters
Attn: S. Hamp
B. Hermann
J. Holm
A. Kapoor
D. Krivitsky
M. Williams
P.O. Box 5400
Albuquerque, NM 87115

1 United States Department of Transportation
Hazardous Materials Safety
Attn: R. Boyle
Washington, DC 20590

1 United States Nuclear Regulatory Commission
Nuclear Material Safety & Safeguards
Attn: E. Easton
11545 Rockville Pike
Rockville, MD 20852

1 International Atomic Energy Agency
Division of Radiation and Waste safety
Attn: Richard R. Rawl
Head, Transport safety Unit
Wagramerstrasse 5,
P.O. Box A-1400
Vienna
Austria

1 International Maritime Organization
Maritime Safety Division
Attn: Hartmut Hesse
Head, Cargoes and Facilitation Section
4 Albert Embankment
London, SE1 7SR
U. K.

1 British Nuclear Fuels Limited
Attn: Roger Cheshire
Senior manager, Terminals and Licensing
Risley
Warrington
Cheshire WA3 6AS
England

1 Edlow International Co.
Attn. Rod Fisk and Holly Tomasik
1666 Connecticut Avenue NW, Suite 201
Washington, DC 20009

1 Gesellschaft fur Anlagen und
Reaktorsicherheit (GRS) mbH
Attn: F. Lange
E. Hoermann
Schwertnergasse 1
D-50667 Koln
Germany

1 Hapag-Lloyd Container Linis GmbH
Attn: Christoph Zwanzleitner,
Containerservice Ballindamm 25
20095 Hamburg
Germany

1 MacGregor (USA) Inc.
Attn: Mike Jamer
20 Chapin Road, Unit 1012
Pine Brook, NJ

1 Nuclear Cargo & Service, GmbH and
Transkem Spedition GmbH
Attn: Holger Goncz
Rodenbacher Chaussee 6
D-63457 Hanau
Germany

1 Spliethoff's Bevrachtingskantoor B.V.
Attn: Hans Wouter Valk
Radarweg 36
1042 Amsterdam
Netherlands

3 Power Reactor and Nuclear Fuel
Development Corporation
Nuclear Material Control Division
Attn: T. Ito
K. Shibata
T. Yagi, Deputy Director
9-13, Akasaka, 1-Chome
Minato-Ku, Tokyo, 107-8445
Japan

1 Power Reactor and Nuclear Fuel
Development Corporation
Tokai Works
Technology Development Coordination
Division Nuclear Material Management
Section
Attn: T. Kitamura, General Manager
4-33 Muramatsu, Tokai
Ibaraki, 319-1112
Japan

1 F. Armingaud
ISPN/DSMR/SSTR
60-68, Av. du General Leclerc
B.P. No. 6
F-92265 Fontenay-aux-Roses
Cedex
France

1 A. J. Cappeto
Environmental Protection Specialist
Military Sealift Command, Atlantic
Military Ocean Terminal, Bldg. 42-4
Bayonne, NJ 07002

1 Nicole Dellero
Department Etudes et Synthesis
Transnucleaire - Nusys
9, Rue Christoph Colomb
75008 Paris
France

1 B. Desnoyers
COGEMA
Service des Transport
B.P. No. 4
F-78141 Velizy Villacoublay
Cedex
France

1 Ann-Margret Ericsson
AMC Konsult AB
Kammakargatan 6
S-111 40 Stockholm
Sweden

1 B. Hall
Damage Control Officer
Military Sealift Command, Atlantic
Military Ocean Terminal, Bldg. 42-4
Bayonne, NJ 07002

1 M. Hussain
Nuclear Transport Limited
Risley, Warrington
Cheshire WA3 6AS
United Kingdom

1 Robert J. Heid
Engineering Computer Optecnomics, Inc.
1356 Cape St. Claire Road
Annapolis, MD 21401

1 E. P. Pfersich
Chief, Packaged Cargo Section
Hazardous Materials Branch
United States Coast Guard
2100 Second St. SW
Washington, DC 20593

1 P. C. Reardon
PCR Technologies
8416 Yeager Dr. NE
Albuquerque, NM 87109

1 R. C. Richards
U.S. Coast Guard R&D Center
1082 Shennecossett Road
Groton, CT 36615-1384

1 M. Claude Ringot
Cabinet d'Etudes Nucleaires
57 1, Les Monts Lories
91440 Bures-sur-Yvette
France

1 T. Schneider
CEPN
Service des Transport
B.P. No. 48
F-92263 Fontenay-aux-Roses
Cedex
France

1 Clinton J. Shaffer
ITS Corporation
6000 Uptown Blvd, NE, Suite 300
Albuquerque, NM 87110

1 Gheorghe Vieru
Institute for Nudlear Research
0300 Pitesti, P.O. Box 78
Romania

1 C. N. Young
Department of Transport
Floor 4/16
76 Marsham Street
London SW1P 4DR
United Kingdom

SANDIA NATIONAL LABORATORIES, INTERNAL DISTRIBUTION

1	MS0724	J. B. Woodard, 6000
1	MS0715	R. E. Luna, 6130
1	MS0766	D. E. Ellis, 6300
1	MS0718	F. L. Kanipe, 6341
1	MS0718	G. S. Mills, 6341
1	MS0718	S. K. Neuhauser, 6341
10	MS0718	J. L. Sprung, 6341
1	MS0718	R. F. Weiner, 6341
10	MS0718	H. R. Yoshimura, 6341
1	MS0717	D. J. Ammerman, 6342
1	MS0717	G. F. Hohnstreiter, 6342
1	MS0717	J. A. Koski, 6342
1	MS0977	S. J. Bespalko, 6524
1	MS0977	J. D. Smith, 6524
1	MS0720	K. B. Sorenson, 6804
1	MS0720	C. D. Massey, 6806
1	MS9018	Central Technical Files, 8940-2
2	MS0899	Technical Library, ~~4414~~ 4916
2	MS0619	Review and Approval Desk, 12690, For DOE/OSTI

Report Number (14) SAND--98-1171/1
TTC--1525/1

Publ. Date (11) 199805
Sponsor Code (18) DOE/EM, XF
UC Category (19) UC-2000, DOE/ER

ph